VACCINE-INDUCED INNATE IMMUNE RESPONSES AND EXAMINATION OF EXOSOMES IN MAREK'S DISEASE VIRUS (MDV) PATHOGENESIS AND VACCINATION

by

Naga Venkata Sabarinath Neerukonda

A dissertation submitted to the Faculty of the University of Delaware in partial fulfillment of the requirements for the degree of Doctor of Philosophy in Animal and Food Sciences

Fall 2018

VACCINE-INDUCED INNATE IMMUNE RESPONSES AND EXAMINATION OF EXOSOMES IN MAREK'S DISEASE VIRUS (MDV) PATHOGENESIS AND VACCINATION

by

Naga Venkata Sabarinath Neerukonda

Approved: _____
Limin Kung, Jr., Ph.D.
Chair of the Department of Animal and Food Sciences

Approved: _____
Mark W. Rieger, Ph.D.
Dean of the College of Agriculture and Natural Resources

Approved: _____
Douglas J. Doren, Ph.D.
Interim Vice Provost for Graduate and Professional Education

I certify that I have read this dissertation and that in my opinion it meets the academic and professional standard required by the University as a dissertation for the degree of Doctor of Philosophy.

Signed: _____

Mark S. Parcells, Ph.D.
Professor in charge of dissertation

I certify that I have read this dissertation and that in my opinion it meets the academic and professional standard required by the University as a dissertation for the degree of Doctor of Philosophy.

Signed: _____

Erin L. Bernberg, Ph.D.
Member of dissertation committee

I certify that I have read this dissertation and that in my opinion it meets the academic and professional standard required by the University as a dissertation for the degree of Doctor of Philosophy.

Signed: _____

Deni S. Galileo, Ph.D.
Member of dissertation committee

I certify that I have read this dissertation and that in my opinion it meets the academic and professional standard required by the University as a dissertation for the degree of Doctor of Philosophy.

Signed: _____

Ryan J. Arsenault, Ph.D.
Member of dissertation committee

I certify that I have read this dissertation and that in my opinion it meets the academic and professional standard required by the University as a dissertation for the degree of Doctor of Philosophy.

Signed: _____

Carl J. Schmidt, Ph.D.
Member of dissertation committee

ACKNOWLEDGMENTS

First and foremost, I would like to thank my advisor Dr. Mark Parcells for the financial and intellectual input he extended for me to carry out this work. His encouragement at every step of the way helped me to excel and address the challenges associated with the graduate research, which concomitantly modulated my thought process and allowed me to evolve into a full-fledged researcher. I would also like to thank all the past and the present members of Parcells lab for their support and help during my graduate career. Finally, I would like to thank my family for their unconditional love and support.

TABLE OF CONTENTS

LIST OF TABLES

LIST OF FIGURES

ABSTRACT

Marek's disease (MD) is a T cell lymphoproliferative disease of chickens caused by an alphaherpesvirus known as Marek's Disease Virus (MDV). MD is the first neoplastic lymphoma to be successfully prevented by vaccination. MD vaccines are not sterilizing and do not limit pathogenic MDV1 transmission, but reduce early viremia and prevent tumor formation. MD vaccines are administered either via *in ovo* or sub-cutaneous inoculation on embryonic day (E18) and 1-day post-hatch, respectively. Currently in the US, commercial broilers are mass vaccinated *in ovo* with bivalent HVT (FC126) and SB-1 vaccine, whereas breeders and layers are vaccinated with either CVI988 alone, or in combination with HVT, in order to induce long term protection. Bivalent HVT/SB-1 was introduced during early 1980's following the emergence of very virulent (vv) strains in response to near ubiquitous use of HVT as the vaccine of choice. Supplementing SB-1 to HVT was found to confer protective synergism and reduce MD condemnation rates by an average of 78% compared to HVT alone (1, 2). Despite being in use since early 1980s, the mechanisms of vaccine protection, in particular the synergistic protection conferred by bivalent HVT/SB-1 combination, still remains obscure. Furthermore, to broaden the protection provided by MD vaccines to other avian pathogens, HVT has been employed as a vector to carry immunogenic antigens belonging to a range of avian viral pathogens (e.g. IBDV VP2, NDV –HN or –F, ILTV gB). The bivalent vaccine is composed of viruses that are genomically distinct compared to CVI988 (attenuated MDV1) yet induces a high level of protection against a very virulent challenge.

Putative mechanisms of vaccine-induced protection include replication in MDV1 target cells to stimulate innate immune responses during the first few days post-vaccination. Rapid induction of non-specific innate immune signaling is sufficient to polarize the immune system towards T_{H1} phenotype, leading to a CD8+ CTL response, as opposed to T_{H2} and T_{REG} polarization seen during MDV1 infection or lymphoma formation. In line with this, early post vaccination, induction of Type I IFNs and Interferon stimulated genes (ISGs), but not pro-inflammatory cytokines was found to be a critical mechanism for MD vaccine mediated protection.

Innate immune stimulation of Antigen Presenting Cells (APCs, such as macrophages, B-cells, and dendritic cells) and CD8+ CTL responses towards shared epitopes (structural glycoproteins, capsid, and tegument proteins) are implicated in protective immune responses, whereas antibodies play a limited role in protection, given the cell-associated nature of MDV1. Presumably, MD vaccines elicit continual anti-viral CD8+ CTL responses via a low-level of replication, a limited-establishment of latency, and periodic reactivation. We hypothesize that systemic T_{H1} patterning by MD vaccines is mediated by exosomes secreted by APCs and present in the serum of protected chickens. Antigenic peptide-complexed MHC-I+ and MHC-II+ exosomes, secreted by APCs, may function by direct or indirect antigen presentation to naïve CD8+ and CD4+ T cells, respectively, resulting in the generation of effector CD8+ CTLs and CD4+ T_{H1} cells. In line with our hypothesis, we identified a greater abundance of tumor suppressor-targeting miRNAs and lower-abundance MDV-1 miRNAs in serum exosomes derived from CVI-988 vaccinated and protected chickens. In addition, transcripts corresponding to structural glycoproteins, tegument proteins, and immediate-early transactivator ICP4 appeared to be transferred via

exosomes in order to mediate CD8+ CTL responses. Furthermore, peptides corresponding to ICP4 were found in the exosomes suggesting a role played by the exosomal transfer of ICP4 in mediating CD8+ CTL responses.

In contrast, we hypothesized that exosomes secreted by latently-infected and transformed CD4+ T_{REG}-like cells in the serum of infected chickens are immune suppressive towards APCs, and CD8+ CTLs, resulting in a permanent phase of immune suppression. Moreover, we hypothesized that lymphoma-derived exosomes contribute to disease progression in the form of profound immune suppression, increased tumor metastasis, and overall tumor load. Serum exosomes derived from MDV-inoculated or contact-exposed, unvaccinated birds displaying MD lesions carried oncogenic miRNAs (OncomiRs) and MDV-1 miRNAs at a greater abundance. Furthermore, peptides corresponding to latent protein UL36 major tegument protein and UL47 tegument protein were found and suggest potential immune suppressive functions of these exosomes.

Finally, exosomal miRNA biomarkers associated with MD vaccine-mediated protection and immunosuppression, respectively include mir-146b and mir-21, whereas exosomal protein biomarkers associated with MD-vaccine mediated protection versus pathogenesis include COL22A1, IGFBP5, and pantetheinase respectively.

Chapter 1

INTRODUCTION

1.1 Marek's Disease

Marek's disease (MD) is a T cell lymphoproliferative and neuropathic disease caused by a cell-associated alphaherpesvirus known as Marek's Disease Virus (MDV). MD was first described in 1907 by a Hungarian veterinarian named Jozsef Marek as "*generalized polyneuritis"*(3). In the honor of his original contribution, the disease was later named after him in 1962 (4). Earlier description of MD include the involvement of central and peripheral nervous systems with the disease frequently described as *polyneuritis*, *paralysis of domestic fowl* or *neuromyelitis gallinarum* (3, 5, 6). In the late 1920's, Pappenheimer and his colleagues identified lymphomas in six out of sixty field cases of paralysis and described it as "*neurolymphomatosis gallinarum*" based on the similarity in the composition of visceral lymphomas and lymphoid infiltrates in the nervous tissue of affected chickens (6, 7). From the time since poultry production began to expand in its density, beginning of 1950, a high incidence of visceral tumors along with pre-existing neurological lesions was reported in younger chickens of around 8-10 weeks of age, referred to as "acute leukosis". The earlier form of MD seen during 1920s, 1930s and 1940s was referred to as "classical MD" in an effort to discriminate from acute form of MD. Earlier, lymphomas caused

by MDV were confused with another disease known as “Lymphoid leukosis” and both the diseases were frequently referred together as Avian Leukosis Complex (8, 9). In 1967, the isolation of acute MDV strain HPRS16 as a cell-associated primary causative agent of MD was reported in chicken kidney cells co-cultured with tumor cells, tumor infiltrated liver cells and MD-infected blood (10). Furthermore, histological lesions of MD were reproduced upon intra-abdominal inoculation of Rhode Island reds with CPE-positive monolayers confirming Koch’s postulates.

1.2 Marek’s Disease Virus (MDV)

In cultured chicken or duck embryo fibroblast cells, MDV-1 naked nucleocapsids seen in nucleus ranged ~ 100nm whereas primary enveloped nucleocapsids seen in perinuclear space ranged ~ 150-170nm (11). In the feather follicular epithelium (FFE), the enveloped particles seen in the cytoplasm ranged ~ 273-400nm (12). MDV-1 genome is enclosed in an icosahedral capsid made of 162 capsomers and the capsid is in turn surrounded by a protein rich tegument layer. Outer most layer of the virus particle is a lipid envelope derived from cellular membranes and is embedded with various cellular and viral glycoproteins.

Based on its ability to infect lymphocytes and slow growth *in vitro*, MDV-1 was initially classified under the subfamily *Gammaherpesvirinae*, along with its other member EBV (9). However, upon sequencing and restriction fragment analysis of MDV-1 genome, it was found to contain Class E type genome, reflecting the similarity with alphaherpesviruses HSV1 & 2 and VZV (13, 14). Hence, it was later classified under the subfamily *Alphaherpesvirinae*. MDV isolates were grouped in the genus *Mardivirus* (Marek’s disease like virus) which encompass 3 distinct serotypes of MDV. MDV-1 serotypes include all oncogenic viruses and their attenuated

derivatives. MDV-2 serotypes include non-oncogenic viruses that naturally infect chickens. MDV-3 or *Meleagrid herpesvirus-1* (MeHV-1) include a non-oncogenic virus that infect turkeys, also known as herpes virus of turkeys (HVT). All three serotypes share similar genomic organization in that the genomes are composed of unique long (U_L) and unique short (U_S) sequences flanked by inverted repeats both terminally (TR_L and TR_S) and internally (IR_L and IR_S). Terminal and internal repeats flanking each unique region are identical in sequence and are in inverted orientation. The overall genomic organization and the individual gene arrangement in the unique regions is similar among all three serotypes and resemble with that of HSV and VZV whereas the genus or virus specific genes are primarily located in the repeat regions. Additionally, the repeat regions also encode virus specific micro-RNAs (miRNAs). Although there lacks a sequence conservation among miRNAs of different MDV serotypes, the genomic location of miRNAs is conserved (15). Genome wide expression of MDV-1 encoded RNAs occurs during lytic replication whereas expression patterns during the phase of latency and transformation are restricted to repeat regions flanking the unique long region or the unique short region that contain latency associated transcript (LAT) (16, 17). Genes encoded in the repeat regions with an implicated role in determining MDV-1 pathogenicity or oncogenicity include oncogene *meq* (18), viral telomerase RNA *(vTR)* (19), viral interleukin 8 *(vIL-8)*(20), repeat long open reading frame 4 (RLORF4) (21) and phosphoprotein 38 complex (pp38) (22).

1.3 MD Pathogenesis

The Cornell Model of MDV pathogenesis proposed by Calnek and his colleagues at the Cornell University consists of four phases: 1) Early cytolytic phase

2) Latent phase 3) Secondary cytolytic phase 4) Phase of Transformation (23). The timing and severity of these phases may vary in accordance with the virulence level and dose of virus used for infection, host genotype and the age during exposure.

1.3.1 Early Cytolytic Phase

MDV-1 infection begins with inhalation of keratin enclosed, cell free or cell associated virus shed along with desquamated feather follicular epithelial dander by the infected birds into surrounding poultry house environment. MDV-1 in dander can persist in the poultry house environment for weeks to several months (24). Following inhalation, the virus is phagocytozed by the recruited phagocytes (macrophages and B cells) either directly or upon an initial round of replication in lung epithelium (25). Infected B cells and macrophages carry the virus to primary (bursa and thymus) and secondary lymphoid (spleen) organs where the virus is transmitted to its predominant target cell, B lymphocyte, to undergo productive-restrictive replication.

Although B cells are the predominant infected cell type, some of the activated but not the resting CD4+ T cells are also infected via antigen presenting interactions with infected APCs. Both infected B cells and some of the activated CD4+ T cells undergo apoptosis resulting in lymphoid depletion and atrophy. As a result, a transient early immune suppression ensues. The spleen then becomes the major site of viral replication. MDV-1 infection was recapitulated *in vitro* in B cells and its subsequent transfer to activated CD4+ T cells, with each cell type maintained in the presence of soluble CD40L and anti-TCR$\alpha_V\beta_1$ antibody respectively. In the *in vitro* infection model, an efficient infection of CD4+$\alpha_V\beta_1$-TCR2 cells was observed whereas $\gamma\delta$ TCR1 cells were poorly infected (26). Another study demonstrated *in vitro* productive-restrictive replication of attenuated CVI-988 in KUL01$^+$CD45$^+$ BMMs and

BMDCs (27). In chickens with fully functional immune system (3 weeks of age), rapid cytolytic infection occurs and viremia levels peak at 3-7 days' post infection (dpi) whereas in infected day old chicks viremia levels peak 7 days later, at 10-14 dpi.

MDV-1 lytic replication during the cytolytic phase initiates an innate immune response characterized by the production of pro-inflammatory cytokines such as IL-1α/β, IL-6, IL-8 along with Type I and II interferons. This innate immune response drives the virus to undergo latency in activated CD4+ TCR2 and TCR3 cells. By 7-10dpi, lytic gene expression and viral genome replication is completely repressed marking a shift from cytolytic phase to latency.

1.3.2 Latent Phase

Transcriptionally active chromatin (H3K9ac and H3K4me3 marks) was found around the *meq* and the miRNA gene promoters in both lymphoblastoid cell lines and primary lymphoma with bound Meq-c-Jun heterodimers. Meq homodimers were found enriched at the lytic origin of replication (OriLyt), located next to the lytic gene pp38. This region was found enriched with repressive histone modifications (H3K27 and H3K9me3) (28). During latency, viral genome integration occurs within and near host telomeres via telomeric repeat (TMR) arrays located in *alpha* like sequences (*a-like sequences*) at the genome termini or between internal repeat segments. High integration efficiency correlates with efficient tumor formation and subsequent reactivation (29). A recent study has elegantly demonstrated viral genome integration during latency (oncogenic and vaccine MDV) via FISH as a predominantly chromosome associated/telomere integrated, whereas during cytolytic phase, chromosome associated state was observed (30). MDV-1 undergoes latency primarily in the activated CD4+ TCR2+ and TCR3+ T cells. Latently-infected CD4+ T cells

rapidly proliferate and disseminate the virus to various visceral and peripheral sites by blood resulting in viremia.

1.3.3 Secondary Cytolytic Phase

As the innate immune response maintaining the latency wanes, the virus reactivates resulting in a second phase of cytolytic infection from 14-21dpi. Secondary cytolytic phase is seen at the peripheral sites (e.g. adrenal glands, kidneys, Schwann cells and feather follicular epithelium) with fully productive virus replication occurring only in feather follicular epithelium (FFE). Cell-free and cell-associated virus is shed along with feather dander throughout the life of chicken even in vaccinated and protected chickens (12). Virus shed along with dander is ready to begin a new infection cycle. US2, UL13 and glycoprotein C were found to be essential for horizontal transmission (31).

1.3.4 Phase of Transformation

During latency, some of the latently infected CD4+ T cells will proliferate and give rise to lymphomas due to direct actions of oncogene *meq*, its spliced variants and other gene products (*vTR*, MDV1-miRNAs) (32). Frank lymphomas can be appreciated in multiple visceral organs including heart, kidneys, spleen, gonads, intestines and proventriculus. The efficiency of MDV-1-mediated transformation depends upon the robustness of lytic replication in order to generate sufficient number of latently infected CD4+ T cells necessary for transformation. Consequently, deletion of lytic gene products (vIL-8, pp38) resulted in lowered lytic replication thus reduced tumor formation efficiency (20, 33). *In vivo*, lymphoma microenvironment is a composite of neoplastic, inflammatory and immune cell infiltrates (34). Transformed

component of MD lymphomas depict T_{REG}-like immunophenotype and are characterized as $CD4^+$, $TCR\alpha\beta^+$, MHC I^{hi}, MHC II^{hi}, IL-$2R\alpha^+$, $CD28^{lo}$, $pp38^-$, gB^-, and express high amounts of Hodgkin's Reed Sternberg Antigen ($CD30^{hi}$) (35, 36). MDV-1 tumors are monoclonal or oligoclonal in nature and a permanent phase of immune suppression ensues due to the transformed T_{REG}-like immune phenotype of lymphomas (37).

1.4 MDV1 gene products associated with pathogenicity and oncogenicity

MDV1-encoded gene products play a critical role in rapid development of tumors as early as 3 weeks post infection. Molecular approaches including comparative genomics of MDV serotypes, deletion and insertional mutagenesis, identification of genomic alterations during the attenuation process and characterization of MDV-1 gene products in MD lymphoblastoid cell lines have implicated genes located in transcriptionally active repeat regions to be essential for pathogenicity. These genes include oncogene *meq*, viral interleukin-8 (vIL-8), phosphoprotein 38 complex (pp38), viral telomerase RNA (vTR) and finally, MDV1-encoded miRNAs.

1.4.1 Oncogene *meq*

Oncogene *meq*, named after **M**arek's **E**coRI-**Q**-encoded protein, codes for a 339 aa. basic leucine zipper (bZIP) protein that is consistently expressed at higher levels in MDV-1-induced primary lymphomas and lymphoma derived transformed cell lines. Meq fulfills several of the criteria for being a primary oncogene. Overexpression of Meq in Rat-2 and DF-1 fibroblasts resulted in morphological transformation, apoptosis resistance, serum- and anchorage-independent growth (38).

Conversely, deletion of both the copies of *meq* in the repeat regions flanking the unique long region of very virulent MDV-1 genomes (RB1B and rMd5) resulted in a loss of viral oncogenicity (32, 39). Finally, oncogene *meq* is present only in MDV-1 serotypes and its attenuated derivatives but absent in non-oncogenic MDV serotypes (serotypes 2 & 3). Upon comparison of coding sequences of *meq* among strains of distinctive virulence, mutations that correlate with pathotype virulence were identified (40). Furthermore, maximum likelihood based selection analyses of *meq* proteins spanning the virulence spectrum have indicated the evidence of adaptive evolution driven by the positive selection with an overall $dN/dS \sim 1.54$ (41). Positive selection appears to reflect viral adaptation against host defenses specifically, innate immune responses elicited early upon vaccination, conferring an overall advantage for the virus to evade or subvert vaccine induced innate patterning (41).

Meq contains an N-terminal bZIP (56-129aa) that is homologous to *jun/fos* family oncogenes and a C-terminal proline rich activation domain (129-339aa) similar to *Wilm's tumor suppressor* (*WT-1*) (42). MDV-1 strains of mildly virulent (CU-2) and virulent (BC-1, JM-1) classification, a Hungarian 1973 isolate (M1) and an attenuated MDV1 derivative (CVI-988) encode longer forms of *meq,* ca. 398-339aa. in length due to an in-frame insertion of 59-60aa. containing proline rich repeats (40, 43). As a transcription factor, Meq localizes in nucleus, nucleolus and Cajal body granules (44). Basic regions rich in arginine and lysine, referred to as basic regions 1 (BR1) & 2 (BR2) contain nuclear and nucleolar localization signals (NLS and NoLS) (45). BR1 extends from 30-35aa and acts as NLS. BR2 extends from 62-78aa and acts as both NLS and NoLS. Meq interacts with cyclin dependent kinase-2 (Cdk2) in Cajal bodies and nucleolar periphery during G1/S transition and S phases of cell cycle (46). Cdk2

mediated phosphorylation of Meq on serine 42 ostensibly reduces its DNA binding ability and shuttles it to cytoplasm. Meq also has a putative nuclear export signal (NES) that is presumed to play a role in cell-cycle dependent translocation. Functional consequences of Cdk2 interaction and different localizations is unknown.

Proline rich repeats (PRRs) in the C-terminal domain (129-339aa.) of *meq* when fused to Gal4 DNA Binding Domain (DBD) transactivates reporters containing Gal4 DNA binding sites (Vaithilingaraja Arumugaswami Ph.D. thesis; 2004). Truncation analyses of C-terminal domain indicated terminal 33aa. to be critical for the transactivation potential of Meq although PRRs are required for a full transactivation potential. This 33aa. region do not contain any major structures except a putative RNA-binding motif. On the other hand, when only the PRR is analyzed in the reporter assays for its transactivating ability, this region displayed transrepression analogous to *WT-1* repression domains (47). Furthermore, virulence correlating mutations were located predominantly in PRRs where a second position in tandem proline rich repeats (PPPP) is substituted with glutamine or alanine (P(P→Q/A)PP) in the strains of higher virulence. It has been hypothesized that these substitutions decrease the transrepression potential of *meq*, with Meq proteins belonging to the strains of higher virulence having greater transactivation potential. In line with this hypothesis, C-terminal domains of higher virulent strain *meqs* when fused to Gal4-DBD display greater transactivation potential in reporter assays.

By virtue of its bZIP domain at the N-terminus, Meq forms homo- or heterodimers with cellular and viral bZIP domain containing proteins. For its transforming ability, both homo- and hetero-dimerization properties are essential (48, 49). Upon hetero-dimerization with cellular bZIP protein *c-Jun*, it binds to AP1 and

AP-1 like motifs in the promoters of target genes and regulates expression of genes involved in cell proliferation, differentiation and apoptosis (38). These include upregulation of JTAP-1, JAC, Hb-EGF and Bcl-2 and downregulation of pro-apoptotic genes Fas and DAP5 in Meq-transformed DF-1 cell line (38). Knock-down of either Meq or c-Jun in these cells using RNAi led to a decrease in cell proliferation and downregulation of JTAP-1, JAC and Hb-EGF pointing to the critical role played by c-Jun pathway in the transforming ability of Meq (38). Other upregulated target genes of Meq include c-ski, a proto-oncogene that suppresses transcriptional activity of Smads and thus intercepts TGF-β signaling (38). Finally, Meq also forms heterodimers with other cellular bZIP proteins JunB, Fos, CREB, ATF-1, -2, -3, DDIT3 and NFIL3 *in vitro* (50).

In MSB-1 lymphoblastoid cell line established from spleen lymphoma induced by vMDV (BC-1) and harboring MDV2 (SB-1), Meq-Jun heterodimers bound to AP-1 motifs in *meq* promoter, whereas, homodimers bound to ACACA motifs in the lytic replication origin (Ori_{Lyt}) which also included a bidirectional promoter for lytic genes pp38/24 and pp14 (28). This binding resulted in an activation of *meq* promoter and repression of lytic gene promoters demonstrating that Meq acts a lytic/latent switch. In addition, Meq-Jun heterodimers bind AP-1 motifs in IL-2 gene promoter, although IL-2 dependent or independent nature of MD lymphoblastoid cell lines is obscure (35).

Other cellular partners of Meq include p53, Rb, $p27^{kip1}$, S-phase Kinase associated protein 2 (Skp2), CtBP1 and Hsp70 (51-55). PxxP motifs in the proline rich repeats of Meq C-terminus serve as binding modules for SH3-domain containing proteins (51). Meq-p53 interaction is via zipper and C-terminal tetramerization domain respectively (51). Meq interaction with p53 leads to a decrease in transcriptional and

apoptotic functions of p53. Meq interaction with Rb is via LACHE or LARHE motif located at the end of bZIP domain (53). In this regard, LACHE motif in oncoproteins of other tumor viruses was found to bind STING to inhibit cGAS-STING DNA sensing or signaling pathway and downstream Type I IFN production (56). Meq interaction with $p27^{kip1}$ and skp2 likely deregulates cell cycle check points leading to transformation. Meq also interacts with chromatin regulator protein CtBP1 via PLDLS motif in its N-terminus (54). PLDLS mutation to AVEFT on vvMDV (RB1B) backbone abolishes the interaction of Meq with CtBP1 resulting in complete loss of oncogenicity (54). Upon interaction with DNA binding proteins containing PLDLS motif, CtBP1 is recruited to target loci as a dimer in complex with histone deacetylases (HDACs), Small Ubiquitin MOdifier (SUMO) and H3K9 histone methyl transferases resulting in histone modification and repression of target chromatin (54). CtBP1 plays a critical role during development, differentiation, proliferation, apoptosis and cellular adhesion. Meq-CtBP1 interaction is presumed to be involved in the regulation of metastasis and T-cell apoptosis (54). Finally, Meq interaction with Hsp70 results in its recruitment to nucleus (55). Hsp70 plays pro-tumorigenic role by apoptosis inhibition and promoting cell survival (55).

One of the key features of MD lymphomas is overexpression of CD30 a.k.a Hodgkin's Reed Sternberg Antigen. Putative Meq binding sites (n=15) in chicken CD30 promoter and Meq-induced transcription from CD30 promoter is responsible for $CD30^{hi}$ phenotype of MD lymphomas or lymphoblastoid cell lines (35, 57). Meq induced CD30 transcription is genotype-specific with MD susceptible lines displaying higher induction compared to resistant lines. $CD30^{hi}$ phenotype promotes cell survival by NFκB activation, confers T_{h2}/T-regulatory phenotype and antagonizes cell

mediated cytotoxic responses (35, 57, 58). $CD30^{hi}$ cells from vMDV (GA) primary lymphomas display greater nuclear localization of NFκB with NFκB enhancing *meq* transcription, thus establishing a feed forward loop between Meq and CD30 (58). This feed-forward loop could be one of mechanisms necessary to maintain cell survival during MDV T-cell transformation.

During latency, in addition to Meq, two other splice variants (Meq/vIL8 and Meq/vIL8ΔExon3) with a possible role in lymphomagenesis are expressed (59). Meq/vIL-8 is a 212aa. protein containing first 100aa of Meq fused to exon 2 and 3 of vIL-8. Concurrent studies in our lab identified Polycomb Repressive Complex-1 (PRC1) component Bmi-1 as Meq/vIL-8 interaction partner. Due to the presence of PLDLS motif, bZIP DBD, lack of a transactivation domain and their ability to interact with Bmi-1, Meq/vIL8 and Meq/vIL8ΔExon3 function to transrepress target loci. Despite the lack of transactivation potential, Meq/vIL8 and Meq/vIL8ΔExon3 induced proliferation upon overexpression in chicken peripheral blood mononuclear cell line (HTC). In this regard, only Meq/v-IL8 had the potential to inhibit Staurosporin-induced apoptosis in DF-1 cell line but not Meq/vIL8ΔExon3 pointing to different functions of each splice variant. Fluorescence resonance energy transfer (FRET) and Fluorescence recovery after photobleaching (FRAP) techniques demonstrated that Meq and Meq/vIL-8 although localized to nucleus, nucleolus and Cajal bodies, exhibited distinctive mobility (44). Meq displayed higher mobility whereas Meq/vIL-8 displayed slower mobility similar to structural components (44). Furthermore, in Meq and Meq/vIL-8 co-transfected cells, Meq/vIL-8 was exclusively localized to Cajal bodies. In light of these findings, Meq and Meq/vIL8 are predicted not to interact or heterodimerize. Finally, Meq/vIL8 and Meq/vIL8ΔExon3 were found to bind lytic

promoters (ICP4 and pp38/14) and Meq promoter in chromatin IP (ChIP-seq) studies (28).

1.4.2 Phosphoprotein 38 (pp38) complex

Two phosphoproteins pp38 and pp24 constitute the pp38 complex. pp38 and pp24 proteins originate from a common promoter and share common amino terminus of 65aa (60, 61). They are encoded in the junctions formed by unique long and terminal or internal repeat long regions. Initially thought to be a latent protein or important for tumorigenicity, later studies identified pp38 to be expressed during cytolytic infection and FFE (62). Further evidence supporting this notion came from studies with rMd5Δpp38 virus, a pp38 deletion mutant constructed from a vv MDV (Md5) using overlapping cosmid clones (33). This deletion mutant displayed no defects in replication *in vitro.* However, in chickens infected with rMd5Δpp38, early cytolytic infection was severely impaired which in turn resulted in low level infection of target cells for transformation and finally, a very low level of tumor incidence compared to parental rMd5 (33). Furthermore, the ability of rMd5Δpp38 to reactivate in splenocyte-CEF coculture remained comparable to that of rMd5 despite lower number of latently infected T-cells. Two other splice variants of pp38 were reported that predominantly expressed during latency although the functional significance of these proteins remain elusive (61).

1.4.3 Viral Interleukin-8 (vIL-8)

vIL-8 is an MDV1-encoded protein located upstream of *meq* gene in the repeat regions flanking the U_L region of MDV1 genome. vIL-8 transcript is made of 3 exons (20). Exon I codes for hydrophobic amino acids and likely has a signal peptide

whereas Exons II and III code for mature, secreted protein. vIL-8 is a viral homolog of cellular IL-8, a CXC chemokine with prototypic signal peptide and 4 positionally conserved cysteines (20). Cellular IL-8 contains a conserved ELR motif preceding CXC motif and functions to promote recruitment of neutrophils (20). vIL-8 possesses DKR motif instead of ELR motif and is a potent chemoattractant for macrophages, B-cells and CD4+CD25+ regulatory T cells, the target cells of MDV1 (63).

A vIL-8 knock-out virus constructed on RB1B backbone, RB1BvIL-8ΔsmGFP displayed poor cytolytic infection and a low level of oncogenicity due to decreased ability to infect and undergo cytolytic infection in MDV1 target cells (20). Similar findings were observed with vIL-8 knock-out virus constructed on rMd5 strain backbone, rMd5ΔvIL-8 (64). Cell population analyses of infected spleens indicated a greater number of B cells and a decreased number of activated T-cells in rMd5ΔvIL-8-infected spleens compared to rMd5-infected spleens. Furthermore, an RB1B deletion mutant lacking only Exon I of vIL-8, constructed to ensure expression of splice variants of RLORF4/5 and *meq*, displayed properties comparable to that of a deletion mutant lacking full length vIL-8 (63). Spliced variants containing Exon III and/or Exon II of the vIL-8 including Meq/vIL8, Meq/vIL8ΔExon3, RLORF5a/vIL-8 and RLORF4a/vIL-8 were reported whose functions are not fully elucidated and thus remain obscure (59).

RLORF4 and 5 are present between *meq* and vIL8 genes in the same orientation in the repeat regions of MDV1 genome. Both RLORF4 and RLORF5a transcripts were found to be expressed in MDV1 lymphoblastoid cell lines. Deletions in RLORF4 gene were identified in several attenuated strains (21). Deletion of RLORF4 but not RLORF5a severely attenuated MDV-1 oncogenicity (21). An RB1B

BAC-based recombinant expressing either enhanced green fluorescence protein (eGFP) or red fluorescence protein (RFP) fused independently in frame with RLORF4 retained oncogenicity. However, eGFP and RFP were expressed unfused with RLORF4 underscoring the transcriptional complexity in the repeat regions of the MDV1 genome (65).

1.4.4 Viral telomerase RNA (*vTR*)

Upstream and anti-sense to vIL-8, MDV1 encodes a telomerase RNA subunit of cellular telomerase holoenzyme known as viral telomerase RNA (vTR) (66-68). MDV1 vTR shares 88% homology with cellular telomerase RNA (cTR)(19, 66). *In vitro* telomerase activity assays confirmed the functionality of vTR which displayed higher activity compared to cTR. Expressed during both lytic and latent phases of infection, vTR promoter displayed 2-6-fold higher activity compared to cTR promoter in *in vitro* assays (19, 66-68). Furthermore, vTR displayed greater interaction with cellular telomerase reverse transcriptase (cTERT) compared to cTR.

When mutated to abolish its ability to interact with cTERT, MDV-1 encoding a mutant vTR that does not contribute to telomerase activity efficiently induced lymphomas as the wild type virus indicating transforming properties of vTR independent of its telomerase activity. In line with this, when overexpressed in DF-1 cells, vTR induced transformation based on its ability to induce proliferation, soft agar colony formation and change in cell morphology (69). Two mutant viruses, one lacking vTR (vTR^{-}) and the other having *vTR* promoter replaced with that of chicken ($vPchTR^{+/+}$) were assessed for their growth characteristics and oncogenicity (70). Both mutant viruses displayed *in vitro* growth characteristics similar to that of parent virus. The mutant viruses, however, displayed reduced tumor incidence and dissemination.

Furthermore, upon mutating the template sequence of *vTR* (AU5- named after 5 consecutive AU bases), AU5 mutant completely lacked the ability to induce lymphomagenesis and displayed delayed proliferation of quail QT35 cancer cell line upon tetracycline induced expression compared to parental vTR (71). Based on similar interacting partners of *vTR* and EBV-encoded RNAs (EBER1 and EBER2), including Rpl22, the ability of EBERs to complement *vTR* loss in MDV1 was assessed on RB1B backbone (72). Mutant viruses either lacking *vTR* or having EBER1/2 in place of *vTR* displayed comparable *in vitro* growth characteristics with that of parent RB1B. In addition, partial and successful complementation of *vTR* loss by EBER1 and EBER2 respectively, indicated conserved functions of herpesvirus RNAs in promoting transformation (72).

Finally, deep sequencing of attenuated vv+MDV1 (648A) displayed 4 deletions in *vTR* that affected its secondary structure (73). In MSB1 lymphoblastoid cell line, *vTR* transcriptional regulation was found to be under the control of *c-myc* but not *meq* (74).

1.4.5 UL36-encoded major tegument protein (MTP)

All herpesviruses have an ubiquitin specific protease (USP) encoded in the N-terminus of MTP (75, 76). USP activity is conferred by 4 absolutely conserved amino acids (C, D, H, Q). MTP is expressed both during lytic and latent phases of infection. A BAC-based RB1B recombinant with USP active site cysteine mutated to alanine ($MDV1^{USP/C98A}$) is a USP-dead recombinant that displayed comparable *in vitro* growth kinetics with that of parent virus (76). $MDV\text{-}1^{USP/C98A}$ however displayed severe reduction in MD tumor incidence although MDV-1 replication was unaffected *in vivo* (76). Deletion of a 22aa cysteine box containing active site cysteine residue severely

impaired viral replication in *in vitro* studies (75). These findings indicate both USP structure or stability and protease activity are essential for MDV-1 replication and lymphomagenesis (75).

Finally, HSV1 USP homologue was shown to deubiquitinate polyubiquitinated IκBα and monoubiquitinated PCNA to inhibit HSV1 DNA-induced IFN-β or NF-κB activation and DNA damage responses respectively to facilitate infection (77, 78). Furthermore, HSV1 USP was shown to interact with ESCRT1 component TSG101 and deubiquitinate TSG101 (79).

1.4.6 UL47 tegument protein

UL47 is a late gene expressed during lytic infection with very low and high abundances in CEFs and FFE respectively (80). MDV-1 encoding UL47-eGFP fusion was constructed on pRB-1B background (80). UL47-eGFP recombinant displayed comparable plaque sizes with that of parent *in vitro* in addition to indistinguishable pathogenicity in infected chickens. UL47-eGFP expressed at low levels in the infected CEF and lymphocytes, and localized to nucleus with a punctate pattern (80). In contrast, UL47-eGFP expressed to a higher level in FFE and displayed cytoplasmic localization. It was hypothesized that the lower and higher expression levels of UL47 in lymphocytes and FFE is directly related to cell associated and cell free patterns of MDV-1 respectively (80).

1.4.7 MDV-encoded glycoproteins

MDV-1 genome encodes for 11 glycoproteins including glycoprotein B (gB), gC, gD, gE, gH, gI, gK, gL, gM, gN, and gp82 (40). Among these, gB, gH/gL complex, gE/gI complex and gM/gN are not essential for virus growth *in vitro* (81-83).

Three splice variants of gC including two smaller transcripts coding for variant proteins lacking transmembrane domains, thus secreted forms, were identified (84). *In vitro*, gC cell surface expression is limited to 5%, with predominant expression of secreted forms. gC expression is non-essential for replication *in vitro*, but is essential for horizontal transmission in chickens (84, 85). gD is expressed to a very low to no expression in cultured cells (86, 87). In infected chickens, gD is expressed to a very low level in FFE (86). gD expression is not essential for viral replication, pathogenicity and horizontal transmission (86-88).

gL lacks a transmembrane domain and its cell surface expression and stability is via complex formation with gH. Herpesviral gH/gL is essential and have a conserved role in receptor binding and fusion or cell to cell spread (89, 90). A deletion of 12nt coding for TKTN amino acids in vv+MDV (T-King a.k.a TK-2A) was found to confer greater virulence in contact-exposed chicks vaccinated with bivalent HVT/SB-1 (40, 91). A recombinant MDV-1 carrying this deletion on pRB1B background, however displayed indistinguishable *in vitro* and *in vivo* replication kinetics and unaltered pathogenicity (92).

1.4.8 Phosphoprotein 14 (pp14)

Pp14 is an MDV-1-encoded protein. Pp14 is expressed as two isoforms by two mature bicistrionic mRNAs that differ in 5' leader sequences due to alternative splicing or promoter usage (93-96). The presence and absence of 5'leader IRES dictates which isoform is produced and isoforms differ in their N-terminal sequences. Bicistrionic mRNA with 5' leader sequence is 2-3-fold higher in abundance in MDV-1-infected CEF and MDV-1-transformed MSB1 cell line (96). The other cistron in the bicistrionic RNA encodes 12kDa RLORF9 whose translation is via an IRES in the

inter-cistrionic region. Deletion of IRES did not affect MDV-1 replication or oncogenicity (96). Based on its immediate-early expression kinetics, cytoplasmic localization and presence of PEST protein-turnover domains, it was proposed to be involved in the regulation of intracellular host response (97).

A recombinant virus lacking exon 2 of pp14 (pRB1BΔ-pp14) displayed similar *in vitro* growth kinetics as parent virus but infected chickens displayed no neurological lesions and infected chickens displayed higher survival rate indicative of a role in neurovirulence (98).

1.4.9 Viral Lipase (vLIP)

vLIP identified in MDV-1, -2 and -3 is a 756aa protein that shares a significant homology with pancreatic lipase in its α/β hydrolase domain (99, 100). The first 32aa of vLIP contains a signal peptide and is encoded in Exon 1 whereas Exon 2 codes for the rest of the protein. vLIP catalytic triad is composed of SNH instead of SDH in its hydrolase domain (99). *In vitro* vLIP displayed late kinetics, glycosylated and secreted into surrounding medium but lacks lipase activity (99). Two vLIP recombinants were constructed, one lacking the homologous region of vLIP and the other with an alanine substitution of nucleophile serine in its catalytic triad. Both recombinant mutants displayed reduced tumor incidence and greater survival rate compared to parental and revertant viruses. Mutations in vLIP were shown to be associated with either attenuation or increase in virulence, depending on the nature of mutations (73).

1.4.10 Latency Associated Transcripts (LATs)

MDV genome encodes 2 copies of LAT in the inverted repeats flanking the unique short region, anti-sense to major immediate early transactivator, infected cell

protein 4 (ICP4) (101-103). LAT gene encodes several LATs including 2 MDV-1 small RNAs (MSRs) and a large unspliced 10kb LAT (102). LATs are predominantly localized to nucleus and are expressed in MD lymphoblastoid cell lines (102). In infected cells, LAT expression is not seen until at late stages of infection when the cells are no longer permissive to lytic replication. MSRs were mapped to ICP4 translation initiation site and contain 2 complementary recognition sequences (102). MSRs were hypothesized to promote ICP4 translational repression thus lytic replication. Viral reactivation in MSB-1 cell line is associated with decreased LAT expression concomitant with a rise in ICP4 mRNA.

1.4.11 Infected Cell Protein4 (ICP4)

ICP4 is an immediate early transactivator encoded in repeat regions flanking the unique short region. MDV-1 ICP4 contains serine rich N terminus, NLS in region 3 with regions 2 & 4 displaying high degree of conservation with HSV1 ICP4 (104). Syngenic cell mediated immune responses towards ICP4 was found to be a major factor in defining the genetic resistance towards MD in $B^{21}B^{21}$ chickens (105). Downstream of ICP4 and anti-sense are several MDV-1-encoded cluster 3 miRNAs predicted to repress ICP4 mRNA translation in the event of its transcriptional read-through (106).

1.4.12 MDV-encoded miRNAs

MDV-1 encodes 14 miRNAs encoded in two clusters. Cluster 1 miRNAs a.k.a *meq* clustered miRNAs flank oncogene *meq* (106-111). *meq* clustered miRNAs, present in cluster 1 and 2 at 5’ and 3’ regions of oncogene *meq* respectively, include MDV1-miR-M9, -M12, -M2, -M3, -M4, -M5, -M1, -M11, -M31. Cluster 3 miRNAs

a.k.a LAT cluster are present at the 5' end of LAT, downstream and antisense to ICP4 (109, 111). LAT cluster include MDV1-miR-M6, -M7, -M8, -M10 and –M13. MDV2 and HVT also encode 18 and 17 miRNAs respectively. Although miRNAs lack sequence homology among of the different MDV serotypes, their genomic location is conserved. The MDV1 *meq*-clustered miRNAs are expressed at much greater levels in vv+MDV1 tumors, compared to vvMDV1 tumors, whereas LAT-clustered miRNA expression levels remained unchanged (106).

Among the *meq*-clustered miRNAs, MDV1-mir-M4 shares seed sequence with cellular mir-155 and KSHV K12-11, with predominant expression (72%) seen in MDV1 tumors. Furthermore, deletion or mutating just 2nt of M4 seed region on pRB1B background abolished viral oncogenicity (112, 113). Replacing M4 with cellular mir-155 restored the oncogenic potential of recombinant RB1B. Cellular miR-155 plays a critical role in immune cell (B-, T-) cell development and its expression is downregulated in MD tumors and lymphoblastoid cell lines (113). miR-155 function is complemented by MDV1-M4 and their shared target genes include c-Myb, GPM6B, RREB, BCL2L13, PDCD6, LAT, HIVEP2, c/EBP, PU.1 and JARID2. A HVT recombinant expressing MDV1-mir-M4 displayed improved replication characteristics but was not tumorigenic (E.Bernberg, R.Morgan 2015 Microbial Systems Symposium). Ectopic over expression of MDV-1 *meq* cluster miRNAs or recombinant HVT carrying *meq* cluster miRNAs abolished Type I IFN and ISG induction in CEF upon HVT infection indicating immune suppressive nature of MDV-1-encoded miRNAs (E.Bernberg, R.Morgan. Microbial Systems symposium 2016 and 2017). Additional targets of MDV1-encoded miRNAs include ICP4, ICP27, UL28, UL32 and RLORF8 suggesting a role in the regulation of lytic versus latent infections (110).

Finally, several cellular miRNAs were found differentially expressed in MDV1 transformed cells including upregulation of gga-miR-21, -150 and -223 (114, 115).

1.5 Immunity to MDV

Immune response to MDV includes both non-specific innate and specific adaptive immunity. Innate immune responses are elicited immediately upon detection of viral PAMPs during infection whereas adaptive immune responses are shaped by 5-7dpi. Cytokines produced upon innate stimulation and antigen presentation play a major role in patterning the adaptive immunity (116, 117).

1.5.1 Innate Immunity

During MDV infection, macrophages and NK cells are the main effectors to promote innate immune responses. NK cells function by promoting death in the target cells by either death receptor ligation or delivery of granular contents leading to extrinsic or intrinsic pathways of apoptosis (116). The cytotoxic effects of NK cells during MDV-1 infection were demonstrated by cell based assays and transcriptional analysis of infected spleens (118-121). Splenocytes from 10 day old chicks infected with RB1B demonstrated NK cell cytotoxicity against RAV2 transformed LSCC-RP9. Furthermore, an enhanced expression of NK cell markers perforin, granzyme and NK lysin was found by 7dpi in RB1B-infected chickens (122). In addition, given the cell associated nature of MDV-1 and since MDV-1 infection is known to down regulate MHC-I expression on infected CEF, NK cells play an important role in controlling infected cells by "recognition of missing self" mechanism (123). An early and sustained NK cell activity was found in splenocytes from B^{21} resistant chickens compared to an abrupt loss in activity in splenocytes from B^{19} susceptible chickens

(119). NK cell cytotoxicity was also demonstrated *in vitro* against MDCC-PA9 lymphoblastoid cell line established from HPRS19-infected chicken lymphomas (124). MD bivalent vaccine HVT/SB1 was found induce a significantly higher NK cell cytotoxic activity in N-2 compared to P-2 birds against LSCC-RP9 (120).

Macrophages play an important role during various stages of MD pathogenesis in addition to inducing innate immune responses. Macrophages serve to transport the virus from lung to lymphoid organs at the beginning of infection. Macrophages were found to support productive restrictive replication *in vitro* and *in vivo* based on the expression of lytic transcripts ICP4, pp38 and gB (125, 126). Macrophages from MDV-1-infected chickens exhibited enhanced phagocytic indices and plaque inhibiting activity *in vitro,* more so in macrophages from susceptible line (127). Macrophages induce iNOS and nitric oxide production to inhibit MDV-1 replication *in vitro* and *in vivo*. A higher level of iNOS activity is responsible for immune-mediated pathology observed with higher virulent strains of MDV-1 (128-130). Selection for excessive NO production was found to be detrimental to the host and enhanced the susceptibility to MDV-1, indicating intermediary levels of NO is beneficial to the host (131). Finally, upon pathogen sensing, macrophages produce Type I IFN, which inhibit MDV-1 replication *in vitro* and *in vivo* upon oral administration (132).

1.5.2 Acquired Immunity

Humoral and cell-mediated immune responses constitute acquired or adaptive immune responses. Due to cell-associated nature of MDV-1, humoral immune responses play a very limited to no role in immunity against MDV-1. The presence of maternal antibodies (mAbs) against MDV delays the onset of infection and reduced disease severity. MAbs also prevent lymphoid organ atrophy associated with higher

virulent MDVs. On the other hand, presence of mAbs also interfere with MD vaccines, for instance cell free-HVT resulting in reduced vaccine efficacy. Antibodies against MDV-1 glycoproteins are produced during infection of which anti-gB antibodies are considered to be crucial. Antibodies may promote Fc-mediated Ab-dependent cellular cytotoxic (ADCC) responses by NK cells.

A recombinant Fowl Pox Virus (FPV-) based vaccine expressing vMDV (GA) gB induced neutralizing Abs against gB and protected chickens from vvMDV challenge. Antibodies are hypothesized to play a role in immunity by cell free virus neutralization, infected cell opsonization, preventing cell-cell spread and ADCC. HPRS16 induced tumors express higher levels of HRS Ag CD30 and induction of anti-CD30 Abs in genetically resistant chickens was observed following infection.

Due to the cell-associated nature of MDV1, cytotoxic T-lymphocyte responses (CTL) are critical in immunity against MD. Lymphocytes isolated from vaccinated chickens either inhibited MDV-1 replication in chicken kidney cells or promoted apoptosis in MD lymphoblastoid cell line MSB1. Furthermore, in chickens depleted of CD8+ T cells via treatment with an antibody against CD8, challenge viral titers were much greater compared to untreated vaccinated chickens. REV-transformed chicken cell lines (RECC) expressing MDV-1 glycoprotein (gB), pp38, *meq* and ICP4 were lysed by syngenic CTLs isolated from spleens of SB1-vaccinated chickens. These findings however are questionable as SB1 lacks *meq* and in line with this, no CD8+ T cell priming occurs towards Meq-derived epitopes. The immune phenotype of CTLs was characterized as CD3+CD4-CD8+TCRαβ1.

1.5.3 Cytokine responses

Cytokines produced during innate immune stimulation play a critical role in shaping adaptive immune responses. Cytokine classes include pro-inflammatory (IL-1β, IL-6 and IL-8), Type I (IFN-α, -β, -λ) & II interferons (IFNγ), T helper 1 cytokines (IL-12p70), T helper 2 cytokines (IL-4, IL-5 and IL-13), and finally T regulatory cytokines (TGF-β and IL-10). Type I IFNs were shown to inhibit MDV replication *in vitro* and *in vivo* (132-134). Co-administration of recombinant cytokines such as cMGF or IFNγ with sub-optimal vaccine HVT reduced the tumor incidence against very virulent RB1B (135, 136). IFNγ upregulation following MDV-1 infection was observed in several studies. IFNγ treatment has an inhibitory effect on MDV replication *in vitro*. In addition, *in vivo* infection studies in susceptible and resistant lines by vMDV (GA) indicated differential IFNγ expression with resistant lines expressing early and greater levels of IFNγ compared to susceptible lines. This differential expression was however not observed in another study. Comparison of cytokine profiles in $CD30^{hi}$ versus $CD30^{lo}$ cell populations from GA/22 induced MD lymphomas indicated an increase in IFN-γ mRNA and protein levels in $CD30^{hi}$ compared to $CD30^{lo}$ populations. Exogenous expression of IFN-γ via plasmid injection led to a reduction in MD tumor incidence in HVT vaccinated and RB1B challenged chicks. On the contrary, KD of endogenous IFN-γ via rAAAV expressing shRNA did not affect tumor incidence indicating that IFN-γ is not in and of itself associated with MD resistance or immunity against MD. Furthermore, recent *in vivo* studies in our lab identified that MDV-1 infection upregulates SOCS1 negating the effects of IFNγ on IFNGR.

Apart from IFN-γ, upregulation of IL-1β, iNOS, IL-6, IL-8 and IL-18 was also observed during MDV-1 infection. Among these, IL-6 and IL-8 were found

upregulated in susceptible lines whereas IL-1β and IL-8 were found upregulated in resistant lines. In the brains of chickens infected with vv+MDV (RK-1), greater levels of IFN-γ, iNOS, IL-1β, IL-6 and IL-8 due to pro-inflammatory cytokine storm and cytokine mediated neuropathy were observed. (129, 137). Similarly, in chickens displaying transient paralysis following infection with vvMDV (RB-1B), transcriptional upregulation of IFN-γ, IL-6, IL-10 and IL-18 was observed compared to RB-1B-infected asymptomatic chickens. Along these lines, selection for excessive NO production in a commercial chicken line was found to be detrimental and increased the susceptibility to MDV-1, indicating that intermediary levels of NO are more beneficial to the host.

In RB-1B-infected chicken spleens upregulation of T_{H2} transcription factor GATA3 was observed at 14dpi. In line with this, upregulation of T_{H2} cytokines IL-4, IL-13 and IL-10 was observed during the cytolytic phase of infection. GO-term enrichment analysis of cytokines profiles in $CD30^{hi}$ versus $CD30^{lo}$ cells in lymphoma micro environment identified the dominant phenotype to be T_{H2} and T_{REG-} in $CD30^{hi}$ lymphomas. Furthermore, in spleen tissues of vMDV (GA)-infected resistant and susceptible lines, pro- T_{H1} and anti- T_{H2} profiles were identified whereas susceptible line tissue lesions displayed pro-$T_{H2/REG}$ and anti-T_{H1} profiles.

1.5.4 MD Vaccine responses

Clear underlying mechanisms of vaccine mediated immunity are still being understood. MD Vaccines do not prevent super infection, replication and horizontal transmission of field strains. Vaccines only reduce early cytolytic infection of MDV1 target cells and thus prevent subsequent tumor formation. It is presumed that, by reducing the number of infected CD4+$\alpha_V\beta_1$- TCR2 cells undergoing latency, vaccines

prevent those cells that are eligible for transformation. Attenuated serotype 1 vaccine CVI-988 is antigenically more identical to that of oncogenic MDV-1 serotype and generates maximal protective responses. On the other hand, MDV serotypes 2 (SB-1) & 3 (HVT) display similarity to MDV-1 at the level of structural (capsid, tegument and glyco-proteins) proteins and lack latently expressed MDV1-gene products. Even then, bivalent HVT/SB-1 combination confers synergistic protection against vvMDV challenge compared to either serotype administered alone.

Enhanced NK cell activity has been observed in response to MD vaccination. Enhanced IFNγ indicative of T_{H1} phenotype and CD8+ CTLs against various MDV-1 gene products upon vaccination was aforementioned. On the contrary, elevated expression of IL-4, IL-13 and IL-10 during cytolytic infection and IL-6, IL-10 and IL-18 during transformation was observed in the spleens of unvaccinated and MDV1-infected chickens indicative of polarization of immune system towards T_{H2} phenotype.

1.5.5 MD Vaccination and MDV evolution

MD vaccines were the first to successfully prevent neoplastic lymphomas. HPRS16*(att)* was the first vaccine introduced, and was generated by the serial-passaging of an acute MD-causing virus, HPRS16, in chicken kidney cells (138). HPRS16*(att)* was soon replaced by the non-oncogenic herpesvirus of turkey (HVT). HVT vaccines are available as both cell-associated, and cell-free, lyophilized vaccines. Lyophilized vaccines can be stored at $4^{o}C$, and don't require storage in liquid nitrogen. This feature of lyophilized HVT enables its usage in countries where liquid nitrogen is unavailable. However, the efficacy of cell-free HVT is reduced compared to cell-associated HVT due to neutralization by maternal antibodies (139).

Widespread adoption of HVT to control virulent MDV (vMDV) led to the emergence of very virulent MDVs (vvMDVs), RB1B and Md5, during the late 1970s (140). Bivalent vaccine (HVT/SB-1), introduced during early 1980s by supplementing HVT with the non-oncogenic MDV2 strain, SB-1, was found to confer protective synergism and induced complete protection against vvMDVs (1). The protective synergism observed with HVT/SB-1 was not dose-dependent, since a dose as low as 80 PFU of SB-1 with 2000 PFU of HVT or 80 PFU of HVT with 400 PFU of SB-1 resulted in a higher protection index than 2000 PFU of HVT or 2000 PFU of SB-1, administered singly (141).

After the introduction of bivalent vaccination, another notable increase in virulence occurred during the early 1990s, with the emergence of very virulent plus MDV (vv+MDV) (142). Upon emergence of vv+MDVs, an attenuated MDV1, CVI988 (Rispens), in use in Europe since 1973, was licensed for use in the US in 1994 (143, 144). Antigenically, CVI988 (Rispens) displays greater homology to MDV1, and is the gold standard among MD vaccines.

MD vaccines are administered either via sub-cutaneous inoculation at day 1 post-hatch, or via *in ovo* inoculation on embryonic day 18 (E18), when the eggs are transferred from the incubator to the hatcher. Inoculation *in ovo* is performed by automated, multiple-head injectors that deliver the vaccine inoculum into the amniotic fluid. Following *in ovo* inoculation, HVT replicates extensively in the embryonic lung during the first 24-72hr (145, 146). *In ovo* vaccination was found to be advantageous in terms of mass vaccination, reduced labor costs, and the accelerated development of protective immunity by several days, as well as in hastening the maturation of chicken immune system (146-150)

To further broaden the protection conferred by HVT to other avian pathogens, the concept of recombinant HVT (rHVT) was introduced during early 90s (151-153). rHVTs have been constructed to encode immunogenic antigens belonging to various other avian pathogens such as IBDV (VP2), NDV (-F or –HN), ILTV (gB, gD, gI) and IAV (HA) in the non-essential loci of HVT genome under the influence of either a strong viral or eukaryotic promoter (152, 154-158). rHVT replication in lymphoid cells allows induction of antibody and cell-mediated immune responses towards the transgene in addition to stimulating immunity to MDV1 (152). rHVTs offers several advantages compared to live vaccines, which pose the significant risk of bird-to-bird transmission, reversion to virulence, and other unwanted immune suppressive side effects (152).

In chickens, administration of CpG-ODN along with traditional vaccine regimens, was found to enhance the vaccine efficacy via an adjuvant effect. This adjuvant effect of CpG, when delivered via various routes, including *in ovo,* was demonstrated against a wide range of bacterial, viral, and protozoal infections. This was due to a proposed mechanism of T_{H1}-mediated IL-12 and IFN-γ production (159, 160). In commercial broilers, *in ovo* CpG administration via carbon nanotubes or liposomes was found to protect day old chicks (60% protection) from *E. coli* or Sal*monella typhimurium* challenge (161). Finally, other studies demonstrated CpG-ODN-mediated adjuvant effects upon MDV, IBV, and ALV-J vaccinations (162-164). Administering CpG-ODN *in ovo* along with MD vaccines is convenient and advantageous in terms of fast administration, reduced labor costs, and conferring of increased anti-viral effects in addition to those conferred by the vaccine. Furthermore,

combining CpG-ODN with a recombinant MD vaccine, such as HVT-LT, might enhance the protective ability of this moderately effective vaccine.

Despite the efforts of vaccination to reduce MD incidence, the increasing virulence of MDV-1 has been an ongoing problem. A maximum likelihood based selection analyses identified non-synonymous substitutions in the coding sequence of oncogene *meq* under positive selection (residues -77, 80, 115, 119, 139, 176, 276, 379, and 385) (dN/dS ~ 1.54) and the time of divergence of *meq* locus coincides with the widespread use of live MD vaccines (165). An attractive hypothesis is positive selection of *meq* is a means of viral adaptation to evade host innate immune defenses activated early times post vaccination.

1.6 Hypothesis of Research

MD is a lymphoproliferative disease of chickens caused by an acute-transforming alphaherpesvirus, MDV1. MD is the first neoplastic disease to be effectively controlled by vaccination. MD vaccines presumably elicit continual anti-viral cytotoxic T-cell and antibody responses towards shared epitopes, via a low-level of replication, a limited establishment of latency, and periodic reactivation. Cytotoxic T-cells (CTLs) and macrophages have been implicated in protective immune responses. While antibodies limit virus replication of MDVs *in vivo*, antibodies are not protective in and of themselves. MD lymphomagenesis involves the proliferation and transformation of latently-infected CD4+ T cells into a T_{H2}/T_{REG} immunophenotype, resulting in profound immune suppression and visceral lymphoma formation. In contrast MD vaccines induce pro-T_{H1} and CD8+ CTL responses. Polarization towards a T_{H1} phenotype during vaccination and towards a T_{H2}/T_{REG} phenotype in lymphoma progression appears to occur within a few days post-vaccination, suggesting that

signal integration during innate immune activation plays a crucial role in subsequent adaptive immune polarization.

In addition, innate immune signaling appear to block the ability of pathogenic MDV1 to shift the patterning of latently-infected T-cells to become malignantly-transformed regulatory T-cells (T_{REG}). Accordingly, the hypothesis addressed by the current work include

1) Early Type I IFN induction and IFN signaling with in the first few days post *in ovo* vaccination is vital to polarize the immune system towards pro-T_{H1} and CD8+ CTL response
2) Systemic T_{H1} patterning observed during MD vaccine-mediated protection is conferred by exosomes secreted by antigen presenting cells, that are present in the serum of protected chickens.
3) Conversely, TEXs secreted in the serum of tumor-bearing birds, or in the supernatant medium of MD-transformed cell lines are immune suppressive and will interfere with innate patterning elicited during the establishment of vaccine-mediated protection.

1.7 Specific Objectives

To address the above hypotheses, we have developed the following objectives:

1. To identify signal integration events post *in ovo* vaccination using individual monovalent vaccine strains, HVT and SB-1, and the bivalent HVT/SB-1, via targeted gene expression analyses using a panel of primers based on classes of innate, acquired, and immune-patterning genes.

2. To identify the proteomic and transcriptomic profiles of serum exosomes from vaccinated and protected chickens to identify exosomal signatures common to protection.
3. To identify the proteomic and transcriptomic profiles of serum exosomes from tumor-bearing birds and MD lymphoblastoid cell line supernatants to identify exosomal signatures associated with immune suppression and lymphomagenesis.

Chapter 2

INNATE IMMUNE RESPONSES TO BIVALENT HVT/SB-1 *IN OVO* VACCINATION AND MECHANISTIC BASIS OF BIVALENT HVT/SB-1 SYNERGISM

Currently used bivalent vaccine in US is composed of viruses (FC126 and SB1) that lack the *meq* oncogene encoded by MDV-1 serotypes. Hence in an ideal case scenario, one would presume no CD4+ or CD8+T cell priming against the MHC associated antigenic peptides derived from *meq* which plays a major role in the switch from lytic replication to latency and also MDV1 mediated lymphomagenesis. In contrast to this, CD8+TCRαβ1 CTLs from SB-1 vaccinated chickens were demonstrated to lyse REV transformed cell lines expressing ICP4, ICP22, *meq* and gB at lower levels (105). However, the amount of specific lysis has never been confirmed at the protein level arguing against the relevance of findings pointing to *meq*-epitope specific lysis.

Vaccines must be able to present shared T cell epitopes (presumably structural glycoproteins, capsid and tegument proteins) with the pathogen in order to elicit a primary immune response. In the case of MDV-1, transformed T cells arise from the latently infected CD4+ T cells and none of the latency associated genes are encoded by either HVT or SB1 (*meq*, splice variants of *meq*, *vTR*, USP) yet they block tumor formation (105). In addition, shared viral structural proteins such as gB, gC and gE are

expressed only during lytic replication but not in a transformed cell. Hence their involvement in anti-tumor response can be precluded. Apart from structural antigens, commonly upregulated lymphoproliferative tumor surface antigens such as MATSA were found unlikely targets in an *in vitro* cytotoxicity assay (166). The exact mechanism of bivalent vaccine mediated immunity, anti-viral/anti-tumor is still unknown.

Our main hypothesis is that the innate sensing during the earlier times post vaccination provides non-specific protection by production of Type I IFNs and IFN-stimulated genes (ISGs) to limit lytic replication of pathogenic MDV1. Type I IFNs promote lifelong protection by induction of strong Th1 polarization mediated CD8+ cytotoxic T cell responses. By limiting the initial cytolytic replication or the number of infected CD4+ target T cells, the number of cells undergoing latency are alleviated. Thus, the number of cells eligible for transformation is completely abolished.

For testing our hypothesis, we first examined the gene expression patterns of a panel of selected innate and acquired immune genes mentioned in Table 1.1 at various time points in an attempt to establish timing of innate sensing and Type I IFN induction, in the spleens of chickens *in ovo* vaccinated with bivalent HVT/SB-1. In addition to investigating the induction of bivalent vaccine mediated non-specific and specific responses *in vivo* we also studied the mechanisms of synergistic protection conferred by bivalent vaccine components *in vitro*, in an orthogonal spleen cell infection model described in detail much later.

2.1 Materials and Methods

2.1.1 Isolator Study I

2.1.1.1 Experimental Design

90 fertile commercial broiler eggs (Hubbard x Cobb) obtained from Allen family foods Inc. Seaford DE, were divided into 3 groups of 30 each, on embryonic day 18 (ED18) of incubation. The first group were assigned controls and left unvaccinated. The second group received 1:10 dilution of bivalent HVT/SB-1 (500PFU/250PFU) via *in ovo* route while the third group received 1X commercial dose of bivalent HVT/SB-1 (5000PFU/2500PFU) via *in ovo* route. *In ovo* immunization was carried out manually by briefly puncturing the shell at the broad end of the egg using a sterile 18 guage needle. The vaccine was precisely delivered into the embryo by inserting a full length 22 guage, 2.5 cm long needle attached to a tuberculin syringe into the punctured hole made at the broad end until it reached the embryo. Post *in ovo* immunization, embryonated eggs were wax sealed and incubated separately in hatching trays according to the treatment. Post hatch, chickens were wing banded and housed separately according to the treatment in BSL-2 isolation units located in the Allen laboratory at the University of Delaware with feed and water provided *ad* libitum.

2.1.1.2 Sample collection

On day 3, 7 and 14 time points post hatch, chickens from each treatment (n=10 per time point) were removed from the isolators in the following sequence; 1. Unvaccinated, 2.1:10 dilution dose vaccinated, 3.1X commercial dose vaccinated. Chickens were humanely euthanized by cervical dislocation for the purpose of

collecting spleen and right lung. Post collection, organs were immediately placed in RNA *later* (Ambion Inc.) and preserved at 4^0C overnight before transferring the tissues to -80^0C.

2.1.1.3 Sample preparation

For the purpose of preliminary pilot experiment, we processed tissues, both spleen and lung isolated from 4 randomly selected birds per treatment from each time point. Total RNA was extracted from 30mg of tissue using an AllPrep DNA/RNA/Protein Mini Kit (Qiagen, USA) according to the manufacturer's instructions. Sample quantity and quality (260:280nm ratio) was measured and confirmed using Nanodrop 1000 Spectrophotometer (Thermo Scientific, Waltham, MA) and Agilent Bioanalyzer. Reverse transcription was performed in 20µl reactions using 1µg of total RNA and random hexamers from a High Capacity cDNA Reverse Transcription Kit (Applied Biosystems, USA). Reverse transcription was carried out in the following four steps: Step 1: 25°C for 10 min; Step 2: 37°C for 120 min; Step 3: 85°C for 5 min; Step 4: 4°C until samples are removed. Final amount of cDNA was diluted 10-fold in nuclease free water for the purpose of gene expression analysis.

2.1.1.4 qRT-PCR and gene expression analyses

Quantitative real time PCR was carried in a 20µl reaction mixture consisting of 10 µl iQ™ SYBR® Green Supermix (Bio-Rad, Hercules, CA), 8.2µl of nuclease free H2O, 1 µl of final cDNA, and 0.4 µl each of forward and reverse primers in a Bio-Rad iCycler MyiQ5 PCR Thermal Cycler. The following cycle times were used: Initial denaturation step at 95°C for 3 minutes followed by 40 cycles of two-step real time detection of SYBR green products (Step 1: 95°C for 10 seconds; Step 2: 58°C for 30

seconds). Following amplification, melt curve analysis was performed in the following steps: Step 1: 95°C for 1 minute; Step 2: 55°C for 1 minute; Step 3: 81 cycles of increasing temperatures from 55°C to 95°C at 10 second, 0.5°C intervals per cycle. Melt curves were examined to exclude any possibility of non-specific amplification such as primer dimers or genomic DNA contamination.

2.1.1.5 Primer Design

Gallus gallus sequences for the selected target genes were obtained from ensemble genome browser (http://www.ensembl.org/index.html). Quantitative real-time PCR primers listed in Appendix A were designed in the exon sequences flanking the intronic regions using Integrated DNA Technologies PrimerQuest (SM) (http://www.idtdna.com/Primerquest/Home/Index) program. Primers were designed in a manner such that the amplicon sizes fell between 90-150 bp and melting temperatures within 58-60^{0}C.

2.1.1.6 Two step testing and Data analysis:

Due to increased sample size (33 genes x 3 time points x 2 treatments x 8 samples per treatment), we adopted and tested a two-step strategy in order to identify differentially expressed genes between treatments at different time points. In the first step, samples from each treatment, on each time point were pooled at the cDNA level. For the purpose of cDNA pooling, equal amounts of cDNA were used. Selected genes were first analyzed on pools and normalized to the geometric mean (GM) of three endogenous reference genes (β-actin, G6PDH, Ubiquitin). In the second step, the differentially expressed genes showing relative expression greater than 2 fold in the

first step were selected and validated with individual samples in each treatment from each time point.

Threshold crossing point (Ct) value outputs given by the Biorad iQ5 optical system software (version 2) were input in REST® 2009 program (Qiagen Inc) (53). REST program calculates the relative expression ratios on the basis of PCR efficiency (E) and crossing point deviation (ΔCt) value between target gene and the GM of selected endogenous reference genes. The differences in expression between control and treated samples were assessed in group means for statistical significance by pair wise fixed reallocation randomisation test. In our study, the PCR efficiency values were calculated using LinReg PCR 11.0 program by inputting the raw fluorescence data outputs for all the samples and genes analyzed in the study (54). PCR efficiency was found to be ≥1.98 among all the samples indicating highly efficient reverse transcription and qPCR reaction and a lack of PCR inhibition factors. Hence an E value of 1 was inputted in REST for data analysis. Statistical significance is represented at $p < 0.05$ level.

2.1.2 *In vitro* spleen cell infection study

2.1.2.1 Cell culture and viruses employed

Spleen cell homogenates were prepared from spleens isolated from 9wk old SPF leg horns raised in BSL-2 isolation units. Briefly, spleens from each bird (n=6) were homogenized separately in glass tenbroeck tissue grinders containing incomplete M199 media (HyClone, GE Healthcare). Spleen cell homogenates from each bird were seeded longitudinally in six 24 well dishes, one for each time point and grown in modified Iscove's Dulbecco medium (IDM) supplemented with 20% fetal bovine

serum (Atlanta Biologicals), 10% chicken Serum (Life Technologies, [LT]), 10% tryptose phosphate broth (TPB), 1X Insulin/Transferrin/Selenium (ITS, LT), 1X Non-essential amino acides (NEAA, LT), 4 mM L-glutamine (LT), 2 mM sodium pyruvate (LT), 2 μm 2-mercaptoethanol (LT), 1X PSN antibiotics (LT) and 1X fungizone (LT). All the dishes were left at 410C in 5% CO2 humidified chamber. Treatments were performed in an orthogonal manner such that splenocytes from each bird received diluent only control, Monovalent HVT (5000PFU), SB1 only (2500PFU) and bivalent HVT/SB1 combination. Treatment dishes were harvested at respective time points (2, 6, 24, 48, 72 and 96 hrs) post vaccine treatments upon careful removal of supernatants containing non-adherent cells and direct addition of RLT lysis buffer (Qiagen Inc.). Bottom of the dishes were mechanically streaked using a pipette to ensure successful harvesting of adherent mono layers. Non-adherent fractions in supernatants were pelleted by centrifugation and the supernatants were stored at -80oC for cytokine characterization. Non adherent pellet fractions are combined with adherent cell lysates. Sample RNA/DNA/Protein isolation, reverse transcription and qRT-PCR analysis was performed exactly as described in sub-sub-sections 2.1.1.3 and 2.1.1.4. All target genes were normalized to reference gene GAPDH using comparative ΔΔCt method by REST software.

2.2 Results

2.2.1 Differential expression of spleens and lungs of Isolator Study I treatments

In the first step of our two step testing strategy, we identified differentially expressed (DE) genes (Relative expression ratio > 2 fold) that were common to both spleen and lung on Day 3 and Day 14 post hatch. These included Type I IFN

responsive genes (MX1, RSAD2, OASL), IFN-γ, MDA5/IFIH1 and TAP1 (Table 2.2). Only DE gene unique to spleen was IL-10, while in the lung the same had exceedingly higher Ct value (>35 cycles) above the detection limit in some samples while in the others it was undetected (N/A or Ct>40 cycles). DE genes found unique to lung include SOCS1, IL-4, IL-18, CD38, MARCO and STAT1. Relative expression ratios of selected genes among the pooled cDNA samples from spleen and lung at various times post hatch were included in Table 2.2.

We extended these findings and confirmed them on individual samples from respective organ tissues in the second step. Expression patterns from the individual spleen samples well correlated with what we have initially observed in the pooled samples. There was a significant induction of Type I IFN responsive genes (MX1, OASL, RSAD2) on day 3 post hatch whereas on day 14 post hatch, although there was a significant induction, the levels observed were substantially lower than that of day 3 (Table 2.3). The levels of IL-10 mRNA significantly peaked on Day 14. In addition, there was a significant up-regulation of MDA5/IFIH1 on day 3 post hatch. We have also analyzed two additional genes, EIF2AK and TLR2, since their relative expression ratios were close to 2 among the pools on day 3 post hatch. However, while there was no significant change associated with EIFAK2, TLR2 was significantly down-regulated on day 7 post hatch.

Among the lung profiles, the expression patterns of Type I IFN responsive genes (MX1, RSAD2, OASL) well correlated with what we have observed in the pooled samples except that RSAD2 was not statistically significant on Day 3 (*p value* ~ 0.103) despite 2.1-fold increase in expression (Table 2.4). Finally, there was a significant induction of TAP1 on day 14 post hatch. No significant changes were

observed among the remaining genes identified in our pooled samples. Although there was greater than 2-fold induction of IL-18, STAT1 and MARCO on day 7 the results were not statistically significant (Table 2.4).

Since early induction of Type I IFN responsive genes (MX1, RSAD2, OASL) was observed in full dose bivalent HVT/SB-1 vaccinated spleens, we investigated the timing of induction of above genes in the spleens obtained from chicks that are *in ovo* vaccinated with one tenth dilution of bivalent HVT/SB-1. Whereas there was a slight induction of MX1 during the earlier time point (D3 post-hatch), there was a significant induction of OASL. In addition, MX1 expression levels peaked much later in a delayed manner compared to full dose *in ovo* vaccinated spleens (Table 2.5).

2.2.2 Mechanistic basis of synergism observed upon bivalent HVT/SB-1 vaccination *in vitro* in a spleen cell infection model

Upon investigating relative gene expression profiles of target genes including TLR3, MyD88, IFN-α, IFN-γ, Type I IFN responsive genes (MX1, OAS), pro-inflammatory markers (IL-1β, IL-18, iNOS, LITAF, IFN-γ), anti-inflammatory cytokine IL-10 and T cell patterning molecules (T-bet, GATA3), no significant induction of target genes was observed at 6, 24 and 48hrs post vaccine treatment. However, by 72hour post treatment, which corresponds to the day of hatch, a significant induction of greater than 2-fold was observed among some of above mentioned target genes (Figure 2.4). These include pattern recognition receptor TLR3 which upon sensing viral dsRNA perturbates in the induction of Type I interferons (IFN-β and α). Type I interferons released into the supernatants act via Type I interferon receptors to induce ISGs (MX1, OAS) via STATs conferring anti-viral state

among infected and surrounding cells. Consistently, significant induction of ISGs (MX1, OAS) was observed.

Additionally, induction of pro-inflammatory markers IL-1β, iNOS and IFN-γ were also observed. Activated NK cells which upon recognition of missing self on the surface of infected cells (MHC I down regulation) release IFN- γ. IFN- γ upon release acts on macrophages to enhance its phagocytic function leading to induction of iNOS and pro-inflammatory cytokine production (IL-1β) as seen in our results. However, no induction of T cell patterning molecules (Tbet, GATA3) was observed. Induction of acquired immune patterning molecules may occur presumably at much later time point upon action of released IFN-γ on activated CD4+ T helper cells.

In terms of vaccine treatments, SB-1-induced additive effect in terms of ISG induction and IFN-γ in bivalent vaccine treatments compared to monovalent HVT-only or SB-1 only treatments. This earlier induction might confer non-specific protection against challenge. Since the spleen cell infection model mimics an *in vitro* setting of fully functional immune system, our results might be closer to what happens upon vaccination in older chickens with fully developed immune system. In addition, this model, provides an opportunity to study single bird responses to different vaccines or virulent viruses in a longitudinal manner with an added advantage of multiple sampling from a single bird. This model can also be applied to study the responses to different vaccines or vaccine + challenge on a variety of genetic backgrounds (resistant vs susceptible) which precludes bird to bird variation or the requirement for large scale bird experiments which incur significant costs and labor.

2.3 Discussion

In the spleen, differential upregulation *(fold change >2, p <0.05)* of Type I IFN responsive genes MX1, RSAD2, OASL was observed on day 3. Significant up-regulation of type I interferon responsive genes on day 3 indicates potential replication of vaccine virus which upon recognition by innate immune sensors lead to a strong induction of Type I interferons (IFN-α/β) at an earlier time point. Type I IFNs produced act in an autocrine or paracrine manner on surrounding cells or tissue to induce downstream JAK-STAT signaling leading to transactivation of interferon stimulated responsive elements (ISREs). This enhanced induction of Type I interferons and their responsive elements collectively induce an anti-viral state limiting cytolytic infection and replication upon early exposure of MDV1 on the day of hatch.

Microarray analysis of splenic responses in susceptible (7_2) lines infected with RB1B at 2 weeks post hatch found significant upregulation of Type I IFN responsive MX1, RSAD2, OASL on Day 3 and 4 post infection (167). In the same study, differential upregulation of MX1 was observed in resistant (6_1) lines compared to susceptible lines on Day 2, 3 and 4 post infection, exactly during the cytolytic phase of infection. Induction of pattern recognition receptor MDA5/IFIH1 on day 3 post hatch also indicates early sensing and signaling of replicating vaccine virus in our study. As chickens lack RIG-1, MDA5 functions as a dominant sensor of uncapped viral RNA during viral replication.

Abdul-Careem *et al* have demonstrated HVT replication via significant induction of gB transcripts on Day 2, 4 and 7 post hatch upon embryonic immunization with HVT in SPF chickens (168). In our case, we performed embryonic immunization with bivalent HVT/SB-1 in commercial broiler chickens with the

sampling time points being Day 3, Day 7 and Day 14 post embryonic immunization. In addition, there was a significant upregulation of interleukin 10 on day 7 and 14, cytokine which is secreted by many immune cells (APCs, T helper type 1 (Th1) and regulatory T cells) and was known to play dual biological role (immune stimulatory and immune regulatory)(169). Although there was an observed induction of IL-10 on day 3 similar to Day 7, it was not significant (*p value ~ 0.2*). The splenic up-regulation of IL-10 along with IFN-γ was also observed in other studies during earlier cytolytic phase upon embryonic immunization with monovalent HVT and/or very virulent RB1B MDV (170, 171). In other studies, this earlier induction followed an increasing trend during later time points of infection or vaccination consistent with what we have observed in our study. Although other studies have suggested an immune suppressive role of IL-10, earlier induction of IL-10 possibly plays a dual biological role (169) during MDV vaccination or infection. IL-10 is a potent stimulator of NK cells and enhances proliferation (172), cytotoxic function (173, 174) and IFN-γ production (175, 176) by NK cells *in vitro. In vivo* in an acute MCMV infection model, blockade of IL-10R markedly reduced the number of activated NK cells in spleen and lung with a concurrent increase in viral DNA load (177). In addition to decreased NK cell responsiveness there was an increased apoptosis of activated NK cells suggesting IL-10 contributes to antiviral innate immunity during acute infection by restricting activation-induced death in NK cells. Along with immune-stimulatory role, IL-10 also plays an immune modulatory role by suppressing pro-inflammatory cytokine production, APC maturation, co-stimulatory molecule expression and T-regulatory cell development in an effort to limit pro-inflammatory damage. NK cells play an important role in mediating earlier protection against cytolytic MDV1 infection and

this earlier induction of IL-10 might play a role in mediating functional activation of NK cells while the induction of IL-10 on day 14 may have more of a suppressive role.

Since we observed the induction of early interferon responsiveness as one of the important mechanisms of bivalent vaccine mediated protection, we extended these findings from full dose vaccinated chickens to one tenth dose vaccinated chickens. Dilution of MD vaccines is a common practice, especially in the commercial broiler operations among developing nations in an effort to reduce the cost of vaccination per chicken. In addition to vaccine dilution, factors such as storage conditions (liquid nitrogen storage), improper handling, improper vaccine reconstitution and delays in vaccine administration post reconstitution also lead to vaccine failures. Other factors such as mixing MD vaccines with antibiotics (178, 179) and joint administration with other vaccines (180, 181) can also significantly reduce MD vaccine titers and efficacy. As a general guideline, the minimum recommended dose of vaccine administration is 2000 PFU of HVT, 1000PFU each of SB1 and CVI988. To confer long term protection among broiler breeders and layers, a minimum titer of 5000 PFU/dose for HVT and 3000 PFU/dose for SB1 or CVI988 (Rispens) were recommended respectively. Commercial vaccine manufacturers normally recommend a much greater and higher dose than minimum protective doses (182).

Standard reference dose for commercial MD vaccines in US must be at least 1000PFU (182, 183). One study by Gimeno *et al* (2011) has demonstrated the effects of diluting monovalent HVT (1:10) and bivalent HVT/SB-1 (1:10/1:5) upon challenge with vvMDV1 MD5 and/or vv+ MDV 648A in commercial meat type chickens. Dilution of vaccines was found to have detrimental effect upon MDV challenge with increased MD incidence and mortality upon vv+ 648A challenge among treatments

receiving diluted vaccines compared to full dose vaccinated chickens. In addition, a profound decrease in relative body weights by 8 weeks was found among survivor groups that received diluted vaccines (HVT or HVT/SB-1) and vv MD5 or vv+ 648A challenge. With respect to titers, lower vaccine titers were found during first 1-week post hatch with a corresponding increase in MDV loads. This early increase in MD loads correlated with increased MD incidence and mortality observed by 8 weeks upon broilers reaching their production age of maturity.

In in the current study, in contrast to responses in full dose vaccinated chickens, chickens that received 1:10 dilution of bivalent HVT/SB-1 displayed delayed or significantly lower induction of interferon responsive genes (MX1 and RSAD2) while the induction of OASL remained significantly higher on day 3 post hatch (see Table 2.5). More importantly, there was a significant down-regulation of IFN-γ on day 3 and 14 post hatch, a possible immune suppressive effect of vaccine dilution. This reduced Type I interferon responsiveness complemented with lack of IFN-γ indicate an insufficient replication of vaccine virus and detrimental effects caused by the vaccine dilution upon MDV1 challenge.

In the lung, significant up-regulation of type I interferon-inducible genes on day 3 (MX1, OASL, RSAD2) suggests that these interferon responses might be important for mediating early protection against invasion of MDV1, whose main route of infection is via inhalation. The significant up-regulation of TAP1 on day 14 is in consensus with the MHC-I processing of antigens and patterning of adaptive immune responses (CD8+ CTL) by that time.

Although induction of IL-18 ($p \sim 0.057$), STAT1 ($p \sim 0.087$) and Macrophage receptor with collagenous structure (MARCO) ($p \sim 0.109$) among individual samples

on day 7 corresponded to pooled samples during respective time points the results weren't significant. IL-18 is a pro-inflammatory cytokine associated with Th1 differentiation and STAT1 is a Type I/II interferon signal transducer. Induction of MARCO on day 7 indicates some level of innate sensing by lung epithelium or APCs recruited to lung. MARCO, is class A scavenger receptor expressed on macrophages and dendritic cells. It was associated with "classical" macrophage activation and IL-12 production, whose expression was enhanced *in vitro* upon treatment of macrophage cell lines with Th1 adjuvants (184). Macrophage type-I and type-II class-A scavenger receptor (MSR-A) knockout mice are more susceptible to Listeria monocytogenes or herpes simplex virus 1(HSV1) (185). However, it was recently determined that MARCO scavenger receptor is exploited by HSV1 to mediate adsorption onto human keratinocytes and gain entry into the cell. It was suggested that, by this mechanism, HSV1 evades cell surface innate immune recognition by TLR2 while gaining viral entry into the cell (186). In addition to heparin sulfate proteoglycans (HSPGs), HSV-1 gC bound to MARCO with a higher affinity than HSPGs causing receptor mediated endocytosis and co-localized along with MARCO onto the cell surface upon replication. MARCO plays an important role in innate sensing by recognizing wide variety of ligands (TLR/NLR/RLR ligands, apoptotic cells) and was known to differentially regulate cell surface TLR activation while enhancing endosomal TLR or cytosolic NLR activation by increasing the ligand availability by internalization. Among the remaining genes identified in pools, IFN-γ and IL-4 couldn't be validated on individual samples due to higher Ct values greater than 35 while the Ct values in our pooled samples were ~31 cycles for both the genes. The induction of SOCS1 at

all the time points examined among the pools was purely false positives as they did not correlate upon validation with individual samples.

Finally, based on our study, significant induction of Type I IFN responsive genes (MX1, RSAD2 and OASL) upon vaccination against MDV1 on Day 5 post *in ovo* vaccination or Day 3 post hatch, a time point when replication of vaccine viruses peak, can serve as an index for monitoring successful *in ovo* vaccination. Additionally, MX1, RSAD2 and OASL can serve as biomarkers for successful vaccination along with reduced challenge viral titers as assessed by qPCR. MX1, RSAD2 and OASL may mediate protection by inhibiting the replication of challenge virus in the target cell during early cytolytic phase resulting in reduced viremia levels. On the other hand, Type I IFN responsive gene induction was also demonstrated upon challenge with vvMDV RB-1b. The differences associated with their timing and magnitude of induction with vaccine versus challenge viruses deserve further attention. Furthermore, bivalent HVT/SB-1 signaling synergism occurs at the level of both Type I & II IFN induction and pro-inflammatory cytokine production as observed in the *in vitro* spleen cell infection study as early as 72hr post vaccination corresponding to the day of hatch. The two step testing strategy followed in the current study can be successfully applied to screen differentially expressed genes under the conditions where there is an increased sample or treatment size with a necessity to analyze numerous genes using qRT-PCR. One limitation found associated with this strategy was a lack of correlation among the pooled and individual treatments in the first and second step respectively, for the genes expressed with a higher Ct value (~30).

Table 2.1: Selected genes and their functional names

Accession no.	Gene	Functional name	Function
AB088533.1	MX1	Myxovirus resistance 1	Type I/III ISG
EU427332.1	RSAD2	Radical-S adenosyl domain 2	Type I/II/III ISG
AB002585.13	OASL	2'-5' oligoadenylate synthetase like gene	Type I/III ISG
AJ621254.1	IL-10	Interleukin 10	Treg cytokine
NM_205149.1	IFN-γ	Interferon gamma	Th1 cytokine
NM_001193638.1	MDA5	Interferon inducible helicase 1	dsRNA sensor
NM_001135968.1	TAP1	Transporter of antigenic peptide	MHC I processing
NM_001031323.1	EIF2AK	Eukaryotic initiation factor 2 alpha kinase (PKR)	Translation
NM_001161650.1	TLR2	Toll like receptor 2	Di/triacylated lipopeptide sensor
NM_205427.1	IFN-α	Interferon alpha	Type I interferon
NM_205420.1	GATA6	GATA Transcription factor 6	Immune cell differentiation
XM_004948616.1	LGP2	DEXH box polypeptide 58	MDA5 regulator
NM_001137648.1	SOCS1	Suppressor of cytokine signaling 1	M2 patterning
NM_205372.1	IRF7	Interferon regulatory factor 7	Type I IFN inducer
NM_001030962.1	MyD88	Myeloid differentiation 88 adapter	TLR4/7/8/21 Adapter
NM_204305.1	G6PDH	Glyceraldehyde-6-phospate dehydrogenase	Reference control
NM_001007079.1	IL-4	Interleukin 4	Th2 cytokine
XM_001231236.3	PLSCR1	Phospholipid scramblase 1	Type I/II/III ISG
XM_416333.4	PARP12	Poly ADP ribose polymerase	Type I/II/III ISG
NM_00120	CD38	Pan leukocyte marker	Leucocyte surface

1388.1			marker
NM_204524.1	IL-1β	Interleukin 1beta	pro-inflammatory cytokine
NM_001097537.1	TNFRSF13B (TACI)	transmembrane activator, calcium modulator, and cyclophilin ligand interactor	
U57603.1	UB	Polyubiquitin	Reference control
NM_001007824.1	β-ACTIN	Beta actin	Reference control
NM_204608.1	IL-18	Interleukin 18	Th1 cytokine
NM_204961.1	INOS	Inducible Nitric oxide synthetase enzyme	pro-inflammatory enzyme
NM_001011688.2	TLR7	Toll like receptor 7	Endosomal ssRNA sensor
NM_204736.1	MARCO	Macrophage receptor with collagenous structure	Classical M1 type
NM_001012914.1	STAT1	Type I/II/III interferon signaling	Signal tranducer

Table 2.2: Heat map summary of targeted gene differential expression at various time points post hatch (Day 3, Day 7, Day 14) in spleen and right lung cDNA pools of chickens *in ovo* vaccinated with bivalent HVT/SB1. Data are represented as relative expression ratios (fold changes) obtained upon comparing cDNA pools from full dose bivalent HVT/SB-1 vaccinated to unvaccinated treatments.

	Pooled spleen profiles			*Pooled lung profiles*		
Gene Symbol	**Day 3**	**Day 7**	**Day 14**	**Day 3**	**Day 7**	**Day 14**
MX1	25.63	0.93	2.99	8.75	5.03	12.75
RSAD2	12.92	1.67	2.20	3.74	1.24	3.57
OASL	9.56	0.57	1.51	6.50	1.15	3.19
IL-10	2.83	2.07	23.40	Ct > 35	Ct > 35	Ct > 35
IFN-γ	2.81	0.71	2.22	0.93	3.38	6.35
IFIH1	2.25	0.98	1.51	1.29	2.04	2.21
TAP1	2.23	1.50	1.28	1.92	1.78	2.78
EIF2AK	2.00	0.93	1.67	1.82	1.22	1.56
TLR2	1.93	0.59	0.25	0.87	0.45	0.51
IFN-α	1.87	0.98	1.14	1.66	1.10	1.98
GATA6	1.78	0.82	0.82	1.13	1.21	1.28
DHX58	1.66	1.17	0.71	0.51	0.55	0.95
SOCS1	1.36	1.26	1.49	3.63	2.07	3.21
IRF 7	1.33	1.30	1.14	1.66	1.24	1.77
MyD88	1.25	1.08	1.11	1.72	0.81	1.31
G6PDH	1.23	1.35	0.82	0.54	1.43	1.49
IL-4	1.21	1.43	1.44	5.52	15.47	4.20
PLSCR1	1.20	1.09	1.26	1.19	1.02	1.31
PARP12	1.17	1.03	1.56	1.74	0.82	1.92
CD38	1.13	1.38	1.70	1.19	0.63	2.11
IL-1β	1.12	0.72	0.76	1.27	1.89	1.04
TNFRSF13B	1.03	1.86	1.02	Ct > 35	Ct > 35	Ct > 35
UB	1.01	1.04	1.10	1.07	1.08	1.31
β actin	0.88	0.78	1.06	1.51	0.85	0.62
IL-18	0.83	1.96	1.24	0.96	2.89	1.75
INOS	0.82	1.18	1.18	1.41	0.97	1.54
TLR7	0.80	1.21	1.13	1.20	0.75	1.21
MARCO	0.73	0.65	0.97	1.05	2.62	1.75
STAT1	0.73	1.36	1.38	1.61	2.39	3.06

DE ≥ 2 fold	
2 > DE > 1.5 fold	
1.5 > DE > 1 fold	
1 > DE > 0.5 fold	
DE ≤ 0.5	

Table 2.3: Heat map summary of differential expression (DE) among the individual spleen cDNA samples at various time points post hatch. Data are represented as relative expression ratios (fold changes) obtained upon comparing full dose bivalent HVT/SB-1 vaccinated spleens (n=4) to unvaccinated spleens (n=4). Asterisk* denotes statistical significance at *p<0.05 level*.

Gene	Day3	Day7	Day14
MX1	12.5*	0.8	2.4*
RSAD2	8.4*	1.0	0.9*
OASL	9.3*	0.4	2.1*
IL-10	2.5	2.9	9.1*
IFN-γ	1.7	0.5	1.2
IFIH1	2.2*	0.5	1.1*
EIF2AK	1.47	0.405	1.2
TLR2	0.548	0.37*	0.856

DE ≥ 2 fold p<0.05	
DE ~ 2 fold	
DE ~ 1 fold	
DE ~ 0.5	
DE ≤ 0.5 p<0.05	

Table 2.4: Heat map summary of differential expression (DE) among the individual lung cDNA samples at various time points post hatch. Data are represented as relative expression ratios (fold changes) obtained upon comparing full dose bivalent HVT/SB-1 vaccinated spleens (n=4) to unvaccinated spleens (n=4). Asterisk* denotes statistical significance at *p<0.05 level*.

GENE	DAY 3	DAY 7	DAY 14
MX1	8.04*	3.3*	4.56*
TAP1	0.98	1.56	2.71*
OASL	10.38*	0.68	2.65*
RSAD2	2.1	1.3	2.4*
CD38	1.5	0.74	2
MARCO	0.52	2.68	1.87
SOCS1	0.76	1.72	1.68
STAT1	0.82	2.5	1.68
IL-18	1.04	2.28	1.14
IFIH1	1.24	1.02	0.95
IFN-γ	Ct > 35	Ct > 35	Ct > 35
IL-4	Ct > 35	Ct > 35	Ct > 35

DE ≥ 2 fold p<0.05	
DE ~ 2 fold	
DE ~ 1 fold	
DE ~ 0.5	
DE ≤ 0.5 p<0.05	

Table 2.5: Heat map summary of differential expression (DE) among the individual spleen cDNA samples at various time points post hatch. Data are represented as relative expression ratios (fold changes) obtained upon comparing 1:10 dilution dose bivalent HVT/SB-1 vaccinated spleens (n=4) to unvaccinated spleens (n=4). Asterisk* denotes statistical significance at *p<0.05 level.*

GENE	DAY3	DAY7	DAY14
MX1	2.40	6.14	5.7*
OASL	12.1*	1.60	3.80
IFN-γ	0.07*	0.80	0.32*
IFIH1	1.67	1.06	1.57
RSAD2	0.325*	0.41	1.18

DE ≥ 2 fold p<0.05	
DE ~ 2 fold	
DE ~ 1 fold	
DE ~ 0.5	
DE ≤ 0.5 p<0.05	

Figure 2.1: Differential expression *(fold change>2, p<0.05)* of immune signaling genes at 6hpt in an *in vitro* spleen cell infection model. The bar graph shows the fold change (Y-axis) associated with various immune signaling molecules (X-axis). Vaccine treatments are color coded as shown on right, HVT (green), SB1 (red) and HVT-SB1(blue). Asterisks mark *p<0.05*.

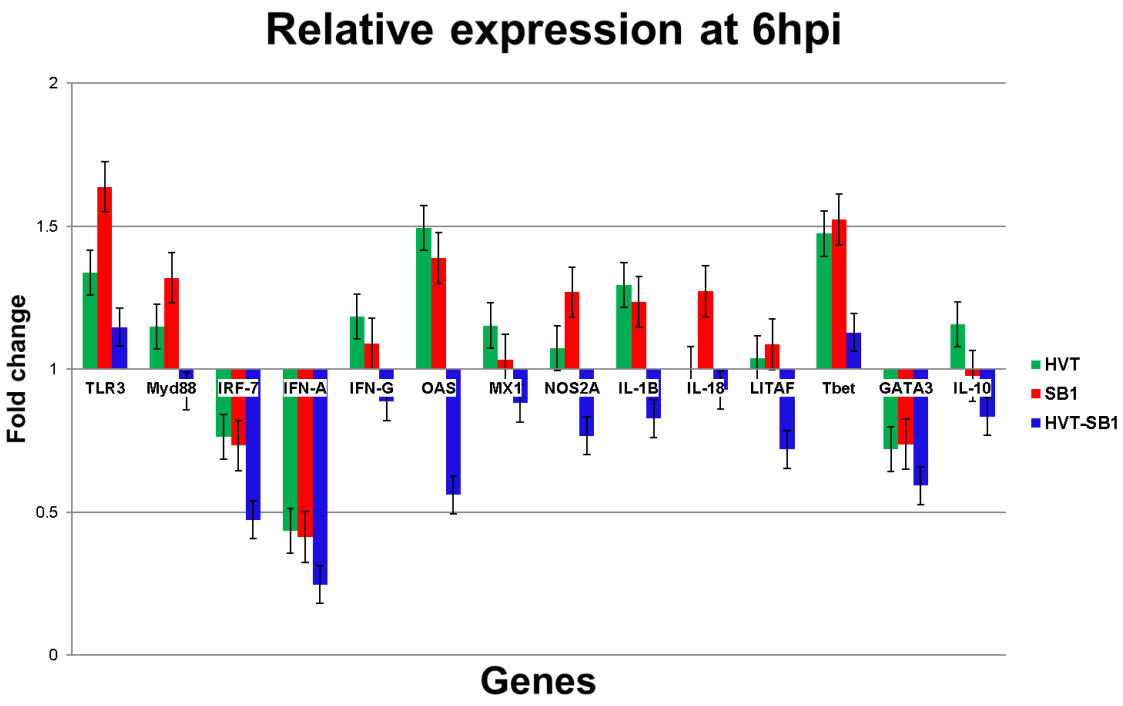

Figure 2.2: Differential expression *(fold change>2, p<0.05)* of immune signaling genes at 24hpt in an *in vitro* spleen cell infection model. The bar graph shows the fold change (Y-axis) associated with various immune signaling molecules (X-axis). Vaccine treatments are color coded as shown on right, HVT (green), SB1 (red) and HVT-SB1(blue). Asterisks mark *p<0.05*.

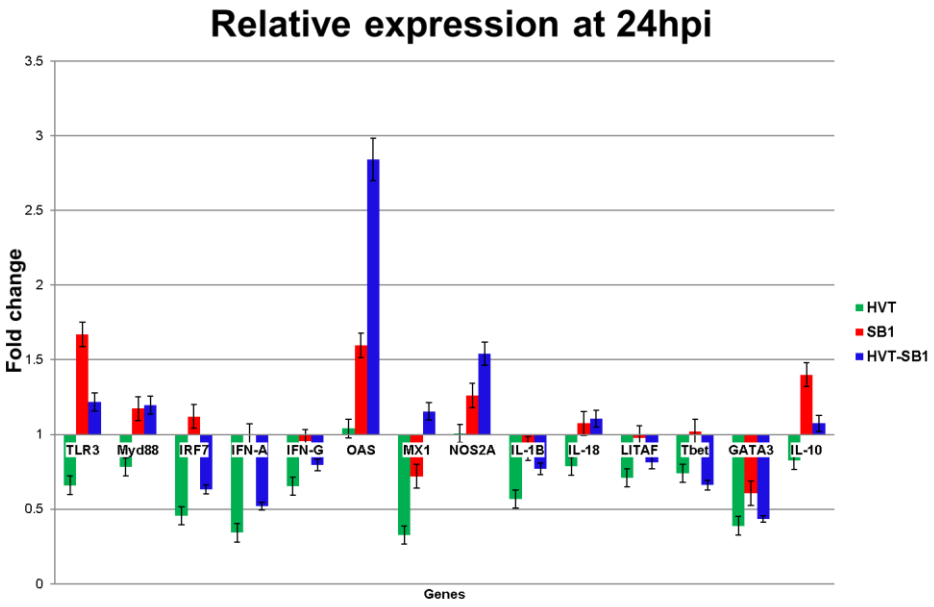

Figure 2.3: Differential expression *(fold change>2, p<0.05)* of immune signaling genes at 48hpt in an *in vitro* spleen cell infection model. The bar graph shows the fold change (Y-axis) associated with various immune signaling molecules (X-axis). Vaccine treatments are color coded as shown on right, HVT (green), SB1 (red) and HVT-SB1(blue). Asterisks mark *p<0.05*.

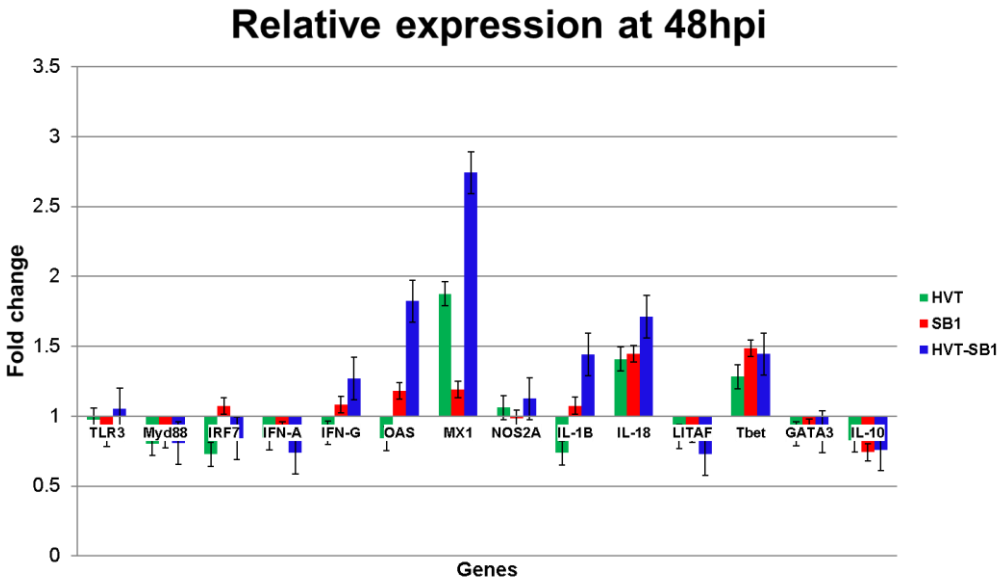

Figure 2.4: Differential expression *(fold change>2, p<0.05)* of immune signaling genes at 72hpt in an *in vitro* spleen cell infection model. The bar graph shows the fold change (Y-axis) associated with various immune signaling molecules (X-axis). Vaccine treatments are color coded as shown on right, HVT (green), SB1 (red) and HVT-SB1(blue). Asterisks mark *p<0.05*.

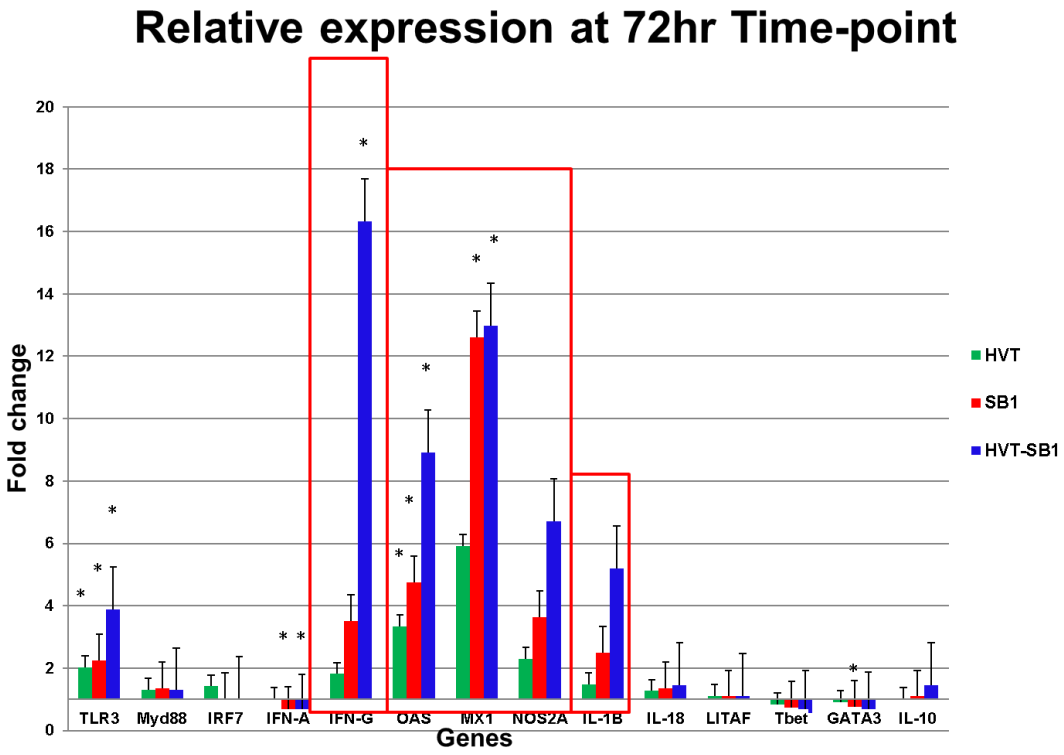

Figure 2.5: Differential expression *(fold change>2, p<0.05)* of virus specific glycoprotein B. The bar graph shows the fold change (Y-axis) at various hours post treatment (X-axis). Vaccine treatments are color coded as shown on right, HVT (green), SB1 (red), HVT (light blue) and SB1(navy blue) components of bivalent HVT-SB1.Asterisks mark *p<0.05*.

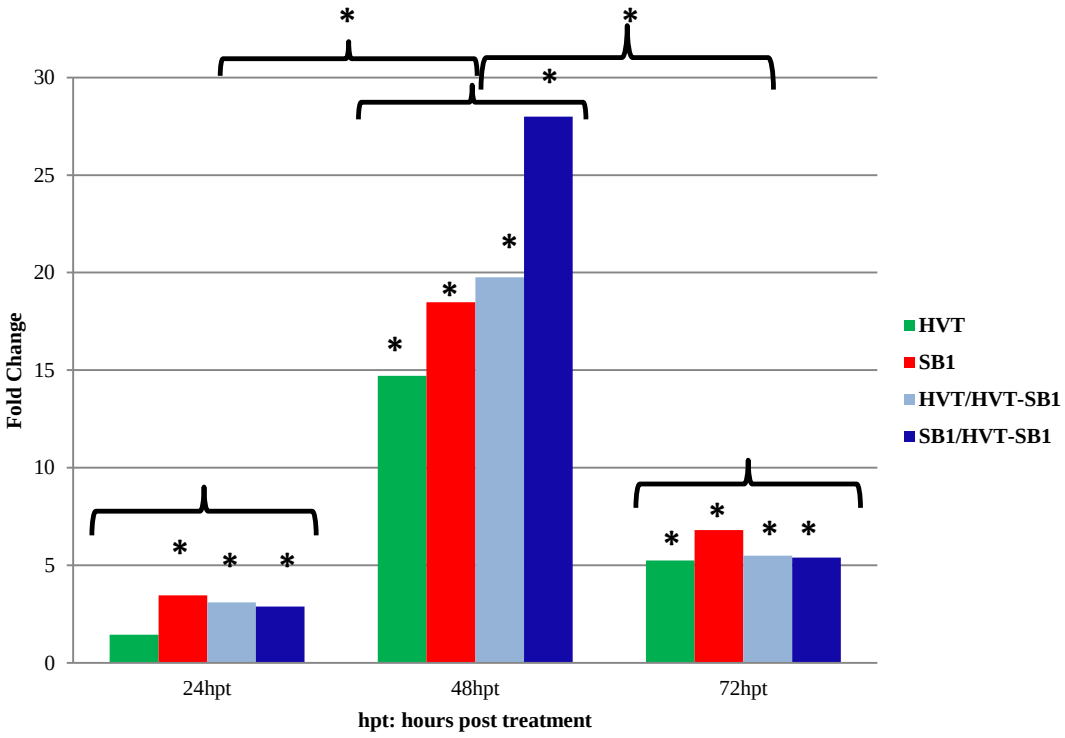

Chapter 3

APPLICATION OF QPCR IMMUNE ARRAY TO ASSESS IMMUNE RESPONSES TO LIVE AND RECOMBINANT MD VACCINES

3.1 Introduction

Our studies analyzing the innate immune responses to bivalent HVT-SB1 in Chapter 1 suggested that induction of Interferon Stimulated Genes (ISGs) occur as early as 3-day post hatch or 5-day post *in ovo* vaccination in meat type commercial broilers. This means that innate sensing and production of Type I interferons (IFN-β or –α) occurs even prior to the analyzed time points in the former study. It is evident in the *in vitro* spleen cell infection model that ISG induction occurs as early as 72hr post vaccination. In addition, studies in our lab analyzing immune responses to recombinant HVT-IBD carrying VP2 structural protein of IBDV have detected innate immune gene expression as early as 24hr post *in ovo* vaccination. Cytokines produced in response to innate sensing of pathogen associated molecular patterns (PAMPs) by pattern recognition receptors (PRRs) play an important role in shaping subsequent adaptive immunity. In the current study, we continue to test our hypothesis that early Type I IFN induction and signaling polarize the immune system towards a pro-Th1 and Th1-mediated CD8+ CTL responses in contrast to pathogenic MDVs which induce a transformed and immune suppressive T_{REG} phenotype. In addition, the

adjuvant effect of DNA based liposome mix (DLM) in enhancing vaccine efficacy was tested. To test our hypothesis, we employed an expanded panel of qPCR primers targeting avian Anti-Microbial Peptides (AMPs), pro- and anti-inflammatory cytokines, Interferons and ISGs, Immune modulatory proteins and transcription factors, sirtuins and cell population Markers.

PRRs form the first line of defense by sensing PAMPs of the invading pathogen. PRR sensing and downstream signaling leads to activation of transcription factors such as IRF7 and NFκB leading production of Type I/III interferons and pro-inflammatory cytokines respectively. Type I/III interferons bind to their receptors IFNAR1/2 and IL-28RA/10R2 respectively, leading to phosphorylation, dimerization and nuclear translocation of STAT1/2 in complex with IRF9 to stimulate ISG transcription. Various ISGs work in concert to contain various stages of virus replication beginning with viral entry, viral mRNA transcription, translation, DNA replication, virus assembly and finally, egress. Several classes of the following PRRs exist in chicken: Toll like receptors (TLRs), Retinoic acid like receptors (RLRs) Nucleotide Oligomerization Domain leucine rich repeat like receptors(NLRs), C-type Lectin receptors (CLRs).

The chicken TLR repertoire comprise TLR1la, TLR1b, TLR2t1, TLR2t2, TLR3, TLR4/MD2, TLR5, TLR6, TLR7, TLR15 and TLR21. These receptors exist on either on cell surface (TLR1la, TLR1b, TLR2t1, TLR2t2, TLR4/MD2, TLR5, TLR15) or endosomal (TLR3, TLR4/MD2, TLR5, TLR6, TLR7, TLR21) membranes (187). TLRs upon sensing their respective ligands such as di-or tri-acylated lipopeptides (TLR2/6 or TLR1/2 complexes respectively) LPS (TLR4) ssRNA (TLR7), dsRNA (TLR3), unmethylated CpG DNA (TLR21) recruit adaptor proteins such as Myd88

(all TLRs except TLR3) and TRIF (TLR3 and 4) to activate downstream kinases IRAK1 and 4 leading to activation of transcription factors IRF7 and NFκB to induce Type I/III interferons and pro-inflammatory cytokines respectively. In HD11 macrophage cell line, unmethylated CpG mediated activation of TLR21 and subsequent iNOS production was known to be dependent on clathrin mediated endocytosis and endosomal acidification and was sensitive to inhibitors of PKCα, p38MAPK, MEK1/2 and IκB phosphorylation(188)

The chicken RLR repertoire include cytosolic RNA helicases MDA5 (myeloid differentiation associated gene 5) and LGP2 (Laboratory of genetics and physiology 2) (189). In contrast to mammalian MDA5, chicken MDA5 preferentially senses short dsRNA or polyI:C to unravel its caspase recruitment domain (CARD). MDA5 CARD interacts with Mitochondrial Anti-Viral Signaling (MAVS/IPS1/VISA/Cardiff) on mitochondrial membranes via CARD-CARD interactions leading to recruitment and activation of TBK1/IKKε kinase complex that phosphorylates IRF3, leading to its dimerization and nuclear translocation to induce TypeI/III interferons. Chicken LGP2 lacks CARD signaling domain but was found to function by enhance MDA5 function by binding dsRNA in a less co-operative manner than MDA5 (190). In addition, chickens also possess cytosolic DNA sensor cGAS (2'-3'cyclic –GAMP synthase) which upon sensing foreign DNA synthesizes 2'-3' cyclic GMP-AMP, a ligand for endoplasmic reticulum (ER) localized Stimulator of Interferon Genes (STING) (191). Chickens lacks AIM2 DNA sensor (191). Poly I:C mediated activation of MDA5 or plasmid DNA mediated activation of cGAS induces MHC-I and MHC-II cell surface expression in DF-1 fibroblast cell line (Dr Parcells personal comm.).

Members of NLR family recognize various PAMPs such as dsRNA or Damage associated molecular patterns (DAMPs) such as ATP, K^+, reactive oxygen species and assemble into inflammasomes. Inflammasomes recruit and cleave caspase 1 which processes proforms of IL-1β and IL-18 into mature forms for secretion (192). Full activation of inflammasomes require 2 signals. First signal is a priming signal where TLR-mediated NFκB activation induces expression of IL-1β and IL-18 mRNAs and their pro-forms and the second signal being inflammasome assembly to activate caspase 1 and processing of pro-forms of IL-1β and IL-18 into their mature forms.

The cytokines produced in response to PRR sensing and activation in antigen presenting cells (dendritic cells, macrophages and B cells) determine the nature of polarization of naïve CD4+ T helper cells into various subsets during antigen presentation. Th1 polarizing cytokines including IL-12 and IFN-γ are produced by classical M1 macrophages and NK cells. Th2 subset polarizing cytokines include IL-4 and IL-2. T_{REG} polarizing cytokines include IL-10, TGF-β and IL-2. Finally, subset defining transcription factors such as Tbet and GATA3 determine the differentiation of naïve T cells into Th1 and Th2 phenotypes respectively.

Sirtuins 1-7 are the Silent Information Regulator proteins that possess deacetylase and ADP ribosyl transferase activity. Sirt-1, -6, -7 are predominantly nuclear where as Sirt-3, -4, -5 are mitochondrial. Sirt-2 is primarily cytoplasmic but can localize to nucleus (193). However, depending upon the cell type, metabolic status and stress signal, they can show altered localization and activity. They play an important role in the regulation of metabolism and aging. More importantly, Sirtuin 1 also possess anti-inflammatory activity in endothelial cells and lowers NFκB activation by deacetylation resulting in lower levels of pro-inflammatory cytokines

(IL-1β, IL-6 and TNFα), iNOS and ICAM1. This activity is associated with vasoprotective effects of Sirt-1 in cardiovascular disease and aging.

Three major classes of anti-microbial peptides (AMPs) are described in chickens. β-defensins, cathelicidins (CATH) and liver-expressed antimicrobial peptide-2 (LEAP-2). β-defensins (AvBDs) are cysteine rich cationic peptides that possess anti-microbial activity against gram positive or gram negative bacteria. AvBDs were presumed to function via insertion and pore formation on microbial membrane leading to their disruption. Human β-defensins, HBD2 &3 were found to co-internalize with HIV1 and neutralize the virus within the endosomal compartment via unknown mechanisms suggesting a potential anti-viral mechanism (194). In addition, AvBDs also appear to possess immune modulatory role. DT-40 B cell line demonstrated chemotaxis towards HEK293T cells expressing duck rAvBD2 (195-197). AvBD13 enhanced proliferation of splenocytes stimulated with concanavalin A or LPS and induced higher levels of IgG and IgM in the serum of chickens (195, 196). AvBD13 was found to induce expression of CD80, CD86 and NFκB in TLR4 dependent manner leading to induction of IL-12 and IFN-γ and was proposed to be a TLR4 ligand (198). Finally, LPS and CpG-ODN mediated induction of AvBD1 & 3 was found to be dependent on IL-1β induction and interaction with IL-1R in hen vaginal cells (199).

Similar to AvBDs, avian cathelicidins also possess anti-microbial activity towards a wide range of gram positive or gram negative bacteria and fungi (200, 201). Chicken LEAP-2 was shown to possess anti-microbial activity towards *Salmonella enterica typhimurium* strain (202). Finally, thymosin β4 functions as an anti-inflammatory peptide in its oxidized state and is involved in promoting tissue

resolution and wound healing (203). Treatment of HTCs with either LPS or PGN appears to have no change in thymosin β4 expression levels and it was induced by monocytes or macrophages in the presence of glucocorticoids (204, 205).

In the current study, we employed an expanded panel of qPCR primers targeting avian Anti-Microbial Peptides (AMPs), pro- and anti-inflammatory cytokines, Interferons and ISGs, Immune modulatory proteins and transcription factors, sirtuins and cell population markers to analyze responses to bivalent HVT+SB1 *in ovo* vaccination. This study is part of an industry funded trial that compelled us to study the adjuvant effects of an DNA liposome mix on the efficacy of MD vaccines HVT+SB1 and HVT-LT+SB1 (HVT based recombinant vaccine encoding glycoprotein B of Infectious Laryngotracheitis virus (ILTV)).

ILT is an economically important and highly contagious respiratory disease in densely populated poultry production areas that causes production losses due to increased mortality, reduced egg production, delayed weight gain and increased susceptibility to other respiratory pathogens due to disruption of respiratory barrier (155, 206). Control of ILT is dependent upon vaccination and strict biosecurity. Current vaccination against ILT in US includes use of either live attenuated (Chick embryo origin (CEO) or tissue culture origin (TCO) vaccines) or recombinant viruses (herpes virus of turkey (HVT) or Fowl pox virus (FPV) carrying ILT glycoproteins). To curtail the risk of infection and unacceptable economic losses, long lived birds are vaccinated with live attenuated vaccines whereas their use in short lived broilers is limited to the events of large outbreaks of disease. CEO vaccines are licensed for administration via spray or drinking water on mass applications. This method of administration can lead to poor mass vaccination. Successful mass vaccination is

dependent upon the vaccine virus making contact with the nasal epithelium via aspiration of vaccine through external nares or choanae (207). Lack of uniformity in successful vaccination can result in adverse reactions due to insufficient attenuation of vaccine virus, tendency to become latently infected carriers, shedding and regaining virulence upon bird to bird passage. Despite these drawbacks CEO vaccines are still being used to control the disease. A safer alternative to CEO would be the use of HVT or FPV recombinants carrying ILTV genes. Current HVT vectored products carry glycoprotein genes of ILTV (gI or gD or gB) and are licensed for *in ovo* administration whereas FPV vectored product (gB and UL32) is licensed for wing web inoculation only. HVT vectored products are advantageous in terms of mass administration to broilers *in ovo,* lack of bird to bird transmission and lack of reversion to virulence (208-210). Moreover, they can serve to protect against both MD and ILT.

In chickens, administration of CpG-ODN along with traditional vaccine regimens was found to enhance the vaccine efficacy via adjuvant effects. This adjuvant effect of CpG when delivered via various routes, including *in ovo* route, was demonstrated against a wide range of bacterial, viral and protozoal infections. For instance, CpG with a stable phosphorothioate backbone when administered via oral or intravenous or subcutaneous routes was found to reduce eimeria oocyst shedding and enhance weight gain in susceptible 3 week old TK line of chickens. This was due to a proposed mechanism of Th1 mediated IL-12 and IFN-γ production (159, 160). In commercial broilers, *in ovo* CpG administration via carbon nanotubes or liposomes was found to protect day old chicks (60% protection) from E. coli or Salmonella typhimurium challenge(161). In addition CpG-ODN was proven to enhance the protection mediated by LaSota NDV vaccine and LPAI H4N6 virosomes by

enhancing both Ab-mediated and cell mediated immunity (161, 211). Finally other studies demonstrated the ability of CpG-ODN mediated adjuvant effects during MDV, IBV and ALV-J vaccinations (162-164).

Administering CpG-ODN *in ovo* along with MD vaccines is convenient and advantageous in terms of fast administration, reduced labor costs and conferring an adjuvant effect on the vaccine alongside which it is administered. Furthermore, combining CpG-ODN with recombinant MD vaccine such as HVT-LT might enhance the protective ability of this moderately effective vaccine. Henceforth the main goal of the current study was to assess CpG-ODN mediated adjuvant effect on MD vaccine responses when administered *in ovo*.

3.2 Materials and Methods

3.2.1 Cell culture and Viruses

The DNA/liposome-based adjuvant (DLM, a.k.a., Bay98, Victrio®) was obtained from Bayer Health Care (Animal Health). The DLM was administered alongside MD vaccines *in ovo* at a dose of 0.15µg. All the vaccine viruses were propagated in secondary CEF derived from specific pathogen free (SPF) embryos of single comb, white leghorn chickens (Sunrise Farms, Catskill, NY). Secondary CEF were grown and maintained in M199 medium supplemented with 3% bovine serum (gibco), 1X antimycotic (fungizone; Invitrogen) and 1X antibiotic mix PSN (penicillin G, streptomycin, and neomycin; Invitrogen, Inc., Gaithersburg, MD).

3.2.2 Non-interference of DLM

One of the main aims of the current study is to study the non-interfering effect of DLM adjuvant on bivalent HVT+SB-1 and bivalent recombinant HVT-LT+SB-1

vaccine efficacy and whether co-administration with DLM accelerated vaccine mediated immunity. In addition, based on the DLM analog (Zelnate) effects seen in cattle, mechanistically, if DLM functions by enhancing anti-bacterial immunity via AMPs and reducing immune mediated pathology (neutrophil influx) seen during shipping fever (*M.parahemolytica*). To assess this, the effect of Victrio® alone, or in combination with MD vaccination (with HVT + SB1, or HVT-based recombinant vaccine, Vectormune HVT-LT + SB1) was compared to diluent-inoculated embryos at E19 (24 hrs post-vaccination), E21 (72 hrs post-vaccination, at hatch) and at 3, 5, 12 and 15 days post-hatch. Treatment groups include Diluent only, Victrio® only (DLM), HVT + SB1, HVT + SB1 and 0.15µg DLM, HVT-LT + SB1, HVT-LT + SB1 and 0.15µg DLM. Treatment doses were tabulated in Table 3.1.

3.2.3 Sampling strategy

Spleen samples were isolated from each treatment at the respective time point and pooled in triplicates to generate 3 pools from a total of 9 embryos per treatment. Pooled spleen samples were snap frozen in individual cryobags and stored at -80 degrees for further processing. In addition, whole blood was obtained from embryos and allowed to coagulate at 4 degrees to collect serum. Serum was subsequently stored at -80^0 c for LT antigen ELISA.

3.2.4 RNA isolation and gene expression analyses

Total RNA was isolated using RNeasy Midi Kit (Qiagen) as per manufacturer's instructions. Quantity and quality of RNA was confirmed using NanoDrop ND-1000 Spectrophotometer (Thermo scientific) and Agilent 2100 BioAnalyzer (Agilent Technologies Inc.) respectively. For cDNA synthesis, 1µg of

RNA from each sample was reverse transcribed using High-Capacity cDNA Reverse Transcription Kit (Applied biosystems) as per manufacturer's instructions. The resulting cDNA was diluted 1:10 and stored at 4 degrees. qRT-PCR was performed using MyiQ2 Two color Real-Time PCR detection system (BIO-RAD, Hercules, CA) in a 20µl reaction containing 1µl of cDNA, forward and reverse primers (0.4µM), 10 µl of iTaq™ Universal SYBR® Green Supermix (Bio-rad) and nuclease-free water. Melt curve analysis was performed by heating from 55°C to 95°C in the increments of 0.2°C/sec to exclude the possibility of non-specific amplification. List of target genes and their respective primer sequences were tabulated in the Table 3.2. Relative gene expression is calculated by ΔΔCt method using REST (Relative software expression tool, http://www.gene-quantification.de/rest.html) upon normalization to internal reference gene GAPDH (212).

3.2.5 ELISA

Serum ELISA was performed to determine Anti-LTgB titres by following manufacturer's instructions provided in the commercial ELISA kit (CEVA-Biomune, Lenexa, KS). This provides a read out against the recombinant protein gB carried by the HVT vector. ELISA was carried out to investigate if DLM coadministration accelerated the development of gB specific antibodies.

3.2.6 Viral Replication Kinetics

Total DNA was isolated from spleen samples using Qiagen DNA tissue kit following manufacturer's instructions. To analyze the effect of DLM on vaccine virus replication, we quantified the Ct values pertaining to cellular β-actin, HVT gB and SB-1 gB genes by quantitative PCR (Biorad). Briefly 50ng of DNA was run in

duplicates in a 20µl reaction containing 1µl of cDNA, forward and reverse primers (0.4µM), 10 µl of iTaq™ Universal SYBR® Green Supermix (Bio-rad) and nuclease-free water. Upon obtaining Ct values, relative quantification of viral DNA loads was calculated as cellular β-actin Ct/ HVT or SB-1 gB Ct x 100.

3.2.7 Statistical analysis

Differences in gene expression levels between diluents treated and rest of the treatments were assessed in group means for statistical significance by pair wise fixed reallocation randomization test by REST software(213).

3.2.8 Research Compliance

All animal studies were carried out using approved Agriculture Animal Care and Use Committee (AACUC) protocols. The protocol for this specific study was approved 3/9/10 and approval number - (22) 04-15-10b R.

3.3 Results

3.3.1 ELISA

In one of our past studies where the effects of DLM on the efficacy of recombinant HVT-IBD (HVT vectored IBD VP2 gene) were analyzed, an increased rate of seroconversion towards IBD was observed (mean anti-IBDV titers were 391.5 (± 555.74) in HVT-IBD-vaccinated versus 533.5 (± 273.9) in HVT-IBD+DLM-vaccinated chickens) HVT-IBD+DLM-vaccinated chickens. In addition, a significantly higher number of chickens tested seropositive in HVT-IBD+DLM treatment group (70.83%) compared to HVT-IBD group (20.83%) although DLM displayed no significant difference in % MD protection (Upendra Katneni Doctoral

dissertation). Our ELISA results indicate a high level of non-specific background signal especially on the day of hatch, day 3 and day 5 post hatch (Fig. 3.1). If a significant amount of maternal antibody towards LT were to be present, a more consistent pattern of anti-LTgB would have been observed among all the time points until day 15 post hatch. These results beg for right dilution (1:100) of serum samples prior to the assay to achieve specificity and sensitivity. However, the lack of antibody response on day 12 and day 15 post hatch in all treatments, including DLM coadministered treatments indicate no effect of DLM on the development of anti-LTgB antibodies. Other studies analyzing the LTgB seroconversion in response to FPV-LT or HVT-LT vaccination, detected Anti-gB antibodies by 5-6 weeks and no acceleration of antibody responses was observed upon co-administration of HVT vectored products with DLM (214).

3.3.2 Gene Expression Analyses

Results of the gene expression analyses will be described for the treatments (DLM, HVT+SB1, HVT+SB1+DLM, HVT-LT+SB1, HVT+SB1+DLM) in the following heirarchy 1. AMPs 2. Pro-inflammatory cytokines 3. Interferon and Interferon stimulated genes 4. Immune modulatory cytokines, suppressors of cytokine signaling and transcription factors 5. Sirtuins 6. Cell population markers. Concurrently, correlation with vaccine viral replication and the effects of DLM on vaccine viral replication will be explained.

3.3.2.1 Anti-microbial peptides (AMPs)

In the chickens treated with DLM alone, no significant induction of avian β defensins (AvBD) 1-4 or cathelicidins 1-3 was observed (Table 3.2). In fact, a

significant down regulation of AvBDs-5, -10 and LEAP2 was observed. On the contrary, a 2.4-fold induction of thymosin β4 was observed within 24hrs with basal levels seen among rest of the time points. Previous studies have ascribed an anti-inflammatory role to the naturally occurring sulfoxide derivative of thymosin β4 in addition to its antimicrobial and tissue remodeling functions (203-205). This appears to be the MOA seen in cattle treated with DLM. In HVT+SB1 vaccinated groups, although no induction of AvBDs 1-4 was observed, coadministration of DLM with this vaccine appears to have an additive effect. We observed a significant induction of AvBDs 1-4 in HVT+SB1+DLM vaccinated group ranging from 2.69 fold to 20.82 fold within 24 hours post vaccination (Table 3.2). Similar to effects seen in DLM alone treatment, significant down regulation of AvBD5 &10 and LEAP2 was observed in HVT+SB1 and HVT+SB1+DLM vaccinated groups. This pattern of downregulation persisted until hatch in HVT+SB1treatment. In HVT-LT+SB1 and HVT-LT+SB1+DLM treatments similar patterns of expression were observed with AvBDs 1-4 with greater levels of AvBD-2 seen in HVT-LT+SB1 group. AvBD10 and LEAP-2 remained significantly downregulated as other treatments. Thymosin β4 appeared to be upregulated similarly in all the treatments. The induction of AvBDs appeared to be very immediate within 24hours post vaccination and transient although in the case of HVT-LT+SB1+DLM treatment, induction of AvBDs 1, 2 and 4 was extended until hatch (Table 3.2).

3.3.2.2 Pro-inflammatory cytokines

A significant downregulation of pro-inflammatory cytokine IL-1β was observed in all treatments including DLM alone treatment within 24hrs. In DLM alone treatment, a significant down regulation of IL-8 and NOS2A was observed at 24hr

time point whereas no significant changes were observed with IL-4, IL-6 and IFN-γ at any time point (Table 3.3). A significant induction of IL-18 was observed by DLM alone at 24hrs, indicating a Th1 biased response, similar to what had been seen in neonatal chicks i.m. treated with CpG (160). HVT+SB1 treatment displayed similar expression pattern as DLM only, with a significant upregulation of IL-18. Addition of DLM to HVT+SB1 appears to enhance the immediate expression (24hr) of IL-18, IL-8, NOS2a and IFN-γ and subsequent down regulation of IL-8, IL-18 and NOS2A at 72hr time point (Table 3.3). In HVT-LT+SB1 group, a significant induction of IL-8 and IL-18 was observed at 24hr. At later time points (3, 5, 12 and 15 days post-hatch), a comparable induction of IFN-γ and a late induction of IL-4 and IL-6 on Day 15 was observed. Interestingly, the IL-4 and IL-6 induction at 15 dph was preceded by downregulation on 12 dph. Addition of DLM to HVT-LT+SB1 appear to induce similar levels of IL-18 (Table 3.3). However, levels of IL-8 and NOS2A appear to be dampened.

3.3.2.3 Interferon and Interferon Stimulated Genes (ISGs)

DLM alone treatment lead to a significant induction of ISGs, MX1 and OASL with in 24hr. The induction of ISGs appeared biphasic. Immediate upregulation by 24hr was followed by a decreased expression at hatch and a sustained expression at 3, 5 and 12 dph for OASL (Table 3.4). Similar pattern of expression is seen with MX1 with a more sustained expression on D12 ph. Type I IFNs promote maturation of innate cells such as dendritic cells and macrophages leading to increased expression of MHC I and MHC II (Table 3.4). However, no significant change in MHC I and II transcript levels was observed. HVT+SB1 group displayed an initial down regulation followed by a potent induction of MX1 on the day of hatch. These levels sustained

until day 3 post hatch for MX1 (Table 3.4). A modest upregulation of MHC I and II was observed at 24hrs followed by falling to levels similar to controls by hatch was seen. Addition of DLM appeared to slightly enhance the levels of MHC I and II. Furthermore, addition of DLM appears to sustain the levels of MX1 and OASL similar to what had been observed with HVT+SB1. Similar to the initial observations made with HVT+SB1, HVT-LT+SB1 group displayed an initial downregulation of MX1 and OASL by 24hr followed by higher levels seen on hatch and D3ph. A modest increase in MHC I and II was observed in HVT-LT+SB1 similar to HVT+SB1. Addition of DLM to HVT-LT+SB1 appear to either dampen or delay the induction of ISGs MX1 and OASL respectively (Table 3.4).

3.3.2.4 Immune modulatory cytokines, suppressors of cytokine signaling and transcription factors indicative of T helper phenotypes

A significant down regulation of SOCS1 and anti-inflammatory cytokine IL-10 was observed with all the treatments. A significant induction of IL-10 was observed by D15 post hatch in all the treatments indicating immune regulation as the vaccine viruses enter latency at this time point (Table 3.5). These patterns of IL-10 followed IL-4 and IL-6 on D15ph, cytokines associated with T helper type 2 response. A similar pattern of significant upregulation was observed by 24hr with regards to Tbet, GATA3 and IL-12p40 subunit with vaccine treatments and DLM added vaccine treatments. HVT+SB1 group displayed a down regulation of SOCS1 & 3 by 24hrs (Table 3.5). This coordinated induction of IL-12p40 and down regulation of SOCS1 & 3 indicates M1/T_H1 patterning of immune system. DLM, in general appeared to have a rapid effect on the induction of genes by HVT+SB1. However, this effect was not sustained

or have long term patterning effects as seen during later time points (D5, D12 and D15 post hatch) (Table 3.5).

3.3.2.5 Sirtuins

Among sirtuins, sirtuin 1 & 6 are of particular interest as they appear to modulate innate and acquired immune signaling. Sirtuin 1 functions by deacetylating NFκB complex resulting in dampened pro-inflammatory cytokines such as IL-1β, IL-6 and TNFα in endothelial cells (193). Sirtuin 6 functions in aging and telomere maintainance. Furthermore, it associates with RelA and acts as co-repressor for NFκB responsive genes such as IL-6, TNFα and MCP1 (183). DLM alone displayed downregulation of SIRT3 on 24hr time point whereas SIRT 5 & 6 were upregulated (Table 3.6). None of the other time points displayed significant differences suggesting that the effects of sirtuins are immediate and anti-inflammatory. Bivalent HVT+SB1 vaccination induced several of these Sirtuins (Sirt -1, -2, -5, -6) whereas SIRT-3 remained significantly down regulated by 24hrs. Effects of SIRT-1 &-6 are evident on the lack of induction of pro-inflammatory cytokines IL-1β, IL-6 and IL-8. Addition of DLM to HVT+SB1 appeared to enhance the level of all the sirtuins examined (SIRT1-6) by 24hrs (Table 3.6). SIRT-3 was found to be down regulated in DLM alone and HVT+SB1 groups but together there was a significant induction by 24hr although the levels were down regulated by hatch. The induction of SIRT-1 & -6 parallels with a lack of IL-1β on 24hr although the same do not apply for IL-8 and IL-18 (Table 3.3). The same pattern was seen in Vectormune HVT-LT+SB1 group where a significant induction of all except SIRT-3 was observed (Table 3.6). Consistent with the induction of SIRT-1 & -6, a lack of IL-1β but not IL-8 or IL-18 was observed by 24hr (Table 3.3). Addition of DLM to HVT-LT+SB1displayed significant induction of

SIRT-1, -4, -5 & -6. But the level of induction was lower than vaccination alone. By hatch the levels of SIRT-1, -2, -4, -5 & -6 remained undetectable whereas SIRT-3 was significantly downregulated.

3.3.2.6 Cell population Markers

To monitor various cell populations, we analyzed the transcript levels of cell surface markers such as BU.1 (B cells), CD3 (T cells and intracellular transcripts for NK cells), CD4 (T helper cells), CD8α (cytotoxic T cells, some NK cells & dendritic cells), CD107α (NK cells and CD8+ CTLs)(215), CD11c (macrophages and dendritic cells). In DLM alone treatment, a significant down regulation of BU.1 and CD8α was observed on 24hr. Although a 4.5-fold non-significant induction of CD3 was observed on 24 hr time point, a greater level of significant induction (16 fold) was observed by hatch (Table 3.7). This however correlated with only a slight induction of CD8 on the day of hatch indicative of immature T cells. In HVT+SB1 treatment, a significant induction of CD3 and CD11c was observed on 24hr time point. This induction of CD3 was extended on day 3 post hatch similar to DLM alone. However, no contemporary induction of either CD4 or CD8 was observed indicative of immature T cells ($CD4^-$ $CD8^-$). The increase in CD11c indicates an influx of splenic macrophages. Similar to DLM alone treatment, a significant down regulation of BU.1 was observed (Table 3.7). DLM addition to HVT+SB1 led to a greater level of induction of all cell population markers (CD3, CD4, CD8, CD107a CD11c and BU.1) by 24hr (Table 3.7). A greater level of CD3 induction was observed on day 3 post hatch similar to DLM or HVT+SB1 alone treatment and this overlapped with CD4 induction suggesting an influx of $CD3^+CD4^+$ T cells. An absence of $CD8^+$ however indicates lack of cell mediated response. In Vectormune HVT-LT+SB1 treatment, a significant induction of

CD3, CD8α, CD4, CD107a was observed, all indicative of NK and T cells ($CD3^+$ $CD4^+$ and $CD3^+$ $CD8^+$ $CD107a^+$) (Table 3.7). No change in BU.1 was observed except on day 5 post hatch, a significant down regulation was observed possibly due to lytic replication of vaccine virus in the target B cells. On day 12 post hatch, a significant induction of CD4 and CD8 was observed indicative of successful patterning of T helper and CTL responses. In combination with DLM, a significant induction of CD3, CD8, CD107a and CD11c was discerned. This is indicative of a modest activation of NK cells ($CD3^+$ $CD107^+$) or CTLs ($CD3^+$ $CD8^+$ $CD107^+$) and an influx of macrophages (CD11c). A marked induction of CD3 accompanied by CD4 was observed on day 3 post hatch indicative of increase in $CD4^+$ T helper cells. A higher level of CD4 and CD8 was also observed on 12 days post hatch similar to HVT-LT+SB1 treatment.

3.3.2.7 DLM effects on vaccine virus replication

To analyze the effect of DLM on the replication of vaccine virus, we used quantitative PCR to measure the threshold cycle values of cellular β actin and HVT/SB1 gB. We did this because of the caveats associated with vaccine virus re-isolation procedure and an advantage of higher sensitivity of detection (8 log) by qPCR. A past study done in our lab failed to re-isolate HVT+SB1 to a sufficient extent from commercial broilers (1-2 PFU per million cells at week 1 & none at week 2). Furthermore, with virus specific primers targeting non conserved regions of glycoprotein B, threshold cycles corresponding to DNA genomes of each virus can be accurately quantified. None of the vaccine viruses were detected in the DLM only treatment. No difference in the kinetic onset of HVT+SB1 replication was observed with or without DLM, although a greater level of SB1 was detected on day 3 and 5

post hatch (Fig. 3.2, 3.3). DLM appeared to accelerate the replication of HVT-LT as early as the day of hatch whereas this virus was undetectable in the HVT-LT+SB1 only treatment (Fig. 3.4, 3.5). No significant difference at other time points was observed.

3.4 Discussion

In a previous study where we analyzed the adjuvant effects of DLM on HVT-IBD vaccine, we observed an increased seroconversion towards IBD VP2 transgene (U. Katneni, doctoral dissertation). This enhanced antibody response; however, did not correlate with MD protection. In fact, comparable indices of lacking protection were observed upon TK (vv+MDV) challenge among HVT-IBD and HVT-IBD+DLM groups. This could be due to the vv+ challenge used in this study that can overwhelm the effects seen with DLM.

In a follow up study addressing the effects of DLM on the efficacy of HVT and HVT+SB1 in SPF chickens, the chicks were challenged with a more relevant RB1B (passage 10) strain. However, this virus appeared more virulent than the reference RB1B and a lack of protection was seen among HVT+SB1 and HVT+SB1+DLM groups (Dr. Parcells, personal comm.).

In the current study, based on immediate effects observed within 24hrs in response to HVT-IBD+DLM, we examined gene expression profiles in the spleens of chickens vaccinated with HVT+SB1 and HVT-LT+SB1, either alone or in combination with DLM. In the ELISA, we observed a lack a seroconversion towards LT antigen (gB) for the time frame examined. However, there was a significant amount of non-specific background that precluded us to evaluate the seroconversion rates in response to DLM. In addition, previous studies indicated that the timing of

development of LT specific antibodies to vector-based vaccination is about 34-37 days. Hence a later time point would have been relevant in assessing seroconversion towards LT. In a previous study, CpG when administered to 5 day old chickens, a delay in the onset of MD was observed although no difference in tumor incidence was observed (216).

The splenic avian β-defensin (AvBD) expression profiles observed in response to MD vaccination were consistent with the previously reports (217, 218). Tissue specific expression of AvBDs 1-7 was restricted to bone marrow whereas AvBD1 and 2 were also highly expressed in lung. AvBD8-13 were found highly expressed in liver, kidney, testicle, ovary, male and female reproductive tracts (218). No AvBDs were found to be expressed at basal levels in spleen. In a necrotic enteritis (*E. maxima* + *C.perfringens*) challenge model performed in Ross and Cobb line commercial broiler chickens, AvBD1 and 7 were upregulated in spleen, with a greater extent of upregulation seen in Ross line chickens (217). In our study, we observed greater level of splenic upregulation of AvBD1, 2 and 3 in groups receiving MD vaccines (bivalent HVT+SB-1, bivalent HVT-LT+SB-1) with or without DLM, indicative of systemic anti-microbial effects caused upon MD vaccination.

Examination of ISG and pro-inflammatory cytokine gene induction patterns revealed a clear role played by innate Type I IFNs in promoting early protection against MD challenge with no or very limited role played by pro-inflammatory cytokines. Supporting this hypothesis is Sirt-1 upregulation and its anti-inflammatory actions (IL-1β down regulation). ISG and CD11c expression overlapped, suggestive of Type I IFN production caused upon innate dendritic cell flux. In addition, Type I IFNs were recently demonstrated to cause activation of CD8+ CTL responses which could

be a possible mechanism occurring upon MD vaccination (219). Consequently, future studies must focus upon how higher virulent strains of MDV-1 overcome the early protection conferred by deregulating the Type I IFN induction, IFN signaling and individual ISG encoded functions. In addition, the innate immune evasion mechanisms employed by MDV-1 or innate immune evasive functions of MDV-1 proteins must be investigated for a rational vaccine design to contain future MD outbreaks.

Finally, bivalent HVT/SB-1 vaccination resulted in a coordinated induction of IL-12p40 and down regulation of SOCS1 & 3 indicative of M1/T_H1 patterning. These findings reflected our past finding comparing immune responses in rMd5- versus rMd5ΔMeq-inoculated SPF chicks where upregulation of IL-12p70 subunits (p40 and p35) along with SOCS1 downregulation was observed in rMd5ΔMeq-inoculated chickens.

Figure 3.1: ELISA graph shows the signal/positive(S/P) ratios for ILTV ELISA. Mean negative control and positive control limits of detection are shown as dotted lines (green and red, respectively).

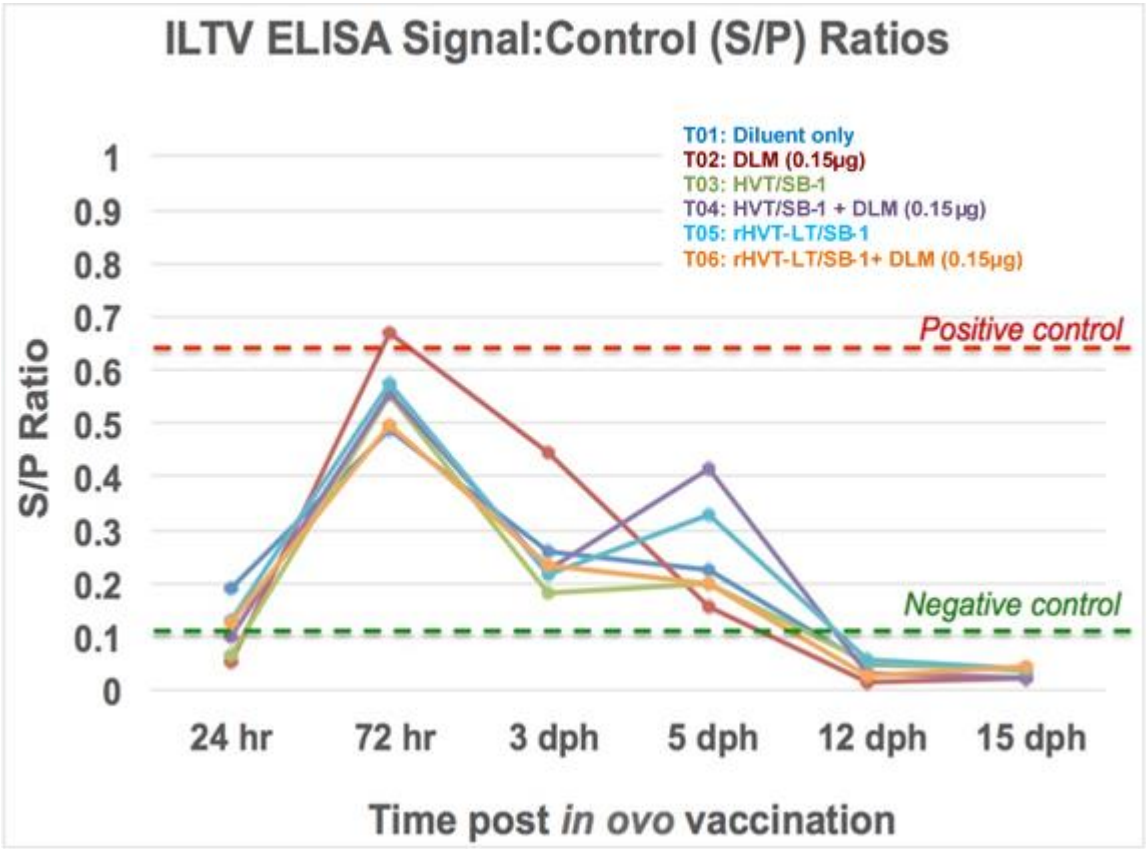

Figure 3.2: Replication kinetics of HVT (blue) and SB-1 (red) viruses in the spleens at various time post *in ovo* vaccination with bivalent HVT/SB-1. Error bars display standard error of mean (SEM).

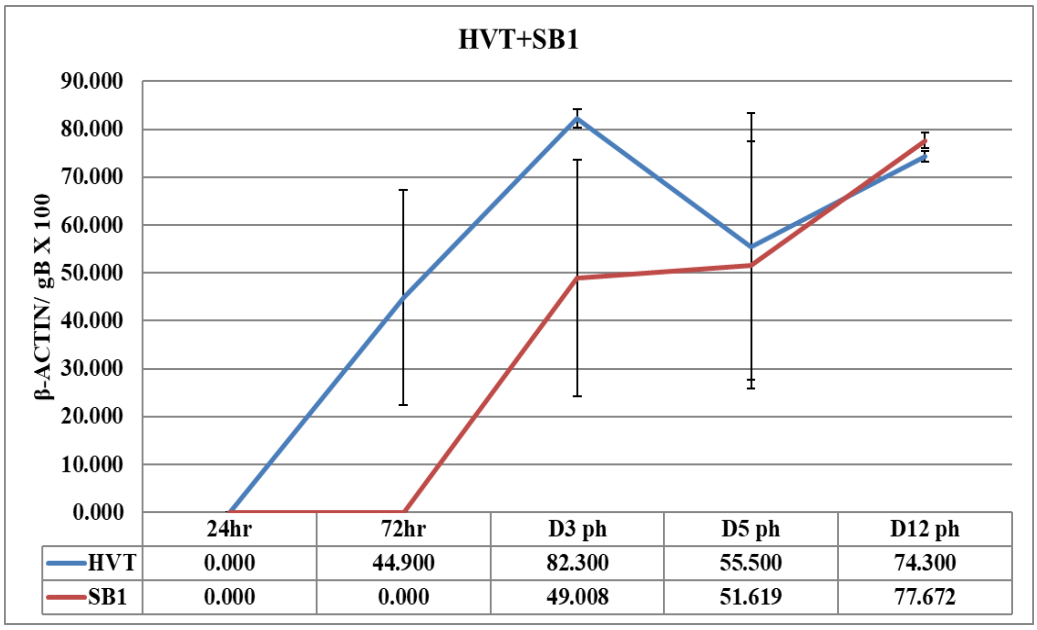

	24hr	72hr	D3 ph	D5 ph	D12 ph
HVT	0.000	44.900	82.300	55.500	74.300
SB1	0.000	0.000	49.008	51.619	77.672

Figure 3.3: Replication kinetics of HVT (blue) and SB-1 (red) viruses in the spleens at various time post *in ovo* vaccination with bivalent HVT/SB-1+DLM. Error bars display standard error of mean (SEM).

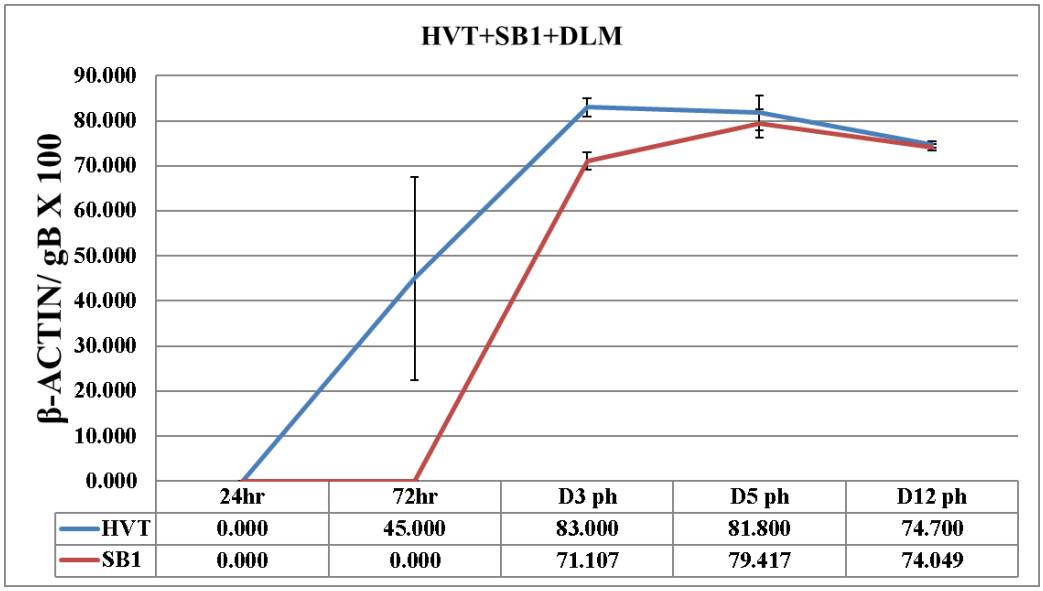

	24hr	72hr	D3 ph	D5 ph	D12 ph
HVT	0.000	45.000	83.000	81.800	74.700
SB1	0.000	0.000	71.107	79.417	74.049

Figure 3.4: Replication kinetics of HVT (blue) and SB-1 (red) viruses in the spleens at various time post *in ovo* vaccination with bivalent HVT-LT/SB-1. Error bars display standard error of mean (SEM).

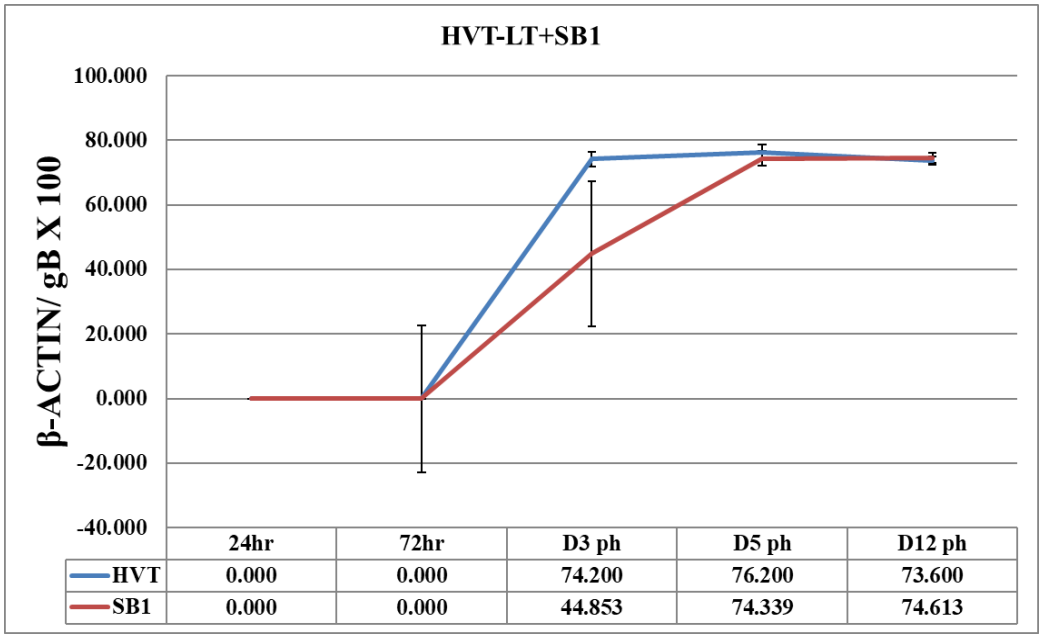

	24hr	72hr	D3 ph	D5 ph	D12 ph
HVT	0.000	0.000	74.200	76.200	73.600
SB1	0.000	0.000	44.853	74.339	74.613

Figure 3.5: Replication kinetics of HVT (blue) and SB-1 (red) viruses in the spleens at various time post *in ovo* vaccination with bivalent HVT-LT/SB-1+DLM. Error bars display standard error of mean (SEM).

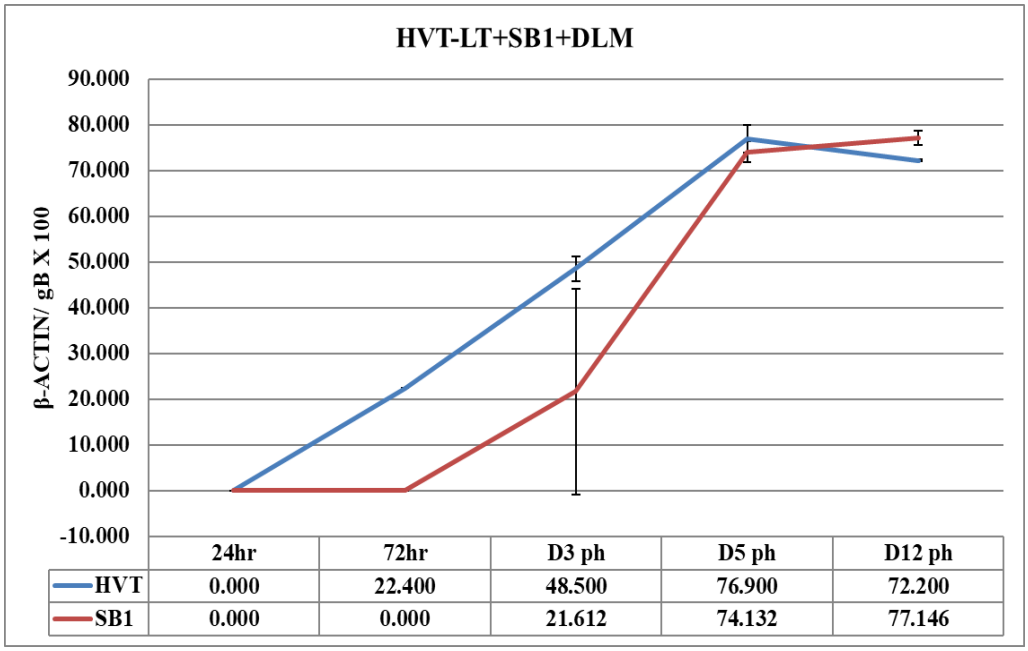

	24hr	72hr	D3 ph	D5 ph	D12 ph
HVT	0.000	22.400	48.500	76.900	72.200
SB1	0.000	0.000	21.612	74.132	77.146

Figure 3.6: Relative expression of Type I/II IFNs, ISGs, pro-inflammatory cytokines, and IL-12 family cytokine subunits in the spleens at various time points post *in ovo* vaccination with bivalent HVT/SB-1. Relative expression at 24, 72, 144 (D3 post hatch), 192 (D5 post hatch) and 360 (D12 post hatch) hr post *in ovo* vaccination was indicated in blue, red, green, purple and cyan bars respectively.

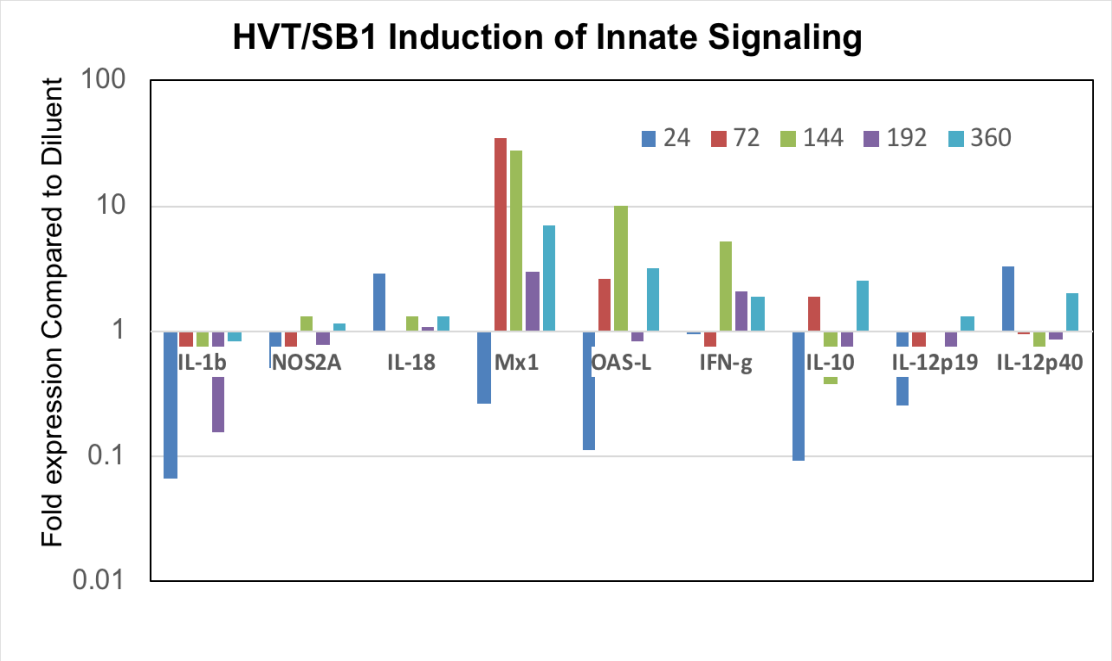

Table 3.1: Study treatments and target doses

Study treatment	Back-titration of PFU per bird
Diluent only (Merial)	0
Victrio® only (Bayer)	0
HVT + SB1	4100 (HVT) 2820 (SB1)
HVT + SB1 and 0.15µg DLM	3820 (HVT) 1740 (SB1)
HVT-LT + SB1 (Vectormune)	5720 (HVT-LT) 1940 (SB1)
HVT-LT + SB1 (Vectormune) and 0.15µg DLM	3860 (HVT-LT) 1400 (SB1)

Table 3.2: Relative gene expression and *p* values of anti-microbial peptides including avian β defensins (AvBDs), Cathelicidins (CATHs), and Thymosin-β4 at various time points post vaccination. Treatment T02, T03, T04, T05 and T06 indicate DLM only, HVT/SB-1, HVT/SB1+DLM, HVT-LT/SB-1, HVT-LT/SB1+DLM respectively. Negative - Ct values greater than 35. ND- Not Determined.

Treatment/Gene	T= 24 hrs	p value	T=72 hrs	p value	T=3 dph	p value	T=5 dph	p value	T=12 dph	p value	T=15 dph	p value
T02 - AVBD-1	0.833	0.513	0.871	0.793	ND							
T03 - AVBD-1	1.263	0.593	0.513	0.214								
T04 - AVBD-1	**7.029**	0.299	0.524	0.338								
T05 - AVBD-1	**9.759**	0.063	0.865	0.699								
T06 - AVBD-1	**6.119**	0	2.158	0.296								
T02 - AVBD-2	1.028	0.765	0.744	0.462	1.323	0.638	ND					
T03 - AVBD-2	2.526	0.247	0.754	0.501	1.009	0.98						
T04 - AVBD-2	**20.821**	0.338	0.597	0.463	2.189	0.159						
T05 - AVBD-2	**30.981**	0.037	1.117	0.967	1.866	0.287						
T06 - AVBD-2	**14.588**	0.136	3.819	0.034	0.776	0.815						
T02 - AVBD-3	0.642	0.412	Negative		ND							
T03 - AVBD-3	1.502	0.493										
T04 - AVBD-3	**4.779**	**0.299**										
T05 - AVBD-3	**4.936**	**0.034**										
T06 - AVBD-3	**4.542**	**0**										
T02 - AVBD-4	0.712	0.29	0.495	0.495	ND							
T03 - AVBD-4	0.489	0.101	0.382	0.107								
T04 - AVBD-4	**2.694**	**0.386**	0.586	0.199								
T05 - AVBD-4	1.972	0.27	1.064	0.552								
T06 - AVBD-4	**2.861**	**0**	1.836	0.415								
T02 - AVBD-5	**0.406**	**0.03**	0.912	0.905	1.344	0.371	ND					
T03 - AVBD-5	0.677	0.367	**0.502**	0	0.704	0.207						
T04 - AVBD-5	1.186	0.796	0.291	0.15	1.366	0.386						
T05 - AVBD-5	0.883	0.937	**0.425**	0	**2.287**	0.072						
T06 - AVBD-5	0.765	0.373	1.023	0.905	1.192	0.972						
T02 - AVBD-10	**0.164**	0	1.045	0.824	0.531	0.517	ND					
T03 - AVBD-10	**0.055**	0	0.559	0.037	0.384	0.208						
T04 - AVBD-10	0.095	0.299	0.193	0.344	1.562	0.592						
T05 - AVBD-10	**0.004**	0	**0.121**	0.027	8.417	0.276						
T06 - AVBD-10	**0.011**	0.034	0.14	0.217	2.44	0.572						
T02 - LEAP2	0.193	0.034	1.159	0.558	ND							
T03 - LEAP2	**0.099**	0	0.631	0.279								
T04 - LEAP2	0.492	0.813	0.213	0.234								
T05 - LEAP2	**0.052**	0.053	0.177	0								
T06 - LEAP2	**0.052**	0.063	0.277	0.2								
T02 - Thymosin-β4	2.44	0.112	0.717	0.291	1.295	0.312	0.751	0.726	0.859	0.78	ND	
T03 - Thymosin-β4	**2.526**	0	0.751	0.192	1.636	0.183	0.809	0.722	0.97	0.848		
T04 - Thymosin-β4	**8.168**	0	0.937	0.707	2.09	0.096	0.948	0.915	0.812	0.362		
T05 - Thymosin-β4	**8.206**	0	1.059	0.767	1.338	0.445	1.647	0.679	1.151	0.444		
T06 - Thymosin-β4	**5.217**	0	1.045	0.745	1.395	0.221	1.257	0.838	0.851	0.44		
T02 - CathB1	Negative											
T03 - CathB1												
T04 - CathB1												
T05 - CathB1												
T06 - CathB1												

Treatment/Gene	T= 24 hrs	p value	T=72 hrs	p value	T=3 dph	p value	T=5 dph	p value	T=12 dph	p value	T=15 dph	p value
T02 - Thymosin-β4	2.44	0.112	0.717	0.291	1.295	0.312	0.751	0.726	0.859	0.78	ND	
T03 - Thymosin-β4	**2.526**	0	0.751	0.192	1.636	0.183	0.809	0.722	0.97	0.848		
T04 - Thymosin-β4	**8.168**	0	0.937	0.707	2.09	0.096	0.948	0.915	0.812	0.362		
T05 - Thymosin-β4	**8.206**	0	1.059	0.767	1.338	0.445	1.647	0.679	1.151	0.444		
T06 - Thymosin-β4	**5.217**	0	1.045	0.745	1.395	0.221	1.257	0.838	0.851	0.44		
T02 - Cathelicidin 1	1.424	0.607										
T03 - Cathelicidin 1	**5.696**	0.199										
T04 - Cathelicidin 1	**14.791**	0.119										
T05 - Cathelicidin 1	**3.588**	0.313										
T06 - Cathelicidin 1	**7.692**	0.107										
T02 - Cathelicidin 2	0.807	0.741										
T03 - Cathelicidin 2	**4.075**	0.199										
T04 - Cathelicidin 2	**6.543**	0.274										
T05 - Cathelicidin 2	**0.051**	**0.034**										
T06 - Cathelicidin 2	0.243	0.163										
T02 - Cathelicidin 3	1.181	0.819										
T03 - Cathelicidin 3	**2.362**	0.256										
T04 - Cathelicidin 3	**5.229**	0.278										
T05 - Cathelicidin 3	**1.927**	0.726										
T06 - Cathelicidin 3	0.732	0.948										

Table 3.3: Relative gene expression and *p* values of pro-inflammatory cytokines (IL-1β, IL-6, IL-18), Nitric oxide synthase (NOS2A) and chemokine IL8 aka KC/CXCL8 at various time points post vaccination.
Treatment T02, T03, T04, T05 and T06 indicate DLM only, HVT/SB-1, HVT/SB1+DLM, HVT-LT/SB-1, HVT-LT/SB1+DLM respectively. Negative - Ct values greater than 35. ND- Not Determined.

Treatment/Gene	T= 24 hrs	p value	T=72 hrs	p value	T=3 dph	p value	T=5 dph	p value	T=12 dph	p value	T=15 dph	p value
T02 - IL-1B	**0.04**	0	0.381	0.107	1.512	0.536	0.191	0.087	**0.061**	0	ND	
T03 - IL-1B	**0.067**	0.029	0.536	0.286	0.564	0.107	0.157	0.514	0.843	0.434		
T04 - IL-1B	0.14	0.101	1.045	0.793	0.564	0.107	1.257	0.82	0.137	0.034		
T05 - IL-1B	**0.19**	0	1.023	0.934	0.649	0.516	1.67	0.593	0.935	0.418		
T06 - IL-1B	**0.143**	0.063	1.269	0.65	0.564	0.107	0.24	0.548	**0.068**	0.034		
T02 - IL-18	**3.109**	0.092	**0.201**	0	0.885	0.443	1.329	0.596	1.089	0.688	ND	
T03 - IL-18	2.848	0.107	0.986	0.9	1.326	0.374	1.087	0.8	1.304	0.584		
T04 - IL-18	**11.081**	0	0.792	0.498	0.663	0.385	1.087	0.801	1.243	0.504		
T05 - IL-18	**8.225**	0	1.335	0.418	**0.482**	0	1.22	0.801	1.278	0.537		
T06 - IL-18	**7.013**	0.011	0.057	0.208	0.916	0.916	0.737	0.693	1.595	0.119		
T02 - NOS2A	0.483	0.1	1.217	0.35	0.747	0.361	1.05	0.9	1.414	0.635	ND	
T03 - NOS2A	**0.508**	0	0.674	0.434	1.335	0.26	0.79	0.795	1.159	0.66		
T04 - NOS2A	3.264	0.235	0.502	0.2	0.975	0.862	0.48	0.488	1.057	0.85		
T05 - NOS2A	0.701	0.646	0.272	0.019	0.654	0.309	1.079	0.856	0.959	0.84		
T06 - NOS2A	0.702	0.284	0.58	0.034	0.572	0.206	0.617	0.522	1.316	0.527		
T02 - IL-6	Negative								2.445	0.299	**4.67**	0
T03 - IL-6									0.699	0.412	**11.632**	0.063
T04 - IL-6									0.729	0.605	**2.908**	0.063
T05 - IL-6									0.386	0.233	**4.189**	0
T06 - IL-6									0.58	0.325	0.389	0.063
T02 - IL-8	**0.681**	**0.746**	0.425	0.295	1.214	0.116	1.505	0.709	0.857	0.102	ND	
T03 - IL-8	**1.401**	**0.591**	**0.599**	0.099	1.157	0.196	1.266	0.9	0.542	0.019		
T04 - IL-8	**4.574**	**0.029**	**0.505**	0.067	0.565	0.016	1.231	0.833	0.526	0.034		
T05 - IL-8	**2.633**	**0**	0.735	0.101	0.666	0.135	1.733	0.518	1.234	0.299		
T06 - IL-8	**1.157**	**0.203**	0.048	0.053	0.481	0.016	1.209	0.848	0.831	0.154		

Table 3.4: Relative gene expression and *p* values of Type I & II IFNs and IFN stimulated genes (ISGs MX1, OASL, MHC I, MHC II). Treatment T02, T03, T04, T05 and T06 indicate DLM only, HVT/SB-1, HVT/SB1+DLM, HVT-LT/SB-1, HVT-LT/SB1+DLM respectively. Negative - Ct values greater than 35. ND- Not Determined.

Treatment/Gene	T= 24 hrs	p value	T=72 hrs	p value	T=3 dph	p value	T=5 dph	p value	T=12 dph	p value	T=15 dph	p value
T02 - IFN-a	0.275	0.153	1.58	0.426	0.52	0.22	0.704	0.514	2.822	0.4	ND	
T03 - IFN-a	0.384	0.245	0.761	0.596	0.343	0	0.079	0	0.663	0.635		
T04 - IFN-a	2.114	0.713	0.309	0.192	0.903	0.603	0.117	0.034	1.014	0.953		
T05 - IFN-a	0.343	0.287	0.497	0.295	0.857	0.697	0.159	0	0.079	0.133		
T06 - IFN-a	0.251	0.162	0.161	0.2	3.622	0.092	0.55	0.338	0.55	0.338		
T02 - Mx	**4.209**	0.099	0.776	0.395	1.823	0.631	0.32	0.379	**6.665**	0.063	ND	
T03 - Mx	**0.26**	0.037	**35.017**	0	**27.987**	0.072	2.976	0.199	**6.948**	0.029		
T04 - Mx	**4.5**	0.233	**34.456**	0	**58.62**	0.072	**12.467**	0	**6.306**	0		
T05 - Mx	0.472	0.114	**15.491**	0.034	**4.801**	0.072	1.786	0.601	**4.479**	0.029		
T06 - Mx	1.094	0.9	**4.438**	0	**6.148**	0.072	1.927	0.437	**6.148**	0.029		
T02 - OAS-L	**1.963**	0.102	0.547	0.13	1.516	0.63	3.802	0.495	**4.616**	0	ND	
T03 - OAS-L	**0.111**	0	2.591	0.071	**10.126**	0.072	0.843	1	3.19	0.105		
T04 - OAS-L	1.316	0.693	1.625	0.251	**41.451**	0.072	1.896	0.753	2.25	0.205		
T05 - OAS-L	**0.21**	0	0.827	0.702	**52.104**	0.088	8.594	0.208	0.809	0.835		
T06 - OAS-L	**0.357**	0.063	0.493	0.2	**78.068**	0.072	2.537	0.57	**4.307**	0		
T02 - IFN- ɣ	0.977	0.801	0.623	0.2	1.526	0.223	1.149	0.671	1.184	0.694	2.822	0
T03 - IFN- ɣ	0.961	0.852	0.705	0.392	5.134	0.08	2.099	0.286	1.901	0.063	4.959	0.1
T04 - IFN- ɣ	1.936	0.341	0.712	0.303	5.401	0.072	4.337	0.164	1.072	0.544	2.373	0.192
T05 - IFN- ɣ	0.654	0.412	0.502	0.105	2.573	0.072	11.081	0.072	1.53	0.033	2.124	0.41
T06 - IFN- ɣ	0.597	0.308	0.739	0.307	1.823	0.084	11.184	0.088	2.214	0.029	1.347	0.705
T02 - MHC I	1.892	0.251	0.734	0.295	0.984	0.925	0.905	0.826	1.24	0.23	ND	
T03 - MHC I	**2.77**	0.048	1.04	0.814	1.353	0.175	0.81	0.745	1.104	0.426		
T04 - MHC I	**6.233**	0	1.154	0.547	1.959	0.072	1.077	0.968	0.989	0.699		
T05 - MHC I	2.417	0.483	1.028	0.86	1.149	0.602	0.419	0.238	**1.344**	0		
T06 - MHC I	1.437	0.635	0.024	0.188	1.613	0.395	0.636	0.613	1.363	0.033		
T02 - MHC II	1.512	0.564	**0.38**	0.04	1.275	0.468	1.457	0.101	0.97	0.849	ND	
T03 - MHC II	2.412	0.42	0.663	0.099	1.491	0.249	1.203	0.105	1.115	0.55		
T04 - MHC II	4.823	0.092	0.739	0.396	1.04	0.873	1.392	0.033	0.937	0.643		
T05 - MHC II	**5.54**	0	**0.729**	0	0.704	0.286	1.625	0.792	1.115	0.498		
T06 - MHC II	2.491	0.306	0.092	0.606	1.087	0.867	0.883	0.293	1.074	0.719		

Table 3.5: Relative gene expression and *p* values of Immune patterning molecules for M1 macrophage (SOCS3) M2 macrophage (SOCS2 & 3), Th1 (Tbet, IL-12p40 subunit), Th2 (GATA3, IL-4, IL10, IL-13), Nitric oxide synthase (NOS2A) and IL-12p19 subunit at various time points post vaccination. Treatment T02, T03, T04, T05 and T06 indicate DLM only, HVT/SB-1, HVT/SB1+DLM, HVT-LT/SB-1, HVT-LT/SB1+DLM respectively. Negative - Ct values greater than 35. ND- Not Determined.

Gene Analysis/Treatment	T= 24 hrs	p value	T=72 hrs	p value	T=3 dph	p value	T=5 dph	p value	T=12 dph	p value	T=15 dph	p value
T02 - SOCS1	**0.469**	0	0.885	0.741	1.146	0.729	0.843	0.693	1.963	0.194	ND	
T03 - SOCS1	0.419	0.1	0.675	0.267	1.853	0.072	0.935	0.9	1.082	0.806		
T04 - SOCS1	2.591	0.375	0.556	0.253	2.423	0.072	1.64	0.46	0.986	0.9		
T05 - SOCS1	0.734	0.292	0.408	0.188	0.877	0.629	0.849	0.688	0.663	0.367		
T06 - SOCS1	0.459	0.063	**0.114**	0	1.209	0.661	1.04	0.953	0.903	0.653		
T02 - SOCS2	0.669	0.278	1.141	0.616	1.087	0.616	0.833	0.67	0.984	0.887	ND	
T03 - SOCS2	1.569	0.107	0.756	0.327	1.146	0.561	0.712	0.667	0.885	0.411		
T04 - SOCS2	**2.969**	0	0.739	0.1	1.035	0.988	0.859	0.824	0.841	0.254		
T05 - SOCS2	**2.153**	0	0.935	0.642	0.664	0.107	0.606	0.409	0.959	0.772		
T06 - SOCS2	1.165	0.631	0.074	0.26	0.94	0.837	0.548	0.415	0.835	0.163		
T02 - SOCS3	0.471	0.187	0.97	0.798	1.167	0.709	0.887	0.625	1.478	0.4	ND	
T03 - SOCS3	0.498	0.102	**0.636**	0	1.392	0.26	0.839	0.854	0.709	0.323		
T04 - SOCS3	4.141	0.17	0.403	0.2	1.064	0.678	0.993	0.963	0.658	0.357		
T05 - SOCS3	1.289	0.601	0.354	0.067	0.472	0.107	0.559	0.397	0.461	0.034		
T06 - SOCS3	0.865	0.901	**0.093**	0	0.979	0.912	0.441	0.468	0.545	0.139		
T02 - Tbet	1.576	0.293	0.685	0.188	1.082	0.881	1.441	0.207	0.905	0.973	ND	
T03 - Tbet	2.09	0.107	0.809	0.307	1.203	0.454	1.467	0.167	1.495	0.248		
T04 - Tbet	**8.263**	0	0.822	0.323	**0.241**	0	1.647	0.1	1.012	0.929		
T05 - Tbet	**4.367**	0	0.646	0.311	**0.115**	0.028	2.777	0.279	1.102	0.635		
T06 - Tbet	**2.949**	0	0.839	0.602	**0.218**	0	0.944	0.9	1.464	0.214		
T02 - GATA3	1.945	0.616	0.649	0.208	0.984	0.948	**2.255**	0	1.012	0.719	ND	
T03 - GATA3	3.775	0.237	1.055	0.898	0.979	0.821	1.883	0.105	1.54	0.259		
T04 - GATA3	**6.884**	0	1.012	0.809	0.879	0.9	1.558	0.386	0.989	0.953		
T05 - GATA3	**6.574**	0.053	1.007	0.934	**0.434**	0	1.866	0.739	1.097	0.317		
T06 - GATA3	**4.521**	0	Negative		0.705	0.32	0.419	0.261	1.498	0.033		
T02 - IL-10	**0.092**	0.087	1.888	0.306	0.374	0.259	0.685	0.967	2.573	0.56	22.264	0.2
T03 - IL-10	**0.042**	0	0.788	0.9	0.542	0.639	0.68	0.9	1.237	0.934	25.398	0.034
T04 - IL-10	**Negative**		0.195	0.253	0.689	0.728	0.603	1	0.816	0.759	49.982	0
T05 - IL-10	**0.021**	0	**0.173**	0	0.378	0.307	0.421	0.621	**0.116**	0	80.635	0
T06 - IL-10	**0.02**	0.034	0.197	0.253	0.557	0.618	0.535	0.713	0.394	0.432	6.049	0.101
T02 - IL-13	Negative		0.732	0.328	0.91	0.726	2.319	0.306	0.968	0.9	1.316	0.807
T03 - IL-13			1.033	0.933	0.73	0.191	1.729	0.305	1.173	0.184	1.548	0.406
T04 - IL-13			0.875	0.395	0.311	0.067	1.151	0.793	0.867	0.549	1.558	0
T05 - IL-13			1.157	0.8	**0.218**	0	1.64	0.749	1.079	0.637	1.411	0.414
T06 - IL-13					0.44	0.175	0.391	0.194	1.067	0.652	1.266	0.207
T02 - p19	0.327	0.102	0.666	0.412	1.045	0.981	0.799	0.738	2.751	0.299	ND	
T03 - p19	0.252	0.154	0.445	0.099	1	0.801	0.672	0.695	1.313	0.543		
T04 - p19	0.651	0.913	0.303	0.2	0.694	0.294	0.699	0.596	1.478	0.516		
T05 - p19	**0.137**	0	0.231	0.101	**0.555**	0	0.916	0.623	0.311	0.168		
T06 - p19	0.117	0.081	Negative		1.451	0.675	0.369	0.308	0.669	0.465		
T02 - p40	1.461	0.56	0.469	0.147	1.072	0.787	1.509	0.298	1.441	0.518	ND	
T03 - p40	**3.249**	0.037	0.955	0.962	0.611	0.092	0.869	0.861	2.033	0.25		
T04 - p40	**4.438**	0.037	1.122	0.801	0.348	0.016	1.141	0.754	1.474	0.447		
T05 - p40	**3.109**	0.037	1.467	0.299	0.293	0.013	1.295	0.794	1.548	0.53		
T06 - p40	**2.346**	0.037	0.156	0.139	0.513	0.028	0.568	0.293	2.335	0.009		
T02 - IL-4	Negative								4.218	0.336	12.936	0.152
T03 - IL-4									1.323	0.872	30.344	0.295
T04 - IL-4									1.089	1	**12.042**	0
T05 - IL-4									0.062	0.123	**36.674**	0
T06 - IL-4									0.45	0.453	1.372	0.713

Table 3.6: Relative gene expression and *p* values of sirtuins (SIRT-1, -2, -3, -4, -5 and -6) at various time points post vaccination. Treatment T02, T03, T04, T05 and T06 indicate DLM only, HVT/SB-1, HVT/SB1+DLM, HVT-LT/SB-1, HVT-LT/SB1+DLM respectively. Negative - Ct values greater than 35. ND- Not Determined. Gene expression analyses was not determined for the remaining time points.

Gene Analysis/Treatment	T= 24 hrs	p value	T=72 hrs	p value
T02 - SIRT1	1.231	0.747	0.322	0.024
T03 - SIRT1	2.502	0.121	0.658	0.338
T04 - SIRT1	**10.411**	0	0.642	0.2
T05 - SIRT1	**15.348**	0	1.251	0.446
T06 - SIRT1	**5.063**	0	Negative	
T02 - SIRT2	1.055	0.801	0.64	0.107
T03 - SIRT2	1.682	0.104	0.717	0.107
T04 - SIRT2	3.249	0.112	0.847	0.306
T05 - SIRT2	**3.613**	0	0.645	0.174
T06 - SIRT2	**3.249**	0	Negative	
T02 - SIRT3	0.22	0.116	0.761	0.099
T03 - SIRT3	**0.158**	0	**0.524**	0
T04 - SIRT3	2.597	0.415	**0.301**	0
T05 - SIRT3	0.603	0.57	0.314	0.008
T06 - SIRT3	0.361	0.131	0.063	0.016
T02 - SIRT4	0.667	0.492	0.747	0.236
T03 - SIRT4	1.146	0.822	0.604	0.136
T04 - SIRT4	**4.947**	0	0.473	0.068
T05 - SIRT4	**2.44**	0	0.541	0.117
T06 - SIRT4	**1.591**	0	Negative	
T02 - SIRT5	1.977	0.105	0.768	0.31
T03 - SIRT5	**2.789**	0	0.95	0.707
T04 - SIRT5	**6.409**	0	0.859	0.62
T05 - SIRT5	**9.232**	0	1.197	0.388
T06 - SIRT5	**5.242**	0	Negative	
T02 - SIRT6	**1.866**	0	0.491	0.148
T03 - SIRT6	**2.129**	0	0.689	0.307
T04 - SIRT6	**5.911**	0	0.655	0.053
T05 - SIRT6	**6.438**	0	0.643	0.101
T06 - SIRT6	**2.815**	0	Negative	

Table 3.7: Relative gene expression and *p* values of cell population markers representing immature and mature T cells (CD3), T helper cells (CD4), cytotoxic T cells and a lower proportion of dendritic cells (CD8), B cells (BU.1), Natural Killer cells and cytotoxic T cells (CD107), dendritic cells (CD11c) and macrophages (CD18) at various time points post vaccination. Treatment T02, T03, T04, T05 and T06 indicate DLM only, HVT/SB-1, HVT/SB1+DLM, HVT-LT/SB-1, HVT-LT/SB1+DLM respectively. Negative- Ct values greater than 35. Gene expression analyses was not determined for the remaining time points.

Gene Analysis/Treatment	T= 24 hrs	p value	T=72 hrs	p value	T=3 dph	p value	T=5 dph	p value	T=12 dph	p value
T02 - CD3	4.521	0.092	0.45	0.155	**16.074**	0.029	0.686	0.54	0.699	0.092
T03 - CD3	**8.112**	0	**0.475**	0	**43.111**	0.072	0.658	0.54	1.146	0.664
T04 - CD3	**23.807**	0.034	0.634	0.26	**208.9**	0.072	0.916	0.749	0.767	0.199
T05 - CD3	**29.514**	0	0.667	0.265	**219.286**	0.072	0.734	0.514	0.839	0.571
T06 - CD3	**18.679**	0.029	0.92	0.793	**188.271**	0.029	0.835	0.948	1.151	0.555
T02 - CD8A	**0.416**	0	0.751	0.692	**1.643**	0.029	0.881	0.586	1.372	0.087
T03 - CD8A	1.178	0.713	0.753	0.128	1.335	0.272	0.968	0.837	1.991	0.063
T04 - CD8A	**10.056**	0	0.64	0.101	0.912	0.49	0.961	0.953	1.54	0.15
T05 - CD8A	3.689	0.16	0.697	0.295	0.73	0.323	**0.402**	0.063	**2.023**	0.033
T06 - CD8A	**2.567**	0	0.643	0.204	0.922	0.905	0.461	0.506	**2.928**	0.048
T02 - CD4	0.435	0.101	**0.606**	0	0.944	0.74	1.021	0.9	1.79	0.279
T03 - CD4	0.373	0.102	0.55	0.2	1.617	0.267	0.537	0.433	2.555	0.1
T04 - CD4	4.469	0.107	0.686	0.754	3.06	0.159	0.742	0.702	2.099	0.2
T05 - CD4	1.713	0.361	0.903	0.9	1.097	0.694	1.263	0.71	**2.526**	0
T06 - CD4	1.122	0.9	**0.17**	0	2.526	0.175	1.424	0.556	**3.597**	0
T02 - CD107/LAMP1	1.61	0.606	1.159	0.656	1.17	0.429	0.905	0.9	1.275	0.188
T03 - CD107/LAMP1	**3.767**	0.029	1.693	0.697	1.248	0.559	1.149	0.749	1.069	0.564
T04 - CD107/LAMP1	**16.488**	0	1.17	0.701	0.742	0.604	1.04	0.9	0.767	0.486
T05 - CD107/LAMP1	**14.723**	0	1.573	0.308	0.599	0.309	0.477	0.3	1.045	0.553
T06 - CD107/LAMP1	**2.139**	0	1.22	0.621	0.618	0.206	0.457	0.506	1.176	0.512
T02 - BU.1	**0.2**	0.034	1.35	0.265	1.04	0.828	0.509	0.342	0.714	0.31
T03 - BU.1	**0.237**	0.053	1.159	0.299	1.146	0.578	0.545	0.429	0.742	0.189
T04 - BU.1	2.777	0.409	0.851	0.506	1.263	0.379	0.588	0.514	1.021	0.929
T05 - BU.1	0.81	0.592	0.709	0.402	1.509	0.487	**0.322**	0	0.914	0.559
T06 - BU.1	1.721	0.308	1.217	0.199	1.617	0.792	0.222	0.207	0.734	0.43
T02 - CD11c	1.454	0.607	0.363	0.101	0.95	0.783	1.968	0.59	0.666	0.428
T03 - CD11c	**4.459**	0.17	0.643	0.263	0.767	0.123	1.404	0.813	**0.705**	0
T04 - CD11c	**5.016**	0.256	0.569	0	0.568	0.022	0.809	0.661	0.933	0.619
T05 - CD11c	**1.733**	0.621	0.563	0	0.483	0.171	0.935	0.9	1.217	0.22
T06 - CD11c	**3.272**	0.306	Negative		0.979	0.9	0.388	0.214	**1.341**	0.046
T02 - CD18	Negative		0.543	0.072	0.837	0.567	1.12	0.313	1.077	0.639
T03 - CD18			0.652	0.291	0.95	0.928	0.948	0.505	1.064	0.856
T04 - CD18			0.643	0.088	0.875	0.509	0.772	0.305	1.079	0.299
T05 - CD18			0.554	0.081	0.694	0.197	0.792	0.953	**1.251**	0.033
T06 - CD18			0.065	0.379	1.115	0.774	**0.456**	0.038	**1.551**	0.033

Chapter 4

COMPARISON OF SIZE, CONCENTRATION, AND MIRNA EXPRESSION PROFILES OF SERUM EXOSOMES PURIFIED VIA ULTRACENTRIFUGATION AND TOTAL EXOSOME ISOLATION (TEI) REAGENT

4.1 Introduction

Extracellular vesicles (EVs) are phospholipid bilayer-enclosed, spherical particles released by a variety of cell types into biological fluids such as blood, urine, breast milk, bile, bronchoalveolar lavage, genital, cerebrospinal, ascitic and amniotic fluids, as well as by cultured cells *in vitro* (220-226). Based on their size, origin, and biogenesis, they are categorized into microvesicles, exosomes and apoptotic bodies (227).

Microvesicles range in size from 100-1000 nm and directly bud from the plasma membrane (PM) (228). Exosomes range in size from 30-150 nm and originate in late endosomes or multi-vesicular bodies (MVBs) upon inward invagination of the endosomal-limiting membrane. MVB fusion with the PM leads to the release of exosomes into the extracellular space (228). Apoptotic bodies range in size between 50-5000 nm and originate from cells undergoing apoptosis via a blebbing mechanism (228).

Among EVs, exosomes are considered crucial vehicles for intercellular communication as they carry functionally active messenger RNAs (mRNAs), micro RNAs (miRNAs), proteins, and lipids between cells to mediate a range of biological effects upon target cell binding and uptake (228). The ease of collection of biological fluids (e.g. blood, urine), and capacity of exosomes to reflect the physiological or pathological state of the originating cell, led to the proposition that exosomal miRNAs and/or proteins can serve as excellent biomarkers for disease diagnosis or prognosis (228-230). Amid growing enthusiasm in utilizing exosomes for biomarker identification and discovery, there lacks a technical standardization in the procedures employed to purify and analyze EVs, including exosomes (231). The influence of various procedures on exosome size, integrity, and recovery, and its effect on their RNA and protein content remains unclear. Hence, there is a need to provide a definition of "best practices" and standardization of exosome purification procedures (231).

Current exosome purification procedures in use include classical differential ultracentrifugation (UC) (232), density gradient UC (sucrose/iodixanol) (233, 234), size exclusion chromatography (SEC) (234), ultrafiltration (235), marker-based immune affinity isolation (236), microfluidic devices (237), commercial polymer-based precipitation reagent kits (ExoQuick^{TM} , System Biosciences), Total Exosome Isolation reagent (TEI, Invitrogen), miRCURY (Qiagen) (238-240) and volume excluding polymers (Polyethylene Glycol [PEG], dextran and polyvinyls) (241).

For further enrichment of exosome fractions from culture or biological fluids, paired combinations of aforementioned methods have been employed including microfiltration paired with UC, UC paired with density gradient UC, and PEG paired

with an UC wash (241). Among above procedures, UC is the conventional gold standard procedure which is technically-laborious, time-consuming, requires special equipment and training, making it unsuitable for use in a routine diagnostic laboratory (232, 242).

Alternatively, commercial precipitation reagent kits currently available offer quick and easy procedures that require low input sample with no specialized equipment or training (243). Furthermore, a handful of studies evaluated the qualitative and quantitative performance of UC versus various commercial precipitation reagent kits, in terms of exosome recovery and downstream miRNA/protein expression from human serum (242, 244-249). These studies reported superior exosome recovery and greater exosomal miRNA and/or protein content by the commercial precipitation reagent kits compared to traditional UC. On the other hand, no study has thus far evaluated the performance of a commercial exosome precipitation reagent kit in comparison to UC in terms of exosome recovery from animal serum.

In the present work, we performed a comparative study of exosome purification procedures, UC versus TEI reagent, to determine to what extent the selected exosome purification procedure influenced size, concentration, integrity and miRNA content of serum exosomes from Marek's Disease Virus-infected chickens (250). By employing Illumina high-throughput sequencing platform, we identified significant and differentially-expressed (SDE) exosomal miRNAs in the serum of CVI988-vaccinated and protected leghorns, and unvaccinated leghorns that were found to be tumor-bearing (Chapter 5 of present thesis). In the present chapter, we validated the expression of (6) *G.gallus* (gga-) and (4) MDV-1(MDV1-) SDE

miRNAs, selected based on their expression ranging from low (gga-mir-21, MDV1-mir-M4, -M12, -M6 and –M8) to high (gga-mir-146b, -10b, -2188, -27b, and -99a) in exosomes purified from CVI988-vaccinated and protected leghorn sera referred to as "Vaccinate Exosomes" (VEX) compared to exosomes purified from MD tumor-bearing unvaccinated leghorn sera referred to as "Tumor Exosomes" (TEX).

4.2 Materials and Methods

4.2.1 Serum Sample sources and collection

Serum exosomes were purified from commercial broiler chickens used in a vaccine trial. Specific samples are detailed in Table 4.1 (below). Essentially, commercial broilers were either inoculated with the TK2a-strain of virus (Shedders), unvaccinated (Contact-exposed, challenge controls) or vaccinated at one day-of-age with a 1X commercial dose (~3,500 PFU) of a CVI988 (Rispens) vaccine and placed in contact with two-week old, MDV-inoculated (vv+MDV, strain TK2a-inoculated) "shedder" chickens, as described previously (91, 213).

At cull (MD+, MDV-inoculated chickens) or necropsy (vaccinated and protected chickens), whole blood was collected via cardiac puncture using a 10 cc syringe with 18-gauge needle with no anticoagulant. For obtaining sera, syringes were stored at 37˚C for 1 hr and then left at 4˚C overnight. Serum samples collected and stored at -80˚C until processed for exosome purification, as described below. The vaccine efficacy study was approved under IACUC protocol #64R-2016-0, addendum 1 and USDA APHIS permit # 130630.

4.2.2 Exosome purification

Exosome purification was carried out by Ultracentrifugation (UC) and Total Exosome Isolation (TEI) precipitation solution procedures. In order to avoid miRNA expression differences due to inter-bird variations, serum samples from the same bird were used for both exosome purification procedures (see Table 4.1).

4.2.2.1 Ultracentrifugation (UC)

Ultracentrifugation was carried out as described by Thery *et al* (233). Exosome fraction from 1mL serum was purified by four consecutive centrifugation steps. Serum was diluted with equal volume of PBS and centrifuged at 300 ×*g* for 10 min followed by 2000 × *g* for 30 min to pellet cells and cell debris, respectively. Next, a centrifugation step was performed at 12,000 ×*g* for 45 min to pellet microvesicles, followed by the transfer of supernatants to 1.5 ml polyallomer ultracentrifuge tubes (Beckman Coulter, Fullerton, CA). Ultracentrifugation was performed for an hour at 110,000 × *g* (Beckman Coulter Optima MAX, TLA-55 fixed angle rotor, *k-factor* 66). Exosome pellets were re-suspended and washed in 1ml PBS and the ultracentrifugation step was repeated. All centrifugation steps were performed at 4˚C. Final exosome pellets were re-suspended in 1X PBS and aliquots were stored at -80˚C.

4.2.2.2 Total Exosome Isolation precipitation (TEI)

Exosomes were purified from 200 µl of serum using TEI reagent (Invitrogen) according to manufacturer's recommendations. Briefly, 1/5 volume of TEI reagent was combined with serum and incubated at 4˚C for 30 min. The mixture was centrifuged at 10,000 ×g for 10 min at room temperature. Supernatants were aspirated and exosome pellets were re-suspended in 1X PBS.

4.2.3 Nanoparticle tracking analysis (NTA)

Concentration, mean size, and size distribution profile of particles purified via UC or TEI reagent were evaluated using a Nanosight NS300 instrument (Malvern, Worcestershire, UK) and analyzed with NTA 3.2 Dev Build 3.2.16 software. The following post-acquisition analysis settings were selected: minimum detection threshold 4, automatic blur, and automatic minimum expected particle size. Samples were diluted 1:20 (TEI) or 1:100 (UC) in PBS to obtain concentration profiles directly comparable between particles purified from 200 µl input serum (TEI) versus 1ml input serum (UC). This dilution strategy allowed us to achieve measured mean particle concentration $0.6–4x10^9$/ml. For each sample, five 1 min videos were recorded and analyzed in batch processing mode. Videos were recorded at camera level 9 with minimum expected particle size, track length, and blur setting, all set to default.

4.2.4 Transmission Electron Microscopy (TEM)

TEM analyses of exosomes was performed on nickel TEM glow discharged grids (Electron Microscopy Sciences), 400 mesh with a formvar-coated carbon film. Grids were floated on the drops of purified exosome-PBS suspensions to allow adsorption for 5 min and then were wicked off with a filter paper. TEI reagent purified exosomes were diluted 1:10 before adsorption to prevent vesicle overcrowding and allow greater resolution. Following a series of washes in water, grids were negatively-stained in a solution of 1% uranyl acetate and a phospholipid stain. Air-dried grids were observed under TEM (Zeiss Libra 120) at 80 kv and imaged using a Gatan Ultrascan 1000 2k x 2k CCD camera in the bioimaging core at the Delaware Biotechnology Institute at the University of Delaware. For each set of analyses, at

least 20 fields were imaged of exosomes purified by each method, representative images are shown.

4.2.5 RNA isolation, reverse transcription and qRT-PCR analysis

For total RNA isolation, 100 µl of exosome-PBS suspensions were combined with 1ml Trizol reagent (Invitrogen™) and total RNA (m/miRNAs) extraction was carried out according to manufacturer's recommendations. Total RNA (0.5µG) isolated via Trizol procedure was DNAse treated (Ambion) before polyadenylation and reverse transcription (90 min at 37˚C) with an Oligo-dT primer that contained a universal tag on its 5' end (Universal mir-RT; Qiagen Inc.,) (251). For qRT-PCR expression analyses of miRNAs, cDNAs were diluted 1:4 and subjected to a first PCR cycle with a forward primer specific to the miRNA of interest. Subsequent PCR cycles were carried out by the miRNA specific forward primer and a reverse primer spanning the universal tag (see Table 4.2).

Exosomal miRNA expression in VEX relative to TEX was calculated upon normalization to the global geometric means of C_t values. Reaction conditions included 1 µl of the diluted cDNA in a 20 µl total reaction volume consisting of 10 µl iTaq SYBR® Green Supermix (Bio-Rad, Hercules, CA), 8.2 µl of nuclease-free water and 0.4 µl (250 nM) of each forward and reverse primer. All reactions, including no template controls and no reverse transcription controls, were performed in duplicates. Cycling conditions included a PCR activation step (15 min at 95°C) followed by 40 cycles of denaturation (15 secs at 94°C), annealing (30 secs at 55°C) and extension (30 secs at 70°C). Following amplification, melt curve analysis was performed at temperatures ranging from 55-95˚C in 0.5 ˚C˚ increments (81 cycles) for 2-3 sec per

cycle to confirm lack of non-specific amplification. Primer sequences are provided in Table 4.2.

4.2.6 Statistical analysis

For statistical analyses, MS excel and GraphPad Prism 5 (GraphPad Software, CA, USA) were used. miRNA C_t values were presented as C_t means ± SD. To compare significant differences in miRNA C_t values between VEX and TEX, an unpaired t-test was used. For correlation analyses between purification methods, the Pearson's correlation coefficient was calculated. The significance threshold was set to a fold change ≥ 2 with a $p\ value \leq 0.05$.

4.3 Results

4.3.1 Comparison of size, yield and integrity of particles purified by UC and TEI reagent kit

Size, size distribution, and concentration profile of particles purified by UC and TEI reagent were quantified through NTA. The size distribution profile of particles purified by either UC or TEI reagent fell within the anticipated exosome size range of 30 – 150 nm. Mean diameters of UC-purified particles were 106.3 ± 46.3 nm and 105.6 ± 41.9 nm for VEX and TEX, respectively with an overall mean of 106 nm (Fig. 4.1A). TEI reagent-purified particles displayed slightly higher mean diameter of 121 ± 57.1 nm and 184.1 ± 50.9 nm for VEX and TEX, respectively with an overall mean diameter of 152.6 nm. The diameter of a majority of UC-purified particles was ca. 73 and 74.9 nm for VEX and TEX, respectively, whereas a majority of TEI reagent-purified particles had a diameter of 77.6 and 181.1 nm for VEX and TEX, respectively (Fig. 4B, 4C, 4D, 4E). Overall, TEI reagent-purified particles displayed

significantly higher overall size compared to UC-purified particles. Particle concentrations in UC- and TEI reagent-purified fractions fell within the range of 0.6-1 and 2 - 4 billion per mL of serum, respectively. Although the TEI reagent yielded slightly higher number of particles/ml, this difference was not statistically different (Fig. 4F).

4.3.2 Visualization of exosome morphology by TEM

Upon finding that the diameters of particles purified by both the procedures fell within the expected size range of exosomes, we further confirmed the morphological integrity of purified particles via TEM, a well-accepted technique for nanoparticle validation. Negative staining of VEX and TEX particles purified by each procedure displayed typical spherical morphology within the anticipated size range of exosomes (Fig. 4.2). Interestingly, although TEM is not a quantitative technique, we found a greater number of exosomes per field in TEI-purified fractions and this number appeared slightly higher for TEX compared to VEX (Fig. 4.2) (252). Furthermore, as described in the methods section, TEI-purified particles had to be diluted 1:10 before adsorption onto TEM grid to prevent vesicle overcrowding. Overall, our TEM analysis verified that both the procedures successfully isolated exosomes with an acceptable size range and morphology.

4.3.3 Exosomal miRNA analysis by RT-qPCR

As we surmised that there may be differences in the expression of chicken and MDV miRNAs in exosomes purified by different methods, we examined the expression of select miRNAs (UC, n = 6; and TEI reagent, n = 6) by qRT-PCR. Both purification procedures permitted the detection of all analyzed miRNAs above the

detection limit (C_t < 35) (Table 4.3). Based on the raw C_t values, the miRNA threshold detection levels were on average 2.35 cycles lower in TEI reagent-purified exosomes, with an average of 0.96 and 3.73 cycles lower C_t values observed in VEX and TEX, respectively. These data indicate that the total miRNA content in TEI reagent-purified exosomes is higher than that of UC-purified exosomes. The most and the least abundant miRNAs in VEX were similar between the purification procedures.

In contrast, the most and the least abundant miRNAs in TEX were quite different between the purification procedures. For instance, in TEX, gga-mir-27b-3p and -10b-5p were of highest and lowest abundance, respectively, in TEI-reagent purified exosomes, as opposed to gga-miR-2188-5p and -146b-5p in UC-purified exosomes (Table 4.3).

In terms of miRNA expression in VEX, a strong correlation was observed between the two purification procedures (Fig. 4.3A, Pearson r = 0.85, $p<0.0001$), whereas in TEX, weak correlation was observed between the two purification procedures (Fig. 4.3B, Pearson r = 0.55, $p<0.0016$).

Finally, relative miRNA expression levels in VEX compared to TEX also exhibited a strong correlation between the two purification procedures (Fig. 4.3C, Pearson r = 0.9, $p <0.003$). Expression of miRNA was uniquely dependent on the exosome purification procedure. However, in TEI-purified exosomes, MDV1-mir-M4, gga-mir-2188 and –mir-146b displayed 2.2-, 2.6- and 2.1-fold higher expression in VEX compared to TEX respectively (Fig. 4.3D). Similarly, gga-mir-99a and -21 displayed 2- and 4-fold greater level repression, respectively.

4.3.4 Protein content of TEI-reagent purified exosomes

Upon confirming greater particle recovery and miRNA content of exosomes purified by TEI-reagent we further confirmed the protein content of TEI-reagent purified exosomes by probing for one of the molecules of antigen presentation expressed in exosomes (MHC I). We picked MHC class I due to the current lack of antibodies to detect exosome marker proteins (CD63, CD81, tsg101, Alix) in chicken. We were able to successfully detect MHC I both in VEX and TEX while UC-purified exosomes from HTC culture supernatants served as controls (Fig 4.4).

4.4 Discussion

In the present study, we compared the efficiency of two different exosome purification procedures, one based on serial ultracentrifugation steps and the other based on a polymer-based precipitation solution that is available commercially. Our starting sample was chicken serum obtained from an MD vaccine trial using commercial meat-type chickens that were either CVI988-vaccinated and protected against MD (as determined at necropsy) or unvaccinated and showed MD clinical signs, including visceral tumors. Particles purified by both the procedures were subject to quantitative comparisons in terms of the physical properties of the particles, the particle yield, and the miRNA content. Based on the precedent that cancer patient sera and transformed cell line supernatants harbor greater number of exosomes, we further refined our comparison to exosomes from the serum of vaccinated and protected chickens (VEX) and of unvaccinated tumor bearing chickens (TEX) (253, 254).

Using NTA and TEM imaging, we confirmed that both the procedures isolated particles within the size range of exosomes (30-150 nm) and with the spherical morphology. TEI reagent co-purified particles with greater size compared to UC and

this size heterogeneity was higher for TEX particles. This result contrasted with a previous study, where exosome recovery efficiency of three commonly used commercial kits (ExoQuick, TEI, miRCURY) was compared to UC (247). From pooled human sera, UC yielded particles with greater diameter compared to three commercial kits, although this result was not reproduced when the authors used individual human serum samples. In the same study, all three kits yielded higher number of particles compared to UC.

In another study, where the efficiency of exosome recovery from human serum was compared between UC and ExoQuick, a higher particle yield was demonstrated with ExoQuick (255). In our study although the TEI reagent yielded slightly higher number of particles per mL, the difference was not significant. On the other hand, in our TEM field images, TEI-reagent purified fractions displayed consistently greater number of particles consistent with exosome size and morphology compared to UC-derived fractions. The source for this discrepancy is unknown.

Since NTA is an optical method that cannot distinguish protein aggregates from EVs, we surmise that UC-purified fractions may harbor a significant amount of non-exosomal aggregates of protein or lipoprotein (252). Supporting our conjecture, serum exosomes purified by UC on a 30% sucrose cushion contained significant amounts of albumin and IgG contaminants compared to those purified by ExoQuick™ (255). Additionally, viscous biofluids such as plasma (1.65 *centipoise* [Cp]) and serum (1.4Cp) were found to have lower sedimentation efficiency compared to less viscous cell culture conditioned media (1.1Cp) (256). To overcome this issue, longer ultracentrifugation times were recommended, although ultracentrifugation for periods longer than 4 hrs can lead to vesicle rupture or fusion (255-257).

An additional factor that needed to be considered was the mode of action of polymeric precipitation reagents which capture and collect particles of a certain size range (60–150 nm) conforming to exosome size range in ‘‘polymer nets’’ that can be pelleted by a simple, low or high speed centrifugation using a bench top microcentrifuge (243). Once pelleted, the supernatant containing excess polymer is discarded and the exosomes are resuspended in PBS to dilute any residual polymer and release the exosomes from polymer net. In this regard, polymeric reagents also co-purify protein complexes along with exosomes. Although the purity of particle fractions can be assessed by quantifying albumin and organelle marker proteins, such assessment is beyond the scope of current study.

In the present study, the miRNA expression profile in the serum exosome samples purified with the TEI reagent was compared to those purified using the standard UC method. Among the four MDV1 miRNAs profiled, two belonged to the oncogene *meq* cluster (MDV1-mir-M12 and –M4), whereas the other two belonged to latency-associated transcript (LAT) cluster (MDV1-mir-M8 and –M6) (106). From our high throughput sequencing study of exosomal small RNAs in VEX and TEX from leghorn sera, we noticed a significantly higher expression of both *meq* and LAT cluster miRNAs in TEX relative to VEX (3.4, 10.8, 3.8 and 8.1-fold for -M12, -M4, -M8 and -M6 miRNAs, respectively). Upon qRT-PCR validation of the expression of above miRNAs, we confirmed lower level expression of –M12 and –M8 miRNAs in VEX relative to TEX, at a comparable level in exosomes purified by both the procedures. Intriguingly, -M4 and –M6 miRNAs displayed higher expression in VEX relative to TEX. The reason for this discrepancy is unknown. Although –M12 and –M4 or -M6 and –M8 originate from the same primary transcript, differential post-

transcriptional processing to yield mature miRNAs can lead to differential expression of the mature miRNAs. In addition, selective exosomal incorporation of miRNAs is an active process dependent on nucleotide (nt) motifs in miRNAs known as EXOmotifs that are recognized by SUMOylated hnRNPA2B1 (258). In this regard, -M4 contained CCCU Exomotif that may allow its selective incorporation into exosomes irrespective of VEX or TEX, although –M6 lacked both CCCU and GGAG EXOmotifs.

MDV1-mir-M4 is a functional ortholog of cellular mir-155 and KSHV-mir-K12-11, and whose expression is correlated with the MDV1 virulence (106). MDV1-mir-M4 is a known oncomiR that is nonessential for replication, but is highly-expressed in MD lymphomas or lymphoblastoid cell lines. Mutation of just 2 nts in the seed region of MDV1-mir-M4 diminished the transforming ability of the virus (113). As instances of cellular miRNA expression contrasting with that of exosomes have been previously noted, and as hnRNPA2B1-dependent export of miRNAs in exosomes was proposed to provide a mechanism for eliminating undesired miRNAs, it is possible that MDV1-mir-M4 elimination in VEX may be a mechanism to prevent its cellular accumulation and thus its oncogenic functions (258, 259).

Alternatively, MDV1-mir-M6 and –M8, although co-transcribed from the same cluster, were previously shown to be differentially-expressed. MDV1-mir-M6 was demonstrated to be the least expressed or poorly processed in MDV1 (RB1B) primary splenic tumors and the MSB1 lymphoblastoid cell line by deep sequencing, whereas a higher expression (3.8- and 8.5-fold for -5p and -3p, respectively) was noted in chicken embryo fibroblasts infected by the RB-1B strain of MDV (107, 109). MDV1-mir-M8 expression contrasted with that of –M6, where it displayed greater expression in RB1B primary splenic tumors (3.5-fold) and the MSB1 lymphoblastoid

cell line (23.5-fold) with basal expression in RB1B-infected CEF (106, 109). Exosomal MDV1-mir –M6 and –M8 expression levels in VEX compared to TEX also contrasted with each other and reflected with those observed in RB1B-infected CEF.

Similar to MDV1-mir-M4 and M6, qRT-PCR validation of chicken cellular miRNAs gga-mir-27b, -10b and -99a in VEX contrasted with the results from our high throughput sequencing study. The discrepant results obtained here might be attributed to the differences in our studies. The previous high throughput sequencing was performed on serum exosomes derived from leghorn sera whereas current qRT-PCR validation was performed on serum exosomes obtained from broiler sera. On the other hand, gga-mir-2188, -146b and -21 expression conformed to our high throughput sequencing results with a greater level of upregulation and repression (in VEX relative to TEX) seen in TEI-purified exosomes indicating higher exosome recovery by TEI reagent. With their *bona fide* roles as tumor suppressor miRNAs and oncomiRs respectively, gga-mir-146b and -21 expression correlated with good and poor prognosis in a wide variety of malignancies (260, 261).

Finally, based on the lack of observable difference in MHC I content between VEX and TEX, it is evident that TEX derived from vv+MDV1-infected chickens do express MHC I although aberrant expression of other cell surface antigens (CD3-, CD4-, CD8-, TCR2+, CD28+, MHC-I+) was evident in cell lines transformed by vv+MDV (UA51) (40). In addition, cell surface MHC I is also shed and is present in microvesicles. Hence MHC I is not a genuine exosome marker although it’s a starting point for species that lacked Abs to detect genuine exosome quality control markers.

Despite our findings, we are aware of our study limitations. First, our study selected only one of many available commercial exosome isolation reagent solutions

from various sources; nonetheless we selected the most commonly used kit in the field. Second, our study only employed serum as a starting sample, and it is thus necessary to perform similar studies with other fluids such as plasma, ascites fluid and culture supernatants. Our ultimate intention, however, is to validate the most suitable technique for use in a routine diagnostic laboratory to identify or confirm serum biomarkers indicative of vaccine induced immune protection or systemic immune suppression. Third, we note that confirmation of the biological activity of purified exosomes is of prime importance prior to its translation for diagnostic use, although such confirmation assays are beyond the scope of this study. Fourth, we cannot exclude the lipoprotein or protein aggregate contamination of our purified fractions by both the procedures and the level of purity gained by each procedure will be assessed in our upcoming studies.

Taken together, our results demonstrate that commonly-used method to purify exosomes, UC, is relatively inefficient to recover exosomes from viscous fluid such as serum. While it may be an efficient procedure to purify exosomes from less viscous fluids such as culture media, urine and lavages, it is not the case for serum and also plasma. On the other hand, the use of TEI reagent to purify exosomes from serum is efficient, quick and can be performed with ease to obtain higher particle numbers for miRNA quantification.

Figure 4.1: Size and concentration profiles of particles purified by ultracentrifugation (UC) and Total Exosome Isolation precipitation (TEI) reagent. A. The overall mean size (diameter) of particles yielded by UC and TEI reagent. Significant difference in the particle size between the purification procedures was assessed by Fisher's exact test. Error bars denote standard error of mean (SEM). B-C. Size distribution and concentration profiles of vaccinate exosome (VEX) particles purified by UC (B) and TEI reagent (C). D-E. Size distribution and concentration profiles of tumor exosome (TEX) particles purified by UC (D) and TEI reagent (E). F. The overall particle concentration yielded by UC and TEI reagent. Error bars denote SEM. Asterisk denotes statistical significance *($p \leq 0.05$)*.

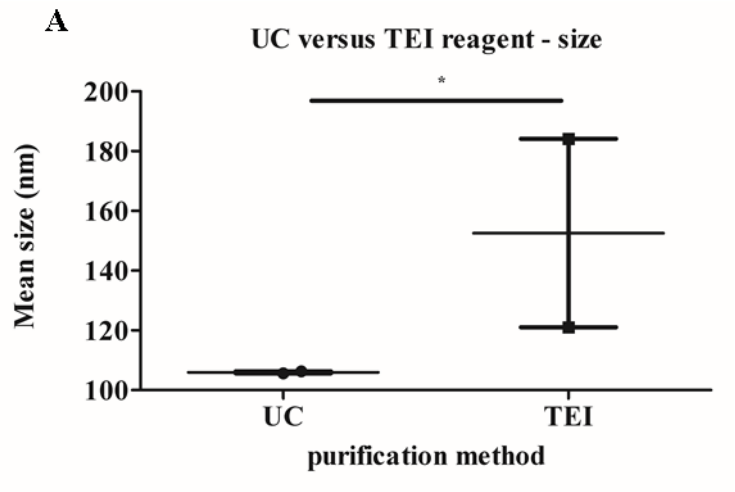
A
UC versus TEI reagent - size
*
200
180
160
140
120
100
Mean size (nm)
UC
TEI
purification method

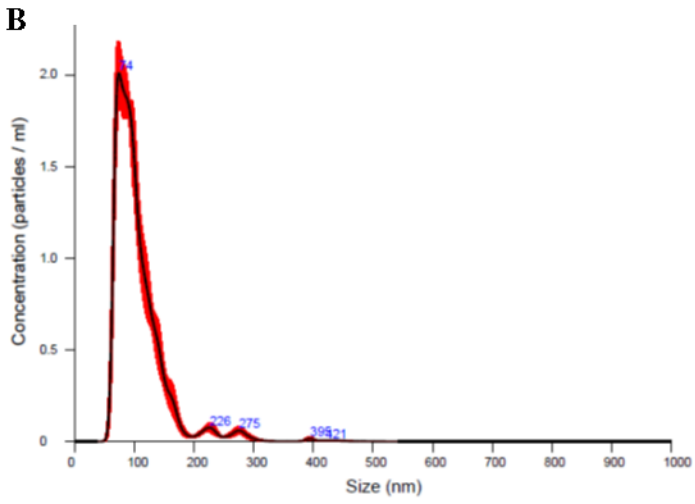
B
2.0
1.5
1.0
0.5
0
Concentration (particles / ml)
0
100
200
300
400
500
600
700
800
900
1000
Size (nm)

C

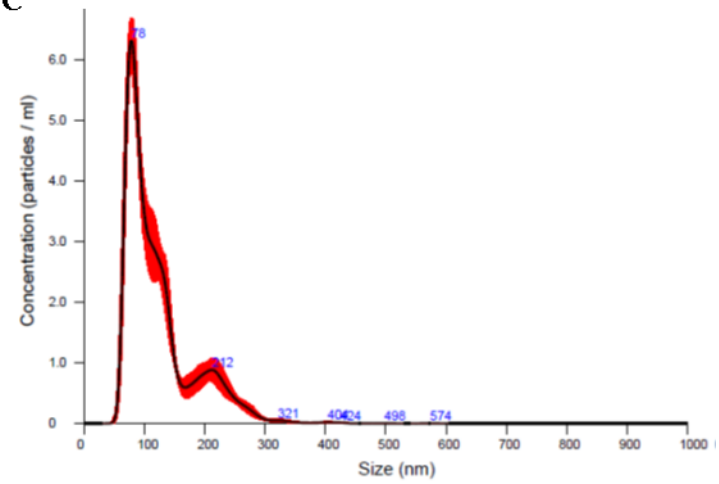
Concentration (particles / ml)
Size (nm)
78
212
321
498
574

D

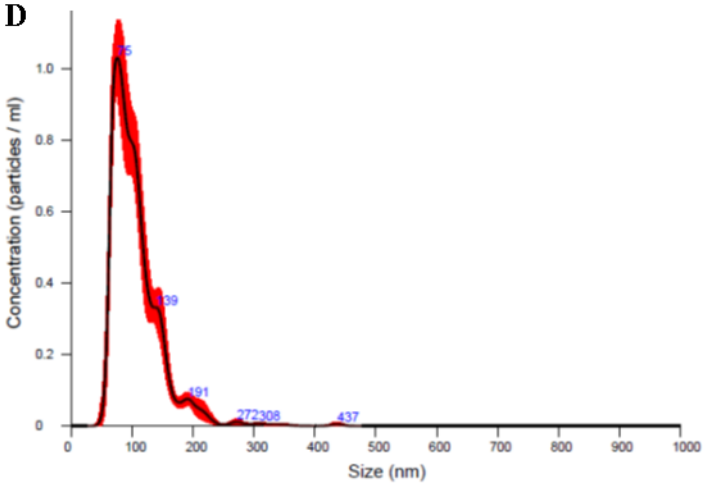
Concentration (particles / ml)
Size (nm)
95
139
191
272308
437

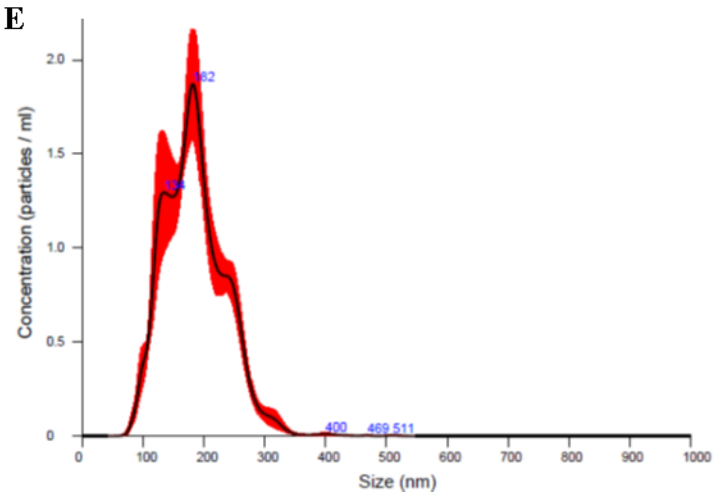
E
Concentration (particles / ml)
2.0
1.5
1.0
0.5
0
382
400
469 511
0
100
200
300
400
500
600
700
800
900
1000
Size (nm)

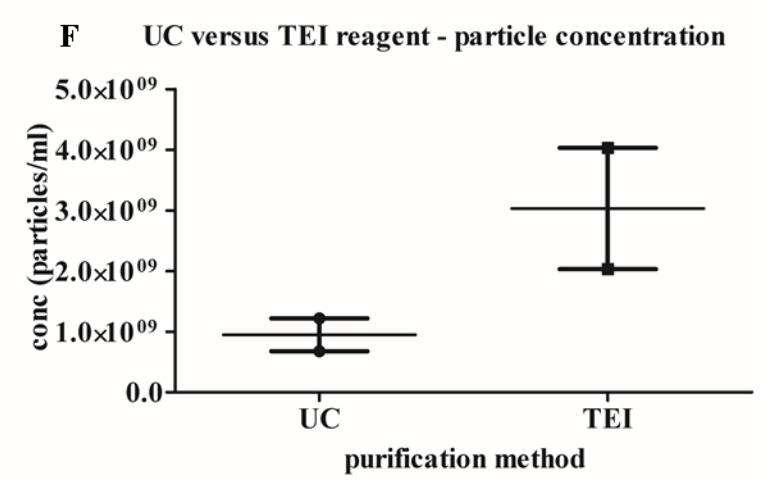
F
UC versus TEI reagent - particle concentration
5.0x10^09
4.0x10^09
3.0x10^09
2.0x10^09
1.0x10^09
0.0
conc (particles/ml)
UC
TEI
purification method

Figure 4.2: Transmission electron microscopic visualization of VEX and TEX purified by UC and TEI reagent. Bar on the left hand corner denotes TEM scale.

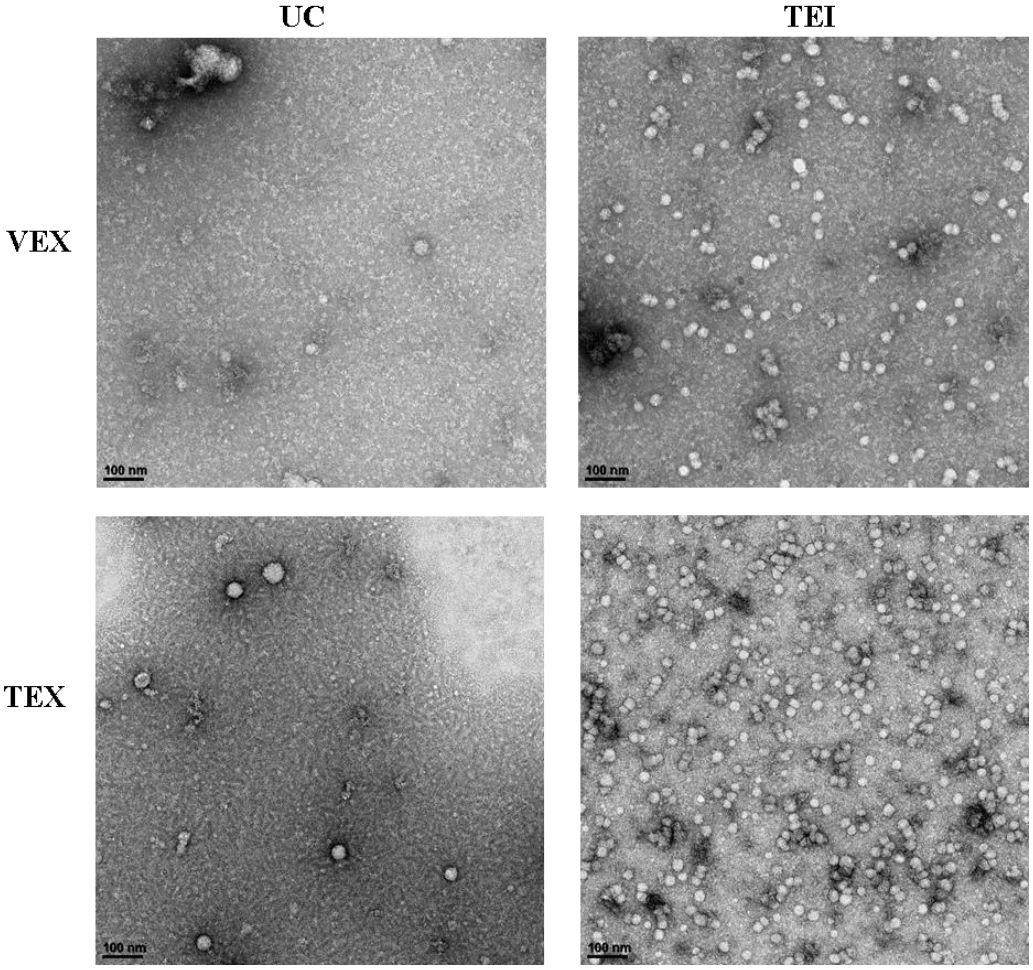

Figure 4.3: Comparison of miRNA expression profiles between purification procedures. Correlation analysis of miRNA expression levels in VEX (A), TEX (B) and VEX/TEX (C) between the exosome purification procedures. Pearson correlation coefficient (r) is indicated for the comparison. Relative MDV-1 and G.gallus miRNA expression in VEX compared to TEX in UC-purified exosomes (grey bars) and TEI-purified exosomes (teal bars). Error bars denote SEM.

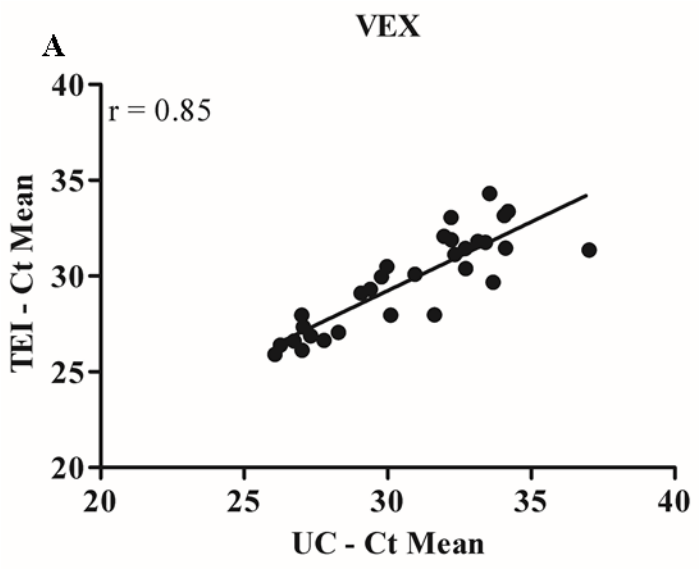
A
VEX
r = 0.85
TEI - Ct Mean
UC - Ct Mean
40
35
30
25
20
20
25
30
35
40

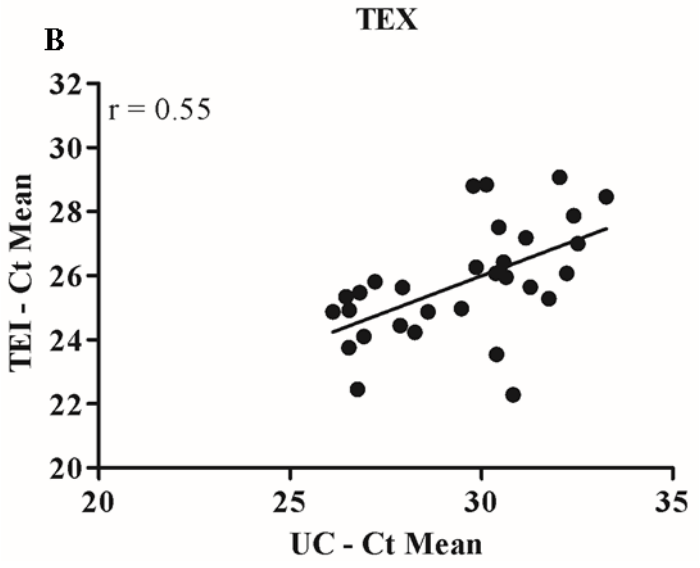
B
TEX
r = 0.55
TEI - Ct Mean
UC - Ct Mean
32
30
28
26
24
22
20
20
25
30
35

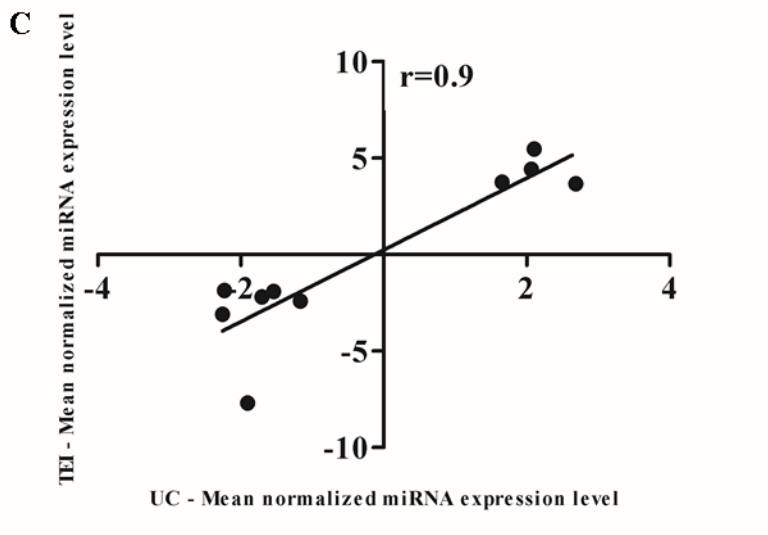
C
r=0.9
10
5
-5
-10
-4
-2
2
4
TEI - Mean normalized miRNA expression level
UC - Mean normalized miRNA expression level

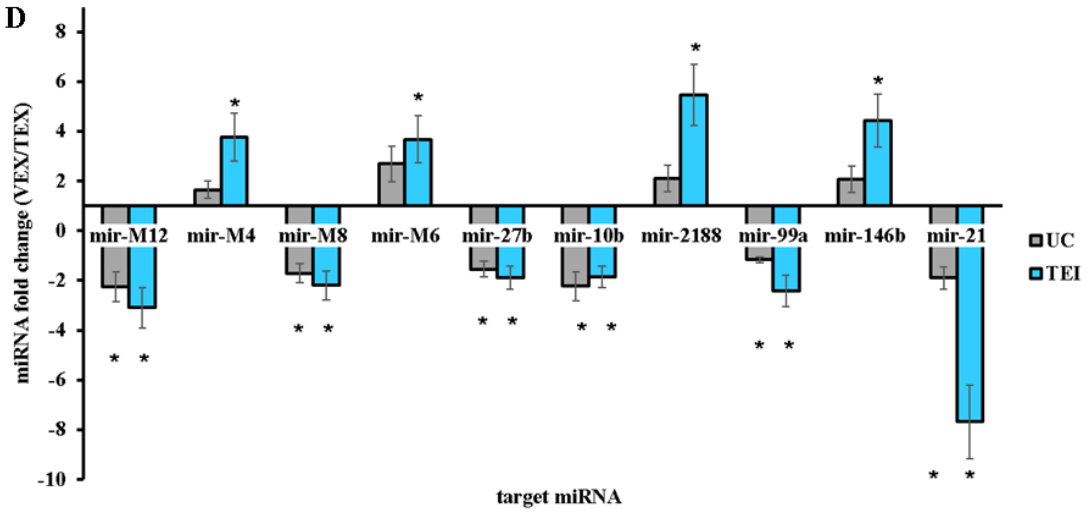
D
8
6
4
2
0
-2
-4
-6
-8
-10
miRNA fold change (VEX/TEX)
mir-M12
mir-M4
mir-M8
mir-M6
mir-27b
mir-10b
mir-2188
mir-99a
mir-146b
mir-21
target miRNA
UC
TEI

Table 4.1: Serum exosome sample sources

Bird Tag	Treatment Group	MD Status	miRNA	NTA	TEM
BL4254	CVI988-vaccinate	Neg. (M)	+	-	-
BL4294	CVI988-vaccinate	Neg. (F)	+	-	-
BL4350	CVI988-vaccinate	Neg. (M)	+	+	+
OR2107	Inoculated Shedder	+ (F, spleen tumor)	+	-	-
OR2232	Inoculated Shedder	+ (F, spleen tumor)	+	-	-
OR2250	Inoculated Shedder	+ (M, heart tumor)	+	+	+

[a] – Serum was obtained from commercial broiler chickens, provided as embryonated eggs by Mountaire Farms, Inc., Millsboro, DE used in a vaccine study comparing CVI988 vaccines

Table 4.2: miRNA Quantification Primers

m/miRNA	Forward primer sequence	reverse primer sequence
gga-miR-2188-5p	AAGGTCCAACCTCACATGTCCT	-
gga-miR-10b-5p	TACCCTGTAGAACCGAATTT GT	-
gga-miR-99a-5p	AACCCGTAGATCCGATCTTGTG	-
gga-miR-146b-5p	TGAGAACTGAATTCCATAGGCG	-
gga-miR-27b-3p	TTCACAGTGGCTAAGTTCTGC	-
gga-miR-21-5p	TAGCTTATCAGACTGATGTTGA	-
MDV1-mir-M12-3p	TGCATAATACGGAGGGTTCT (meq cluster)	-
MDV1-mir-M4-5p	TTAATGCTGTATCGGAACCCTTC (meq cluster)	-
MDV1-mir-M6-5p	TCTGTTGTTCCGTAGTGTTCTC (LAT cluster)	-
MDV1-mir-M8-5p	TATTGTTCTGTGGTTGGTTTCG (LAT cluster)	-
gga-mir-200b-5p	CGTCAGATGTCCGAGTAGAGGGGGAACGGCG TAATACTGCCTGGT	TGTCAGGCAACCGTATTCACCGTGAGTGG TATCATC
gga-mir-26a-5p	CGTCAGATGTCCGAGTAGAGGGGGAACGGCG TTCAAGTAATCCAGG	TGTCAGGCAACCGTATTCACCGTGAGTGG TGCCTAT
gga-mir-101-3p	CGTCAGATGTCCGAGTAGAGGGGGAACGGCG GTACAGTACTGTGAT	TGTCAGGCAACCGTATTCACCGTGAGTGG TTTCAGT
Universal miR-RT primer	-	CGTCAGATGTCCGAGTAGAGGTTTTTTTT TTTTTTTT
Universal reverse	-	CCTCTACTCGGACATCTGACG

Table 4.3: Serum Exosomal miRNA raw C_t values as Detected by qRT-PCR

	VEX		TEX	
miRNA ID	**UC**	**TEI**	**UC**	**TEI**
gga-miR-2188-5p[b]	26.5	26.4	26.1	24.7
MDV1-mir-M4-5p[b]	27.2	26.8	26.9	24.8
MDV1-mir-M6-5p[b]	27.5	27.8	27.3	25.2
gga-mir-27b-3p[b]	29.5	27.7	28.8	23.9
gga-mir-146b-5p[b]	30.2	30.1	30.2	28.4
gga-mir-99a-5p[b]	32.2	30.8	30.2	25.0
MDV1-mir-M12-3p[b]	32.3	30.0	31.5	25.9
gga-mir-21-5p[b]	33.0	30.9	31.5	24.6
MDV1-mir-M8-5p[a,b]	33.9	31.9	32.1	27.0
gga-mir-10b-5p[b]	34.9	32.6	33.0	28.2
Average C_t	30.7	29.5	29.7	25.7

[a] – miRNA level differences in VEX were statistically significant between the purification methods

[b] – miRNA level differences in TEX were statistically significant between the purification methods

Chapter 5

EXAMINATION OF THE ROLE OF EXOSOMES DURING MAREK'S DISEASE VIRUS (MDV) PATHOGENESIS AND IN VACCINE-INDUCED PROTECTION

5.1 Introduction

Extracellular vesicles (EVs) are spherical lipid bilayer limited vesicles released from a variety of biological cells into the extracellular fluids (220). Consequently, these vesicles can be found and isolated from a range of biological fluids including serum, plasma, blood, cerebrospinal fluid, amniotic fluid, breast milk, saliva, urine, semen and bile. Based on the size, origin, physical properties and composition, EVs are mainly classified into three types; 1. Microvesicles (microparticles or ectosomes) originate from plasma membrane (PM) and are of 100-1000nm in diameter. 2. Exosomes originate in endosomes or multivesicular bodies (MVBs) as intraluminal vesicles (ILVs) and are sized between 30-150nm (density: 1.15-1.19g/ml). 3. Apoptotic vesicles arise upon blebbing of cells undergoing apoptosis and range between 50-500nm (262). Current protocols however, cannot distinguish between different types of EVs due to a size overlap among them (263). Methods such as marker based immune affinity isolation (anti-CD63) can enrich exosomes, although marker less exosomes can be excluded by this procedure. Our goal is to characterize the exosomes from MDV-infected chickens or -transformed lymphoblastoid cell lines.

Henceforth, the terminology “exosome” will be used in the rest of description, although the exosome preparations in our studies might contain minor amounts of other EVs.

The term “exosome” was first described in 1981 to refer microvesicles secreted by rat and mouse neoplastic cell lines and had 5’ nucleotidase activity (264). Later in 1987, Stahl and Johnstone *et al.*, independently described exosomes as vesicles of endocytic origin in maturing reticulocytes. These vesicles were shown to contain transferrin receptor (Tfr) and were thought as a mechanism to dispose Tfr upon fusion with plasma membrane as seen under electron microscopy (265, 266). Exosomes (or ILVs) originate in MVB upon inward invagination of endosomal limiting membrane. MVB containing exosomes can either fuse with lysosomes resulting in their degradation or fuse with plasma membrane resulting in exocytic release of exosomes into the extracellular environment. Upon release, exosomes serve as vehicles of intercellular communication by delivering their cargo into the recipient cells upon direct fusion with recipient cell PM or uptake via receptor mediated endocytosis.

5.1.1 Biogenesis (ESCRT-dependent and –independent) and composition

Based on their endosomal origin, ILV budding is driven by endosomal sorting complex required for transport (ESCRT) protein complexes. In fact, the process of exosome formation is analogous to retroviral budding and as such HIV-1 proteins (Nef, Gag, Env and transactivation elements) were found to be packaged in exosomes in order to transfer them to uninfected cells (267-272). Four ESCRT complexes (ESCRT-0,-I,-II and –III) along with their associated proteins (e.g. Alix, VPS34) mediate the cargo sorting, membrane invagination and subsequent scission to generate ILVs (273). ESCRT complexes were initially identified to mediate endosomal sorting

of ubiquitinated proteins and their subsequent degradation in lysosomes (274, 275). The lipid PI3P on endosomal membrane first recruits ESCRT0 complex bound to ubiquitinated proteins. ESCRT-0 recruits ESCRT-I complex which then incorporates ESCRT-II subunits. Both ESCRT-I and –II complexes drive the invagination, while ESCRT-II recruits ESCRT-III complexes into the neck of nascent ILVs to mediate vesicle scission (276-280). Although most ubiquitin chains and ESCRT subunits are removed for recycling, some of the ESCRT components involved in biogenesis remain retained in the exosomes and thus can serve as exosome markers (e.g. Alix, Tsg101, Hrs). However, MVBs are still generated in cells depleted of all four ESCRT subunits indicative of ESCRT independent pathways of MVB biogenesis (281, 282).

Exosomal sorting of proteins such as PMEL, MHC-II and proteolipids in oligodendrocytes are ubiquitination or ESCRT-independent (262, 283, 284). Indeed, tetraspanin (TSPAN) CD63 was demonstrated to sort luminal domain of PMEL in an ESCRT-independent manner (285). Inhibition of neutral sphingomyelinase (nSMase) enzyme that breaks down sphingomyelin in sphingolipid containing lipid rafts into ceramide reduced proteolipid bearing exosome release in oligodendrocytes (282). Thus proteolipid sorting is ceramide dependent and ESCRT independent. Reduced exosomal release and their contents (CD63, CD81, TSG101 including miRNA) was observed upon treatment of various cell lines with nSMase inhibitor manumycin or GW4869 (286-289). As a matter of fact, nSMase inhibitor treatment or nSMase siRNA knock down is frequently used to discriminate exosome dependent transfer or the effect of exosomes between donor and target recipient cells *in vitro*. Additionally, Hsc70 binding to the luminal domain of Tfr and KFERQ motif containing proteins sorts them to exosomes (290, 291).

Once formed, MVBs traffic to the cell periphery to fuse with plasma membrane to mediate exocytic release of exosomes. This traffic is dependent upon co-ordinated action of cytoskeleton, small GTPases (Rab or RAL1) and fusion machinery. Similar to the intracellular vesicle trafficking, Rab GTPases also promote MVB trafficking to the PM. Knockdown or ectopic over expression of dominant negative mutants of Rab-2b,-9a,-5a,-11, 27a,-27b,-35 in various cell lines reduced the number of exosomes secreted into the medium (292-298). Inhibition of Ral GTPases-A or -B resulted in fewer secretion of exosomes in 4T1 mammary tumor cell line (299). The fusion of MVBs to the PM appear to depend on SNAP (Soluble N-ethyl maleimide sensitive fusion Attachment Protein) receptors or SNAREs (262). VAMP7 and NSF ATPase were found to promote MVB exocytosis in K562 erythroleukemic cell line whereas VAMP7 inhibition in MDCK cells was found to inhibit lysosomal exocytosis similar to other epithelial cells suggestive of cell type dependent requirements (300-302).

Exosome cargo is composed of proteins (peripheral membrane associated, transmembrane and soluble hydrophilic), lipids and nucleic acids (miRNA, mRNA). Exosomal protein content varies and depends upon the originating cell. Exosomes originating from APCs such as dendritic cells (DCs), macrophages and B cells contain MHC-I,-II, costimulatory CD80 and CD86 (303-305). In addition, exosomes also contain some common classes of proteins such as TSPANs (CD9, -63, -81, -82), integrins (ICAM-1), chaperones (HSC70 and Hsp90), Milk Fat Globule Epidermal Growth Factor 8 (MFGE8), membrane trafficking proteins (Rab GTPases, Annexins-I, -II, -IV, -V, -VI, -XI, syntaxin), enzymes (GAPDH, ef1α), cytoskeletal proteins (actin, ezrin, moesin), MVB biogenesis proteins (Rab GTPases, TSG101, ALIX, syntenin-1),

and lipid raft proteins (stomatin, flotillin-1). Proteomic analyses of exosomes has identified protein classes mainly belonging to PM, cytosol or endosomes whereas proteins from other cellular compartments or organelles are almost absent (262, 263). Exosomal proteins, lipids and coding or non-coding RNAs identified are incorporated and routinely updated in online databases such as ExoCarta (http://www.exocarta.org) and Vesiclepedia (http://microvesicles.org/) (306).

Lipid composition includes membrane lipids such as phosphotidyl serine (PS), sphingomyelin, ceramide, GM3 ganglioside and cholesterol (294, 307-310). In 2007, exosomes derived from human primary mast cells and mast cell lines (HMC-1 and MC/9) or primary bone marrow derived mast cells from mice were found to contain mRNAs coding for 1300 genes along with miRNAs, expression of which appeared specific to exosomes and contrasted with that of cytoplasmic m/miRNAs of the cells of origin (259). These mRNAs were functional in *in vitro* translation assays and protein coding upon transfer of mouse cell line derived exosomes to human cell lines. Unidirectional transfer of exosomal miRNAs from Jurkat cell line to APC (Raji-SEE B cell line) in the immunological synapse is antigen dependent resulting in the modulation of gene expression in the recipient cells (311). Alteration of exosomal miRNA profiles post maturation of mouse immature bone marrow derived dendritic cells (BMDC) by LPS treatment and functional transfer of exosomal contents to other DCs by fusion or hemifusion was demonstrated to show how exosomes from APCs can fine tune the immune responses in recipient APCs (312). Of particular note is non-cell autonomous gene silencing mediated by exosomal *let-7b,-7d* miRNAs from T_{REG} cells and their function in suppressing T_{h1} cell proliferation and thus IFN-γ secretion (313). *let-7* family of miRNAs, well known to function as tumor suppressors, were

found frequently down regulated in vvMDV RB1B-infected CEF or spleen tumors and vMDV GA strain-infected tumors as well (107, 314). However, the possibility of selective packaging of these miRNAs into exosomes to mediate systemic immune suppression cannot be excluded and is subject of our study. High-through put sequencing of exosomal RNA also allowed the identification of other small ncRNAs such as vault RNA, t-RNA and Y RNA and very limited to no ribosomal RNA (315).

5.1.2 Immune modulatory role of exosomes

5.1.2.1 Exosomes in innate immunity

Exosomes can serve as key carriers for PAMPs, viral antigens, tumor antigens and finally MHCI/II-antigenic peptide complexes to facilitate antigen presentation and adaptive immune patterning. Exosomes isolated from *M. tuberculosis* or *M. bovis*-infected macrophage cultures or infected mice BALF were found to carry PAMPs lipoarabinomannan and 19kDa protein (166). PAMP carrying exosomes upon addition to macrophages *in vitro* or intranasal instillation in mice *in vivo*, stimulated TNF-α production. LPS-stimulated DCs secreted exosomes carrying tumor necrosis factor (TNF) receptors (TNFRI and TNFRII) and pro-inflammatory cytokine TNF-α in addition to canonical MHC-II, CD40, and CD83 molecules. Exosomes from mature DCs when added to intestinal epithelial cells, stimulated production of pro-inflammatory cytokines RANTES, IL-8, MCP-1 and GM-CSF in TNF-α-dependent manner (167). Mouse DC exosomes display TNF family ligands TRAIL and FasL and enhance NK cell cytotoxicity by direct binding to their respective receptors (168). Intradermal injection of mouse DC exosomes increased the number of NK cells in draining lymph nodes and facilitated their activation via IL-15Rα expressed on the

exosomal surface interacting with natural killer group 2-member D (NKG2D) activating receptor on NK cells (169, 170). Exosomes derived from HEK293 cells or immature DCs display HLA-B associated transcript 3 (BAT3) on their surface and via interaction with activating receptor NKp30 facilitated NK cell activation, which in turn led to DC maturation (171).

Exosome preparations from long term DC cultures contaminated with Mycoplasma were found to stimulate B cell proliferation in an antigen-independent manner (172). Allogeneic HCMV-infected HUVECs released exosomes were sufficient to mediate autologous APC-CD4+ T cell mediated interactions in HLA-DR dependent manner and proliferation of naïve and memory CD4+ T cells. Exosomes from HUVEC-infected HCMVs contained gB and were proposed to be the source of rejection towards graft endothelium (173). On the other hand, exosomes derived from LCMV-infected mouse BMDC lacked viral antigens and therefore failed to cross prime CD8+ CTLs (174). In addition, exosomes derived from tumor cell lines or pleural or peritoneal effusions served as vehicles for unique or shared tumor antigens (MART1/Melan A, Trp1, gp100, Her2/Neu), which when primed onto DCs, promoted activation and expansion of autologous MHC I restricted CD8+ CTLs to induce CTL-mediated killing of tumor cell lines *in vitro* or CTL-mediated regression of tumor size *in vivo* (175, 176).

5.1.2.2 Exosomes in adaptive immunity

Due to their ability to vehicle antigens, exosomes can convey their antigenic entities to unprimed or immature APCs such as DCs and B cells, which process and present them by complexing the antigenic peptides with MHC I & II molecules. Furthermore, whole antigen or MHC complexed peptide bearing exosomes were able

to induce antigen specific naïve CD4+ T cell activation *in vivo*. *In vitro,* however, antigen specific CD4+ T cell stimulation failed to occur in the absence of intermediate DCs (316, 317). To activate naïve CD4+ T cells, APC derived exosomes have to be captured by DCs and also, exosomes derived from mature DCs can induce more efficient CD4+ T cell activation than those from immature DCs (318-320). This ability of transferring antigenic entities to DCs and subsequent antigen specific stimulation of naïve CD4+ T cells is referred to as indirect antigen presentation as opposed to direct antigen presentation (see below).

Exosomes derived from mouse mast cell (MC) lines were demonstrated to have a mitogenic effect on cultured splenocytes leading to blast formation and proliferation with IL-2 and IFN-γ production (321). Administration of MC exosomes in mice led to maturation of immature DCs and up-regulation of MHC II, CD80, CD86, and CD40 (322). Exosomes can serve as vehicles of direct antigen presentation by means of preformed peptide-MHC I complexes and co-stimulatory molecules on their surface and thus can directly present to CD8+ T cells. APC derived microvesicles expressing MHC I- peptide complexes in addition to costimulatory B7 and ICAM1 were found to directly activate naïve CD8+ T cells and pattern them into effector CTLs (323). Exosomes derived from DCs treated with viral immunogenic peptides (CMV, EBV and IAV) were able to directly activate autologous CD8+ T cells in a dose dependent manner leading to IFN-γ production (324). Exosomes secreted by ovalbumin (OVA)- peptide pulsed mature BMDCs activated OVA specific MHC class I-restricted T cell hybridomas more efficiently than those from immature BMDCs. Furthermore, cross presentation of MHC I-OVA peptide complexes was also found in BMDC exosomes derived from $TAP^{-/-}$ (Transporter of Antigen Processing) mice

indicating that antigenic peptide loading onto exosomal MHC I is TAP independent unlike MHC I antigenic peptide loading in ER (325). Exosomes secreted by LPS matured DCs were 50-100 fold more potent than immature DC exosomes in activating antigen specific CD8+ CTLs. In addition, mature DC exosomes added to B cells conferred them the ability to prime naïve CD8+ CTLs (319).

5.1.3 Exosomes in viral infection

Similar to Human immunodeficiency virus (HIV1), other viruses such as Epstein Barr Virus (EBV), HSV1, Hepatitis A virus (HAV), Hepatitis B virus (HBV), Hepatitis C virus (HCV), Hepatitis E virus (HEV) and Human T-cell lymphotropic virus (HTLV) were known to exploit exosomes in order to mediate a range of effects beginning with immune suppression or immune modulation to immune evasion by cloaking themselves in exosomes in order to evade Ab-mediated neutralization as seen in the case of HAV and HEV infections (326). Exosomes derived from HCV-infected hepatocytes or patient sera carried full length + sense ssRNA viral genome, permitting receptor independent transfer of viral genome and establishment of productive infection in recipient cells (286, 327-331). Exosomes are exploited to cargo viral proteins (LMP1, Tax, dUTPase enzyme), viral and cellular mRNAs or miRNAs to non-permissive cells to mediate biological effects (332-335). miRNA mediated silencing of target genes such as CXCL11 in monocyte derived DCs and NLRP3 was found to occur via EBV positive B cell line derived exosomes through intercellular transfer of BHRF1-3^{+} and BART-15 miRNAs respectively (336, 337). Although EBV is restricted to B cells, EBV BART miRNAs were found in both B and non B cell fractions in patients with higher EBV loads indicative of exosomal transfer from B-cell to non B-cell fractions (336). Furthermore, mir-200 family members secreted by

oral epithelial cells via exosomes were found to reactivate latent EBV in the nearby tonsillar B cells (338). Finally, Hodgkin-Reed Sternberg (HRS) Ag CD30 is expressed by HRS B lymphoma cell exosomes and can serve to activate CD30L on mast and eosinophilic cells in the tumor microenvironment to amplify pro-inflammatory signals (339). Modified exosomal content was also described in the case of KSHV primary effusion lymphoma (PEL) cell lines where exosomes were found to be enriched in latent protein markers (about one-third) and glycolytic enzymes (340). Tspan enriched exosomes co-purified along with HSV1 virions carried STING protein along with non-coding RNAs such as LAT and mir-H3, -H5, -H6 whose abundance is greater in latently infected cells than in reactivated cells (341). It was surmised that STING carrying exosomes are released to be taken up by uninfected cells, for instance, satellite or neuronal cells, as an innate immune priming mechanism to inhibit viral dissemination resulting in latency and lifelong persistence in the infected host (341).

5.1.4 Tumor derived Exosomes (TEX) mediated immune suppression and tumor promotion

TEX are crucial in promoting angiogenesis, invasion, metastasis and immune suppression (342-346). TEX numbers are significantly elevated in sera of cancer patients and *in vitro* in each of three breast cancer cell line supernatants exposed to hypoxic conditions (253, 254, 347). TEX from tumor cell lines and sera of leukemic patients when co-incubated with primary activated T cells or $CD56^{+}CD16^{+}$ NK cells led to Fas/FasL mediated $CD8^{+}$ CTL apoptosis, down regulated CD3ζ and JAK3 (Janus kinase 3) expression in primary activated T-cells, induced $CD4^{+}CD25^{hi}FOXP3^{+}$ patterning (T_{reg} patterning) and dampened the cytotoxic function of NK cells (348). Neutralizing Abs against TGFβ1 and/or IL-10 carried on exosomal

surface inhibited the ability of TEXs to expand T_{reg} populations (348). Furthermore, TEX differentiated T_{regs} displayed significant expression of FasL, IL-10, TGF-β1, CTLA-4, granzyme B, perforin and promoted suppression of responder cell proliferation (349). TEX express FasL and induce Fas dependent apoptosis of circulating CD8+ CTLs (350, 351). TEX carried ectonucleotidases CD39 and CD79 responsible for immune suppressive adenosine production and transfer them to target cells in tumor micro environment (352). Adenosine binds adenosine A2A receptor to upregulate cAMP production and suppressed effector T cell function (353). Another independent study demonstrated mesothelioma cell line derived TEX decreased IL-2 responsiveness in human $CD4^+$, $CD8^+$ T cell and NK cell populations (354). Apart from impairment of IL-2 mediated CD25 upregulation in all T cell populations except $CD3^+$ $CD8^-$, TEX promoted differentiation of $CD3^+$ $CD25^+$ $Foxp3^+$ T_{regs}. Furthermore, TEX directly hampered NK cell cytotoxic function in this study (354). In another study demonstrating the effects of exosomes from bodily fluids such as amniotic fluid, liver cirrhosis and ascitis fluids (AF) of ovarian carcinoma patients, exosomes from both non-cancerous and cancerous fluids activated and induced differentiation in THP-1 monocyte cell line (355). Exosome treatment of THP-1 cell line led to activation of NFκB and downstream IL-6 induction in TLR2- and TLR4-dependent manner. IL-6 autocrine and paracrine actions led to STAT3 activation. Of considerable interest, primary monocyte derived DCs or macrophages released IL-12p40 into culture supernatants upon AF exosome treatment in a Myd88 dependent manner (355). TEX isolated from melanoma patient sera or cell lines and positive for melanoma antigens inhibited proliferation of activated $CD8^+$ CTLs including melanoma antigen specific

$CD8^+$ CTLs (356). In addition, melanoma TEX expanded $CD4^+CD25^+FOXP3^+$ T regulatory cells and enhanced their suppressor activity *in vitro* (356).

Acute myeloid leukemia (AML) patient plasma TEX express MHC I related sequences (MICA, MICB), TGF-β, latency associated peptide (LAP) and mediate down regulation of NKG2D receptors on the surface of NK cells (347, 357-359). $CD14^+$ monocytes differentiated in the presence of TEX, IL-4 and GM-CSF skewed their differentiation towards a suppressor phenotype ($CD14^+$ HLA-$DR^{-/low}$) which in turn promoted suppression of T-cell functions in a TGF-β–dependent manner (360). Finally, Human Reed Sternberg Antigen CD30 was found on the exosomes exocytosed by malignant Hodgkin lymphoma (cHL) cell lines ($CD30^+$ cHL cell lines) L540, L428, KM-H2 L1236 and in peripheral blood of HL patients (339, 361). Furthermore, in HL patients treated with CD30 antibody drug conjugate (ADC) Brentuximab Vedotin (SGN-35, Adcetris), exosomal CD30 bound ADC and CD30L on the normal nearby bystander cells in the tumor microenvironment to divert ADC toxicity on healthy bystander cells (339).

5.2 Hypotheses of Research

Notwithstanding the role played by exosomes in mediating immune stimulation or immune suppression in the context of a variety of physiologies and pathologies including tumorigenesis, the role played by exosomes in MDV1-mediated immune suppression or MD vaccine induced protection is currently unknown. MD vaccines replicate for a very limited period of time post vaccination yet induce complete protection against tumor formation. Early detection by and stimulation of innate APCs (macrophage, DCs and B-cells) by the vaccine viruses is sufficient to

induce systemic T_{H1} immune patterning observed during the rest of life of the host. Our current hypothesis is based on this observation and as follows:

1. Systemic T_{H1} patterning observed during MD vaccine-mediated protection is mediated by exosomes secreted by antigen presenting cells and is present in the serum of vaccinated and protected chickens.

2. On the contrary, exosomes secreted by latently infected and transformed $CD4^+$ T_{REG}-like cells in the serum of susceptible birds or MD lymphoblastoid cell line supernatants are immune suppressive towards APCs and T_{H1}-patterned $CD8^+$ CTLs.

5.3 Materials and Methods

MDV1 used for vaccination (CVI-988, CEVA Biomune) was delivered at a 1X commercial dose in commercial diluent. Vaccine dosage was determined by back-titration of diluted vaccine on secondary CEF. Under the conditions where exosomes were either purified from cell culture (UD35) supernatants or purified serum exosomes were added to the culture supernatants (CEFs), secondary CEFs, or MDV1-transformed UD35 cells were maintained in serum free media (CEF) or exosome free FBS (Gibco). UD35 (an RB1B based transformed cell line) was maintained in Iscove's DMEM supplemented with 10% Exosome free FBS, 1X insulin transferrin selenium, 10% tryptose phosphate broth, 1X non-essential amino acids, 4 mM L-glutamine, 2 mM sodium pyruvate, 2 μM β-ME, 1X pencillin streptomycin neomycin cocktail and 1X Fungizone (all from Life Technologies).

5.3.1 *In vivo* studies

5.3.1.1 *In vivo* vaccine efficacy study I

Serum or plasma samples collected for exosome purification were a composite of two consecutive *in vivo* vaccine efficacy studies. Sera samples used for exosome purification were obtained at the end of vaccine study before termination and were marked MD+ (n=4) or MD- (n=4) based on scored gross MD lesions (visceral or peripheral lymphomas) and clinical signs (ataxia, torticollis, red leg). *In vivo* studies described here followed natural exposure model of infection known as "shedder model" that has already been described elsewhere (91). Briefly, white leghorns (Hyline W36) obtained from Elizabethtown hatchery and assigned "shedders" were inoculated intra-abdominally (i.a) on the day of hatch with 200-400PFU of TK-2a-infected SPC, neck tagged and placed in colony houses (20/house) 2 weeks prior to the placement of remaining treatments. Groups assigned vaccinates and unvaccinated contacts were eye drop vaccinated on the day of hatch against NDV/IBV and then inoculated i.a. with 2500PFU of attenuated MDV1 CVI-988 (CEVA Biomune). Vaccinates and unvaccinated contacts were cohoused alongside shedders two weeks after shedder placement. Birds were monitored daily with food and water provided *ad libitum*. All the birds were spray boosted with NDV/IBV on the 29th day post hatch. Euthanasia by cervical dislocation, necropsy and lesion scoring was performed on the 49th day post hatch for shedders and the remaining treatments. The vaccine efficacy study was approved under IACUC protocol #64R-2016-0, addendum 1 and USDA APHIS permit # 130630.

5.3.1.2 *In vivo* vaccine efficacy study II

Plasma (MD+) obtained was from a vaccine efficacy study in commercial broilers. Commercial broilers chicks on the day of hatch were eye drop vaccinated with NDV/IBV, neck tagged and i.a inoculated with 200-400PFU of TK-2a-infected SPC. Birds were provided with food and water *ad libitum*. All the birds were spray boosted with NDV/IBV on 29th day post hatch. Euthanasia by cervical dislocation, necropsy and lesion scoring was performed on 49th day post hatch. For isolation of plasma, syringes pre-loaded with heparin were used to obtain whole blood via intracardiac invasion and heparinized whole blood (400units/ml heparin) was spun at 2500xg at 4^{0}C. The vaccine efficacy study was approved under IACUC protocol #64R-2016-0 SOP1.

5.3.2 Exosome purification from serum, plasma and culture supernatants

Exosome purification from sera and plasma samples was done upon serial centrifugation steps (300xg for 10min to remove cells, 2000xg for 30min to remove cell detritus, 10000xg for 45min to remove larger microvesicles) followed by filtration using 0.22µm filter (Millipore). Total exosome isolation reagent precipitation solution (1/10th volume or 20µl) for serum and plasma (TEI, Invitrogen^{TM}) was used to purify exosomes from serum and plasma (200µl volume) respectively following manufacturer's instructions at room temperature.

Exosome purification from UD35 cell line culture supernatants was performed by "ExtraPEG" method of purification as recommended by Rider *et al*;(241). Briefly, after performing serial centrifugation steps to remove cells (500xg for 10min) and cell detritus (2000xg for 30min at 4^{0}C) followed by a filtration (0.22µm filter) step to remove residual cell debris and apoptotic bodies, culture supernatant was combined

with equal volume of 2X PEG (16%) +1M NaCl (M.W. 8000, Sigma) to achieve 8% PEG final concentration. 8% PEG purifies exosomes with the highest purity and less protein aggregates (241). Exosomal protein content was quantified by Pierce BCA assay (Thermo scientific, Waltham, MA).

5.3.3 Exosome particle size and concentration characterization

5.3.3.1 Exosome particle size and concentration characterization via Dynamic Light Scattering

To determine particle size and concentration, exosome samples (stored at −80 °C) were thawed and gently vortexed before further diluting in sterile, particle-free PBS at ratios between 1:250 and 1:1,000 to achieve final particle concentrations consistent with the optimal range of analysis by the instrument (Mobius, dynamic light scattering) at Advanced Materials characterization lab in ISE lab at the University of Delaware.

5.3.4 Transmission Electron Microscopy

TEM analyses of exosomes was performed on nickel TEM grids (Electron Microscopy Sciences), 400 mesh with a formvar coated carbon film. Grids were floated on the drops of purified exosome-PBS suspensions to allow adsorption onto formvar coated carbon grids. Following a series of washes in water, grids are contrasted in a solution of 1% uranyl acetate and a phospholipid stain. Air dried grids are observed under TEM (Zeiss Libra 120) at 80kv at DBI Imaging center.

TEM images were analyzed by ImageJ software (NIH, Frederick, MD) to calculate the size and number of exosomes in each TEM field. TEM field images were scale set using the TEM scale on the left hand corner of each field, duplicated and

band pass filtered at 40 x 30 pixels. Image threshold was set just to select the exosomes and not the grainy background. Exosomes were measured using "analyze particles" function with set area: 500-infinity and circularity: 0.05-1.00. Particle areas were imported into excel and diameters were calculated using area = πr^2 formula.

5.3.5 Small RNA-seq

5.3.5.1 Exosome RNA isolation and RNA quality determination for high through put sequencing of exosomal small RNAs

Serum and plasma samples from *in vivo* vaccine efficacy study I and II respectively were used for high throughput sequencing. Exosomes were precipitated by ExoQuick Solution (System Biosciences) followed by loading of exosome lysate onto SeraMir columns (System Biosciences). Column eluted RNAs were subject to concentration and quality check by Agilent 2100 Bioanalyzer (Agilent technologies). Total RNA concentrations ranged from 0.27-2.27 μg. Bioanalyzer profiles indicated exosomal RNA lengths fell within the range of 20-30 nucleotides (nts) upon comparison with ladder.

5.3.5.2 Small RNA library preparation

Small RNA libraries were prepared by Illumina Truseq™ Small RNA Preparation kit according to manufacturer's instructions. Briefly, small RNAs were adaptor ligated on both 5' and 3' ends followed by reverse transcription with a primer complementary to 3' adaptor. The resultant cDNA products were subject to PCR amplification using a common PCR Primer complementary to 5' end adaptor (RNA PCR Primer 1) and a reverse primer containing a primer index on the 5' end of the region complementary to 3' adaptor. The PCR amplification step allows library

amplification along with index bar coding to facilitate multiplexing during sequencing runs.

The purified cDNA library was subject to cluster generation on Illumina cluster station and then sequenced on Illumina Hiseq Platform. Raw sequencing reads (~50 nt) were obtained using Illumina's Sequencing Control Studio software version 2.8 (SCS v2.8) following real-time sequencing image analysis and base-calling by Illumina's Real-Time Analysis version 1.8.70 (RTA v1.8.70). The extracted sequencing reads were stored in *SampleID_RawData.fq* FastQ files, which were then used in the standard data analyses pipelines described in the next couple of sections.

5.3.6 RNA-seq data analyses

A proprietary pipeline script, ACGT101-miR v4.2 (LC Sciences), was used for sequencing data analysis. Upon obtaining raw sequence reads from the image data, a series of digital filters were applied to exclude unmappable low complexity reads (reads lacking 3' adaptor, adaptors with greater than one mismatch, reads with >32nts after 3' adaptor removal, reads < 15nts after 3' adaptor removal) and generate mappable reads.

5.3.6.1 Generation of unique families of sequenced sequences by sorting raw reads

In this step identical sequenced sequences in the raw read data files were clustered into unique families and a fastq (.fq) file containing unique reads were generated and labeled as *SampleID_unique.fq*. One typical entry of this file is as follows:

@5_18368

AGCAGAGTGGCGCAGCGGAAGCGTGCTGGGC

+

Fffffeffffffffeeedeeeeceeefeee

The first line in the entry indicates sequence identification composed of index and the copy number of sequenced sequences. The second line indicates the read sequence. The fourth line indicates sequencing quality of the corresponding bases using average Phred score.

5.3.6.2 Filtering sequenced sequences

Low complexity or impure sequences during sample preparation, sequencing chemistry, optical digital resolution of sequencing detector and other processes were removed. The remaining filtered sequences with lengths between 15-32 bases were grouped by families and stored in files labeled *SampleID_mappableReads.fq* which were subsequently used to map against reference databases or genomes.

5.3.7 FastQC quality check

FastQC is not performed as part of quality check in AGCTmir-101 pipeline. However, an independent FastQC quality check was performed to spot problem either in the sequencer or starting library material. FastQC was ran in a stand-alone interactive mode to analyze *SampleID_mappableReads.fq* files. FastQC analyses was performed on the University of Delaware High performance computing cluster Biomix (Delaware Biotechnology Institute). FastQC reports were created in HTML versions as a more permanent record.

5.3.8 Mapping mappable reads to reference databases

Mappings were performed on unique sequences against precursor miRNAs (pre-miRNA) and mature miRNA (miR) sequences listed in the miRBase latest

version (v:22) or reference genomes of selected host species or virus. Mappings were also performed on miRNAs of interest against reference genome. Length variation at both 3' and 5' ends and only one mismatch inside the sequence were allowed in the alignment.

5.3.8.1 Mapping unique sequences to miRs in miRBase

The unique sequences in *SampleID_mappableReads.fq* files were mapped against pre-miRNAs of selected species including *Gallus gallus* and zebra finch (*Taeniopygia guttata*). The mapped reads were grouped as 'unique sequences mapped to selected pre-miRNAs in miRBase' while the remaining ones were grouped as 'unique sequences unmapped to selected pre-miRNAs in miRBase'

5.3.8.2 Group 1

The pre-miRNAs to which the unique sequences mapped to pre-miRs in miRBase were further mapped to genomes of *G.gallus* and *T.guttata*. The pre-miRNAs mapped to genomes were selected and unique sequences associated with these pre-miRNAs were grouped as "unique sequences mapped to pre-miRNAs that further mapped to genomes of selected species". This group comprised three subgroups Group 1a, 1b and 1c.

5.3.8.2.1 Group 1a

Unique sequences in this group meet the following criteria: (1) Unique sequences were first mapped to the selected pre-miRNAs in miRbase; (2) these pre-miRNAs were mapped to the genome; (3) the pre-miRNAs /miRs are known pre-miRNAs /miRs of the specific species. Their alignments were presented in the file [Sample]_gp1a_aln.txt. A summary file was also generated as[Sample]_gp1a_sum.txt.

5.3.8.2.2 Group 1b

Unique sequences in this group meet the following criteria: (1) Unique sequences were mapped to the selected pre-miRNAs in miRbase; (2) the pre-miRNAs were mapped to the genome; (3) the pre-miRNAs /miRs are known mirs/miRs of other selected species. Their alignments were presented in the file [Sample]_gp1b_aln.txt. A summary file was also generated as [Sample]_gp1b_sum.txt.

5.3.8.2.3 Group 1c

This group includes unique sequences in Group 1a and 1b. These unique sequences were mapped not only to the locations of known pre-miRNAs /miRs but also to other locations in the genome. Their alignments were presented in the file [Sample]_gp1c_aln.txt. A summary file was also generated as Sample]_gp1c_sum.txt.

5.3.8.3 Group 2

5.3.8.3.1 Group 2a

Unique sequences were included in Group 2a if they meet the following criteria: (1) unique sequences were mapped to the pre-miRNAs of selected species (*G.gallus; Tguttata*); (2) the pre-miRNAs were, however, not mapped to the genome of the specific species; (3) but the unique sequences were mapped to the genome; (4) the extended sequences at the mapped positions of the genome potentially form hairpins. Their alignments were presented in the file [Sample]_gp2a_aln.txt. A summary file was also generated as [Sample]_gp2a_sum.txt.

5.3.8.3.2 Group 2b

Unique sequences were included in Group 2a if they meet the following criteria: (1) unique sequences were mapped to the pre-miRNAs of selected species

(*G.gallus; Tguttata*); (2) the pre-miRNAs were, however, not mapped to the genome of the specific species; (3) but the unique sequences were mapped to the genome; (4) the extended sequences at the mapped positions of the genome potentially CANNOT form hairpins. Their alignments were presented in the file [Sample]_gp2b_aln.txt. A summary file was also generated as [Sample]_gp2b_sum.txt.

5.3.8.4 Group 3

5.3.8.4.1 Group 3a

Unique sequences were included in Group 3a if they meet the following criteria: (1) unique sequences were mapped to the pre-miRNAs of selected species (*G.gallus; Tguttata*); (2) the pre-miRNAs were, however, not mapped to the genome of the specific species; (3) the unique sequences were also not mapped to the genome; (4) the unique sequences were mapped to miRs of selected species. Their alignments were presented in the file [Sample]_gp3a_aln.txt. A summary file was also generated as [Sample]_gp3a_sum.txt.

5.3.8.4.2 Group 3b

Unique sequences were included in Group 3b if they meet the following criteria: (1) unique sequences were mapped to the pre-miRNAs of selected species (*G.gallus; Tguttata*); (2) the pre-miRNAs were, however, not mapped to the genome of the specific species; (3) the unique sequences were also not mapped to the genome; (4) the unique sequences were NOT mapped to miRs of selected species. Their alignments were presented in the file [Sample]_gp3b_aln.txt. A summary file was also generated as [Sample]_gp3b_sum.txt.

5.3.8.5 Mapping unique sequences to selected databases

Mappable unique sequences were mapped to other defined databases such as mRNA, Rfam piRNA and Repbase. Mapped unique sequences were presented in the file [Sample]_others.txt.

5.3.8.5.1 Group 4a

Unique sequences were included in Group 4a if they meet the following criteria: (1) unique sequences were not mapped to the pre-miRNAs of selected species (*G.gallus; Tguttata*); (2) unique sequences were mapped to the genome (3) the extended sequences at the mapped genome positions have the propensity to form hairpins. Their alignments were presented in the file [Sample]_gp4a_aln.txt. A summary file was also generated as [Sample]_gp4a_sum.txt.

5.3.8.5.2 Group 4b

Unique sequences were included in Group 4b if they meet the following criteria: (1) unique sequences were not mapped to the pre-miRNAs of selected species (*G.gallus; Tguttata*); (2) unique sequences were NOT mapped to the genome (3) the extended sequences at the mapped genome positions DONOT have the propensity to form hairpins. Their alignments were presented in the file [Sample]_gp4b_aln.txt. A summary file was also generated as [Sample]_gp4b_sum.txt.

5.3.8.6 No hit

The unique sequences that belong to none of Group 1, Group 2, Group 3, Group 4, and other selected databases are defined as Nohit and presented in file [Sample]_nohit.txt.

5.3.9 Mapping Summary

All groups above (excluding Group 4b and Nohit) were summarized and listed in [Sample]_uni_miRs.txt as mapped miRs or predicted miRs.

5.3.10 Multiple sample comparison

Normalization of sequence counts in each sample (or data set) is achieved by dividing the counts by a library size parameter of the corresponding sample. The library size parameter is a median value of the ratio between the counts a specific sample and a pseudo-reference sample. A count number in the pseudo-reference sample is the count geometric mean across all samples. Sequences were removed if corresponding maximum number of raw reads in all samples is less than 10. In a statistic test, a sequence is removed if the mean value of the normalized reads of all samples involved in the test is less than 10.

Comparisons are made between Vaccinated and protected leghorns (PVL) and Tumor bearing leghorns (TBL); Vaccinated and protected leghorns (PVL) and Tumor bearing broilers (TBB); Tumor bearing leghorns (TBL) and Tumor bearing broilers (TBB). Multiple group comparisons utilized One-way ANOVA as statistical test where as comparisons between two groups utilized Student's t-test to determine significance.

5.3.11 MirDeep2 analyses of MDV1 miRNAs

A UNIX based server installed with PERL-based package miRDeep2 (version 2.0.0.7), initially created by Friedlander *et al.,* was utilized to map reads originating from MDV1 genome (362). The unique sequences in the *SampleID_mappableReads.fq* files were converted in to FASTA format as corresponding *SampleID_mappableReads.fa* files. The FASTA files were filtered to

limit the sequence length to 17 bases as required for miRDeep2 using the following one liner script

```
awk -v min="17" 'BEGIN {RS = ">"; ORS = ""} length($2) >= min {print ">"$0}' SampleID_mappableReads.fa > SampleID.fa
```

The sequence IDs in the filtered FASTA files were modified to MSP_SampleID_xSequenceID using a series of "grep" functions to match miRDeep2 input format. Next, using mapper function (*mapper.pl*) of miRDeep2, all the reads with identical sequence were collapsed to remove redundancy. The collapsed reads were mapped to the pRB1B genome with bowtie, using the options: bowtie –f –n 0 –e 80 –l 18 –a –m 5 –best –strata. The option '-n 0' keeps only alignments with no mismatches in the seed region of a read mapped to the genome. The seed region is defined by '-l 18' option that corresponds to the first 18nt of a read sequence. The option '–e 80' allows only two mismatches in the sequence of the read after the seed region. The option '-m 5' keeps only reads that do not map more than five times to the pRB1B genome. Option '–best –strata' orders the mappings from best to worse alignments and if the mappings with 0 mismatches occur, then mappings with one or two mismatches are not reported. Finally, processed reads and the mappings to the genome are outputted in *.arf* format.

Mapper module output was directly input to the miRDeep2 module to identify known and novel MDV1 miRNAs. In addition, a pRB1B reference genome, FASTA file containing the reads (labelled as *SampleID_mappableReads.fa*), known mature, star and precursor MDV1 miRNAs from the miRBase and mature miRNAs from other herpesviruses (HSV1, HSV2, EBV, KSHV, MGHV, RRV, RLCV, HVS, BHV1, BHV5, PRV, HCMV, MCMV) were added in the input.

The first step of miRDeep2 work flow was to sanity check the format of the input files, so that any format problems that are identified can be corrected by the user before the actual analysis begins. Since known mature, star, and precursor MDV1 miRNAs were input in the miRDeep2 module, they are automatically input into the Quantifier module to ensure that all known MDV1 miRNAs are included in the output, even if they are not scored by miRDeep2.

Second step was by using the mapped reads as guidelines, potential miRNA precursor sequences are excised from MDV1 genome, that is by excising the genomic sequence covered by the mapped read and some flanking sequence.

Third step was the 'bowtie' mapping of reads against the excised potential miRNA precursors.

In fourth step, RNAfold tool was used to predict if the RNA secondary structures that resemble a typical miRNA hairpin exist in each excised potential precursor.

The fifth step involved the miRDeep2 core algorithm estimating the structure and signature of each potential miRNA precursor. If the structure resembles a miRNA hairpin and the reads map with in the hairpin as is typical from Dicer processing, then the potential precursor is assigned a score that reflects the likelihood of it being a genuine miRNA. If not, the potential precursor is discarded. This step of miRDeep2 prevents any chance intersection of false positives due to the ability of a large number of reads forming hairpins but have no connection to miRNA biology.

miRNA expression levels in each sample were determined by dividing the number of mature miRNA reads for a given MDV1 miRNA by the total number of mapped MDV1 reads and multiplying by the total number of mapped MDV1 reads

with the most abundant MDV1 mapped reads [(mature reads) / (total mapped reads) * (total mapped reads 'most abundant')]. In our analyses, as we performed read counts independently for each sample from each bird, miRNA expression levels from miRDeep2 output weren't taken into account except the total read count which is a sum of mature and star read count.

5.3.12 miRNA-gene target prediction

miRNA target prediction was performed using the miRDB online resource and analysis platform (http://www.mirdb.org//). Launched in 2008, it was comprehensively updated where the complete set of miRNA sequences from the miRBase repository were downloaded along with the complete set of *G.gallus* 3'UTR sequences contained in the NCBI RefSeq database (363). In addition, the miRDB target prediction algorithm, MirTarget, which was developed using support vector analysis of high throughput expression data, predicts conserved and non-conserved target genes via weighting target site conservation as a high priority, but not as a strict requirement. MiRDB target scores range between 50 to 100, with a greater score indicating a greater statistical confidence in the target prediction. The FAQ section on the miRDB website indicates "a predicted target with a score > 80 is most likely to be real." Henceforth, targets with scores greater than 80 were considered the most confident gene predictions.

5.3.13 Geneious mapping of transcript reads to MDV1 genome

Quality controlled mappable reads were mapped against pRB1B reference genome (Accession no: EF523390) to produce a contig, using the Geneious read

mapper with 10% allowed gaps per read, word length of 18, and 20% maximum mismatches per read and with structural variant, insertion, and gap finding allowed.

5.3.14 Tumor suppressive effect of vaccinate serum exosomes on the growth and proliferation of UD35 cell line

To determine the effect of CVI-988 vaccinate serum derived exosomes on the growth and proliferation of UD35 cell line, a total of 4 x 10^7 UD35 cells were CFSE labeled in 1X PBS + 1% BSA for 10 min at 37˚C. Labeling is then quenched by growth media addition followed by pelleting via centrifugation and final resuspension in growth media described for UD35 cell line except 10% Exosome free FBS (Gibco) was employed instead of routine FBS. Cells were adjusted to 0.5 x 10^6 cells/ml per well and the following treatments were performed; 1. Medium Only 2. Medium + 5 µg tumor bearing bird exosomes 3. Medium + 5 µg vaccinate serum exosomes 4. Medium + 50 µg vaccinate serum exosomes. Dishes were incubated at 41 ˚C. Post incubation period for various time points (24hr, 48hr, 72hr and 96hr) cells were pelleted in standard flow cytometry tubes (BD Falcon) and fixed in 4% paraformaldehyde. Serial wash steps were performed in 1X PBS + 1% BSA + 0.1% NaN3 and cells were finally resuspended in FACS buffer for acquisition. CFSE labeled cells were processed and handled under foil wrapped conditions. CFSE dye dilution was acquired by BD FACS flow cytometer set at 490nm/517nm excitation/emission. Mean fluorescence for each treatment condition at a particular time point was normalized to dye fluorescence from the input set as time point zero to calculate the Proliferation Index (PI).

5.3.15 UD35 TEX effect on innate signaling induced by canonical innate agonists

To determine immune modulatory or immune suppressive nature of UD35 cell supernatant (sup) derived exosomes (UD35 exo), CEFs were preseeded on eight 6 well

dishes at 6 x 10^5 cells per well and maintained overnight in M199 (Hyclone) medium supplemented with 1% calf serum, 1X PSN and 1X fungizone. Next day, media was removed and refed with M199 base media consisting of the following treatments; 1. Medium only 2. Medium + 0.5 µg UD35 exo 3. Medium + 5 µg UD35 exo 4. Medium + 50 µg UD35 exo. 1-hour post exosome treatment or uptake, each treatment condition was subjected to innate agonists LPS (5µg/ml), poly I:C liposome mix (15µg/ml) and pBKCMV-mCherry DNA liposome mix (100ng/ml). All the treatments were performed in triplicates. Canonical innate agonists LPS, poly I:C and plasmid DNA induce activation and downstream signaling of innate receptors TLR4, MDA5 and cGAS respectively. Treatments were incubated for an additional 24hr followed by media removal and direct addition of RLT lysis buffer to harvest the monolayers for RNA isolation and gene expression analyses.

5.3.16 RNA isolation and miRNA expression analysis

Total exosomal RNA (m/miRNA) was isolated by Trizol procedure (Invitrogen) following manufacturer's recommendations. RNA was DNAse treated (Ambion RNAse free DNAse). For miRNA profiling of serum/plasma exosomes belonging to *in vivo* vaccine efficacy study I and II, 100ng of RNA was subjected to miRNA specific reverse transcription (RT) by a miRNA specific RT primer carrying a 5' universal reverse tag using Superscript IV reverse transcriptase (Invitrogen) following manufacturer's recommendations. cDNA was 1:4 diluted with nuclease free water and 2µl of cDNA was employed in a 20ul reaction composed of 10 µl iTaq universal SYBR® Green Supermix (Bio-Rad, Hercules, CA), 7.8 µl of nuclease free water 0.4 µl (4nM) of miRNA specific forward primer carrying a universal sequence on its 5' end and 0.4 µl (100nM) each of M13 forward and reverse universal primers.

The miRNA specific reverse transcription and qRT-PCR analysis described here followed mir-Q approach that had been already described elsewhere (364). Primers employed produced unique melt curves lacking non-specific amplification. miRNA expression was normalized to the global geometric mean of Ct values by comparative ΔCt method (365). Cellular RNA isolation, reverse transcription and qRT-PCR gene expression analyses was performed as previously described (213).

5.3.17 Proteomic analysis of exosomes

For proteomic analysis, 50 µg of total exosomes were submitted to Dr. Fiona McCarthy and Mr. Ken Pendarvis at the University of Arizona Core Proteomics facility (Keating Bioresearch Building, U. Arizona, Tucson, AZ). Protein extraction from exosomes was performed as described by McCarthy *et al*., (366). Differential detergent fractionation was performed with digitonin followed by Triton X-100 to extract soluble and membrane associated exosomal protein fractions. Protein fractions were treated with a mixture of DNase I (50U; Invitrogen, Carlsbad CA) and RNase A (50 mg; Sigma-Aldrich, St Louis, MO) to digest intact nucleic acids at 37^0C for 30min. Samples were centrifuged at 6,200 × g for 10 min at 10°C to pellet the debris.

An equal volume of 50% trichloroacetic acid (TCA) was added to the sample supernatants, and exosomal proteins were precipitated at −20 °C overnight. The precipitated proteins were pelleted by centrifugation at 6,200× g for 10 min at 10°C, washed with ice-cold acetone and dried at room temperature. The proteins were subsequently resuspended in 0.5 mL of solubilization solution (7M urea, 20 mM Tris-Cl, pH 8.0, 5mM EDTA, 5 mM MgCl2, 4% CHAPS, 1 mM PMSF) and quantitated using the 2-D Quant Kit (GE Healthcare Life Sciences). An aliquot of 0.1 mg of proteins was precipitated again with 50% TCA at −20 °C, followed by centrifugation

and a wash with ice-cold acetone. Samples were resuspended in 0.1 mL of 100 mM ammonium bicarbonate and 5% acetonitrile, reduced with 5 mM dithiothreitol for 10 min at 65 °C, alkylated with 10 mM iodoacetamide for 30 min at 30 °C, and finally digested with 2 μg of sequencing grade trypsin at 37 °C for 16 h. Peptides were desalted using a peptide macrotrap (Michrom Bioresources, Inc.), dried at room temperature, and stored at −80 °C until further processing. Desalted peptides were vacuum centrifuged until dry and resuspended in 2μL of 2 % acetonitrile, 0.1 % formic acid and transferred to low retention vials in preparation for analysis using 1D-LC–MS/MS.

Samples were transferred to low retention HPLC vials for analysis using mass spectrometry. Peptide mass spectrometry was performed upon separation of proteins using a one dimensional Dionex U3000 splitless nanoflow HPLC system operated at 333 nl per minute using a gradient from 2 to 50 %acetonitrile over 4 h. The C18 column, an in-house prepared 75 μm by 10 cm reverse phase column packed with Halo 2.7 μm, 90 A° C18 material (MAC-MOD Analytical), was located in the ion source just before a Proxeon ES562 40 mm, 30 μm id stainless steel emitter. U3000 eluate is analyzed with an LTQ Velos (Thermo Scientific) linear ion trap mass spectrometer at the University of Arizona Proteomics Core facility (367).

Scan parameters for the LTQ Velos Pro were one MS scan followed by 10 MS/MS scans of the 5 most intense peaks. MS/MS scans were performed in pairs, a CID fragmentation scan followed a HCD fragmentation scan. All scans were performed in enhanced resolution mode. Dynamic exclusion was enabled with a mass exclusion time of 3 min and a repeat count of 1 within 30 s of initial m/z measurement.

5.3.17.1 Protein Identification

Mass spectra and tandem mass spectra were used to search subsets of the non-redundant protein database (nrpd) downloaded from the National Center for Biotechnology Institute (NCBI; 06/14/04) using TurboSEQUEST (Bioworks Browser 3.2; ThermoElectron). Analysis was performed on avian non-redundant protein database or NRPD (AVIAN DB; search terms: chicken, gallus, cornix, aves, turkey, and ostrich NOT plant, yeast, bacteria, virus). In addition, a non-avian vertebrate subset of the NR protein database (NAVDB; search terms: mammal, Homo, Rattus, Mus, fish, and excluding the terms used to create the AVIAN DB) was used to identify more proteins. Trypsin digestion was applied in silico to AVIAN DB and NAVDB and included mass changes due to cysteine carbamido-methylation and methionine oxidation. The peptide MS precursor ion mass tolerance was set to 1.5 Da and the fragment ion (MS^2) mass tolerance was set to 1.0 Da. Peptide matches were considered genuine if they were greater than 6 amino acids and consistent with described X correlation and ΔCn values.

5.3.17.2 Bioinformatic analysis of identified proteins

Refseq IDs of identified proteins were mapped to their corresponding UniprotKB IDs and unmapped proteins were mapped against UniProt archive (UniParc) to obtain the closest hit.

Exosomal protein set enrichment analysis was performed by first identifying previously found EV proteins, in the downloaded Vesiclepedia database of vesicular proteins (Version 3, 9 Jan 2015) from www.microvesicles.org/download. Enrichment of cellular compartment Gene Ontology term was performed using FunRich v3 (368).

5.4 Results

5.4.1 Size, concentration and morphological characterization of exosomes

During our initial characterization of size and concentration of exosomes purified from culture supernatants of various transformed cell lines representative of viruses of distinctive virulence, exosomes samples were measured using dynamic light scattering instrument. Each sample was measured 5 times, with 10 data samplings per measurement. Of note, even though exosome-depleted FBS (spun at 100,000 x g for 4 hrs at 4˚C) was employed, there remained substantial numbers of residual exosome-sized particles in the medium only treatment. It is possible that these particles were of large serum protein aggregates or FBS exosome carryovers themselves. The particles observed were spherical, but somewhat smaller in size than anticipated size of exosomes (25 – 35 nm range), but the size tended to increase with subsequent measurements. These were present at ~4.5 x 6.5 x 10^5/analysis volume (1 mM light path) and were therefore at a concentration of ~5 x 10^6/ml (Figure 5.1A). The presence of MDV-mir-M4 in exosomes derived from MDV cell lines and absence of cellular mir-155 or small nuclear U6 RNA demonstrates the integrity of purified exosomes and their content. Cellular mir-155 was detected at a Ct value of 34.72 in CU-91 (REV-transformed) derived exosomes whereas it was undetected in MDV transformed cell line derived exosomes similar to what had been described previously (Figure 5.1B)(106).

For characterizing serum exosomes from *in vivo* vaccine efficacy study I, TEM imaging was performed on one random sample representative of each treatment, for all three treatments (CVI-988 Bird# BL3822 vaccinate and protect serum exosomes, TK-2a contact, Bird# OR1760, serum exosomes and UD35 passage 24 transformed cell

line supernatant exosomes). Upon ImageJ analyses, number of exosomes per TEM field from CVI-988 vaccinate and TK-2a contact serum exosomes were 12 and 17 (Median) respectively from a total of 20 TEM fields (Figure 5.2A, B and C). Number of UD35 derived exosomes per TEM field was significantly higher (Median ~ 173) (Figure 5.2). This greater difference in number between serum and culture supernatant derived exosomes can be due to the amount of starting material used for exosome purification (100µl serum vs 20ml culture supernatants). Alternatively and most relevant, transformed cell lines represent homogenous populations with significantly higher number of exosomes produced than healthy normal cells as described previously (254). Cancer patient sera contain significantly higher number of exosomes per ml compared to healthy individual (4000 trillion vs 2000 trillion)(253). However, at least, exosome numbers from TEM fields weren't significantly different from CVI-988 vaccinate and TK-2a contact sera. Total number of exosomes among all 20 fields reflected the median numbers per field seen with each treatment. A total of 379, 584 and 3420 exosomes were analyzed by ImageJ from CVI-988 vaccinate, TK-2a contact and UD35 supernatant derived exosome treatments respectively (Figure 5.2B).

Area and diameter measurement indicated a median diameter of 30.99nm and 28.9nm for CVI-988 vaccinate and TK-2a contact exosomes respectively conforming to the usual exosomal size range (Figure 5.2C). Diameter of UD35 derived exosomes was intriguingly smaller with a median of 17.3nm (Figure 5.2C). UD35 exosomes were purified using 8% PEG (M.W 8000) solution in an attempt to concentrate larger quantities of culture fluids. PEG in water exists as rigid helical segments and hydrogen bonding of water occurs with oxygens along the disordered parts of helix (369). Disorder and water binding can enhance the osmotic pressure exerted on exosome cell

walls leading to a reduction in the amount of size detected. Either complete removal of PEG from exosome suspension or resorting to ultracentrifugation methods rather than PEG purification should solve this problem. In addition, sample processing and drying during TEM negative staining procedure can cause exosome size alterations.

Finally, visualization of particles by TEM displayed particle morphology identical with that of exosomes with greater number of particles seen in contact serum and UD35 culture supernatant treatments (Figure 5.3)

5.4.2 RNA-Seq results

5.4.2.1 FastQC analyses

FastQC report provided basic statistics, per base sequence quality, per sequence quality score, per base sequence content, per sequence GC content, per base N content, sequence length distribution, sequence duplication levels, over represented sequences and adaptor content.

Basic statistics of read sequences from all samples indicated the number of 'Sequences flagged as poor quality' as 0. In addition, the %GC content of read sequences fell in the range between 48-56%.

Per base sequence quality provides the quality values across all bases at each position in the FastQ file. Mappable reads from all the samples displayed good quality calls at every base position. Base call quality on most platforms usually degrades as the run progresses. However, in our study, since the reads were filtered of low complexity sequences, the base quality of mappable reads was very good with no falling into the orange area at the end of the read (Figure 5.4).

Per sequence quality score report indicated that the sequences are of high quality. Phred scores for the reads from all the samples were ~39 (Figure 5.5).

Per base sequence content indicates the proportion of each base position in the reads for which each of the four normal DNA bases has been called. For a successful sequence run in a random library, it is expected that there would be little to no difference between the different bases, so the lines in this plot must run parallel with each other unless there is an overrepresented sequence in the library that is creating a strong bias. Sample reads from all samples had plots with lines running parallel to each other indicative of a lack of contaminating overrepresented sequence in our libraries (Figure 5.6).

Per sequence GC content measures GC content across the whole length of each sequence in a file and compares it to a modelled normal distribution of GC content. In a random library with no over represented sequences one would expect to see a roughly normal distribution of GC content where the central peak corresponds to the overall GC content of the underlying cellular and viral genomes. GC content of the reads from all samples in our study followed normal distribution that overlapped reference distribution based on modal GC content that is calculated from the observed data (Figure 5.7).

Per base N content represents the base positions that are substituted as N if the sequencer is unable to make a conventional base call with sufficient confidence. Although a very low frequency of Ns (3%) were observed at the first base position of every read, no Ns were called at any of the remaining positions (Figure 5.8).

Sequence length distribution module of FastQC graphs the distribution of fragment sizes in the raw reads file generated by the sequencer. The graph displayed peak at one size (~51bases) indicative of uniform read lengths (Figure 5.9).

No duplicate sequences indicative of enrichment bias or higher level of coverage of a particular target sequence was observed in the raw reads. No sequence duplication was observed among the analyzed reads (Figure 5.10).

A normal high-throughput library contains a diverse set of sequences. Any overrepresentation of a single sequence means that either it is highly biologically significant or that the library is contaminated. For every overrepresented sequence, the program will look for matching contaminants in the database and reports the best hit. Matching hits must be at least 20bp in length and have no more than 1 mismatch. No overrepresented sequences were found in the libraries of raw reads analyzed (Figure 5.11).

5.4.2.2 RNA-seq read statistics

Quadruplicate serum exosome samples from Vaccinated and protected leghorns (PVL), tumor bearing leghorns (TBL), and tumor bearing commercial broilers (TBL) were analyzed to generate 8-27 million raw reads per sample (Table 5.1). Upon removal of reads lacking 3' adaptors, reads < 15nts, and reads > 32 nts, the number of mappable reads constituted 4.8-12 million reads per sample. The length distribution of a majority of mappable reads was 21nts (16%) followed by 22nts (15.2%) and 20nts (13.9%) corresponding to an average size range of miRNA.

Of total number of mappable reads (112.35 million), 27.1% of reads mapped to the *G.gallus* genome (Groups 1a +1b +2a + 2b + 3a + 3b + 4a) where as 8.5% of reads did not map to the genome of selected species (Group 4b). 11.7% of total mappable

reads mapped to others RNAs including rRNA, tRNA, snRNA, snoRNA, piwiRNA and others deposited in the Rfam database (Table 5.2). 7.9% of total mappable reads mapped to *G.gallus* mRNAs. 47.9% of total mappable reads displayed no hit and possibly constituted reads originating from the MDV-1 genome. 6.77% of total mappable reads mapped to pRB1B reference genome (Table 5.3).

Of total number of mappable reads, the number of reads mapped to precursor miRNAs of MDV1 ranged from 0.0018 to 0.85%. These precursor miRNAs include both the mature miRNA strand and the passenger strand of each MDV1 miRNA (Table 5.4).

5.4.2.3 Significant and differentially expressed (SDE) *G.gallus* miRNAs in PVL compared to TBL and TBB

Upregulated *G.gallus* miRNAs that are SDE > 2-fold in PVL compared to TBL included gga-mir-146b, -PC-3p-53, -10b, -2188, -27b, -99a, -26a, -146c, -24, -146a and -23b (Figure 5.13). Among the miRNA that displayed relatively greater expression levels in PVL compared to TBL, miR-146a, -146b and -146c share seed sequence and are predicted to have common targets, but are present on different chromosomal locations (chr13, 6 and 4 respectively). In addition, mir-23b, -27b and -24 are part of a mir-23b-27b-24-1 gene cluster located on chrZ. miRNAs gga-miR-30e and -199 were found to be expressed at relatively same levels in both PVL and TBL (Figure 5.13). Finally, miRNAs that are SDE < 2-fold in PVL compared to TBL included gga-mir-142, -125b, -181a, -let7i, -363, -92, -101, -let-7g, -451, -148a, -21, -7, -15c, -16, -16c and -23b (Figure 5.13). Among the that displayed relatively lower expression levels in PVL compared to TBL, mir-92 and -363 share seed sequence and belong to paralog clusters mir-17-92 (chr1) and mir-106a-363 (chr4) respectively.

Furthermore, let-7i and-7g miRNAs also share seed sequence and are located on chr1 and 15 respectively. In addition, mir-15c, -15 and -16c also share seed sequence and belong mir-15-16 family of miRNAs. mir-15-16 family of miRNAs exist as 4 paralog clusters in vertebrates. Whereas mir-15a/16-1 cluster invariably flanks TRIM13 on chr4, mir-15c-16c flanks HPRT on chr1 and both the clusters share a common 7nt seed sequence. The sequence similarity between the miR-15a/ miR-16-1 and miR-15c/miR-16c clusters led to the hypothesis that they share similar targets to some extent, although it remains to be tested. Conversely, the conservation of both the clusters among most vertebrates suggests that they have at least partially distinct roles, targets and thus functions.

Upregulated *G.gallus* miRNAs that are SDE > 2-fold in PVL compared to TBB included gga-mir-99a, -2188, -10b, -1388, let-7f, -146b, -26a, -27b, -30e, -146c, -23b (Figure 5.14). As mentioned above, only mir-27b and -23b belong to the same 23b-27b-24-1 cluster. miRNAs gga-miR-24 was found to be expressed at relatively same levels in both PVL and TBB. Finally, miRNAs that are SDE < 2-fold in PVL compared to TBL included gga-mir-199, -425, -181a, -92, -let7i, -181a, -126, -148a, -363, -21, -122, -142, -199 and -140 (Figure 5.14).

miRNAs that are commonly upregulated in PVLs comparison to TBB or TBL included, mir-99a, -2188, -10b, -146b, -26a, -27b, -146c and -23b. Likewise, commonly downregulated miRNAs included, mir-92, -363, -148a, -181a and -21.

Upon identifying miRdb predicted targets with a target enrichment score greater than 80, to represent high confidence targets, many of the SDE exosomal miRNAs up or downregulated in PVL and TBL respectively were found to target proto-oncogenes, hence referred to as tumor suppressor miRNAs (Table 5.5). One

exception was mir-10b, known to target HoxD10 in breast cancer. Mirdb identified targets of exosomal miRNAs up or downregulated in TBL and PVL respectively included targets that are both pro-oncogenes and tumor suppressors. Henceforth both OncomiRs and tumor suppressor miRNAs were identified to be upregulated in TBL (Table 5.6).

5.4.2.4 Tumor suppressive function of PVL-upregulated miRNAs on the growth of UD35 cell line

To confirm the putative tumor suppressor function of miRNAs upregulated in PVL, we performed a cell based assay where UD35 cells were treated with each of three treatments; 1. 5 µg TBB serum exosomes, 2. 5 µg PVL exosomes, and 3. 50 µg PVL serum exosomes. Exosomes were solubilized in serum free media and added on to assess their effect on the growth and proliferation of UD35 cell line at various times post exosome treatment (24hr, 48hr, 72hr and 96hr). Growth and proliferation of UD35 cells was assessed by BD FACS flow cytometer using CFSE dye dilution as a read out. Mean fluorescence for each treatment condition was normalized to dye fluorescence from the input at time point zero to calculate the Proliferation Index. A 61% reduction in the proliferation of UD35 cell line was observed by 72hr upon treatment with 50µg of PVL serum exosomes (Figure 5.15). There was, however, a gain in the proliferation in the residual cell populations by 96 hr, although the amount of proliferation still remained 30% lower than that of controls. No significant difference was found among other treatments at all the observed time points.

To investigate whether the reduction in proliferation is due to miRNA mediated post transcriptional regulation, we quantified miRNAs targeting **p**oly**c**omb **g**roup (**PcG**) proteins. Recent studies in our lab identified interactions between *meq*-

vIL-8 or meq-vIL-8ΔExon3 and PcG protein BMI-1. In addition, MD transformed cell lines consistently expressed higher levels of PcG transcripts and proteins (EZH2, BMI-1) and were sensitive to their inhibitors in a dose dependent manner (Nicholas Egan M.S. thesis; Parcells MS unpublished findings). PcG proteins form **P**olycomb **r**epression **c**omplexes (**PRC**1 &2) that serve to repress target loci. Most importantly, PRC2 activity represses key miRNAs involved in maintenance of stem cell like phenotypes during cancer. Interestingly, some the repressed miRNAs targets are PRC components themselves, for instance mir-200b, -200c (RING2, BMI-1, SUZ12), mir-203 (BMI-1) mir-101(EZH2), mir-26a (EZH2, JARID2) (370). Upregulating PcG targeting miRNAs had an inhibitory effect on the proliferation of many cancer cell lines (370). To investigate if the growth inhibitory effect seen upon PVL serum exosome (50μg) treatment of UD35 cell line is mediated by exosomal transfer of miRNAs targeting one or more polycomb group (PcG) proteins, we monitored the expression levels of miRNAs targeting common PcG proteins, gga-mir-200b by qRT-PCR. As expected, mir-200b was greatly expressed in PVL exosomes, whereas basal levels were observed in both MD+ hyline W36 (TBL) and commercial broiler TK-2a contact (TBB) exosomes. Furthermore, qRT-PCR determined expression (4-fold) of mir-200b was comparable to that identified in our RNA-seq experiment (5.6-fold) (Figure 5.16).

Among miRNAs greatly expressed in TBL and TBB compared to PVL, we confirmed the relevance of miRNA-21 that is known to target Programmed cell death 4 (PDCD4) and IL-12p35 to skew the responses toward T_{H2} phenotype (371-373). Targeted deletion of mir-21 in allergen sensitized mice skewed the responses towards T_{H1} phenotype with greater IL-12/IFN-γ production.

5.4.2.5 Immune suppressive function of UD35 exosomes on canonical innate agonist mediated signaling

A cell-based assay was performed where CEFs were pre-treated with 5 or 50 μg of exosomes purified from the supernatants of UD35 cell line and then stimulated with canonical innate agonists LPS, poly I:C and DNA plasmid (mCherry) to activate respective receptors (TLR4, MDA5 and cGAS respectively). Activation of innate receptors leads to downstream induction of Type I IFNs and inflammatory cytokines (IL-12p40 and p35) in an IRF3 and NFKB dependent manner.

In studies performed by Dr Erin Bernberg and colleagues, ectopic over expression of MDV-1 *meq* cluster miRNAs or HVT vectored MDV-1 *meq* cluster miRNAs abolished Type I IFN and ISG induction in CEF upon HVT infection indicating immune suppressive nature of MDV-1 encoded miRNAs (E. Bernberg, R. Morgan. Microbial Systems symposium 2016 and 2017). In our RNA-seq experiment, MDV-1 *meq* cluster miRNAs were upregulated 10-13-fold higher in TBL compared to PVL (see section 5.4.2.4 below).

We reasoned that should there be exosomal transfer of MDV1 miRNAs, the result would be a down modulation of Type I IFN and ISGs induced by these canonical agonists. Upon gene expression analyses, no significant difference in the expression of ISGs or MHC-II was observed in agonist + UD35 exosome treatments compared to agonist only treatment. Intriguingly, an enhanced expression (42-fold) of IL-12p40 subunit was observed in the agonist + UD35 exosome treatment compared to agonist only (8-fold increase). IL-12 subunits p35 and p19 remained significantly down regulated in both the treatments (Fig. 5.17F and G). Increased steady state levels of IL-12p40 indicates miRNA dependent modulation of NFκB pathways as previously

described (374), leading to production of immune suppressive homodimeric IL-12p40 subunits known as IL-12p80 upon TEX treatment (375) (Fig. 5.17E).

5.4.2.6 MDV1 miRNA expression in PVL compared to TBL and TBB

Read numbers of MDV1 miRNAs were also presented in order to describe a greater level of inter-bird variation in miRNA expression (Table 5.7). Although a greater than 2-fold expression of *meq* cluster 1 (except MDV1-mir-M2 and –M5), *meq* cluster 2 (except MDV1-mir-M1) and LAT cluster miRNAs was noted in TBL compared to PVL, none of the changes were statistically significant due to greater inter-bird variation in the number of reads.

On the other hand, a greater magnitude of upregulation was noted in TBB compared to PVL, with a significant upregulation of *meq* cluster 1 (except MDV1-mir-M4 and –M5), *meq* cluster 2 (MDV1-mir-M1 and -M11) and LAT cluster (MDV1-mir-M6 and –M7) miRNAs (Table 5.8 and Figure 5.18).

5.4.2.7 Mapping of reads onto MDV-1 genome

Mappable reads in PVL, TBL and TBB treatments were mapped against pRB1B reference genome (Accession No: EF523390) using Geneious (Biomatters Ltd). Surprisingly, a greater proportion of reads mapped to the reference genome compared to mature MDV-1 miRNAs (compare % of reads mapped to pRB1B reference in Table 5.3 versus % of reads mapped to mature MDV-1 miRNAs by mirDeep2 in Table 5.4). Since the mappable reads obtained in our current study were the result of size selection prior to small RNA sequencing and were further subjected to quality control steps to ensure their size range between 15-32nts, reads mapping to

the coding sequences may be the result of sequencing of fragmented transcripts or incomplete reverse transcription products during sample preparation.

Among the genes that are upregulated in PVL compared to TBL, glycoprotein I (gI), UL42 polymerase subunit neared significance (Table 5.10). In addition, a significant downregulation of UL39 large ribonucleotide reductase was evident in PVL compared to TBL. An overview of percent coverage of reads originating from PVL and TBL exosomes and mapped to MDV-1 genome is shown in Figure 5.19 and 5.20 respectively.

Among the genes that are significantly upregulated in PVL compared to TBB include glycoprotein M (gM), UL11 tegument protein, UL13 serine threonine kinase, UL14 minor tegument protein, Uracil DNA glycosylase, gL, gD, LORF3, US3 serine threonine kinase, ICP4, UL43 membrane protein and UL35 tegument protein (Table 5.11). An overview of percent coverage of reads originating from TBB exosomes and mapped to MDV-1 genome is shown in Figure 5.21.

5.4.3 Proteomic analysis of exosomes

Upon proteomic analyses of serum exosomes from PVL, TBL, TBB, and UD35 supernatant purified exosomes (UD35), we received Refseq IDs of identified peptides. Refseq IDs from each treatment were mapped to corresponding UniprotIDs. Unmapped IDs were BLASTed against UniParc to obtain closest *G.gallus* hits. Corresponding GeneIDs, entry names, gene names and protein names were output for gene enrichment analyses via Funrich_V3 (376) and DAVID (377).

To examine the overlap between data sets among various study treatments and the known vesicular proteins, exosomal proteins from each treatment were compared to those in Vesiclepedia compendium of extracellular vesicle molecular data (378).

For this, proteins from Vesiclepedia database were updated in Funrich_V3 along with our data sets. Funrich_V3 mapped 196/283, 337/467, 366/465, 521/677 total proteins from PVL, TBL, TBB and UD35 treatments respectively. Since Funrich is exclusively human specific and allows users to perform functional enrichment analysis against it using human genes/proteins (376), some of the proteins from our study treatments remained unmapped and thus excluded (For instance, *G.gallus* histones H4-I, H4-II, H4-III, H4-IV, H4-V, H4-VI, whose nomenclature varies with that of human).Among mapped proteins,182/196, 314/337, 334/366, 469/521 proteins from PVL, TBL, TBB and UD35 treatments were previously identified vesicular proteins confirming the sample integrity of exosomes. Finally, comparison to vesiclepedia revealed majority of proteins belonging to subcellular compartments: cytosol, exosomes, nucleus, plasma membrane, extracellular and lysosome in their descending order (Figure 5.22). In addition, unique viral and cellular proteins were identified in each treatment.

Some of the commonly identified exosomal protein functional groups in PVL include membrane receptors (C1r, EphA4), metabolic enzymes (GAPDH, LCAT, PCY1OXL), heat shock proteins (HSPA9), cytoskeletal proteins (ActA, ActB, ActG1, myo1E, tub2, -4, -5, -7), histones (H2A-1/2/4/6, H2B), ribosomal proteins (mRPS31), vesicle trafficking proteins (VAMP1, STXBP4, Arfgef12). MDV-1 protein identified in low abundances was ICP4 (spectral intensity ~0.1)

Among overrepresented proteins identified in PVL that are common to both TBL and TBB include collagen a-1, XXII chain, and IGFBP-complex acid labile subunit isoform). Collagen a-1 XXII (COL22A1) is associated with tissue integrity, myotendinous junctions, and cellular adhesion. It’s presence in exosomes may be associated with their targeting to tissues. The IGFBP-acid labile subunit (ALS), aka,

IGFBP-5 is similarly associated with systemic tissue integrity, and has been previously demonstrated to be expressed in exosomes

Common functional groups of exosomal proteins identified in TBL include β2m, membrane receptors (THRB, TSPAN10, C1r), metabolic enzymes (PKM, ENO1, GAPDH, LCAT), elongation factors (Eef1a2, Eef1B2, Eef2, Eif2s3, eIF4A2), heat shock proteins (HSPA4L, Hspbp1), cytoskeletal proteins (ActA, ActB, ActG2, myl6, my015a, tubb, tuba, DNAH), histones (H3-I,-II,-III,-IV, -V,-VI,-IX, H4-I-II-III-IV-V-VI, H2A-VII H2A-VI, H2A-VIII), ribosomal proteins (RPL-4, -5,-6,-10a,-17, -P1, -P2, RPS-2,-6,-19), vesicle trafficking proteins (VPS13A), chromatin modifying enzymes (KAT5, NSD1 – H3K36me, H4K20me, ATM) and pro-apoptotic protein (BID). MDV-1 proteins detected in TBL includes peptides corresponding to UL36 and UL47 tegument proteins.

Common functional groups of exosomal proteins identified in TBB include β2m, membrane proteins (CD36, CD48, CD5L, CD163L1), membrane receptors (INSR, CFTR, DMBT1), metabolic enzymes (PKM, ENO1, GAPDH, LCAT, PCYOX1L), elongation factors (Eef1a2, Eef2S3),heat shock proteins (Hsp5), cytoskeletal proteins (ActA1, ActB, ActA2, ActBl2, ActG1, myh6, myh7, tubb, tuba), histones (H2B-I,H2B-II,H2B-III,H2B-IV,H2B-VI , H2A-VII H2A-VI, H2A-VIII), ribosomal proteins (RPL-4,-5,-6,-10a,17, -P1, P2, RPS-2,-6,-19), vesicle trafficking proteins (RanBP), transcription factors (JunD, E2F4, YEATS2). The major tegument protein (MTP) encoded by UL36 (MDV049) gene was exclusively detected in TBL and TBB treatments.

5.5 Discussion

5.5.1 Characterization of size, morphology and miRNA content of exosomes

In the present work, exosomal small RNA and protein content was investigated by Illumina small RNA sequencing and LC coupled tandem MS technologies respectively. Exosomes were purified from the serum of MDV1-infected chickens that are either CVI-988 vaccinated and protected or remained unvaccinated and contact exposed to vv+MDV-1 (Tk-2a). In addition, exosomes from the culture supernatants of an RB-1b transformed lymphoblastoid cell line, UD35 were purified and subjected to proteomic analysis along with serum exosomes described above.

Initially, we employed Polyethylene glycol (PEG, m.w. 45 – 60,000 dal. 3.5% wt/wt) in combination with dextran (DEX, m.w. 450 – 650,000 dal. 1.5% wt/wt) to purify exosomes from Medium only and the culture supernatants of CU91 (REV transformed cell line), MSB1 (vMDV-1, BC-1 transformed, also harbors MDV-2), UD35 (vvMDV-1 transformed), and UA53 (vv+MDV-1 transformed) cell lines. Dynamic light scattering (DLS) and qRT-PCR were employed to characterize purified particle size range and miRNA content respectively. DLS profile displayed particle shape as spherical, but somewhat smaller in size than anticipated (25 – 35 nm range), but these tended to increase with subsequent measurements. These were present at ~4.5 x 6.5 x 10^5/analysis volume (1 mM light path) and were therefore at a concentration of ~5 x 10^6/ml. qRT-PCR analysis of exosomal miRNA content indicated a higher abundance of MDV-1-encoded miRNA MDV-1-mir-M4 in MDV-1 transformed cell lines and its absence (below the detection limit) in REV-transformed CU91 cell line. Similarly, lower levels of *G.gallus* miRNA, mir-155, was evident in exosomes from MDV1-transformed cell lines similar to their cellular expression levels

compared to REV-transformed CU91 cell line. These experimental results proved our ability to successfully purify exosomes and characterize their content. However, for the deep sequencing and proteomic profiling of exosome contents, we employed a polymer based precipitation solution kit (TEI for proteomic profiling or ExoQuick for deep sequencing) based on its relative ease, lesser sample processing time and efficient exosome recovery (Chapter 4). Morphology of particles purified by the TEI-reagent was determined by TEM. TEM fields displayed spherical particles conforming to exosome morphology. Upon confirming their morphology, purified exosome samples were sent for proteomic analysis whereas for small RNA sequencing, whole serum samples were sent for exosome purification by ExoQuick method.

5.5.2 Differentially expressed exosomal miRNAs

5.5.2.1 PVL-upregulated exosomal miRNAs

As anticipated, exosomes purified from serum were highly enriched in hundreds of distinct miRNAs. The miRNA profile of exosomes purified from CVI-988 vaccinated and protected leghorns (PVL) and contact exposed tumor bearing leghorns (TBL) or broilers (TBB) was distinct, and yielded a number of significantly up- and down-regulated miRNAs that may indicate potential biomarkers of vaccine induced protection or susceptibility to MD.

PVL serum exosomes contained a host of miRNAs that target proto-oncogenes, hence referred to as tumor suppressor miRNAs, that were found upregulated compared to TBL or TBB serum exosomes. For the current discussion upregulated miRNAs in PVL that are common to both TBL and TBB will be highlighted. In addition, mirDB targets identified to target 3'UTRs of *G.gallus*

mRNAs and are validated in human or mice will be discussed. Interestingly, some of the upregulated exosomal miRNAs belonged to the same family (mir-146 family) or originated from the same cluster (mir-23b-27b-24-1).

5.5.2.1.1 Mir-146 family

mir-146a and -146b share seed sequence, thus have common targets and only differ by two 3' end nucleotides. Both mir-146a and -146b were first identified as endotoxin inducible miRNAs via TLR4 signaling and are induced by 18hr, post LPS treatment in THP1 monocytic cell line during the resolving phase of LPS-induced inflammation (379, 380). mir-146a and -146b thus prevent deleterious consequences of exuberant inflammation or sepsis by acting as negative regulators of NFκB. Both mir-146a and -146b target upstream activators of NFκB including IRAK1 and TRAF6 resulting in dampening of NFκB signaling and pro-inflammatory cytokine production. IRAK1 and TRAF6 were found to be conserved targets of mir-146a, and-146b also in chicken by miRDB. Likewise, upon TCR engagement, T-cell activation and NFκB-mediated mir-146a induction, mir-146a targets IRAK1 and TRAF6 providing a negative feedback on T-cell activation. In line with this, miR-146a gene-deficient mice developed spontaneous chronic inflammation and autoimmune disorders with greater levels of T_{H17} responses characterized by IFNγ and IL-17 production (381, 382). In addition, mir-146a deficiency led to impaired T_{REG} cell function with a loss of immunological tolerance, and fatal immune-mediated pathology characterized by higher IFNγ. mir-146a maintains T_{REG} cell function by directly targeting STAT1. Whereas mir-146a is a direct NFκB target gene, mir-146b induction is STAT3 dependent and is inducible via IL-10 and TGFβ dependent STAT3 activation. In physiologically normal epithelial cells, NFκB activation results in IL-6 production,

and auto- or paracrine actions of IL-6 and the resultant IL-6-STAT3 signaling promoted pri-mir-146b transcription and mature mir-146b production (383). mir-146b functions in a feedback inhibition pathway to inhibit NFκB by targeting IRAK1 and TRAF6.

In ER negative (-) breast cancers including triple – and basal-like tumors, this feedback inhibition pathway is deregulated via mir-146b promoter methylation and transcriptional inhibition of pri-mir-146b. As a result, ER- breast cancers exhibit constitutive activation of NFκB-IL-6-STAT3 axis and upregulation of STAT3 target genes to facilitate proliferation, epithelial to mesenchymal (EMT) transition, motility, migration and invasion (383).

TAL1, a transcription factor that is critical for early hematopoiesis and overexpressed in T-acute lymphoblastic leukemias (T-ALL), is one among the others to silence mir-146-3p. mir-146-3p overexpression led to decreased motility, migration and invasion capacities of all T-ALL cell lines and solid tumors. Henceforth in the context of breast cancer and T-ALL, mir-146b functions as a tumor suppressor

In the chicken, miR-146b-5p is located in an intergenic region (22,683,802–22,683,906) on chromosome (chr) 6 and was found to regulate adipogenesis. Intriguingly, in vMDV GA-infected tumorous spleens and liver tumors mir-146a, -146b and -146c were all found to be significantly upregulated compared to uninfected spleens and PBL controls respectively (115). Conversely in our study, upregulation of mir-146a or b was found in PVL exosomes compared to TBL or TBB exosomes and mir-146c levels were below the set detection limit, setting forth the proposed tumor suppressor actions of mir-146b in the context of MD lymphomas. Supporting evidence comes from our qRT-PCR confirmatory analyses of differentially expressed miRNAs

in VEX compared to TEX (Figure 4.3), where a significant upregulation of mir-146b was found in VEX compared to TEX. Based on these findings, we currently hypothesize that in response to vaccination, innate stimulation of APCs leads to transcriptional induction and exosomal incorporation of mir-146a/b, which in turn promote maintenance of systemic homeostasis in response to vv+MDV-1 challenge. Mir-146b may serve as a biomarker for protection against MD.

5.5.2.1.2 Mir-23-27-24 family

The mir-23-27-24 family consists of 3 members in two paralogs –a and –b. Mature sequences of miR-23a and miR-27a differ by one nucleotide in comparison to their corresponding paralogs miR-23b and miR-27b respectively, whereas miR-24-1 and -2 share the same sequence. Although it is hypothesized that evolutionarily conserved miRNA clusters co-operatively target the same gene or various components of a common biological process, members of mir-23a and b clusters are known to have antagonistic role rather than a co-operative role in modulating effector T cell differentiation (384). Enforced expression of mir-23 cluster led to spontaneous hyperactivation of naïve CD4+ T cells and negatively impacted the differentiation of every T helper cell lineage including T_{h1}, $T_{h2,}$ T_{h17} and iT_{reg} lineages (384). In contrast, overexpression of individual members of clusters had distinct effects. Whereas overexpression of mir-23 negatively impacted the differentiation of T_{h17} and iT_{reg} cell lineages, mir-27 overexpression negatively impacted the differentiation of all T helper cell lineages (384). Mechanistically, mir-27 indirectly targeted T_{h2} master regulator GATA3. Substantiating this, mir-23b was repressed in patient tissues or in mouse models with different types of autoimmunity, including multiple sclerosis, systemic lupus erythematosus, rheumatoid arthritis and experimental autoimmune

encephalomyelitis (385). mir-27b is an immune modulatory miRNA found to target KH-Splicing Regulatory Protein (KSRP) during *Cryptosporidium parvum* infection, which was identified as one of the mir-27b targets by our mirDB analysis. KSRP is a key mediator of RNA decay that binds to the AU-rich elements in the 3' UTRs of iNOS, IL-8 and COX2 mRNAs to facilitate RNA decay. By targeting KSRP, mir-27b indirectly enhanced the stability of iNOS mRNA that contributed to NO production upon TLR4/NFκB signaling during *C.parvum* infection(386).

MiR-23b displayed anti-inflammatory properties by directly repressing NFκB signaling activators, TGF-β activated kinase 1/MAP3K7 binding protein 2 (Tab2), Tab3 and inhibitor of nuclear factor κB kinase subunit α (IKK-α), all of which were also identified by mirDB as high confidence targets (387).

Mir-24 overexpression on the other hand led to T_{h1} and T_{h17} differentiation. In this regard, mir-24 targeted 3'UTRs of T_{h2} cytokine IL-4 and TCF1 transcription factor resulting in greater levels of IFN-γ and IL-17 production. In addition, mir-24 can also target IL-4 expression in an indirect manner as shown for mir-27 mediated targeting of GATA3 by targeting Bmi1, a molecule that stabilizes GATA3 by blocking its proteasome-dependent degradation (388). Based on greater levels of exosomal mir-27b and -24 compared to mir-23b, it is evident that MD vaccination leads to T_{h1} differentiation.

Evidence for the tumor suppressor function of mir-27b comes from the loss of heterozygosity on chr 9 (9q22.3), the breast cancer susceptibility locus at which miR-27b is located was observed in a docetaxel-resistant luminal-type human breast cancer cell line. Mir-27b inhibits the acquisition of cancer stem cell (CSC)-like properties in luminal type breast cancer by targeting the gene ectonucleotide pyrophosphatase/

phosphodiesterase family member 1 (ENPP1)(389). ENPP1, identified as mir-27b target by mirdb, apart from its tumor seeding ability, promotes conventional chemotherapy resistance via upregulation and cell surface localization of ABC drug efflux transporter ABCG2. In addition, it is also involved in type 2 diabetes (T2D) development. Metformin-mediated chemosensitivity of luminal-type breast cancer is via upregulation of mir-27b and mir-27b-mediated targeting of ENPP1 and reduced expression and cell surface localization of ABCG2.

In colorectal cancer cell line SW620 and a xenografted mouse model, mir-27b targeted LIMK1 to promote reduced cell proliferation, G1/S cell cycle arrest, reduced migration and invasion(390) . Furthermore, mir-27b targets VEGFC to inhibit tumor angiogenesis in colorectal cancer.

Overexpression of mir-27b in aggressive ovarian cancer cell lines (Hey1B and ES2) resulted in reduced migration and invasion, and markedly-suppressed capillary-like structure formation and tumor blood vessel formation *in vitro* and *in vivo* respectively. Mir-27b targeted vascular endothelial cadherin (VE-cadherin) in ovarian cancer to mediate above effects (391).

Finally, in A-type retinal pigmental cells (ARPE-19), mir-27b targeted NADPH oxidase 2 (NOX2) mRNA resulting in decreased ROS production and downstream inactivation of PI3K/Akt/Mtor pathway (392). By targeting NOX2, mir-27b reduced mitogen induced proliferation, migration and invasion of ARPE-19 cells.

Conversely, mir-24 was demonstrated to have a tumor suppressor role and suppressed cell proliferation and migration in prostate cancer, arterial smooth muscle cells, vascular muscle cells, nasopharyngeal carcinoma, bladder cancer, and small-cell lung cancer, but is an oncogene in glioma, Hodgkin's lymphoma and SQCC. Ectopic

expression of miR-24-3p inhibited cell migration, growth, and drug sensitivity in five different cell lines including MCF7 (breast), Hep3B (HCC), B16F10 (melanoma), SH-Hep1 (HCC), and PC-3 (prostrate cancer) cell lines by targeting p130Cas/BCAR1 or breast cancer anti-oestrogen receptor(393).

Other upregulated tumor suppressor miRNAs in PVL exosomes included mir-99a, mir-26a, whereas mir-10b is a widely known OncomiR. mir-99a is a tumor suppressor miRNA whose expression level was found to be down regulated in various human cancers including non-small cell lung (NSCLC), cholangio- (CCA), breast, esophageal squamous cell, urothelial renal, renal cell, prostrate and cervical carcinomas (394). Enforced expression of mir-99a resulted in reduced proliferation, migration and invasion of various transformed cell lines and xenografts in tumor mice. Specifically, in CCA, let-7c/mir-99a/mir-125b that are expressed from the same cluster were down regulated. mir-99a overexpression in CCA cell lines MK- and SK-cha-1 resulted in reduced sphere formation, migration and invasion in suspension cultures, transwell and matrigel migration assays respectively. In this regard, mir-99a directly targeted IGF1R and inhibited IL-6-STAT3 pathway to suppress tumorigenicity (394).

Other mir-99a-targeted mRNAs contributing to the mir-99a tumor suppressor functions include E2F2 and EMR2 in NSCLC, mTOR in breast, urothelial renal and cervical carcinomas (395) . In this regard, mir-99a target sequence is highly conserved in vertebrate mTOR 3’ UTRs including that of chicken. By targeting mTOR, mir-99a inhibits the activity of both mTORC1 and 2 complexes whose common catalytic subunit is mTOR. Finally, mir-99a contributes to M2 macrophage polarization in epididymal white adipose tissue by targeting TNFα and improves systemic glucose

tolerance, insulin sensitivity, and dyslipidemia in diabetic mice. Other known targets of mir-99a include Akt1, Hoxa1 and TNFAIP8 (396-398).

5.5.2.1.3 Mir-26a

Mir-26a functions as a tumor suppressor miRNA in nasopharyngeal carcinoma (NPC), breast cancer, lung cancer and hepatocellular carcinoma (HCC) whereas it promotes tumor cell proliferation in glioma and CCA. In EBV positive (+) NPC cell line C666-1, PRC2 component EZH2 was found to be highly expressed. Targeting EZH2 via mir-26a, -101 and -98 led to cell cycle arrest in G0/G1, enhanced apoptosis via BCL2 down regulation and delayed tumor implantation time in mice (399). Furthermore, EZH2 down regulation via mir-26a transfection in NPC cell lines CNE2 and 5-8F led to decreased invasion and migration *in vitro* and metastasis *in vivo* in transplanted tumors. In HCC cell lines MHCC97H and HCCLM3, a significantly lower expression of mir-26a was observed. Ectopic overexpression of mir-26a led to G1/S cell cycle arrest, enhanced apoptosis and decreased proliferation in wound scratch assays *in vitro* (400). Furthermore, orthotopic implantation of mir-26a overexpressing HCCLM3 cells displayed suppressed tumor growth and metastasis *in vivo* with significantly lower primary tumor volumes.

Mir-26a directly targeted IL-6 to abrogate IL-6-STAT3 signaling to suppress STAT3 target genes Bcl-2, Mcl-1, cyclin D1, and MMP2 (400). Additionally, mir-26a targeted hepatocyte growth factor (HGF) which upon binding its receptor c-Met activates downstream PI3K/Akt/Mtor/S6K signaling to mediate VEGF induction. VEGF in turn facilitates angiogenesis by acting on nearby endothelial cells (401). Mir-26a targeting of HGF prevented VEGF mediated angiogenesis. Mir-26a promoted mitochondrial apoptosis by targeting anti-apoptotic Mcl1 in HCC cell lines.

Therapeutic combination of IFNα1b and 5-fluorouracil promoted facilitated HCC cell line apoptosis via p53-mediated upregulation of mir-26a and Mcl1 targeting. Finally, the tumor suppressive effect of mir-26a targeting of EZH2 was also demonstrated in HCC cell lines (402).

In the context of wound healing, mir-26a inhibited hypertrophic scar formation due to excess fibrotic tissue growth and extracellular matrix deposition by targeting Smad2. Wound healing proceeds via platelet release of TGFβ1 in the vicinity of injury and TGFβ1-Smad2/3 signaling and downstream transcription of target genes related to ECM synthesis and degradation. Mir-26a targeting of Smad2 in human skin fibroblasts suppressed cellular proliferation, induced apoptosis and prevented scar formation.

Other validated mir-26a targets include SMAD2, MTDH, CDK6, CCNE1, CCNE2, CCND2, FBXO11, PTEN, RB1, MAP3K2, and GSK-3b (402, 403).

Intriguingly, in vMDV GA-infected tumorous spleens and liver tumors compared to uninfected spleens and uninfected PBLs respectively, mir-26a was found to be significantly down regulated attesting to its tumor suppressor role in the case of MD lymphomas(314). Furthermore, miR-26a was found to be down-regulated in seven independently-derived MDV-transformed lymphoblastoid T cell lines, and ALV and REV transformed lymphoid cell lines (404). Apart from EZH2, another mir-26a target EIF3A was found to be significantly upregulated in tumorous spleen in a different study (115). Overexpression of mir-26a has been shown in many solid malignancies and is generally regarded as a prognostic marker of poor clinical outcome.

5.5.2.1.4 Mir-10b

During breast cancer metastasis, mir-10b transcription is induced by transcription factor Twist which upon targeting homeobox D10 (HOXD10) mRNA results in its translation inhibition(405). As HOXD10 represses prometastatic gene RHOC, HOXD10 targeting by mir-10b results in RHOC derepression and RHOC facilitates migration and metastasis *in vitro* and *in vivo* in MDA-MB-231 metastatic breast cancer cell line and SUM149 cell line transplanted tumors. Silencing mir-10b via antagomir or miRNA sponge is sufficient to inhibit metastasis of 4T1 cell line transplanted primary mouse tumors. Furthermore, a study investigating H4K4me3 and H3K27me3 chromatin marks in the bursas of 14-day old MD susceptible ($L7_2$) and resistant ($L6_3$) line of chickens with and without infection with a partially attenuated vv+MDV strain (648A) has reported higher levels of H3K27me3 repressive mark around gga-mir-10b in the $L6_3$ line compared to $L7_2$, with or without infection. At 10 dpi, only infected birds from $L6_3$ line displayed higher levels of H3K27me3 at gga-mir-10b locus indicative of potential oncogenic functions of mir-10b.

5.5.2.2 PVL-downregulated exosomal miRNAs

Among miRNAs that are significantly downregulated in PVL or conversely upregulated in TBL or TBB included let-7i, mir-363, -92, -142, -148a, -181a, -101 and -21. Among these, mir-181a, -142 and -148a are well known tumor suppressors whereas let-7i, mir-92, -363 and -21 are widely known OncomiRs.

5.5.2.2.1 Mir-92 and -363

Mir-92 is transcribed as part of a polycistrionic mir-17-92 cluster a.k.a oncomir-1, that encodes 6 miRNAs including mir-17, -18a, -19a, -19b-1, -20a and -92a(406). In addition to mir-17-92 cluster, there exists two paralog clusters including

mir-106a-363 (miR-106a, miR-18b, miR-20b, miR-19b-2, miR-92-2 and miR-363) and mir-106b-25 (mir-106b, -93, -25) which encode mir-92 paralogs mir-92a-2, -363 and -25 respectively (407). Although, they are expressed as part of polycistrionic transcript, varying post transcriptional processing results in differential expression of individual mature miRNAs (407). In TBL or TBB, mir-92 and -363 were found to be significantly up regulated. In addition, with a read number less than 2000, thus below the set detection limit, remaining miRNAs of mir-17-92 cluster (mir-17, -19a, -20a), and mir-106a-363 cluster (mir-20b, -106) were found to be significantly up regulated in TBL.

In naïve CD4+ T cells, the mir-17-92 cluster contributes to cell survival and proliferation by mir-19a and -92a targeting of PTEN and Bim, respectively (408). Furthermore, the mir-17-92 cluster was also demonstrated to play a critical role during the T helper cell patterning into various lineages. On the other hand, amplification of mir-17-92 cluster coding region is found in cell lines representative of several types of lymphomas including splenic lymphoma with villous lymphocytes: SLVL), six mantle lymphoma cell lines (REC-1, Jeko-1, Z138, NCEB-1, Granta 519, SP49 and JVM2), ATN-1 (adult T-cell lymphoma cell line), Jurkat (T-cell acute lymphocytic leukemia), HT-1 (T-cell lymphoblastic lymphoma cell line, HTLV-1-negative) and HUT78 (peripheral T-cell lymphoma cell line) (409). Notable upregulation of mir-19a, -20 and -92a was found in the above lymphoma cell lines, whereas mir-17a and -18 were found at lower expression levels. Furthermore, mir-17-92 cluster overexpression in transgenic mice causes B cell lymphomas (410).

The miR-17-92 and mir-106a-363 cluster transcription is c-Myc dependent, which is frequently hyperactive in many types of cancers (411). With respect to cell

cycle control, the miR-17-92 cluster miRNAs were found to be activated by the E2F family of transcription factors but also target the E2F transcription factor family, thereby establishing a negative feedback loop (412). In neuroblastoma cells, miR-17-92 has been shown to target components of the TGF-β signaling pathway to prevent TGF-β-mediated apoptosis (413). TGF-β receptor II is targeted by miR-17 and miR-20, and SMAD2 and SMAD4 are targeted by miR-18a. Likewise in gastric cancer, mir-17-92 cluster and its paralog cluster mir-106b-25 miRNAs silence two main downstream effectors of TGF-β signaling: the cell cycle inhibitor CDKN1A (p21) and the proapoptotic gene BCL2L11 (BIM). Whereas miR-106b and miR-93 suppress p21 expression, which is required for TGF-β-mediated cell cycle arrest, miR-25 silences pro-apoptotic BIM (414). Similarly, miR-17-5p and miR-20a target p21, whereas miR-92 targets BIM. These findings indicate that miR-106b-25 and miR-17-92 cooperatively inactivate the TGF-β pathway. In this regard, gene dosage is critically important in this context as loss of even a single SMAD4 or BIM allele results in haplo-insufficiency phenotypes leading to cancer.

Finally, in tumors induced by KSHV, EBV and HPV16/18, the mir-17-92 clusters were found to upregulated. KSHV latent proteins vFLIP and vCyclin, cellular analogs of FLIP and cyclin D, respectively, upregulate the mir-17-92 cluster in epithelial (SLK) and endothelial (TIVE) cells to target SMAD2 and abrogate TGF-β-mediated apoptosis (415). The two 17/92 cluster miRs, miR18a/19 target the anti-angiogenic secreted factor Tsp-1, thereby promoting angiogenesis in the tumor microenvironment. Conversely miR-17/-20 and miR-92a target Janus kinase 1 (Jak1) and integrin a5 (Itga5) to negatively regulates vascular morphogenesis. In a PAR-CLIP assay performed on EBV-transformed LCLs (LCL35), miR-17/-20/-106 family

was found to target the LMP1 3'UTR during latent EBV infection (416). HPV16 and 18 transformed cell lines, SiHa and HeLa displayed greater intracellular expression of mir-20a and mir-92a, and exosomal mir-92a. This greater expression in cells or exosomes was found to be E6/E7-dependent and was independent of the effect of E6 on p53 (p53 degradation)(417).

The mir-106a-363 cluster was shown to regulate Th_{17} patterning by miR-106a, miR-18b and miR-363-3p targeting of Nfat5 and Rora, leading to a consequent decrease of IL17a/f gene expression and reduction of IL-17a protein production. The Mir-106a-363 cluster is significantly down regulated in Th_{17} -patterned CD4+ T cells.

Exosomes from CD5+ B-cell CD40/IL-4 stimulated CLL cells when incubated with autologous CD4+ T cells transferred mir-363 and resulted in CD4+ T cell activation, proliferation, and motility by mir-363 targeting of CD69 (418). Except in glioma, mir-363 was primarily described as a tumor suppressor miRNA in the context of HCC, CRC, lung adenocarcinoma and NK/T-cell lymphoma. It was demonstrated to target GAP43, E2F3, GATA6, PCNA and BCL2/IGF1 to mediate it effects respectively. Based on greater expression of mir-92 and -363 in TBL or TBB and previous roles as Oncomirs, we currently hypothesize that they play a critical role in MDV-1 lymphomagenesis.

5.5.2.2.2 Let-7i

Interestingly, let-7i along with let-7g is a LPS-regulated miRNA. Whereas TLR4 activation upon LPS treatment or *Cryptosporidium parvum* infection of cholangiocyte cell line (H69) repressed let-7i in a MyD88-dependent manner, overexpression of let-7i directly targeted TLR4 mRNA (419). Let-7g and let-7i belong to the let-7 family of miRNAs that are well known to be down regulated in a variety of

malignancies and function as tumor suppressors. In the same study, although let-7g and -7a were also proposed to target TLR4 mRNA, they were never tested. In addition, liver tissue of mice treated with LPS, upregulated let-7g miRNA in an E2F1 transcription factor dependent manner. Additionally, let-7g was demonstrated to target mRNAs of oxidized-LDL receptor and TGF-β signaling mediators (TGFβRII and Smad2) in vascular smooth muscle cells and endothelial cells respectively. In contrast to their role in many cancers, let-7i was found to be highly upregulated in follicular lymphoma tissues from patients that underwent transformation (FCL-t).

Members of the let-7 family were known to target c-myc expression in Burkitt lymphoma and decreased c-myc expression has been associated with high-grade transformation of FCL to DLBCL. Likewise, let-7a, -7b, -7i and -7f were consistently upregulated in Hodgkin's lymphoma cell lines and tissues irrespective of EBV-infection status. Specifically, let-7a and mir-9 were demonstrated to target PRDM1 (Blimp1) mRNA to inhibit terminal differentiation of plasma cells and promote transformation into HRS cells (420).

Based on greater expression of exosomal let-7i miRNA in TBL and TBB or let-7g miRNA in TBL, we propose that let-7i and -7g may have proto-oncogenic roles in the context of MD lymphomas.

5.5.2.2.3 Mir-21

Mir-21 is a *bona fide* oncomir that was shown overexpressed in virtually all carcinomas and various hematological malignancies including MDV1-induced lymphomas and is transactivated by Meq (421, 422). Mir-21 targets a host of gene products including Myd88 and IRAK1 to promote immune suppression (423). Furthermore, in our qRT-PCR confirmatory analysis of mir-21 expression in TEX, we

found a significant downregulation indicating that mir-21 may be a potential biomarker for MD tumor formation.

5.5.3 Potential MDV-1 transcripts transferred via exosomes

Basing on the reads mapped to MDV1 coding regions, it appears a significant number of mRNAs corresponding to structural genes (glycoprotein M (gM), gI, UL11 tegument protein, UL13 serine threonine kinase, UL14 minor tegument protein, Uracil DNA glycosylase, gL, gD, LORF3, US3 serine threonine kinase, ICP4, UL43 membrane protein and UL35 tegument protein) are incorporated and transferred to target cells resulting in their translation. Since vaccination success relies on CD8+ CTL responses against shared antigens including structural glycoproteins and tegument proteins, it appears that exosomal transfer of mRNAs corresponding to structural genes plays a critical role in CD8+ CTL response towards structural proteins.

5.5.3.1 MDV-1 upregulated miRNAs

MDV-1 miRNAs that displayed significantly greater abundance in TBB include MDV1-mir-M2, -M4, -M5, -M1, –M11, -M6 and -M7. These included *meq* cluster (-M2, -M4, -M5, -M1 and –M11) and LAT cluster (–M6 and –M7) miRNAs. Among high confidence MDV-1 miRNA targets (score > 80) identified by mirDB, MDV1-mir-M1 was found to target subunit of general transcriptional machinery TATA Box associated factor 4 (TAF4) indicative of a general shut down of cellular and viral transcription during latency and limited transcription restricted to latency associated regions (Appendix B). MDVI-mir-M2 and –M4 targets included TNFAIP8, TAB3 and TAB2 indicative of modulation of NFκB signaling mediators (424). In

addition, TAB2 was also identified as a common target of MDV1-mir-M11 (Appendix B). MDV1-mir-M6 targets included components of anti-viral stress granules (YY1, G3BP2, FMR1) that function to sequester cellular and viral messenger ribonucleoproteins with bound ribosomes resulting in translational silencing (425).

5.5.4 Proteomic analysis

Of particular interest, ICP4 was found in low abundances. ICP4 is an immediate early transactivator encoded in repeat regions flanking the unique short region. MDV ICP4 contains serine rich N terminus, NLS in region 3 with regions 2 & 4 displaying high degree of conservation with HSV1 ICP4 (104). Syngenic cell mediated immune responses towards ICP4 was found to be a major factor in defining the genetic resistance towards MD in $B^{21}B^{21}$ chickens (105). Exosomal transfer of ICP4 to APCs and subsequent CTL responses towards conserved ICP4 epitopes appears to be a critical mechanism in inducing protection against MD.

The major tegument protein (MTP) encoded by UL36 (MDV049) gene was exclusively detected in TBL and TBB treatments. MTP is expressed both during lytic and latent infection and encodes an ubiquitin specific protease (USP) in its N terminus that is conserved among all known herpesviruses (426, 427). A C98A protease-dead mutation in its USP catalytic center lead to severe reduction in MD tumor incidence, although MDV replication was unaffected *in vitro* and *in vivo*. HSV1 USP was shown to deubiquitinate polyubiquitinated IκBα and monoubiquitinated PCNA to inhibit HSV1 DNA-induced IFN-β or NF-κB activation and DNA damage responses respectively to facilitate infection (77, 78). In addition, tegument protein VP13/14 encoded by UL47 was detected TBL exosomes. UL47 is a late gene expressed during lytic infection with very low and high abundances in CEFs and FFE respectively (80).

In our study, exosomal UL47 in MD+ birds may be due to reactivating virus selectively packaging UL47 into exosomes for transfer to distant FFE to promote transmission. Finally, innate components, STAT1 and OASL were detected in TBL exosomes. Herpesviral latent infections were known to selectively package innate immune molecules in exosomes in an effort to arm surrounding cells to prevent lytic infection and maintain latency (341).

In TBB, Ada-two-A-containing (ATAC) complex component YEATS2 was detected along with JunD and E2F4 transcription factors. YEATS2 is a YEATS domain-containing protein that serves as a H3K27 acetylated or crotonylated lysine reader of nucleosomal DNA. Upon binding, as part of ATAC complex, it promotes ATAC complex-mediated H3K9Ac marks on the target gene promoters resulting in transcriptional activation (428, 429).

Furthermore, among over represented proteins identified in TBL and TBB exosomes, pantetheinase encoded by the vanin gene was common to TBL and TBB treatments (Table 5.12). Vanin is an enzyme involved in catabolizing intermediate pantetheine to vitamin B5 for recycling in coenzyme A biosynthesis. Vanin 1 contains a GPI anchor sequence and is membrane bound on epithelial and myeloid cells. Vanin-1 is also a potential biomarker for certain inflammatory conditions such as pancreatic cancer associated diabetes (PCAND) and renal injury. By regulating the synthesis of cysteamine and glutathione, vanin-1 affects cellular viability, proliferation and function. In PCAND, neoplastic cells overexpressing vanin-1 displayed greater paraneoplastic islet injury through an increased oxidative stress response. Based on this, we propose exosomal pantetheinase can serve as a biomarker for MD tumors and a spectrophotometric assay to detect a greater level of pantetheinase enzymatic activity

in serum exosome fractions can have a great potential for MD diagnosis. In this regard, enzymatic hydrolysis of *S*-pantetheine-3-pyruvate substrate into *S*-cysteamine-3-pyruvate, which cyclizes in a non-rate-limiting step to give rise to 2H-1,4-thiazin-5,6-dihydro-3-carboxylic acid (aminoethylcysteine ketamine; absorption: 296 nm) was described in the past that can be translated for use in a routine animal diagnostic laboratory (430).

In UD35 exosomes, ER stress induced UPR signaling proteins IRE1α, PDIA3 and GRP78 were detected (212). Tumor cell conditioned media was found to induce "transmissible ER stress" in the macrophages and upregulate pro-inflammatory cytokine production indicative of exosome mediated transfer of UPR signaling components leading to downstream induction of pro-inflammatory cytokines (431, 432).In addition, as RB1B transformed cell lines were known to express greater levels of MHC I, MHC I along with its partner β_2 microglobulin were detected in UD35 exosomes exclusively.

5.5.5 Future directions

Future studies must focus on delineating the biological function of upregulated miRNAs (tumor suppressor function) and downregulated miRNAs (OncomiR function) in PVL exosomes. This can be done at the level of individual miRNA by ectopic over expression of study miRNA or inhibiting miRNA expression by antagomiRs in MD transformed cell lines and assess the effect of over expression or inhibition on their growth, proliferation, invasion and migratory ability.

Similarly, proteomic differences in PVL vs TBL or TBB require additional validation through Western blotting. In addition, serum exosome studies from additional vaccine trials are required to validate the targets observed in these studies.

These current studies provide the basis for numerous testable hypotheses regarding the functions of exosomes in MDV-mediated immune suppression, tumor progression as well as in the coordination of systemic immunity to MDV.

Table 5.1: Read statistics by sample. The sample IDs represent bird tag numbers from which serum exosomes were obtained. The top 4, middle 4 and the bottom 4 IDs represent PVL, TBL and TBB respectively.

sample	# raw reads	# reads containing 3' AD	# reads <15 nt	# reads >32 nt	reads after removing 3' AD	# mappable reads	%mappable
BL4178	15878894	15599035	5521278	306791	9770966	9747686	61.3876886
BL4047	16472545	16067842	3512861	401472	12153509	12121502	73.5860913
BL4062	14407601	13944816	4105438	392874	9446504	9424620	65.4142213
BL4183	26533369	26117394	8946008	797915	16373471	16334950	61.5637992
OR1810	18024380	15387110	5048204	1186664	9152242	9038453	50.1457082
OR1760	13826014	12017955	2163208	1093629	8761118	8725701	63.1107491
OR1838	26009675	20553805	9579761	2370704	8603340	8559904	32.9104612
OR748	16422100	15080874	5954113	780268	8346493	8321176	50.6705963
BL3815	27168090	26425402	20655002	224640	5545760	5539665	20.3903366
BL3841	16544388	15333535	2069158	976561	12287816	12264873	74.133132
BL3850	11567549	11161948	3213609	542988	7405351	7394774	63.9268872
BL3825	8516052	7993111	2806262	291607	4895242	4885568	57.368931

Table 5.2: Summary of percentage reads mapped to *G.gallus* reference genome by AGCT101-miR pipeline script.

	#Seqseq	%Mappable SequSeq
Raw	211,370,657	
Total mappable reads	112,358,872	100%
Group 1a	1,455,913	1.3%
Group 1b	8	0%
Group 2a	27,206,392	24.2%
Group 2b	950,001	0.8%
Group 3a	459,810	0.4%
Group 3b	20,969	0%
Group 4a	480,568	0.4%
Group 4b	9,525,666	8.5%
Mapped to mRNA	8,879,834	7.9%
Mapped to other RNAs (RFam: rRNA, tRNA, snRNA, snoRNA and others)	13,155,489	11.7%
Mapped to Repbase	881,129	0.8%
Mapped to custom database if applicable	0	0%
Nohit	53,784,139	47.9%

Table 5.3: Summary of percentage reads mapped to pRB1B (Accession no: EF523390) reference genome by Geneious version 10.

Bird#	number of mapped reads	% reads mapped
BL3815	11,995 of 164,499 reads were assembled to EF523390 to produce Contig	7.29183764
BL3825	8,335 of 142,807 reads were assembled to EF523390 to produce Contig	5.836548629
BL3841	29,586 of 308,287 reads were assembled to EF523390 to produce Contig	9.596901588
BL3850	36,084 of 340,442 reads were assembled to EF523390 to produce Contig	10.59916227
BL4047	66,270 of 521,568 reads were assembled to EF523390 to produce Contig	12.70591754
BL4062	55,003 of 507,679 reads were assembled to EF523390 to produce Contig	10.83420823
BL4178	57,285 of 463,005 reads were assembled to EF523390 to produce Contig	12.37243658
BL4183	87,058 of 648,748 reads were assembled to EF523390 to produce Contig	13.41938626
OR1760	314 of 1,058,292 reads were assembled to EF523390 to produce Contig	0.02967045
OR1810	64,636 of 985,115 reads were assembled to EF523390 to produce Contig	6.561264421
OR1838	534 of 1,054,877 reads were assembled to EF523390 to produce Contig	0.050622016
OR748	56,629 of 977,840 reads were assembled to EF523390 to produce Contig	5.79123374
All birds	485724 of a total number of 7173159 reads were assembled to EF523390	6.771409919

Table 5.4: Summary of percentage reads mapped to MDV1 precursor miRNAs (-5p and -3p) deposited in miRBase version 22.

sample	# reads mapped to pre-MDV1-miRs	# mappable reads	% mapped reads
BL4178	12126	9747686	0.124398755
BL4047	52574	12121502	0.433725127
BL4062	80168	9424620	0.850623155
BL4183	46897	16334950	0.287096073
OR1810	47867	9038453	0.529592841
OR1760	4123	8725701	0.047251218
OR1838	6219	8559904	0.072652684
OR748	9589	8321176	0.115236116
BL3815	478	5539665	0.008628681
BL3841	224	12264873	0.001826354
BL3850	6891	7394774	0.093187432
BL3825	1864	4885568	0.038153189

Table 5.5: miRdb predicted targets of exosomal miRNAs upregulated in PVL or downregulated in TBL. miRNAs identified in the same color are either belonging to a family (mir-146 family) and share seed sequence or are clustered and co-transcribed as a primary transcript (mir-23b-27-24 cluster)

miRNA	Function	miRdb Predicted mRNA Targets
gga-miR-146b-5p	tumor suppressor	IRAK1, TRAF6, STAT3
gga-miR-10b-5p	OncomiR	HoxD10
gga-miR-2188-5p	Unknown	neuropilin-2a
gga-miR-27b-3p	tumor suppressor	Bmi-1, KSRP, NOX2, VE-CDH, CCNG1, CYP1B1, ENPP1, VEGFC, LIMK1
gga-miR-99a-5p	tumor suppressor	IGF1R, E2F2, EMR, mTOR, Akt, Hoxa1, TNFAIP8
gga-miR-26a-5p	tumor suppressor	EZH2, HGF, SMAD2, MTDH, CDK6, CCNE1, CCNE2, CCND2, FBXO11, PTEN, RB1, MAP3K2, GSK-3b, EIF3A
gga-miR-146c-5p	tumor suppressor	IRAK1, TRAF6, STAT3
gga-miR-24-3p	tumor suppressor	IL-4, TCF1, p130Cas
gga-miR-146a-5p	tumor suppressor	IRAK1, TRAF6, STAT3
gga-miR-23b-3p	tumor suppressor	IKKA, TAB2, TAB3, Src, Akt, FZD7, MAP3K1 , PAK2 TGFβR2 , uPA

Table 5.6: miRdb predicted targets of exosomal miRNAs upregulated in TBL or downregulated in PVL. miRNAs identified in the same color are either belonging to a family (let-7 family) and share seed sequence or are clustered together and co-transcribed as a primary transcript (mir-363-92 cluster, mir-15-16 family)

miRNA	Function	Mirdb predicted mRNA targets
gga-miR-142-5p	tumor suppressor	SOCS1, Sirt-1, SMAD3, CLDN1, PI4KC
gga-miR-125b-5p	OncomiR	BCL2, CBFβ, TRP53INP1, TET2, TNFAIP3, 5-LOX, BIK, MTP18
gga-miR-181a-5p	tumor suppressor	MYBL1, IGF2BP3, SHP2, DUSP6, PTPN22, TLR4, PI3K
gga-let-7i	Oncomir/tumor suppressor	c-myc
tgu-miR-363	OncomiR	CD69, GAP43, E2F3, GATA6, PCNA, BCL2/IGF1
gga-miR-92-3p	OncomiR	Bim, Jak1, Itga5
gga-miR-101-3p	tumor suppressor	Bmi-1
gga-let-7g-5p	Oncomir/tumor suppressor	c-myc
gga-miR-451	tumor suppressor	GATA2, Ywhaz/14-3-3
gga-miR-148a-3p	tumor suppressor	Bach2, Mitf, PTEN, Bim, CUL5
gga-miR-21-5p	OncomiR	TIMP3, PDCD4, MMP2, PTEN, Gata3, and sprouty1, PAIS3
gga-miR-7	OncomiR	Erf2, ERLIN1, LXR, myrip, Pax6
gga-miR-15c-5p	tumor suppressor	DNMT3B
gga-miR-16-5p	tumor suppressor	Bmi-1, CCND1, CCND2, CCND3, CCNE1, Cdk-4, -6, Chk1, Mcm5, cdc25a, p53
gga-miR-16c-5p	tumor suppressor	DNMT3B

Table 5.7. MDVI mature miRNA read numbers in PVL, TBL and TBB serum exosomes as analyzed by miRDeep2 package.

		PVL				TBL				TBB			
		BL3815	BL3825	BL3841	BL3850	BL4047	BL4062	BL4178	BL4183	OR748	OR1760	OR1810	OR1838
meq cluster 1	MDV1-miR-M9-3p	6	4	7	136	2260	3012	371	1086	126	78	973	291
	MDV1-miR-M5-3p	3	40	0	70	559	376	194	617	43	16	62	41
	MDV1-miR-M12-3p	75	469	83	2139	36416	67745	6242	25325	1247	653	6397	1240
	MDV1-miR-M3-5p	54	48	21	378	5085	10561	833	5413	905	377	4788	465
	MDV1-miR-M2-3p	6	74	5	171	4233	6512	1061	3812	129	16	127	40
	MDV1-miR-M4-5p	218	826	72	2541	25556	40784	10083	26760	5537	1726	30356	2126
meq cluster 2	MDV1-miR-M11-5p	1	0	0	3	54	172	53	184	6	0	9	11
	MDV1-miR-M31-3p	0	0	0	0	15	46	7	22	4	0	7	5
	MDV1-miR-M1-5p	1	1	0	39	310	193	105	123	11	2	19	2
LAT cluster 3	MDV1-miR-M8-5p	29	203	7	733	4117	5976	674	2121	811	684	1051	1213
	MDV1-miR-M13-3p	0	0	0	1	8	6	0	2	1	10	24	2
	MDV1-miR-M6-5p	41	119	12	296	5733	8183	1443	4314	308	273	2757	475
	MDV1-miR-M7-3p	3	1	4	14	250	273	106	227	124	29	251	35

Table 5.8. SDE MDV1 miRNAs in TBL or TBB compared to PVL

		TBL/PVL fold change	*p-value*	TBB/PVL fold change	*p-value*
***meq* Cluster1**	M9-3p	9.6	0.22	44.0	0.07
	M5-3p	1.4	0.12	15.5	0.02
	M12-3p	3.4	0.23	49.1	0.08
	M3-5p	13.0	0.26	43.7	0.07
	M2-3p	1.2	0.15	61.0	0.04
	M4-5p	10.9	0.22	28.2	0.03
***meq* cluster 2**	M11-5p	6.5	0.12	115.8	0.05
	M31-3p	4.0	0.20	22.5	0.08
	M1-5p	0.8	0.11	17.8	0.04
LAT cluster 3	M8-5p	3.9	0.31	13.3	0.09
	M13-3p	37.0	0.87	16.0	0.15
	M6-5p	8.1	0.20	42.0	0.04
	M7-3p	20.0	0.25	38.9	0.01

Table 5.10: SDE MDV-1 mRNAs in PVL compared to TBL. Reads mapped to pRB1B reference genome by Geneious. Expression levels are displayed as reads per million mapped reads. Significance between groups was determined by Student's t-test.

		PVL		TBL		TBL/PVL	
MDV gene name	mapping strand	RPKM average	SD	RPKM average	SD	Expression value	*p-value*
MDV 052-c (UL39, large Ribonuc. Red)	forward	8193.43	5483.27	2797.75	330.95	0.34	0.03
MDV 055-c (UL42 DNA polymerase subunit)	forward	10649.45	10717.96	35547.75	17003.69	3.34	0.05
US7, glycoprotein I	forward	116.78	40.12	2073.23	1039.76	17.75	0.06
UL20, membrane protein	reverse	9162.35	4568.96	3096.73	1902.15	0.34	0.09
US2	reverse	4126.25	4693.91	4423.10	2976.00	1.07	0.09
MDV 053-c (UL40 RRs)	forward	19748.90	19661.74	5763.85	781.05	0.29	0.09
MDV 046-b (UL32, glycoprotein B assoc)	reverse	12479.33	3757.13	10755.33	2515.40	0.86	0.09
UL13, PK serine/threonine	reverse	337.98	470.93	1920.30	1597.56	5.68	0.09
UL19, major capsid protein	reverse	4179.83	4342.16	1717.50	1082.00	0.41	0.09
MDV 044-c (UL31, DNA pol assoc.)	reverse	16601.03	15560.72	5398.40	102.90	0.33	0.10
UL11 myristylated tegument protein	reverse	47.50	60.90	412.25	125.85	8.68	0.10
SORF3	reverse	73.28	73.04	494.60	212.23	6.75	0.10

Table 5.11: SDE MDV-1 mRNAs in PVL compared to TBB. Reads mapped to pRB1B reference genome by Geneious. Expression levels are displayed as reads per million mapped reads. Significance between groups was determined by Student's t-test.

		PVL		TBB		TBB/PVL	
MDV gene name	mapping strand	RPKM average	SD	RPKM average	SD	Expression value	*p-value*
UL10, glycoprotein M	forward	110.63	82.68	6849.20	4764.29	61.91	0.05
UL11 myristylated tegument protein	reverse	47.50	60.90	1327.20	750.30	27.94	0.03
UL13, PK serine/threonine	reverse	337.98	470.93	2694.35	1181.41	7.97	0.03
UL14, minor tegument protein	reverse	417.98	388.82	2397.28	1037.12	5.74	0.04
UL-2, Uracil-DNA glycosylase	forward	766.40	1238.91	3353.75	1912.98	4.38	0.00
UL-1 glycoprotein L	forward	952.83	1539.38	3538.43	1974.32	3.71	0.00
US6, glycoprotein D	forward	1856.45	2843.45	6042.78	3958.05	3.26	0.02
LORF3	forward	1951.60	1786.54	5786.90	2271.02	2.97	0.01
US3 serine/threonine kinase	forward	2631.25	1518.44	4527.63	2402.91	1.72	0.03
ICP4	reverse	3785.45	2455.02	5865.23	1208.26	1.55	0.04
MDV 056-b (UL43, membrane protein)	forward	2179.98	1484.82	3160.53	960.25	1.45	0.03
MDV 048-c (UL35)	forward	24231.33	2200.12	15591.90	3270.79	0.64	0.01
MDV 047-b (UL34 membrane phosphoprotein	forward	26555.30	1531.60	11999.83	3606.22	0.45	0.00
MDV 045-c (UL33, DNA packaging)	forward	23135.05	7034.55	9464.68	1914.88	0.41	0.03

Table 5.12: Overrepresented protein in PVL serum exosomes. Over represented proteins in PVL that are commonly identified include COL22A1 and IGFBP5 (bolded). Shown are fold change ratios of spectral counts and *p-values* relative to TBL (yellow) and TBB (cyan).

Table 3. Proteomic Analysis of Serum VEXs: Overrepresented Proteins

Protein (accession)	Vaccine-protected (NI)[1]	Tumor-bearing (NI)[1]	Ratio (protected/tumor)	p-value
Protocadherin-17 (XP_015132312.1)	2.31	0	11,109:1	0.015
Collagen a-1 (XXII) chain (XP_015138660.1)	1.13	0	10,825:1	0.048
IgGFc-binding protein-like protein (XP_428412.5)	0.6	0	2,851:1	0.035
Insulin-like growth factor-binding protein complex acid labile subunit isoform (XP_425222.3)	0.24	0	1,159:1	0.014
Tenascin isoforms (XP_015134827.1)	0.15	0	998:1	0.014
Insulin-like growth factor-binding protein complex acid labile subunit isoform (XP_425222.3)	0.24	0	851:1	0.043
Muellerian-inhibiting factor precursor (NP_990361.1)	0.21	0	733:1	0.043
Collagen a-1 (XXII chain) (XP_015138660.1)	1.13	0.04	27:1	0.039
Transferrin Receptor	0.1	0.01	12:1	0.005
C-reactive protein, pentraxin-related precursor (NP_001300649.1)	2.13	0.43	4.9:1	0.014

[1] – NI = normalized intensity

Leghorn vaccinated and protected chickens vs tumor-bearing leghorn chickens

Leghorn vaccinated and protected chickens vs tumor-bearing broiler chickens

Figure 5.1: **A) Particle radius as measured by Mobius dynamic light scattering**. Y-axis represents particle radius in nm. X-axis represents exosome source. **B) Threshold cycles values of MDV-mir-M4 and cellular gga-mir-155 as measured via qRT-PCR analysis.** Y-axis represents Ct cycle value. X-axis represents exosome source.

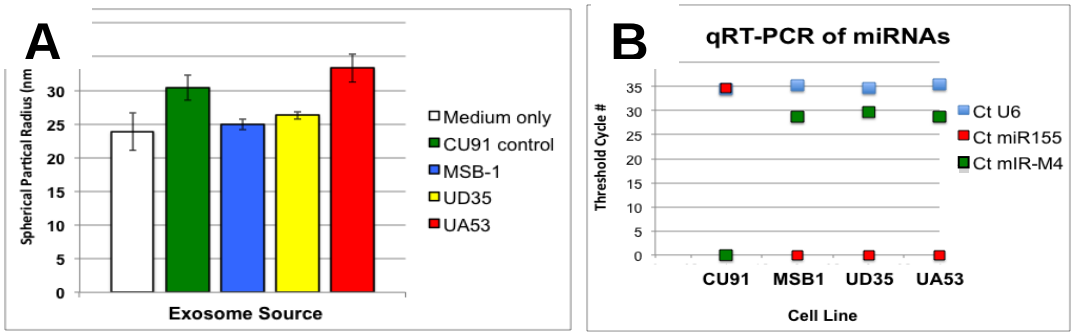

Figure 5.2: ImageJ analyses of number of exosomes per TEM field image (A), total number of exosomes (B) and the average diameter of exosomes in 20 TEM field images. A total of 20 fields per treatment were analyzed. Y-axis represents number of exosomes per image. X-axis represents exosome source.

A.

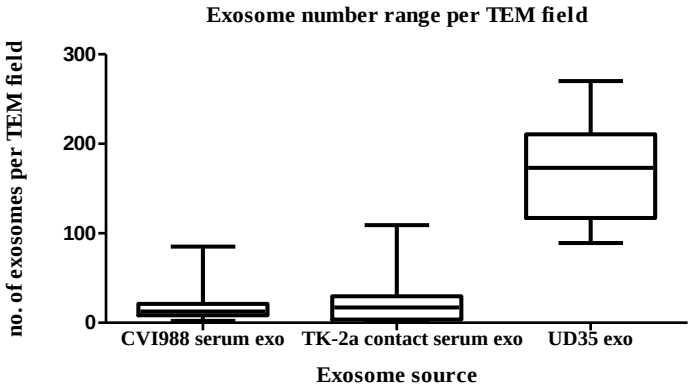

B.

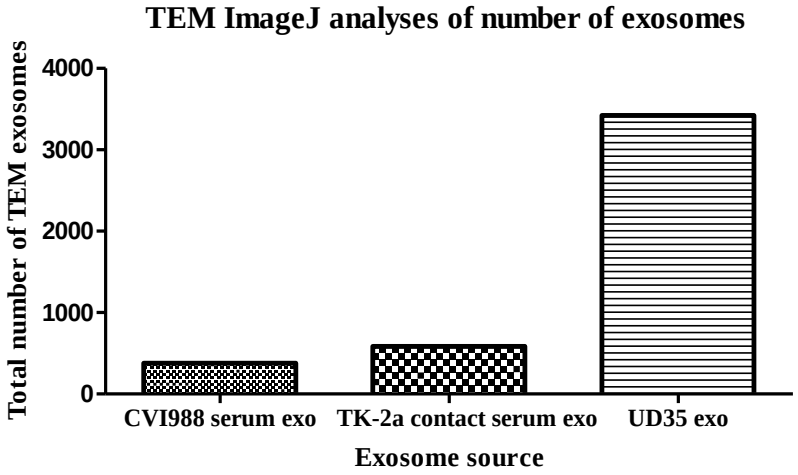
TEM ImageJ analyses of number of exosomes
Total number of TEM exosomes
4000
3000
2000
1000
0
CVI988 serum exo
TK-2a contact serum exo
UD35 exo
Exosome source

C.

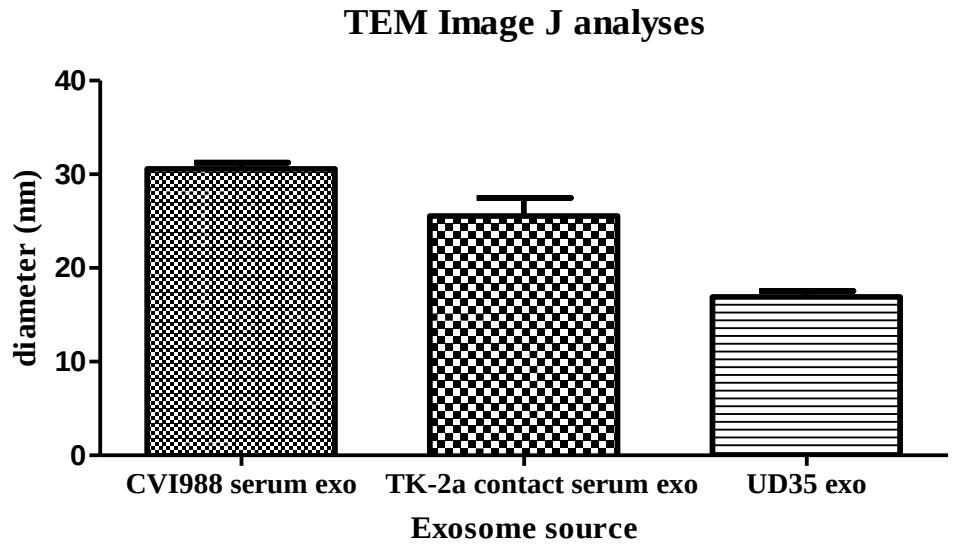
TEM Image J analyses
diameter (nm)
40
30
20
10
0
CVI988 serum exo
TK-2a contact serum exo
UD35 exo
Exosome source

Figure 5.3: TEM analysis of exosomes in the study. Bar on the lower left indicates TEM scale

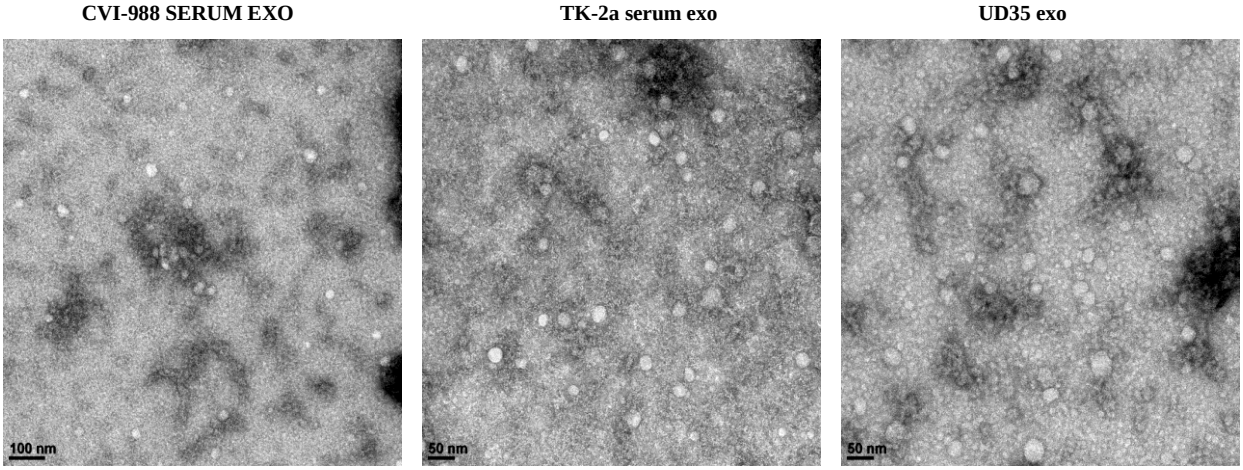

Figure 5.4: Per base sequence quality graph of reads from bird #BL3815. Y-axis and X-axis display quality score and base position respectively. Central red line is the median value. Yellow box represents the inter-quartile range (25-75%). Upper and lower whiskers represent the 10% and 90% points. Blue line represents the mean quality.

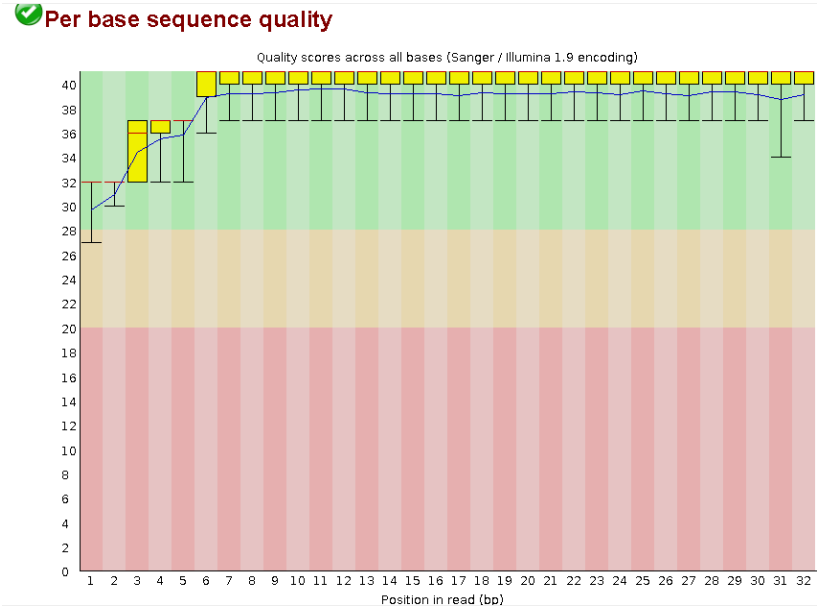

Figure 5.5: Per base sequence quality score of reads from bird #BL3815. Y-axis and X-axis display Phred score and number of reads respectively.

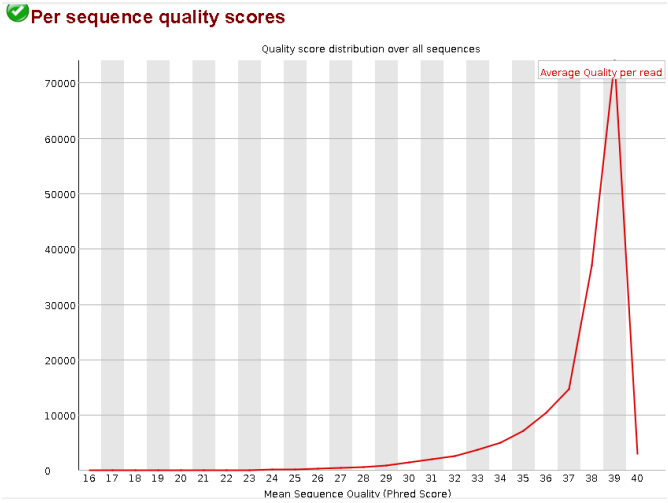

Figure 5.6: Per base sequence content of reads from bird #BL3815. Y-axis and X-axis display % base composition and base position in read respectively.

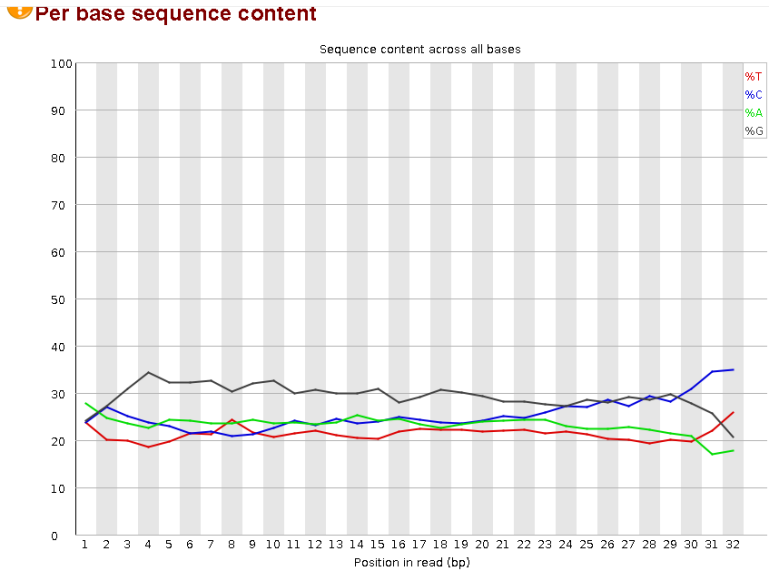

Figure 5.7: Per base GC content of reads from bird #BL3815. Red and blue bell shaped distributions display GC content per read and reference distribution respectively.

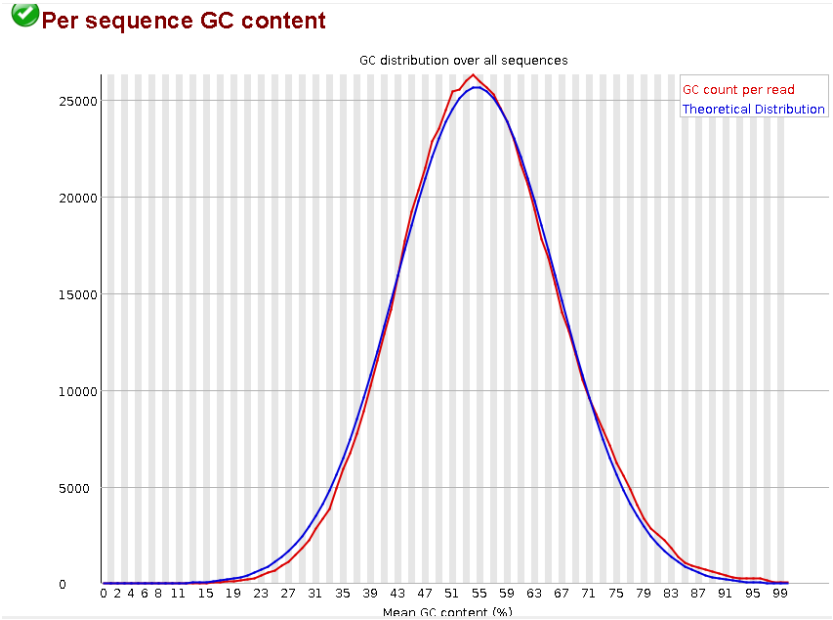

Figure 5.8: Per base N content of reads from bird #BL3815. Red line peaks indicate %N positions across the bases of every read

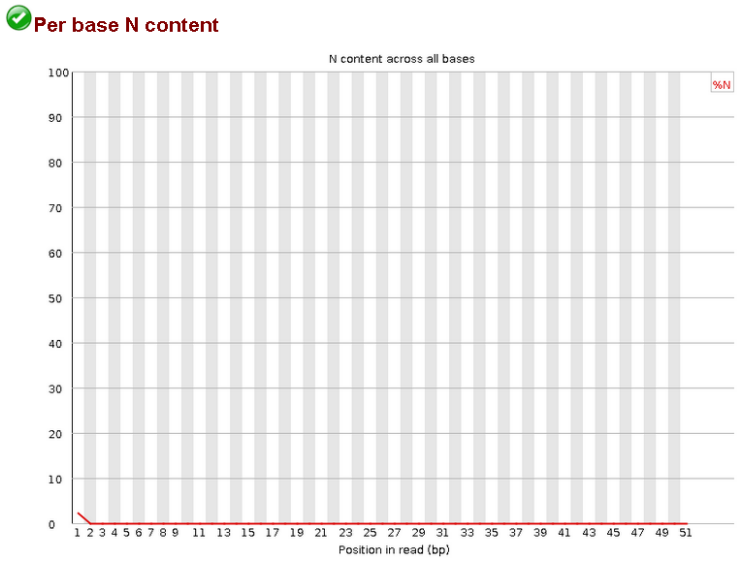

Figure 5.9 Sequence length distribution of reads from bird #BL3815. Red peak at 51bases indicate uniform read lengths generated by the sequencer.

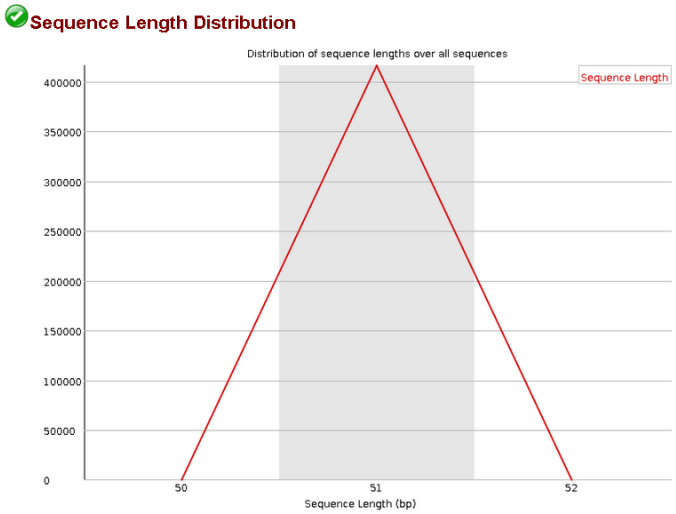

Figure 5.10: Sequence duplication levels of reads from bird #BL3815. Red and blue lines indicate percentage of total and duplicated sequences respectively.

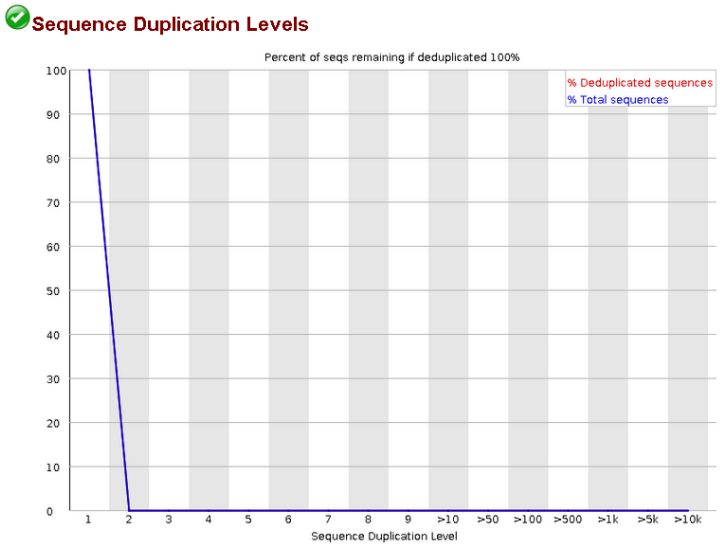

Figure 5.11: Overrepresented sequences in BL3815 raw read library

Figure 5.12: Length distribution of mappable reads

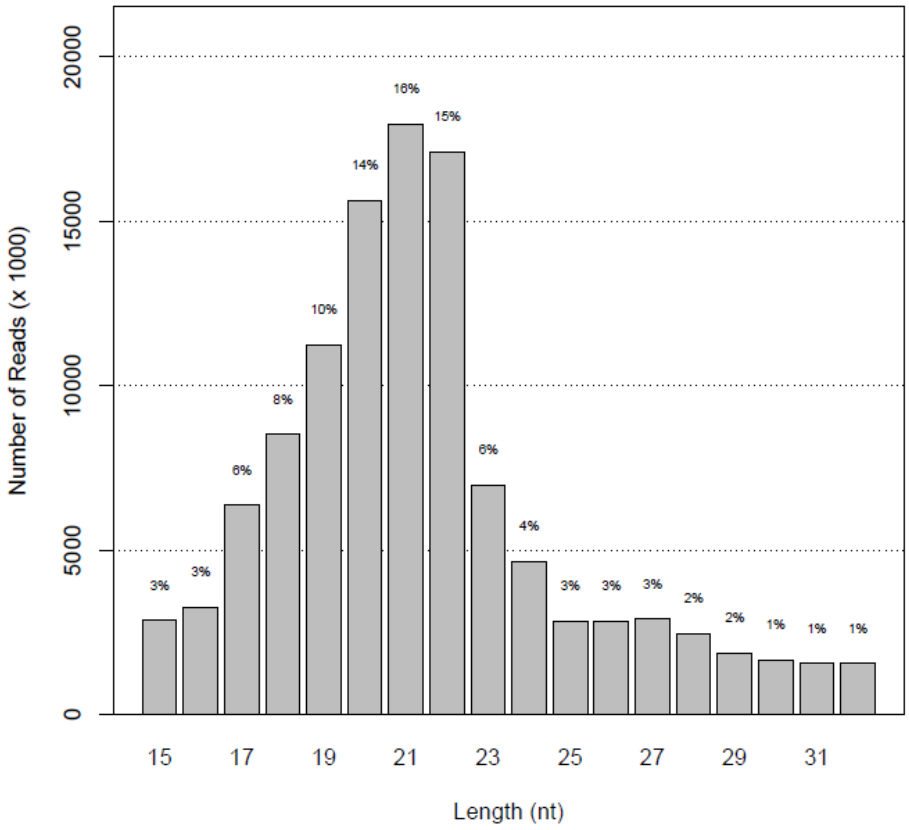

Figure 5.13: SDE miRNAs in Protected and Vaccinated Leghorns (PVL) compared to Tumor-Bearing Leghorns (TBL). Shown on the Y-axis is log_2 fold change and on the X-axis is target mature miRNA.

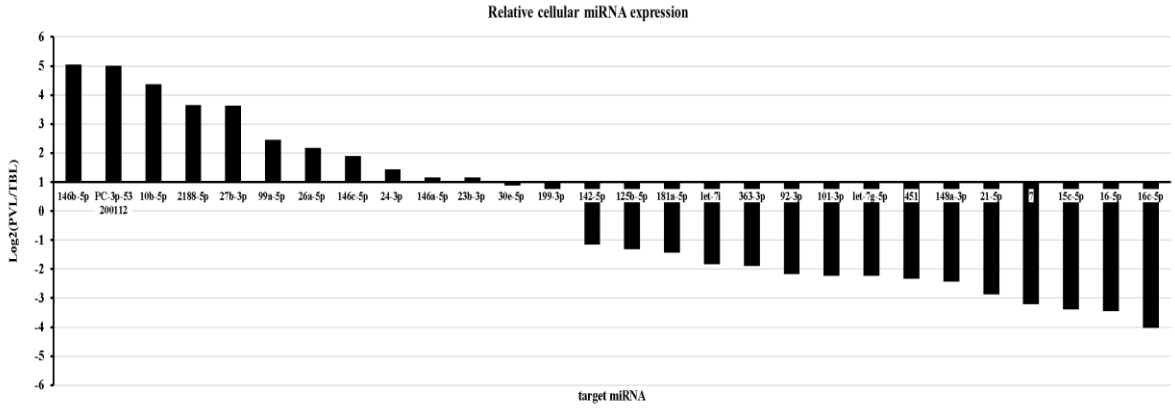

Figure 5.14: SDE miRNAs in Protected and Vaccinated Leghorns (PVL) compared to Tumor-Bearing Broilers (TBB). Shown on the Y-axis is log_2 fold change and on the X-axis is target mature miRNA.

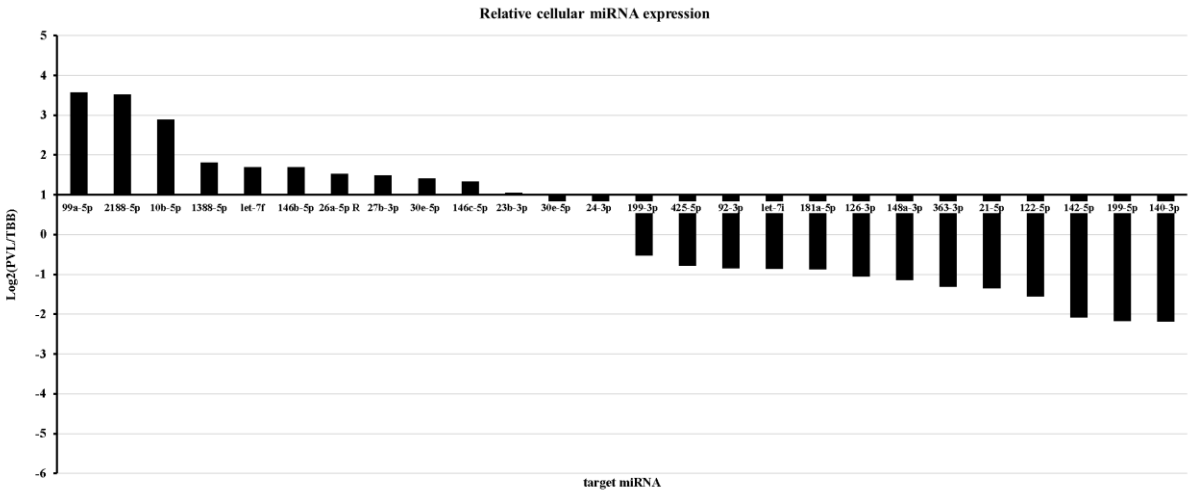

Figure 5.15: Tumor suppressive effect of PVL serum exosomes on the growth and proliferation of UD35 cell line.

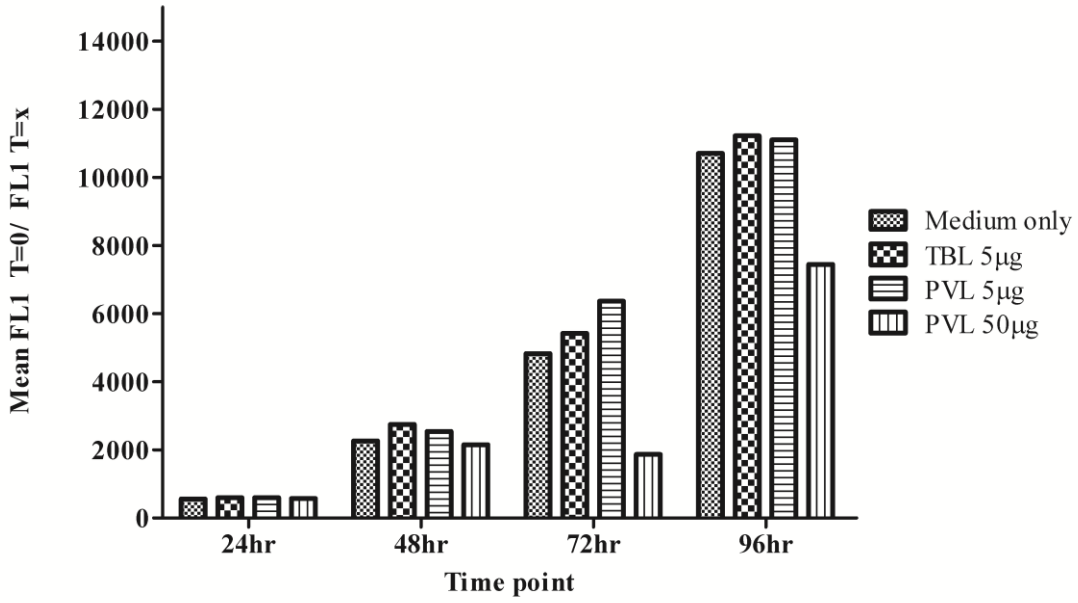

Figure 5.16: Expression of mir-200b in PVL relative to TBL and TBB. Shown on the Y-axis is fold change and on the X-axis is exosome source

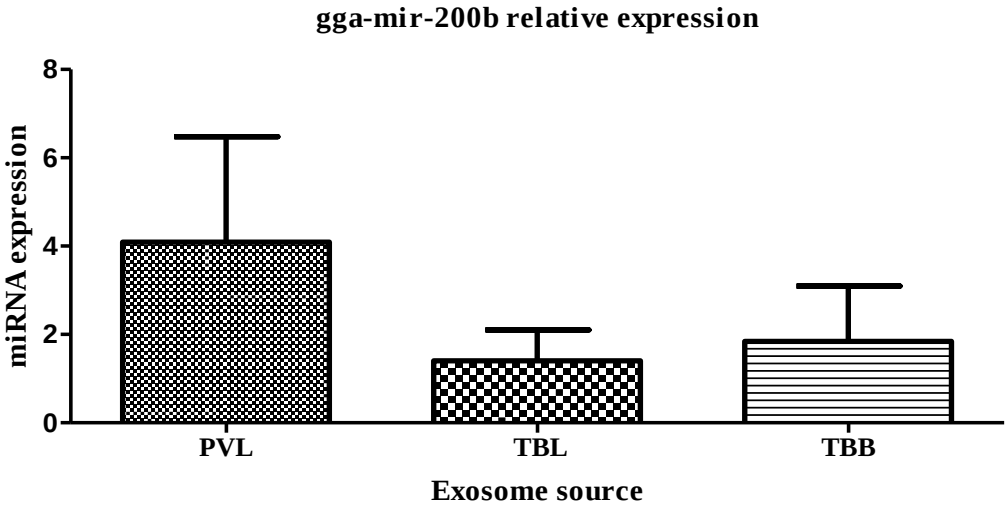

Figure 5.17: Immune suppressive effect of exosomes derived from UD35 cell line supernatants. Shown below are fold changes in target gene expression on Y-axis and innate agonist treatments on X-axis. Graphs A-C and D represent ISGs and MHC II respectively. Graphs E-F represent various IL-12 cytokine family subunits. Agonist only and agonist + UD35 exosomes (exo) were represented in blue and red bars respectively. Asterisks denote significance of $p \leq 0.05$.

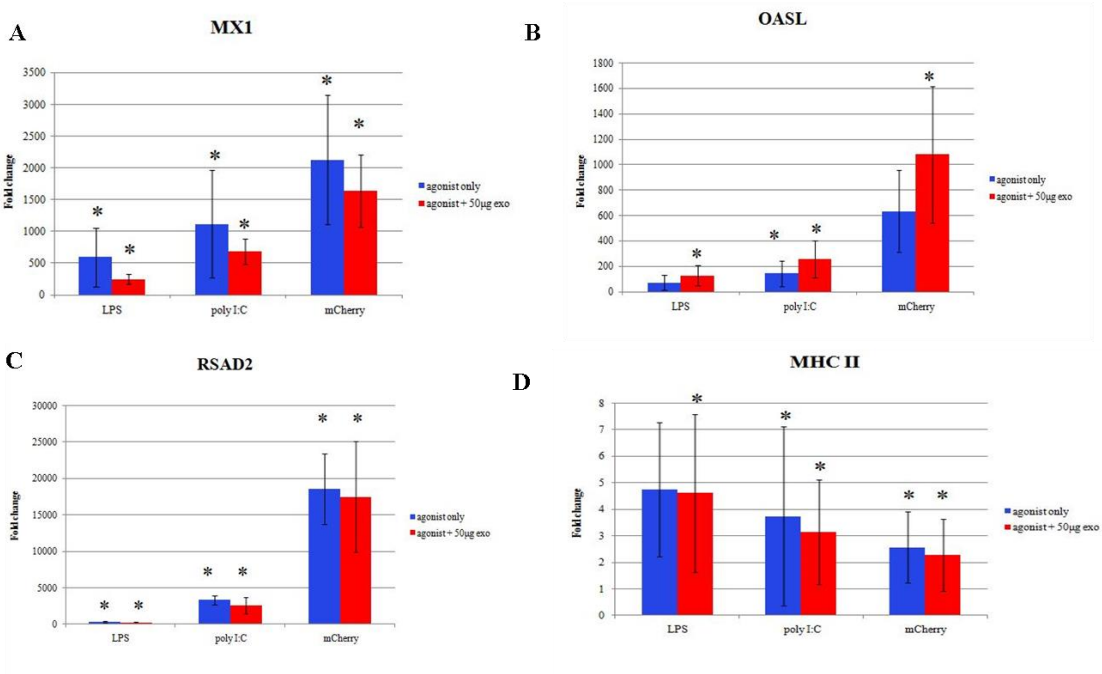

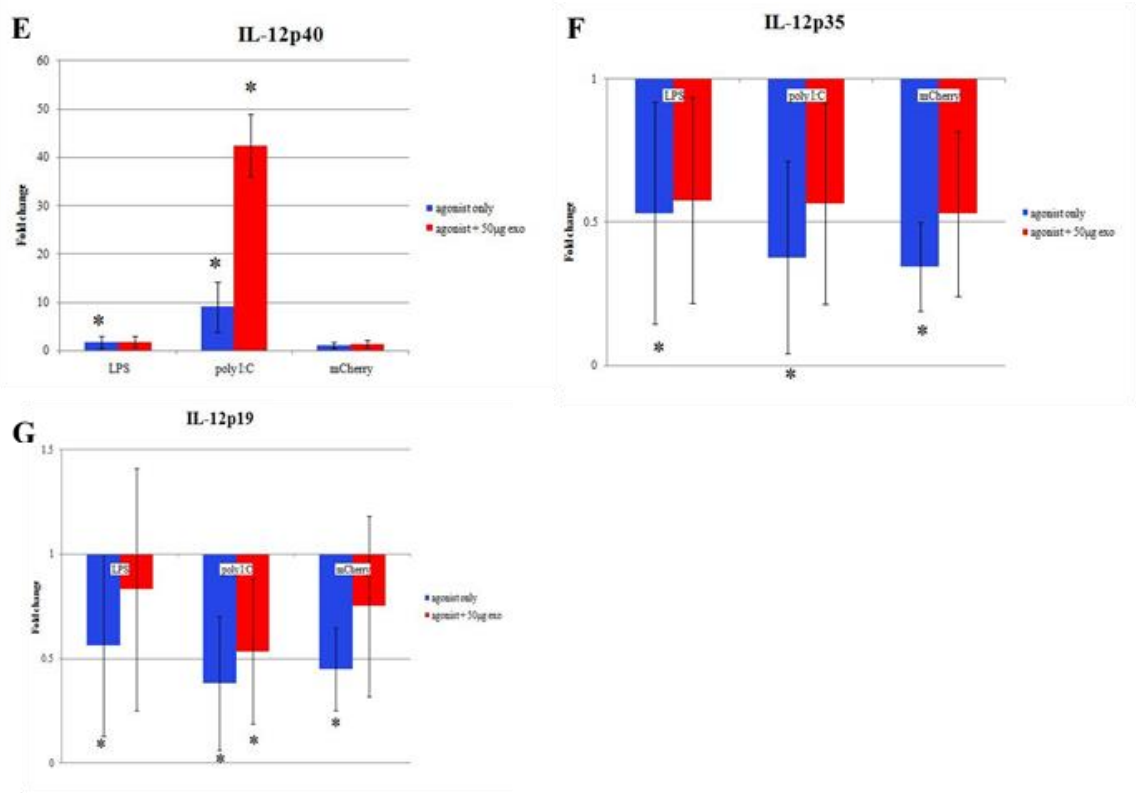
E
IL-12p40
Fold change
60
50
40
30
20
10
0
LPS
poly I:C
mCherry
agonist only
agonist + 50µg exo
F
IL-12p35
Fold change
1
0.5
0
LPS
poly I:C
mCherry
agonist only
agonist + 50µg exo
G
IL-12p19
Fold change
1.5
1
0.5
0
LPS
poly I:C
mCherry
agonist only
agonist + 50µg exo

Figure 5.18. SDE MDV1 miRNAs in TBL (grey bars) and TBB (black bars) compared to PVL. Y-axis denotes $\log_2$ fold change in TBL or TBB compared to PVL. X-axis denotes MDV1 miRNAs. From left to right, *meq* cluster 1 miRNAs (first five), *meq* cluster 2 (next three) and LAT cluster miRNAs (final four). Significance between groups is calculated by two-tailed t-test. Asterisks denote significance of $p \leq 0.05$.

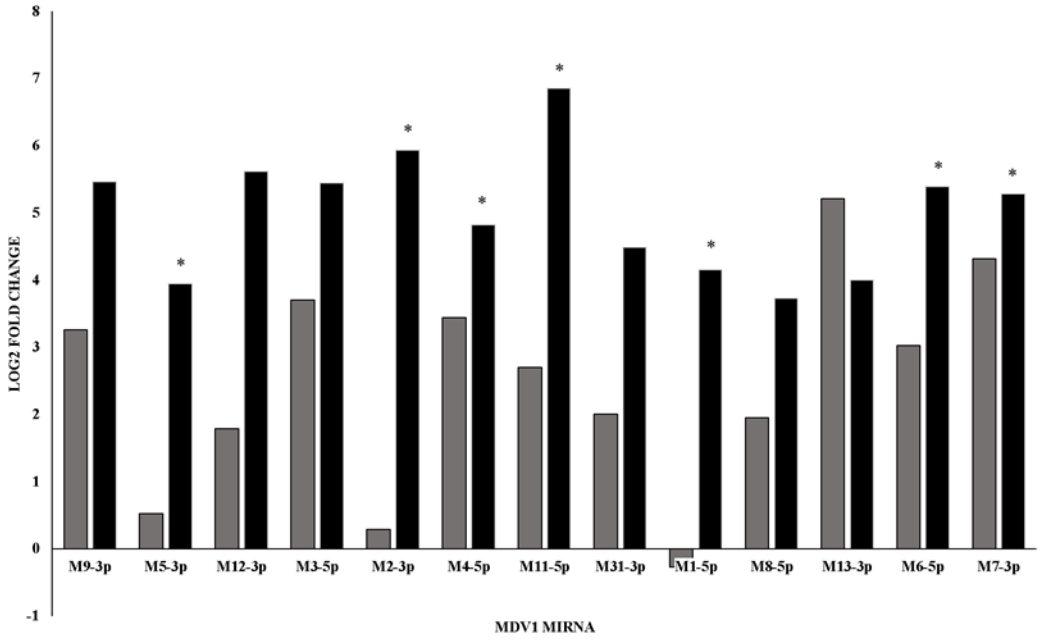

Figure 5.19: PVL reads mapped to pRB1B reference genome by Geneious.

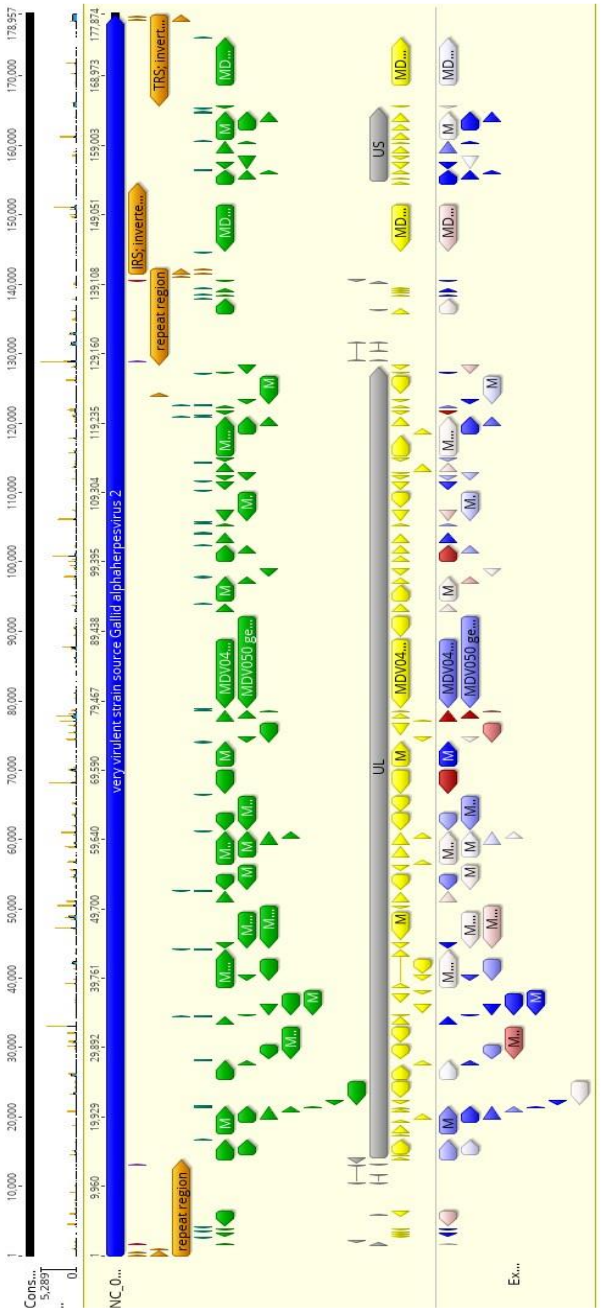

Figure 5.20: TBL reads mapped to pRB1B reference genome by Geneious.

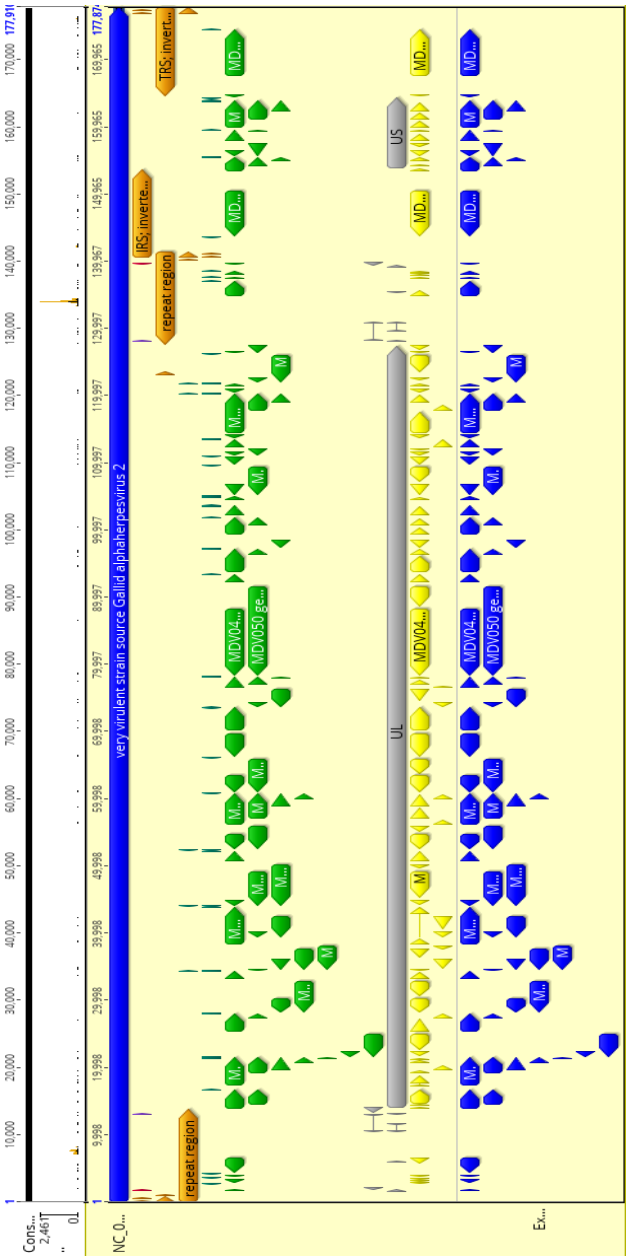

Figure 5.21: TBB reads mapped to pRB1B reference genome by Geneious.

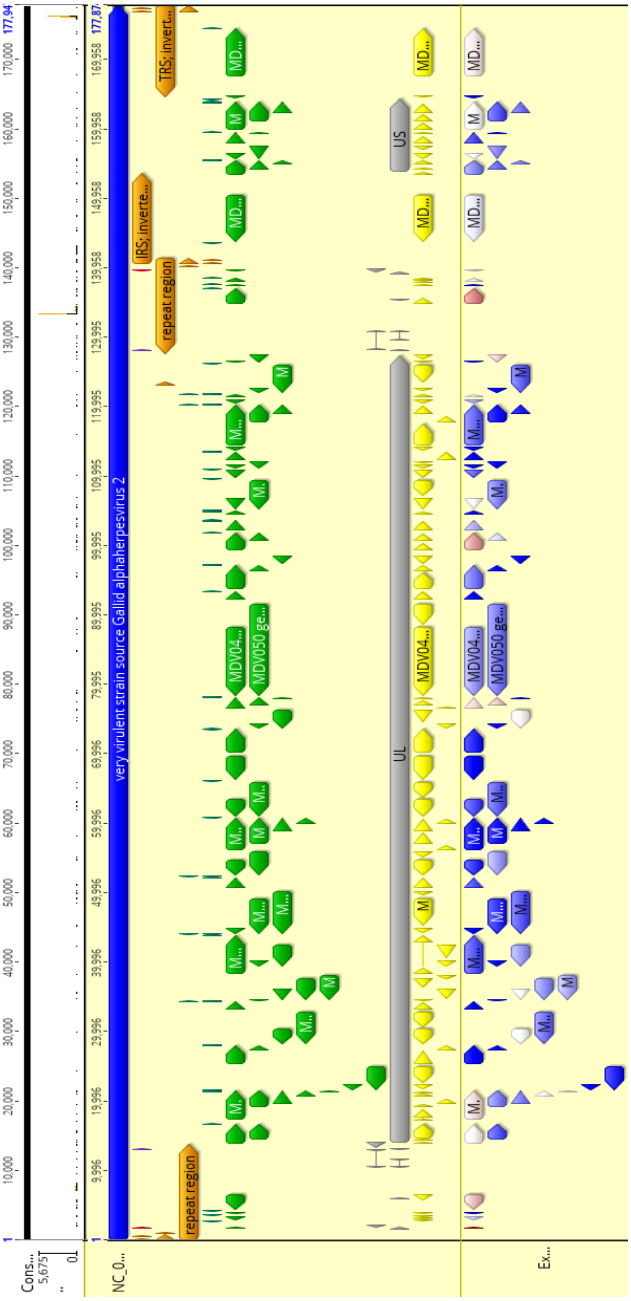

Figure 5.21: Funrich enrichment of exosomal proteins by cellular compartment in PVL (Leghorn protect), TBL (Leghorn tumor), TBB (Leghorn broiler) and UD35 supernatant exosomes.

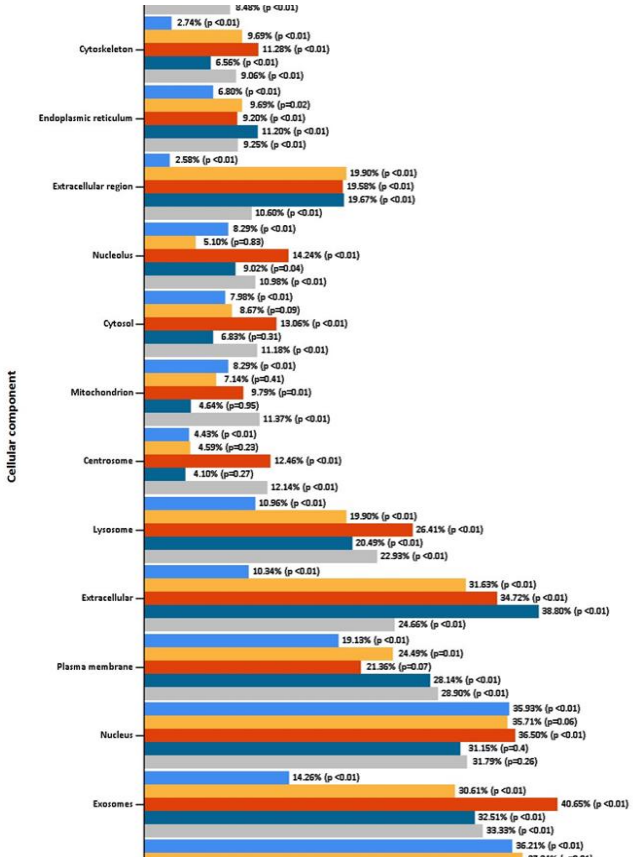

REFERENCES

1. **Calnek BW, Schat KA, Peckham MC, Fabricant J.** 1983. Field trials with a bivalent vaccine (HVT and SB-1) against Marek's disease. Avian diseases **27:**844-849.
2. **Witter RL, Sharma JM, Lee LF, Opitz HM, Henry CW.** 1984. Field trials to test the efficacy of polyvalent Marek's disease vaccines in broilers. Avian diseases **28:**44-60.
3. **Marek J.** 1907. Multiple Nervenentzündung (Polyneuritis). bei Hühnern. Dtsch. Tierärztl. **Wochenschr. 15,417–421**.
4. **PM. B.** 1962. Some observations on the properties of cells from the lesions of Marek's disease and lymphoid leukosis, p. pp.83-89, Proceedings of the Thirteenth Symposium of the Colston Research Society, vol. XIII of the Colston Papers, Butterworth, London.
5. **Kaupp BF.** 1921. Paralysis of the Domestic Fowl. Poultry Science **s2-7:**25-31.
6. **Pappenheimer AW, Dunn, L C. & Cone, V.** 1929a. Studies on fowl paralysis (Neurolymphomatosis gallinarum). I. Clinical features and pathology. . J. Exp. Med. **46:**63-86
7. **Pappenheimer AW, Dunn, L. C. & Seidlin, S. M.** 1929b. Studies on fowl paralysis (Neurolymphomatosis gallinarum). II. Transmission experiments. J. Exp. Med. **49:** 87–102
8. **PM. B.** 1966. Avian leukosis and Marek's disease, p. pp 91-118, XIIIth World's Poultry Congress Symposium Papers, Kiev, Russia.
9. **Osterrieder N, Kamil JP, Schumacher D, Tischer BK, Trapp S.** 2006. Marek's disease virus: from miasma to model. Nat Rev Micro **4:**283-294.
10. **Churchill AE, Biggs PM.** 1967. Agent of Marek's Disease in Tissue Culture. Nature **215:**528-530.
11. **Denesvre C.** 2013. Marek's Disease Virus Morphogenesis. Avian Diseases **57:**340-350.
12. **Calnek BW, Adldinger HK, Kahn DE.** 1970. Feather Follicle Epithelium: A Source of Enveloped and Infectious Cell-Free Herpesvirus from Marek's Disease. Avian Diseases **14:**219-233.
13. **Kishi M, Bradley G, Jessip J, Tanaka A, Nonoyama M.** 1991. Inverted repeat regions of Marek's disease virus DNA possess a structure similar to that of the a sequence of herpes simplex virus DNA and contain host cell telomere sequences. Journal of virology **65:**2791-2797.

14. **Fukuchi K, Sudo M, Lee YS, Tanaka A, Nonoyama M.** 1984. Structure of Marek's disease virus DNA: detailed restriction enzyme map. Journal of virology **51:**102-109.
15. **Waidner LA, Morgan RW, Anderson AS, Bernberg EL, Kamboj S, Garcia M, Riblet SM, Ouyang M, Isaacs GK, Markis M, Meyers BC, Green PJ, Burnside J.** 2009. MicroRNAs of Gallid and Meleagrid herpesviruses show generally conserved genomic locations and are virus-specific. Virology **388:**128-136.
16. **Schat KA, Buckmaster A, Ross LJN.** 1989. Partial transcription map of Marek's disease herpesvirus in lytically infected cells and lymphoblastoid cell lines. International Journal of Cancer **44:**101-109.
17. **Sugaya K, Bradley G, Nonoyama M, Tanaka A.** 1990. Latent transcripts of Marek's disease virus are clustered in the short and long repeat regions. Journal of virology **64:**5773-5782.
18. **Jones D, Lee L, Liu JL, Kung HJ, Tillotson JK.** 1992. Marek disease virus encodes a basic-leucine zipper gene resembling the fos/jun oncogenes that is highly expressed in lymphoblastoid tumors. Proceedings of the National Academy of Sciences of the United States of America **89:**4042-4046.
19. **Fragnet L, Blasco MA, Klapper W, Rasschaert D.** 2003. The RNA subunit of telomerase is encoded by Marek's disease virus. Journal of virology **77:**5985-5996.
20. **Parcells MS, Lin SF, Dienglewicz RL, Majerciak V, Robinson DR, Chen HC, Wu Z, Dubyak GR, Brunovskis P, Hunt HD, Lee LF, Kung HJ.** 2001. Marek's disease virus (MDV) encodes an interleukin-8 homolog (vIL-8): characterization of the vIL-8 protein and a vIL-8 deletion mutant MDV. Journal of virology **75:**5159-5173.
21. **Jarosinski KW, Osterrieder N, Nair VK, Schat KA.** 2005. Attenuation of Marek's disease virus by deletion of open reading frame RLORF4 but not RLORF5a. Journal of virology **79:**11647-11659.
22. **Cui Z, Yan D, Lee LF.** 1990. Marek's disease virus gene clones encoding virus-specific phosphorylated polypeptides and serological characterization of fusion proteins. Virus Genes **3:**309-322.
23. **BW. C.** 1986. . Marek's disease--a model for herpesvirus oncology. Critical reviews in microbiology 12:293-320.
24. **Calnek BW.** Pathogenesis of Marek’s disease, in K. Hirai
(ed): Marek’s Disease, 25–55 (Springer, Berlin).
25. **Baaten BJ, Staines KA, Smith LP, Skinner H, Davison TF, Butter C.** 2009. Early replication in pulmonary B cells after infection with Marek's disease herpesvirus by the respiratory route. Viral immunology **22:**431-444.
26. **Schermuly J, Greco A, Hartle S, Osterrieder N, Kaufer BB, Kaspers B.** 2015. In vitro model for lytic replication, latency, and transformation of an oncogenic alphaherpesvirus. Proceedings of the National Academy of Sciences of the United States of America **112:**7279-7284.

27. **Chakraborty P, Vervelde L, Dalziel RG, Wasson PS, Nair V, Dutia BM, Kaiser P.** 2017. Marek's disease virus infection of phagocytes: a de novo in vitro infection model. The Journal of general virology **98:**1080-1088.
28. **Brown AC, Nair V, Allday MJ.** 2012. Epigenetic regulation of the latency-associated region of Marek's disease virus in tumor-derived T-cell lines and primary lymphoma. Journal of virology **86:**1683-1695.
29. **Kaufer BB, Jarosinski KW, Osterrieder N.** 2011. Herpesvirus telomeric repeats facilitate genomic integration into host telomeres and mobilization of viral DNA during reactivation. The Journal of experimental medicine **208:**605-615.
30. **McPherson MC, Cheng HH, Delany ME.** 2016. Marek's disease herpesvirus vaccines integrate into chicken host chromosomes yet lack a virus-host phenotype associated with oncogenic transformation. Vaccine **34:**5554-5561.
31. **Jarosinski KW, Margulis NG, Kamil JP, Spatz SJ, Nair VK, Osterrieder N.** 2007. Horizontal transmission of Marek's disease virus requires US2, the UL13 protein kinase, and gC. Journal of virology **81:**10575-10587.
32. **Lupiani B, Lee LF, Cui X, Gimeno I, Anderson A, Morgan RW, Silva RF, Witter RL, Kung HJ, Reddy SM.** 2004. Marek's disease virus-encoded Meq gene is involved in transformation of lymphocytes but is dispensable for replication. Proceedings of the National Academy of Sciences of the United States of America **101:**11815-11820.
33. **Reddy SM, Lupiani B, Gimeno IM, Silva RF, Lee LF, Witter RL.** 2002. Rescue of a pathogenic Marek's disease virus with overlapping cosmid DNAs: use of a pp38 mutant to validate the technology for the study of gene function. Proceedings of the National Academy of Sciences of the United States of America **99:**7054-7059.
34. **Payne LN, Roszkowski J.** 1972. The presence of immunologically uncommitted bursa and thymus dependent lymphoid cells in the lymphomas of Marek's disease. Avian pathology : journal of the W.V.P.A **1:**27-34.
35. **Burgess SC, Young JR, Baaten BJ, Hunt L, Ross LN, Parcells MS, Kumar PM, Tregaskes CA, Lee LF, Davison TF.** 2004. Marek's disease is a natural model for lymphomas overexpressing Hodgkin's disease antigen (CD30). Proceedings of the National Academy of Sciences of the United States of America **101:**13879-13884.
36. **Parcells M, Burgess S.** 2008. Immunological aspects of Marek's disease virus (MDV)-induced lymphoma progression, p. 169-191. *In* Kaiser H, Nasir A (ed.), Selected Aspects of Cancer Progression: Metastasis, Apoptosis and Immune Response, vol. 11. Springer Netherlands.
37. **Mwangi WN, Smith LP, Baigent SJ, Beal RK, Nair V, Smith AL.** 2011. Clonal Structure of Rapid-Onset MDV-Driven CD4+ Lymphomas and Responding CD8+ T Cells. PLoS Pathog **7:**e1001337.
38. **Levy AM, Gilad O, Xia L, Izumiya Y, Choi J, Tsalenko A, Yakhini Z, Witter R, Lee L, Cardona CJ, Kung H-J.** 2005. Marek's disease virus Meq

transforms chicken cells via the v-Jun transcriptional cascade: A converging transforming pathway for avian oncoviruses. Proceedings of the National Academy of Sciences of the United States of America **102:**14831-14836.

39. **H. D.** 2011. . The role of Marek's disease virus MEQ gene products on MDV pathogenicity and oncogenicity. University of Delaware, Newark, DE.
40. **Shamblin CE, Greene N, Arumugaswami V, Dienglewicz RL, Parcells MS.** 2004. Comparative analysis of Marek's disease virus (MDV) glycoprotein-, lytic antigen pp38- and transformation antigen Meq-encoding genes: association of meq mutations with MDVs of high virulence. Veterinary microbiology **102:**147-167.
41. **Padhi A, Parcells MS.** 2016. Positive Selection Drives Rapid Evolution of the meq Oncogene of Marek's Disease Virus. PLoS ONE **11:**e0162180.
42. **Levy AM, Gilad O, Xia L, Izumiya Y, Choi J, Tsalenko A, Yakhini Z, Witter R, Lee L, Cardona CJ, Kung HJ.** 2005. Marek's disease virus Meq transforms chicken cells via the v-Jun transcriptional cascade: a converging transforming pathway for avian oncoviruses. Proceedings of the National Academy of Sciences of the United States of America **102:**14831-14836.
43. **Lee S-I, Takagi M, Ohashi K, Sugimoto C, Onuma M.** 2000. Difference in the meq Gene between Oncogenic and Attenuated Strains of Marek’s Disease Virus Serotype 1. Journal of Veterinary Medical Science **62:**287-292.
44. **Anobile JM, Arumugaswami V, Downs D, Czymmek K, Parcells M, Schmidt CJ.** 2006. Nuclear localization and dynamic properties of the Marek's disease virus oncogene products Meq and Meq/vIL8. Journal of virology **80:**1160-1166.
45. **Liu JL, Lee LF, Ye Y, Qian Z, Kung HJ.** 1997. Nucleolar and nuclear localization properties of a herpesvirus bZIP oncoprotein, MEQ. Journal of virology **71:**3188-3196.
46. **Liu J-L, Ye Y, Qian Z, Qian Y, Templeton DJ, Lee LF, Kung H-J.** 1999. Functional Interactions between Herpesvirus Oncoprotein MEQ and Cell Cycle Regulator CDK2. Journal of virology **73:**4208-4219.
47. **Qian Z, Brunovskis P, Rauscher F, Lee L, Kung HJ.** 1995. Transactivation activity of Meq, a Marek's disease herpesvirus bZIP protein persistently expressed in latently infected transformed T cells. Journal of virology **69:**4037-4044.
48. **Suchodolski PF, Izumiya Y, Lupiani B, Ajithdoss DK, Gilad O, Lee LF, Kung H-J, Reddy SM.** 2009. Homodimerization of Marek's Disease Virus-Encoded Meq Protein Is Not Sufficient for Transformation of Lymphocytes in Chickens. Journal of virology **83:**859-869.
49. **Suchodolski PF, Izumiya Y, Lupiani B, Ajithdoss DK, Lee LF, Kung H-J, Reddy SM.** 2010. Both homo and heterodimers of Marek's disease virus encoded Meq protein contribute to transformation of lymphocytes in chickens. Virology **399:**312-321.

50. **Reinke AW, Grigoryan G, Keating AE.** 2010. Identification of bZIP interaction partners of viral proteins HBZ, MEQ, BZLF1, and K-bZIP using coiled-coil arrays. Biochemistry **49:**1985-1997.
51. **Brunovskis P QZ, Li D, F. LL, Kung HJ.** 1996. 5th International Symposium on Marek's Disease, AAAP KS, Pennsylvania, Kellogg center, Michigan State University, East Lansing, Michigan.
52. **S. K.** 2007. Evaluation of the Chicken Cyclin-dependent Kinase Inhibitor 1b, p27 KIP1 in MDV induced Transformation. University of Delaware, Newark, DE.
53. **Kung HJ XL, Brunovskis P, Li D, Liu JL, Lee LF. .** 2001. Meq: An MDV Specific bZIP Transactivator with Transforming Properties, p. 245-260. In Hirai K (ed.), Marek's Disease, vol. 1. Springer, New York.
54. **Brown AC, Baigent SJ, Smith LP, Chattoo JP, Petherbridge LJ, Hawes P, Allday MJ, Nair V.** 2006. Interaction of MEQ protein and C-terminal-binding protein is critical for induction of lymphomas by Marek's disease virus. Proceedings of the National Academy of Sciences of the United States of America **103:**1687-1692.
55. **Zhao Y, Kurian D, Xu H, Petherbridge L, Smith LP, Hunt L, Nair V.** 2009. Interaction of Marek's disease virus oncoprotein Meq with heat-shock protein 70 in lymphoid tumour cells. The Journal of general virology **90:**2201-2208.
56. **Lau L, Gray EE, Brunette RL, Stetson DB.** 2015. DNA tumor virus oncogenes antagonize the cGAS-STING DNA-sensing pathway. Science **350:**568-571.
57. **Shack LA, Buza JJ, Burgess SC.** 2008. The neoplastically transformed (CD30hi) Marek's disease lymphoma cell phenotype most closely resembles T-regulatory cells. Cancer immunology, immunotherapy : CII **57:**1253-1262.
58. **Kumar S, Kunec D, Buza JJ, Chiang H-I, Zhou H, Subramaniam S, Pendarvis K, Cheng HH, Burgess SC.** 2012. Nuclear Factor kappa B is central to Marek’s Disease herpesvirus induced neoplastic transformation of CD30 expressing lymphocytes in-vivo. BMC Systems Biology **6:**123.
59. **Jarosinski KW, Schat KA.** 2007. Multiple alternative splicing to exons II and III of viral interleukin-8 (vIL-8) in the Marek’s disease virus genome: the importance of vIL-8 exon I. Virus Genes **34:**9-22.
60. **Ding J, Cui Z, Lee LF, Cui X, Reddy SM.** 2006. The Role of pp38 in Regulation of Marek’s Disease Virus Bi-directional Promoter between pp38 and 1.8-kb mRNA. Virus Genes **32:**193-201.
61. **Li X, Jarosinski KW, Schat KA.** 2006. Expression of Marek's disease virus phosphorylated polypeptide pp38 produces splice variants and enhances metabolic activity. Veterinary microbiology **117:**154-168.
62. **Gimeno IM, Witter RL, Hunt HD, Reddy SM, Lee LF, Silva RF.** 2005. The pp38 Gene of Marek's Disease Virus (MDV) Is Necessary for Cytolytic Infection of B Cells and Maintenance of the Transformed State but Not for

Cytolytic Infection of the Feather Follicle Epithelium and Horizontal Spread of MDV. Journal of virology **79:**4545-4549.

63. **Engel AT, Selvaraj RK, Kamil JP, Osterrieder N, Kaufer BB.** 2012. Marek's Disease Viral Interleukin-8 Promotes Lymphoma Formation through Targeted Recruitment of B Cells and CD4(+) CD25(+) T Cells. Journal of virology **86:**8536-8545.
64. **Cui X, Lee LF, Hunt HD, Reed WM, Lupiani B, Reddy SM.** 2005. A Marek's Disease Virus vIL-8 Deletion Mutant Has Attenuated Virulence and Confers Protection Against Challenge with a Very Virulent Plus Strain. Avian Diseases **49:**199-206.
65. **Jarosinski KW, Donovan KM, Du G.** 2015. Expression of fluorescent proteins within the repeat long region of the Marek's disease virus genome allows direct identification of infected cells while retaining full pathogenicity. Virus Research **201:**50-60.
66. **Fragnet L, Blasco MA, Klapper W, Rasschaert D.** 2003. The RNA Subunit of Telomerase Is Encoded by Marek's Disease Virus. Journal of virology **77:**5985-5996.
67. **Fragnet L, Kut E, Rasschaert D.** 2005. Comparative Functional Study of the Viral Telomerase RNA Based on Natural Mutations. Journal of Biological Chemistry **280:**23502-23515.
68. **Trapp-Fragnet L, Marie-Egyptienne DT, Fakhoury J, Rasschaert D, Autexier C.** 2012. The human telomerase catalytic subunit and viral telomerase RNA reconstitute a functional telomerase complex in a cell-free system, but not in human cells. Cellular & Molecular Biology Letters **17:**598-615.
69. **Trapp S, Parcells MS, Kamil JP, Schumacher D, Tischer BK, Kumar PM, Nair VK, Osterrieder N.** 2006. A virus-encoded telomerase RNA promotes malignant T cell lymphomagenesis. The Journal of experimental medicine **203:**1307-1317.
70. **Chbab N, Egerer A, Veiga I, Jarosinski KW, Osterrieder N.** 2010. Viral control of vTR expression is critical for efficient formation and dissemination of lymphoma induced by Marek's disease virus (MDV). Veterinary Research **41:**56.
71. **Kaufer BB, Arndt S, Trapp S, Osterrieder N, Jarosinski KW.** 2011. Herpesvirus Telomerase RNA (vTR) with a Mutated Template Sequence Abrogates Herpesvirus-Induced Lymphomagenesis. PLoS Pathogens **7:**e1002333.
72. **Kheimar A, Kaufer BB.** 2018. Epstein-Barr virus-encoded RNAs (EBERs) complement the loss of Herpesvirus telomerase RNA (vTR) in virus-induced tumor formation. Scientific reports **8:**209.
73. **Spatz SJ.** 2010. Accumulation of attenuating mutations in varying proportions within a high passage very virulent plus strain of Gallid herpesvirus type 2. Virus Research **149:**135-142.

74. **Shkreli M, Dambrine G, Soubieux D, Kut E, Rasschaert D.** 2007. Involvement of the Oncoprotein c-Myc in Viral Telomerase RNA Gene Regulation during Marek's Disease Virus-Induced Lymphomagenesis. Journal of virology **81:**4848-4857.
75. **Veiga IB, Jarosinski KW, Kaufer BB, Osterrieder N.** 2013. Marek's disease virus (MDV) ubiquitin-specific protease (USP) performs critical functions beyond its enzymatic activity during virus replication. Virology **437:**110-117.
76. **Jarosinski K, Kattenhorn L, Kaufer B, Ploegh H, Osterrieder N.** 2007. A herpesvirus ubiquitin-specific protease is critical for efficient T cell lymphoma formation. Proceedings of the National Academy of Sciences **104:**20025-20030.
77. **Dong X, Guan J, Zheng C, Zheng X.** 2017. The herpes simplex virus 1 UL36USP deubiquitinase suppresses DNA repair in host cells via deubiquitination of proliferating cell nuclear antigen. The Journal of biological chemistry **292:**8472-8483.
78. **Ye R, Su C, Xu H, Zheng C.** 2017. Herpes Simplex Virus 1 Ubiquitin-Specific Protease UL36 Abrogates NF-kappaB Activation in DNA Sensing Signal Pathway. Journal of virology **91**.
79. **Calistri A, Munegato D, Toffoletto M, Celestino M, Franchin E, Comin A, Sartori E, Salata C, Parolin C, Palù G.** 2015. Functional Interaction Between the ESCRT-I Component TSG101 and the HSV-1 Tegument Ubiquitin Specific Protease. Journal of cellular physiology **230:**1794-1806.
80. **Jarosinski KW, Vautherot J-F.** 2015. Differential expression of Marek's disease virus (MDV) late proteins during in vitro and in situ replication: Role for pUL47 in regulation of the MDV UL46–UL49 gene locus. Virology **484:**213-226.
81. **Schumacher D, Tischer BK, Reddy SM, Osterrieder N.** 2001. Glycoproteins E and I of Marek's Disease Virus Serotype 1 Are Essential for Virus Growth in Cultured Cells. Journal of virology **75:**11307-11318.
82. **Schumacher D, Tischer BK, Fuchs W, Osterrieder N.** 2000. Reconstitution of Marek's Disease Virus Serotype 1 (MDV-1) from DNA Cloned as a Bacterial Artificial Chromosome and Characterization of a Glycoprotein B-Negative MDV-1 Mutant. Journal of virology **74:**11088-11098.
83. **Tischer BK, Schumacher D, Messerle M, Wagner M, Osterrieder N.** 2002. The products of the UL10 (gM) and the UL49.5 genes of Marek's disease virus serotype 1 are essential for virus growth in cultured cells. Journal of General Virology **83:**997-1003.
84. **Jarosinski KW, Osterrieder N.** 2012. Marek's Disease Virus Expresses Multiple UL44 (gC) Variants through mRNA Splicing That Are All Required for Efficient Horizontal Transmission. Journal of virology **86:**7896-7906.
85. **Isfort RJ, Stringer RA, Kung HJ, Velicer LF.** 1986. Synthesis, processing, and secretion of the Marek's disease herpesvirus A antigen glycoprotein. Journal of virology **57:**464-474.

86. **Niikura M, Witter RL, Jang HK, Ono M, Mikami T, Silva RF.** 1999. MDV glycoprotein D is expressed in the feather follicle epithelium of infected chickens. Acta virologica **43:**159-163.
87. **Ono M, Jang HK, Maeda K, Kawaguchi Y, Tohya Y, Niikura M, Mikami T.** 1996. Detection of Marek's disease virus serotype 1 (MDV1) glycoprotein D in MDV1-infected chick embryo fibroblasts. The Journal of veterinary medical science **58:**777-780.
88. **Anderson AS, Parcells MS, Morgan RW.** 1998. The glycoprotein D (US6) homolog is not essential for oncogenicity or horizontal transmission of Marek's disease virus. Journal of virology **72:**2548-2553.
89. **Kaye JF, Gompels UA, Minson AC.** 1992. Glycoprotein H of human cytomegalovirus (HCMV) forms a stable complex with the HCMV UL115 gene product. The Journal of general virology **73 (Pt 10):**2693-2698.
90. **Wu P, Reed WM, Lee LF.** 2001. Glycoproteins H and L of Marek's disease virus form a hetero-oligomer essential for translocation and cell surface expression. Archives of virology **146:**983-992.
91. **Tavlarides-Hontz P, Kumar PM, Amortegui JR, Osterrieder N, Parcells MS.** 2009. A deletion within glycoprotein L of Marek's disease virus (MDV) field isolates correlates with a decrease in bivalent MDV vaccine efficacy in contact-exposed chickens. Avian Dis **53:**287-296.
92. **Shaikh SAR, Katneni UK, Dong H, Gaddamanugu S, Tavlarides-Hontz P, Jarosinski KW, Osterrieder N, Parcells MS.** 2013. A Deletion in the Glycoprotein L (gL) Gene of U.S. Marek's Disease Virus (MDV) Field Strains Is Insufficient to Confer Increased Pathogenicity to the Bacterial Artificial Chromosome (BAC)—Based Strain, RB-1B. Avian Diseases **57:**509-518.
93. **Hong Y, Coussens PM.** 1994. Identification of an immediate-early gene in the Marek's disease virus long internal repeat region which encodes a unique 14-kilodalton polypeptide. Journal of virology **68:**3593-3603.
94. **Hong Y, Frame M, Coussens PM.** 1995. A 14-kDa immediate-early phosphoprotein is specifically expressed in cells infected with oncogenic Marek's disease virus strains and their attenuated derivatives. Virology **206:**695-700.
95. **Tahiri-Alaoui A, Matsuda D, Xu H, Panagiotis P, Burman L, Lambeth LS, Petherbridge L, James W, Mauro V, Nair V.** 2009. The 5' leader of the mRNA encoding the marek's disease virus serotype 1 pp14 protein contains an intronic internal ribosome entry site with allosteric properties. Journal of virology **83:**12769-12778.
96. **Tahiri-Alaoui A, Smith LP, Baigent S, Kgosana L, Petherbridge LJ, Lambeth LS, James W, Nair V.** 2009. Identification of an intercistronic internal ribosome entry site in a Marek's disease virus immediate-early gene. Journal of virology **83:**5846-5853.

97. **Parcells MS, Arumugaswami V, Prigge JT, Pandya K, Dienglewicz RL.** 2003. Marek's disease virus reactivation from latency: changes in gene expression at the origin of replication. Poultry Science **82:**893-898.
98. **Tahiri-Alaoui A, Smith LP, Kgosana L, Petherbridge LJ, Nair V.** 2013. Identification of a Neurovirulence Factor from Marek's Disease Virus. Avian Diseases **57:**387-394.
99. **Kamil JP, Tischer BK, Trapp S, Nair VK, Osterrieder N, Kung HJ.** 2005. vLIP, a viral lipase homologue, is a virulence factor of Marek's disease virus. Journal of virology **79:**6984-6996.
100. **Tulman ER, Afonso CL, Lu Z, Zsak L, Rock DL, Kutish GF.** 2000. The genome of a very virulent Marek's disease virus. Journal of virology **74:**7980-7988.
101. **Cantello JL, Anderson AS, Morgan RW.** 1994. Identification of latency-associated transcripts that map antisense to the ICP4 homolog gene of Marek's disease virus. Journal of virology **68:**6280-6290.
102. **Cantello JL, Parcells MS, Anderson AS, Morgan RW.** 1997. Marek's disease virus latency-associated transcripts belong to a family of spliced RNAs that are antisense to the ICP4 homolog gene. Journal of virology **71:**1353-1361.
103. **Li DS, Pastorek J, Zelnik V, Smith GD, Ross LJ.** 1994. Identification of novel transcripts complementary to the Marek's disease virus homologue of the ICP4 gene of herpes simplex virus. The Journal of general virology **75 (Pt 7):**1713-1722.
104. **Anderson AS, Francesconi A, Morgan RW.** 1992. Complete nucleotide sequence of the Marek's disease virus ICP4 gene. Virology **189:**657-667.
105. **Omar AR, Schat KA.** 1996. Syngeneic Marek's Disease Virus (MDV)-Specific Cell-Mediated Immune Responses against Immediate Early, Late, and Unique MDV Proteins. Virology **222:**87-99.
106. **Morgan R, Anderson A, Bernberg E, Kamboj S, Huang E, Lagasse G, Isaacs G, Parcells M, Meyers BC, Green PJ, Burnside J.** 2008. Sequence conservation and differential expression of Marek's disease virus microRNAs. Journal of virology **82:**12213-12220.
107. **Burnside J, Ouyang M, Anderson A, Bernberg E, Lu C, Meyers BC, Green PJ, Markis M, Isaacs G, Huang E, Morgan RW.** 2008. Deep sequencing of chicken microRNAs. BMC Genomics **9:**185.
108. **Morgan RW, Burnside J.** 2011. Roles of avian herpesvirus microRNAs in infection, latency, and oncogenesis. Biochimica et biophysica acta **1809:**654-659.
109. **Burnside J, Bernberg E, Anderson A, Lu C, Meyers BC, Green PJ, Jain N, Isaacs G, Morgan RW.** 2006. Marek's disease virus encodes MicroRNAs that map to meq and the latency-associated transcript. Journal of virology **80:**8778-8786.

110. **Parnas O, Corcoran DL, Cullen BR.** 2014. Analysis of the mRNA targetome of microRNAs expressed by Marek's disease virus. mBio **5:**e01060-01013.
111. **Yao Y, Nair V.** 2014. Role of virus-encoded microRNAs in Avian viral diseases. Viruses **6:**1379-1394.
112. **Yu ZH, Teng M, Sun AJ, Yu LL, Hu B, Qu LH, Ding K, Cheng XC, Liu JX, Cui ZZ, Zhang GP, Luo J.** 2014. Virus-encoded miR-155 ortholog is an important potential regulator but not essential for the development of lymphomas induced by very virulent Marek's disease virus. Virology **448:**55-64.
113. **Zhao Y, Xu H, Yao Y, Smith LP, Kgosana L, Green J, Petherbridge L, Baigent SJ, Nair V.** 2011. Critical role of the virus-encoded microRNA-155 ortholog in the induction of Marek's disease lymphomas. PLoS Pathog **7:**e1001305.
114. **Tian F, Luo J, Zhang H, Chang S, Song J.** 2012. MiRNA expression signatures induced by Marek's disease virus infection in chickens. Genomics **99:**152-159.
115. **Lian L, Qu L, Chen Y, Lamont SJ, Yang N.** 2012. A Systematic Analysis of miRNA Transcriptome in Marek's Disease Virus-Induced Lymphoma Reveals Novel and Differentially Expressed miRNAs. PLOS ONE **7:**e51003.
116. **Parvizi P, Abdul-Careem MF, Haq K, Thanthrige-Don N, Schat KA, Sharif S.** 2010. Immune responses against Marek's disease virus. Animal health research reviews **11:**123-134.
117. **Schat KA, Xing Z.** 2000. Specific and nonspecific immune responses to Marek's disease virus. Developmental and comparative immunology **24:**201-221.
118. **Sarson AJ, Abdul-Careem MF, Zhou H, Sharif S.** 2006. Transcriptional analysis of host responses to Marek's disease viral infection. Viral immunology **19:**747-758.
119. **Garcia-Camacho L, Schat KA, Brooks R, Jr., Bounous DI.** 2003. Early cell-mediated immune responses to Marek's disease virus in two chicken lines with defined major histocompatibility complex antigens. Veterinary immunology and immunopathology **95:**145-153.
120. **Heller ED, Schat KA.** 1987. Enhancement of natural killer cell activity by Marek's disease vaccines. Avian pathology : journal of the W.V.P.A **16:**51-60.
121. **Sharma JM, Okazaki W.** 1981. Natural killer cell activity in chickens: target cell analysis and effect of antithymocyte serum on effector cells. Infection and immunity **31:**1078-1085.
122. **Sarson AJ, Abdul-Careem MF, Read LR, Brisbin JT, Sharif S.** 2008. Expression of cytotoxicity-associated genes in Marek's disease virus-infected chickens. Viral immunology **21:**267-272.
123. **Hunt HD, Lupiani B, Miller MM, Gimeno I, Lee LF, Parcells MS.** 2001. Marek's disease virus down-regulates surface expression of MHC (B Complex)

Class I (BF) glycoproteins during active but not latent infection of chicken cells. Virology **282:**198-205.
124. **Quere P, Dambrine G.** 1988. Development of anti-tumoral cell-mediated cytotoxicity during the course of Marek's disease in chickens. Annales de recherches veterinaires. Annals of veterinary research **19:**193-201.
125. **Barrow AD, Burgess SC, Baigent SJ, Howes K, Nair VK.** 2003. Infection of macrophages by a lymphotropic herpesvirus: a new tropism for Marek's disease virus. The Journal of general virology **84:**2635-2645.
126. **Chakraborty P, Vervelde L, Dalziel RG, Wasson PS, Nair V, Dutia BM, Kaiser P.** 2017. Marek's disease virus infection of phagocytes: a de novo in vitro infection model. Journal of General Virology **98:**1080-1088.
127. **Powell PC, Hartley KJ, Mustill BM, Rennie M.** 1983. Studies on the role of macrophages in Marek's disease of the chicken. Journal of the Reticuloendothelial Society **34:**289-297.
128. **Djeraba A, Bernardet N, Dambrine G, Quere P.** 2000. Nitric oxide inhibits Marek's disease virus replication but is not the single decisive factor in interferon-gamma-mediated viral inhibition. Virology **277:**58-65.
129. **Jarosinski KW, Njaa BL, O'Connell P H, Schat KA.** 2005. Pro-inflammatory responses in chicken spleen and brain tissues after infection with very virulent plus Marek's disease virus. Viral immunology **18:**148-161.
130. **Xing Z, Schat KA.** 2000. Inhibitory effects of nitric oxide and gamma interferon on in vitro and in vivo replication of Marek's disease virus. Journal of virology **74:**3605-3612.
131. **Buscaglia C, O'Connell PH, Jarosinski KW, Pevzner I, Schat KA.** 2009. Selection for increased nitric oxide production does not increase resistance to Marek's disease in a primary broiler breeder line. Avian Dis **53:**336-340.
132. **Jarosinski KW, Jia W, Sekellick MJ, Marcus PI, Schat KA.** 2001. Cellular responses in chickens treated with IFN-alpha orally or inoculated with recombinant Marek's disease virus expressing IFN-alpha. Journal of interferon & cytokine research : the official journal of the International Society for Interferon and Cytokine Research **21:**287-296.
133. **Volpini LM, Calnek BW, Sneath B, Sekellick MJ, Marcus PI.** 1996. Interferon modulation of Marek's disease virus genome expression in chicken cell lines. Avian Dis **40:**78-87.
134. **Levy AM, Heller ED, Leitner G, Davidson I.** 1999. Effect of native chicken interferon on MDV replication. Acta virologica **43:**121-127.
135. **Djeraba A, Kut E, Rasschaert D, Quere P.** 2002. Antiviral and antitumoral effects of recombinant chicken myelomonocytic growth factor in virally induced lymphoma. International immunopharmacology **2:**1557-1566.
136. **Haq K, Elawadli I, Parvizi P, Mallick AI, Behboudi S, Sharif S.** 2011. Interferon-gamma influences immunity elicited by vaccines against very virulent Marek's disease virus. Antiviral research **90:**218-226.

137. **Nath Neerukonda S, Mahadev-Bhat S, Aylward B, Johnson C, Charavaryamath C, Arsenault RJ.** Kinome analyses of inflammatory responses to swine barn dust extract in human bronchial epithelial and monocyte cell lines. Innate Immunity **0:**1753425918792070.
138. **Churchill AE, Payne LN, Chubb RC.** 1969. Immunization against Marek's Disease using a Live Attenuated Virus. Nature **221:**744-747.
139. **Witter RL, Burmester BR.** 1979. Differential effect of maternal antibodies on efficacy of cellular and cell-free Marek's disease vaccines. Avian pathology : journal of the W.V.P.A **8:**145-156.
140. **Schat KA, Calnek, B.W.,.** 1978. . Characterization of an apparently non-oncogenic Marek's disease virus. J. Natl. Cancer Inst. **60:**1141–1146.
141. **Witter RL, Lee LF.** 1984. Polyvalent Marek's disease vaccines: safety, efficacy and protective synergism in chickens with maternal antibodies. Avian pathology : journal of the W.V.P.A **13:**75-92.
142. **Witter RL.** 1997. Increased virulence of Marek's disease virus field isolates. Avian Dis **41:**149-163.
143. **Rispens BH, van Vloten H, Mastenbroek N, Maas HJ, Schat KA.** 1972. Control of Marek's disease in the Netherlands. I. Isolation of an avirulent Marek's disease virus (strain CVI 988) and its use in laboratory vaccination trials. Avian diseases **16:**108-125.
144. **Rispens BH, van Vloten H, Mastenbroek N, Maas JL, Schat KA.** 1972. Control of Marek's disease in the Netherlands. II. Field trials on vaccination with an avirulent strain (CVI 988) of Marek's disease virus. Avian diseases **16:**126-138.
145. **Gimeno IM, Witter RL, Cortes AL, Reed WM.** 2011. Replication ability of three highly protective Marek's disease vaccines: implications in lymphoid organ atrophy and protection. Avian pathology : journal of the W.V.P.A **40:**573-579.
146. **Sharma JM.** 1987. Embryo vaccination of chickens with turkey herpesvirus: characteristics of the target cell of early viral replication in embryonic lung. Avian pathology : journal of the W.V.P.A **16:**567-579.
147. **Gimeno IM, Faiz NM, Cortes AL, Barbosa T, Villalobos T, Pandiri AR.** 2015. In Ovo Vaccination with Turkey Herpesvirus Hastens Maturation of Chicken Embryo Immune Responses in Specific-Pathogen-Free Chickens. Avian diseases **59:**375-383.
148. **Sharma JM, Graham CK.** 1982. Influence of maternal antibody on efficacy of embryo vaccination with cell-associated and cell-free Marek's disease vaccine. Avian Dis **26:**860-870.
149. **Sharma JM, Lee LF, Wakenell PS.** 1984. Comparative viral, immunologic, and pathologic responses of chickens inoculated with herpesvirus of turkeys as embryos or at hatch. American journal of veterinary research **45:**1619-1623.

150. **Sharma JM, Witter RL.** 1983. Embryo vaccination against Marek's disease with serotypes 1, 2 and 3 vaccines administered singly or in combination. Avian Dis **27:**453-463.
151. **Morgan RW, Gelb J, Jr., Pope CR, Sondermeijer PJ.** 1993. Efficacy in chickens of a herpesvirus of turkeys recombinant vaccine containing the fusion gene of Newcastle disease virus: onset of protection and effect of maternal antibodies. Avian diseases **37:**1032-1040.
152. **Morgan RW, Gelb J, Jr., Schreurs CS, Lutticken D, Rosenberger JK, Sondermeijer PJ.** 1992. Protection of chickens from Newcastle and Marek's diseases with a recombinant herpesvirus of turkeys vaccine expressing the Newcastle disease virus fusion protein. Avian diseases **36:**858-870.
153. **Sondermeijer PJ, Claessens JA, Jenniskens PE, Mockett AP, Thijssen RA, Willemse MJ, Morgan RW.** 1993. Avian herpesvirus as a live viral vector for the expression of heterologous antigens. Vaccine **11:**349-358.
154. **Andoh K, Yamazaki K, Honda Y, Honda T.** 2017. Turkey herpesvirus with an insertion in the UL3-4 region displays an appropriate balance between growth activity and antibody-eliciting capacity and is suitable for the establishment of a recombinant vaccine. Archives of virology **162:**931-941.
155. **Garcia M.** 2016. Current and future vaccines and vaccination strategies against infectious laryngotracheitis (ILT) respiratory disease of poultry. Veterinary microbiology.
156. **Ingrao F, Rauw F, van den Berg T, Lambrecht B.** 2017. Characterization of two recombinant HVT-IBD vaccines by VP2 insert detection and cell-mediated immunity after vaccination of specific pathogen-free chickens. Avian pathology : journal of the W.V.P.A **46:**289-299.
157. **Kapczynski DR, Dorsey K, Chrzastek K, Moraes M, Jackwood M, Hilt D, Gardin Y.** 2016. Vaccine Protection of Turkeys Against H5N1 Highly Pathogenic Avian Influenza Virus with a Recombinant Turkey Herpesvirus Expressing the Hemagglutinin Gene of Avian Influenza. Avian diseases **60:**413-417.
158. **Zhao W, Spatz S, Zhang Z, Wen G, Garcia M, Zsak L, Yu Q.** 2014. Newcastle disease virus (NDV) recombinants expressing infectious laryngotracheitis virus (ILTV) glycoproteins gB and gD protect chickens against ILTV and NDV challenges. Journal of virology **88:**8397-8406.
159. **Dalloul RA, Lillehoj HS, Okamura M, Xie H, Min W, Ding X, Heckert RA.** 2004. In vivo effects of CpG oligodeoxynucleotide on Eimeria infection in chickens. Avian Dis **48:**783-790.
160. **Patel BA, Gomis S, Dar A, Willson PJ, Babiuk LA, Potter A, Mutwiri G, Tikoo SK.** 2008. Oligodeoxynucleotides containing CpG motifs (CpG-ODN) predominantly induce Th1-type immune response in neonatal chicks. Developmental & Comparative Immunology **32:**1041-1049.
161. **Gunawardana T, Foldvari M, Zachar T, Popowich S, Chow-Lockerbie B, Ivanova MV, Tikoo S, Kurukulasuriya S, Willson P, Gomis S.** 2015.

Protection of Neonatal Broiler Chickens Following in ovo Delivery of Oligodeoxynucleotides Containing CpG Motifs (CpG-ODN) Formulated with Carbon Nanotubes or Liposomes. Avian Dis **59:**31-37.

162. **Parvizi P, Abdul-Careem MF, Mallick AI, Haq K, Haghighi HR, Orouji S, Heidari M, Behboudi S, Sharif S.** 2014. The effects of administration of ligands for Toll-like receptor 4 and 21 against Marek's disease in chickens. Vaccine **32:**1932-1938.
163. **Li Y, Meng F, Cui S, Fu J, Wang Y, Cui Z, Chang S, Zhao P.** 2017. Cooperative effects of immune enhancer TPPPS and different adjuvants on antibody responses induced by recombinant ALV-J gp85 subunit vaccines in SPF chickens. Vaccine **35:**1594-1598.
164. **Dar A, Tikoo S, Potter A, Babiuk LA, Townsend H, Gerdts V, Mutwiri G.** 2014. CpG-ODNs induced changes in cytokine/chemokines genes expression associated with suppression of infectious bronchitis virus replication in chicken lungs. Veterinary immunology and immunopathology **160:**209-217.
165. **Padhi A, Parcells MS.** 2016. Positive Selection Drives Rapid Evolution of the meq Oncogene of Marek's Disease Virus. PloS one **11:**e0162180.
166. **Schat KA, Murthy KK.** 1980. In vitro cytotoxicity against Marek's disease lymphoblastoid cell lines after enzymatic removal of Marek's disease tumor-associated surface antigen. Journal of virology **34:**130-135.
167. **Smith J, Sadeyen JR, Paton IR, Hocking PM, Salmon N, Fife M, Nair V, Burt DW, Kaiser P.** 2011. Systems analysis of immune responses in Marek's disease virus-infected chickens identifies a gene involved in susceptibility and highlights a possible novel pathogenicity mechanism. Journal of virology **85:**11146-11158.
168. **Abdul-Careem MF, Hunter BD, Parvizi P, Haghighi HR, Thanthrige-Don N, Sharif S.** 2007. Cytokine gene expression patterns associated with immunization against Marek's disease in chickens. Vaccine **25:**424-432.
169. **Mocellin S, Panelli MC, Wang E, Nagorsen D, Marincola FM.** 2003. The dual role of IL-10. Trends in immunology **24:**36-43.
170. **Abdul-Careem MF, Hunter DB, Lambourne MD, Read LR, Parvizi P, Sharif S.** 2008. Expression of cytokine genes following pre- and post-hatch immunization of chickens with herpesvirus of turkeys. Vaccine **26:**2369-2377.
171. **Heidari M, Zhang HM, Sharif S.** 2008. Marek's disease virus induces Th-2 activity during cytolytic infection. Viral immunology **21:**203-214.
172. **Cai G, Kastelein RA, Hunter CA.** 1999. IL-10 enhances NK cell proliferation, cytotoxicity and production of IFN-gamma when combined with IL-18. European journal of immunology **29:**2658-2665.
173. **Mocellin S, Panelli M, Wang E, Rossi CR, Pilati P, Nitti D, Lise M, Marincola FM.** 2004. IL-10 stimulatory effects on human NK cells explored by gene profile analysis. Genes and immunity **5:**621-630.

174. **Qian C, Jiang X, An H, Yu Y, Guo Z, Liu S, Xu H, Cao X.** 2006. TLR agonists promote ERK-mediated preferential IL-10 production of regulatory dendritic cells (diffDCs), leading to NK-cell activation. Blood **108:**2307-2315.
175. **Shibata Y, Foster LA, Kurimoto M, Okamura H, Nakamura RM, Kawajiri K, Justice JP, Van Scott MR, Myrvik QN, Metzger WJ.** 1998. Immunoregulatory roles of IL-10 in innate immunity: IL-10 inhibits macrophage production of IFN-gamma-inducing factors but enhances NK cell production of IFN-gamma. Journal of immunology **161:**4283-4288.
176. **Carson WE, Lindemann MJ, Baiocchi R, Linett M, Tan JC, Chou CC, Narula S, Caligiuri MA.** 1995. The functional characterization of interleukin-10 receptor expression on human natural killer cells. Blood **85:**3577-3585.
177. **Stacey MA, Marsden M, Wang EC, Wilkinson GW, Humphreys IR.** 2011. IL-10 restricts activation-induced death of NK cells during acute murine cytomegalovirus infection. Journal of immunology **187:**2944-2952.
178. **Colwell WM, Simmons DG, Harris JR, Fulp TG, Carrozza JH, Maag TA.** 1975. Influence of some physical factors on survival of Marek's disease vaccine virus. Avian Dis **19:**781-790.
179. **Eidson CS, Page RK, Kleven SH.** 1978. In vivo and in vitro studies on the effect of gentamicin sulfate on the efficacy of the turkey herpesvirus vaccine. Poult Sci **57:**1519-1525.
180. **Rosenberger JK.**
1983. Reovirus interference with Marek's disease vaccination. In: Proc. Western Poultry Disease Conference, Davis, CA. pp. 50–51.
181. **Islam AF, Wong CW, Walkden-Brown SW, Colditz IG, Arzey KE, Groves PJ.** 2002. Immunosuppressive effects of Marek's disease virus (MDV) and herpesvirus of turkeys (HVT) in broiler chickens and the protective effect of HVT vaccination against MDV challenge. Avian pathology : journal of the W.V.P.A **31:**449-461.
182. **Gimeno IM, Cortes AL, Montiel ER, Lemiere S, Pandiri AK.** 2011. Effect of diluting Marek's disease vaccines on the outcomes of Marek's disease virus infection when challenged with highly virulent Marek's disease viruses. Avian Dis **55:**263-272.
183. **U.S. Department of Agriculture AaPHISCoFRT, Chapter I, part 113–330. Office of the Federal Register, Washington, DC. 2009.**
184. **Jozefowski S, Arredouani M, Sulahian T, Kobzik L.** 2005. Disparate regulation and function of the class A scavenger receptors SR-AI/II and MARCO. Journal of immunology **175:**8032-8041.
185. **Suzuki H, Kurihara Y, Takeya M, Kamada N, Kataoka M, Jishage K, Ueda O, Sakaguchi H, Higashi T, Suzuki T, Takashima Y, Kawabe Y, Cynshi O, Wada Y, Honda M, Kurihara H, Aburatani H, Doi T, Matsumoto A, Azuma S, Noda T, Toyoda Y, Itakura H, Yazaki Y, Kodama T, et al.** 1997. A role for macrophage scavenger receptors in atherosclerosis and susceptibility to infection. Nature **386:**292-296.

186. **MacLeod DT, Nakatsuji T, Yamasaki K, Kobzik L, Gallo RL.** 2013. HSV-1 exploits the innate immune scavenger receptor MARCO to enhance epithelial adsorption and infection. Nature communications **4:**1963.
187. **Keestra AM, de Zoete MR, Bouwman LI, Vaezirad MM, van Putten JP.** 2013. Unique features of chicken Toll-like receptors. Developmental and comparative immunology **41:**316-323.
188. **Crippen TL, Sheffield CL, He H, Lowry VK, Kogut MH.** 2003. Differential nitric oxide production by chicken immune cells. Developmental and comparative immunology **27:**603-610.
189. **Hayashi T, Watanabe C, Suzuki Y, Tanikawa T, Uchida Y, Saito T.** 2014. Chicken MDA5 senses short double-stranded RNA with implications for antiviral response against avian influenza viruses in chicken. Journal of innate immunity **6:**58-71.
190. **Uchikawa E, Lethier M, Malet H, Brunel J, Gerlier D, Cusack S.** 2016. Structural Analysis of dsRNA Binding to Anti-viral Pattern Recognition Receptors LGP2 and MDA5. Molecular cell **62:**586-602.
191. **Vitak N, Hume DA, Chappell KJ, Sester DP, Stacey KJ.** 2016. Induction of interferon and cell death in response to cytosolic DNA in chicken macrophages. Developmental and comparative immunology **59:**145-152.
192. **Broz P, Dixit VM.** 2016. Inflammasomes: mechanism of assembly, regulation and signalling. Nature reviews. Immunology **16:**407-420.
193. **Haigis MC, Sinclair DA.** 2010. Mammalian sirtuins: biological insights and disease relevance. Annual review of pathology **5:**253-295.
194. **Quinones-Mateu ME, Lederman MM, Feng Z, Chakraborty B, Weber J, Rangel HR, Marotta ML, Mirza M, Jiang B, Kiser P, Medvik K, Sieg SF, Weinberg A.** 2003. Human epithelial beta-defensins 2 and 3 inhibit HIV-1 replication. Aids **17:**F39-48.
195. **Soman SS, Arathy DS, Sreekumar E.** 2009. Discovery of Anas platyrhynchos avian beta-defensin 2 (Apl_AvBD2) with antibacterial and chemotactic functions. Molecular immunology **46:**2029-2038.
196. **Soman SS, Nair S, Issac A, Arathy DS, Niyas KP, Anoop M, Sreekumar E.** 2009. Immunomodulation by duck defensin, Apl_AvBD2: in vitro dendritic cell immunoreceptor (DCIR) mRNA suppression, and B- and T-lymphocyte chemotaxis. Molecular immunology **46:**3070-3075.
197. **Soman SS, Sivakumar KC, Sreekumar E.** 2010. Molecular dynamics simulation studies and in vitro site directed mutagenesis of avian beta-defensin Apl_AvBD2. BMC bioinformatics **11 Suppl 1:**S7.
198. **Yang Y, Jiang Y, Yin Q, Liang H, She R.** 2010. Chicken intestine defensins activated murine peripheral blood mononuclear cells through the TLR4-NF-kappaB pathway. Veterinary immunology and immunopathology **133:**59-65.
199. **Sonoda Y, Abdel Mageed AM, Isobe N, Yoshimura Y.** 2013. Induction of avian beta-defensins by CpG oligodeoxynucleotides and proinflammatory cytokines in hen vaginal cells in vitro. Reproduction **145:**621-631.

200. **van Dijk A, Tersteeg-Zijderveld MH, Tjeerdsma-van Bokhoven JL, Jansman AJ, Veldhuizen EJ, Haagsman HP.** 2009. Chicken heterophils are recruited to the site of Salmonella infection and release antibacterial mature Cathelicidin-2 upon stimulation with LPS. Molecular immunology **46:**1517-1526.
201. **Feng F, Chen C, Zhu W, He W, Guang H, Li Z, Wang D, Liu J, Chen M, Wang Y, Yu H.** 2011. Gene cloning, expression and characterization of avian cathelicidin orthologs, Cc-CATHs, from Coturnix coturnix. The FEBS journal **278:**1573-1584.
202. **Townes CL, Michailidis G, Nile CJ, Hall J.** 2004. Induction of cationic chicken liver-expressed antimicrobial peptide 2 in response to Salmonella enterica infection. Infection and immunity **72:**6987-6993.
203. **Evans MA, Smart N, Dube KN, Bollini S, Clark JE, Evans HG, Taams LS, Richardson R, Levesque M, Martin P, Mills K, Riegler J, Price AN, Lythgoe MF, Riley PR.** 2013. Thymosin beta4-sulfoxide attenuates inflammatory cell infiltration and promotes cardiac wound healing. Nature communications **4:**2081.
204. **Kannan L, Rath NC, Liyanage R, Lay JO, Jr.** 2007. Identification and characterization of thymosin beta-4 in chicken macrophages using whole cell MALDI-TOF. Annals of the New York Academy of Sciences **1112:**425-434.
205. **Young JD, Lawrence AJ, MacLean AG, Leung BP, McInnes IB, Canas B, Pappin DJ, Stevenson RD.** 1999. Thymosin beta 4 sulfoxide is an anti-inflammatory agent generated by monocytes in the presence of glucocorticoids. Nature medicine **5:**1424-1427.
206. **Gimeno IM, Cortes AL, Guy JS, Turpin E, Williams C.** 2011. Replication of recombinant herpesvirus of turkey expressing genes of infectious laryngotracheitis virus in specific pathogen free and broiler chickens following in ovo and subcutaneous vaccination. Avian pathology : journal of the W.V.P.A **40:**395-403.
207. **Robertson GM, Egerton JR.** 1981. Replication of infectious laryngotracheitis virus in chickens following vaccination. Australian veterinary journal **57:**119-123.
208. **Bublot M, Pritchard N, Swayne DE, Selleck P, Karaca K, Suarez DL, Audonnet JC, Mickle TR.** 2006. Development and use of fowlpox vectored vaccines for avian influenza. Annals of the New York Academy of Sciences **1081:**193-201.
209. **Esaki M, Godoy A, Rosenberger JK, Rosenberger SC, Gardin Y, Yasuda A, Dorsey KM.** 2013. Protection and antibody response caused by turkey herpesvirus vector Newcastle disease vaccine. Avian Dis **57:**750-755.
210. **Fakhrul Islam AF, Walkden-Brown SW, Groves PJ, Underwood GJ.** 2008. Kinetics of Marek's disease virus (MDV) infection in broiler chickens 1: effect of varying vaccination to challenge interval on vaccinal protection and

load of MDV and herpesvirus of turkey in the spleen and feather dander over time. Avian pathology : journal of the W.V.P.A **37:**225-235.

211. **Linghua Z, Xingshan T, Fengzhen Z.** 2007. Vaccination with Newcastle disease vaccine and CpG oligodeoxynucleotides induces specific immunity and protection against Newcastle disease virus in SPF chicken. Veterinary immunology and immunopathology **115:**216-222.
212. **Neerukonda SN, Katneni UK, Bott M, Golovan SP, Parcells MS.** 2018. Induction of the unfolded protein response (UPR) during Marek's disease virus (MDV) infection. Virology **522:**1-12.
213. **Neerukonda SN, Katneni UK, Golovan S, Parcells MS.** 2016. Evaluation and validation of reference gene stability during Marek's disease virus (MDV) infection. Journal of virological methods **236:**111-116.
214. **Godoy A, Icard A, Martinez M, Mashchenko A, Garcia M, El-Attrachea J.** 2013. Detection of infectious laryngotracheitis virus antibodies by glycoprotein-specific ELISAs in chickens vaccinated with viral vector vaccines. Avian Dis **57:**432-436.
215. **Wattrang E, Dalgaard TS, Norup LR, Kjaerup RB, Lunden A, Juul-Madsen HR.** 2015. CD107a as a marker of activation in chicken cytotoxic T cells. Journal of immunological methods **419:**35-47.
216. **Parvizi P, Abdul-Careem MF, Mallick AI, Haq K, Haghighi HR, Orouji S, Heidari M, Behboudi S, Sharif S.** 2014. The effects of administration of ligands for Toll-like receptor 4 and 21 against Marek's disease in chickens. Vaccine **32:**1932-1938.
217. **Hong YH, Song W, Lee SH, Lillehoj HS.** 2012. Differential gene expression profiles of beta-defensins in the crop, intestine, and spleen using a necrotic enteritis model in 2 commercial broiler chicken lines. Poult Sci **91:**1081-1088.
218. **Xiao Y, Hughes AL, Ando J, Matsuda Y, Cheng JF, Skinner-Noble D, Zhang G.** 2004. A genome-wide screen identifies a single beta-defensin gene cluster in the chicken: implications for the origin and evolution of mammalian defensins. BMC Genomics **5:**56.
219. **Welsh RM, Bahl K, Marshall HD, Urban SL.** 2012. Type 1 Interferons and Antiviral CD8 T-Cell Responses. PLoS Pathogens **8:**e1002352.
220. **Neerukonda S, Egan N, Parcells M.** 2017. Exosomal Communication during Infection, Inflammation and Virus-Associated Pathology. J Cancer Ther Sci. 1(1).
221. **Admyre C, Johansson SM, Qazi KR, Filen JJ, Lahesmaa R, Norman M, Neve EP, Scheynius A, Gabrielsson S.** 2007. Exosomes with immune modulatory features are present in human breast milk. Journal of immunology **179:**1969-1978.
222. **Alegre E, Sanmamed MF, Rodriguez C, Carranza O, Martin-Algarra S, Gonzalez A.** 2014. Study of circulating microRNA-125b levels in serum exosomes in advanced melanoma. Archives of pathology & laboratory medicine **138:**828-832.

223. **Conde-Vancells J, Rodriguez-Suarez E, Embade N, Gil D, Matthiesen R, Valle M, Elortza F, Lu SC, Mato JM, Falcon-Perez JM.** 2008. Characterization and comprehensive proteome profiling of exosomes secreted by hepatocytes. Journal of proteome research **7:**5157-5166.
224. **Hegmans JP, Bard MP, Hemmes A, Luider TM, Kleijmeer MJ, Prins JB, Zitvogel L, Burgers SA, Hoogsteden HC, Lambrecht BN.** 2004. Proteomic analysis of exosomes secreted by human mesothelioma cells. The American journal of pathology **164:**1807-1815.
225. **Nilsson J, Skog J, Nordstrand A, Baranov V, Mincheva-Nilsson L, Breakefield XO, Widmark A.** 2009. Prostate cancer-derived urine exosomes: a novel approach to biomarkers for prostate cancer. British journal of cancer **100:**1603-1607.
226. **Rabinowits G, Gercel-Taylor C, Day JM, Taylor DD, Kloecker GH.** 2009. Exosomal microRNA: a diagnostic marker for lung cancer. Clinical lung cancer **10:**42-46.
227. **Lawson C, Vicencio JM, Yellon DM, Davidson SM.** 2016. Microvesicles and exosomes: new players in metabolic and cardiovascular disease. The Journal of endocrinology **228:**R57-71.
228. **Yanez-Mo M, Siljander PR, Andreu Z, Zavec AB, Borras FE, Buzas EI, Buzas K, Casal E, Cappello F, Carvalho J, Colas E, Cordeiro-da Silva A, Fais S, Falcon-Perez JM, Ghobrial IM, Giebel B, Gimona M, Graner M, Gursel I, Gursel M, Heegaard NH, Hendrix A, Kierulf P, Kokubun K, Kosanovic M, Kralj-Iglic V, Kramer-Albers EM, Laitinen S, Lasser C, Lener T, Ligeti E, Line A, Lipps G, Llorente A, Lotvall J, Mancek-Keber M, Marcilla A, Mittelbrunn M, Nazarenko I, Nolte-'t Hoen EN, Nyman TA, O'Driscoll L, Olivan M, Oliveira C, Pallinger E, Del Portillo HA, Reventos J, Rigau M, Rohde E, Sammar M, Sanchez-Madrid F, Santarem N, Schallmoser K, Ostenfeld MS, Stoorvogel W, Stukelj R, Van der Grein SG, Vasconcelos MH, Wauben MH, De Wever O.** 2015. Biological properties of extracellular vesicles and their physiological functions. Journal of extracellular vesicles **4:**27066.
229. **Ailawadi S, Wang X, Gu H, Fan GC.** 2015. Pathologic function and therapeutic potential of exosomes in cardiovascular disease. Biochimica et biophysica acta **1852:**1-11.
230. **Zhao L, Liu W, Xiao J, Cao B.** 2015. The role of exosomes and "exosomal shuttle microRNA" in tumorigenesis and drug resistance. Cancer letters **356:**339-346.
231. **Witwer KW, Buzas EI, Bemis LT, Bora A, Lasser C, Lotvall J, Nolte-'t Hoen EN, Piper MG, Sivaraman S, Skog J, Thery C, Wauben MH, Hochberg F.** 2013. Standardization of sample collection, isolation and analysis methods in extracellular vesicle research. Journal of extracellular vesicles **2**.

232. **Théry C, Zitvogel L, Amigorena S.** 2002. Exosomes: composition, biogenesis and function. Nature Reviews Immunology **2:**569.
233. **Thery C, Amigorena S, Raposo G, Clayton A.** 2006. Isolation and characterization of exosomes from cell culture supernatants and biological fluids. Current protocols in cell biology **Chapter 3:**Unit 3 22.
234. **Lobb RJ, Becker M, Wen SW, Wong CS, Wiegmans AP, Leimgruber A, Moller A.** 2015. Optimized exosome isolation protocol for cell culture supernatant and human plasma. Journal of extracellular vesicles **4:**27031.
235. **Merchant ML, Powell DW, Wilkey DW, Cummins TD, Deegens JK, Rood IM, McAfee KJ, Fleischer C, Klein E, Klein JB.** 2010. Microfiltration isolation of human urinary exosomes for characterization by MS. Proteomics. Clinical applications **4:**84-96.
236. **Nakai W, Yoshida T, Diez D, Miyatake Y, Nishibu T, Imawaka N, Naruse K, Sadamura Y, Hanayama R.** 2016. A novel affinity-based method for the isolation of highly purified extracellular vesicles. Scientific Reports **6:**33935.
237. **Contreras-Naranjo JC, Wu H-J, Ugaz VM.** 2017. Microfluidics for exosome isolation and analysis: enabling liquid biopsy for personalized medicine. Lab on a Chip **17:**3558-3577.
238. **Cheng Y, Schorey JS.** 2013. Exosomes carrying mycobacterial antigens can protect mice against Mycobacterium tuberculosis infection. European Journal of Immunology **43:**3279-3290.
239. **Kadiu I, Narayanasamy P, Dash PK, Zhang W, Gendelman HE.** 2012. Biochemical and Biologic Characterization of Exosomes and Microvesicles as Facilitators of HIV-1 Infection in Macrophages. The Journal of Immunology **189:**744-754.
240. **Alvarez ML.** 2014. Isolation of Urinary Exosomes for RNA Biomarker Discovery Using a Simple, Fast, and Highly Scalable Method, p. 145-170. *In* Alvarez ML, Nourbakhsh M (ed.), RNA Mapping: Methods and Protocols. Springer New York, New York, NY.
241. **Rider MA, Hurwitz SN, Meckes Jr DG.** 2016. ExtraPEG: A Polyethylene Glycol-Based Method for Enrichment of Extracellular Vesicles. Scientific reports **6:**23978.
242. **Ding M, Wang C, Lu X, Zhang C, Zhou Z, Chen X, Zhang CY, Zen K, Zhang C.** 2018. Comparison of commercial exosome isolation kits for circulating exosomal microRNA profiling. Analytical and bioanalytical chemistry **410:**3805-3814.
243. **Peterson MF, Otoc N, Sethi JK, Gupta A, Antes TJ.** 2015. Integrated systems for exosome investigation. Methods **87:**31-45.
244. **Rekker K, Saare M, Roost AM, Kubo AL, Zarovni N, Chiesi A, Salumets A, Peters M.** 2014. Comparison of serum exosome isolation methods for microRNA profiling. Clinical biochemistry **47:**135-138.
245. **Royo F, Diwan I, Tackett MR, Zuniga P, Sanchez-Mosquera P, Loizaga-Iriarte A, Ugalde-Olano A, Lacasa I, Perez A, Unda M, Carracedo A,**

Falcon-Perez JM. 2016. Comparative miRNA Analysis of Urine Extracellular Vesicles Isolated through Five Different Methods. Cancers **8**.

246. **Royo F, Zuniga-Garcia P, Sanchez-Mosquera P, Egia A, Perez A, Loizaga A, Arceo R, Lacasa I, Rabade A, Arrieta E, Bilbao R, Unda M, Carracedo A, Falcon-Perez JM.** 2016. Different EV enrichment methods suitable for clinical settings yield different subpopulations of urinary extracellular vesicles from human samples. Journal of extracellular vesicles **5:**29497.
247. **Helwa I, Cai J, Drewry MD, Zimmerman A, Dinkins MB, Khaled ML, Seremwe M, Dismuke WM, Bieberich E, Stamer WD, Hamrick MW, Liu Y.** 2017. A Comparative Study of Serum Exosome Isolation Using Differential Ultracentrifugation and Three Commercial Reagents. PloS one **12:**e0170628.
248. **Alvarez ML, Khosroheidari M, Kanchi Ravi R, DiStefano JK.** 2012. Comparison of protein, microRNA, and mRNA yields using different methods of urinary exosome isolation for the discovery of kidney disease biomarkers. Kidney international **82:**1024-1032.
249. **Saenz-Cuesta M, Arbelaiz A, Oregi A, Irizar H, Osorio-Querejeta I, Munoz-Culla M, Banales JM, Falcon-Perez JM, Olascoaga J, Otaegui D.** 2015. Methods for extracellular vesicles isolation in a hospital setting. Frontiers in immunology **6:**50.
250. **Neerukonda SN, Egan N, Patria J, Assakhi I, Tavlarides-Hontz P, Modla S, Munoz E, Hudson M, Parcells MS.** 2018. Comparison of exosomes purified via ultracentrifugation (UC) and Total Exosome Isolation (TEI) reagent from the serum of Marek's disease virus (MDV)-vaccinated and tumor-bearing chickens. Journal of virological methods.
251. **Zeka F, Mestdagh P, Vandesompele J.** 2015. RT-qPCR-Based Quantification of Small Non-Coding RNAs, p. 85-102. *In* Rederstorff M (ed.), Small Non-Coding RNAs: Methods and Protocols. Springer New York, New York, NY.
252. **van der Pol E, Hoekstra AG, Sturk A, Otto C, van Leeuwen TG, Nieuwland R.** 2010. Optical and non-optical methods for detection and characterization of microparticles and exosomes. Journal of thrombosis and haemostasis : JTH **8:**2596-2607.
253. **Kalluri R.** 2016. The biology and function of exosomes in cancer. The Journal of clinical investigation **126:**1208-1215.
254. **King HW, Michael MZ, Gleadle JM.** 2012. Hypoxic enhancement of exosome release by breast cancer cells. BMC cancer **12:**421.
255. **Caradec J, Kharmate G, Hosseini-Beheshti E, Adomat H, Gleave M, Guns E.** 2014. Reproducibility and efficiency of serum-derived exosome extraction methods. Clinical biochemistry **47:**1286-1292.
256. **Momen-Heravi F, Balaj L, Alian S, Trachtenberg AJ, Hochberg FH, Skog J, Kuo WP.** 2012. Impact of biofluid viscosity on size and sedimentation efficiency of the isolated microvesicles. Frontiers in physiology **3:**162.

257. **Cvjetkovic A, Lotvall J, Lasser C.** 2014. The influence of rotor type and centrifugation time on the yield and purity of extracellular vesicles. Journal of extracellular vesicles **3**.
258. **Villarroya-Beltri C, Gutiérrez-Vázquez C, Sánchez-Cabo F, Pérez-Hernández D, Vázquez J, Martin-Cofreces N, Martinez-Herrera DJ, Pascual-Montano A, Mittelbrunn M, Sánchez-Madrid F.** 2013. Sumoylated hnRNPA2B1 controls the sorting of miRNAs into exosomes through binding to specific motifs. Nature Communications **4:**2980.
259. **Valadi H, Ekstrom K, Bossios A, Sjostrand M, Lee JJ, Lotvall JO.** 2007. Exosome-mediated transfer of mRNAs and microRNAs is a novel mechanism of genetic exchange between cells. Nature cell biology **9:**654-659.
260. **Correia NC, Fragoso R, Carvalho T, Enguita FJ, Barata JT.** 2016. MiR-146b negatively regulates migration and delays progression of T-cell acute lymphoblastic leukemia. Sci Rep **6:**31894.
261. **Ma X, Kumar M, Choudhury SN, Becker Buscaglia LE, Barker JR, Kanakamedala K, Liu MF, Li Y.** 2011. Loss of the miR-21 allele elevates the expression of its target genes and reduces tumorigenesis. Proceedings of the National Academy of Sciences of the United States of America **108:**10144-10149.
262. **Thery C, Ostrowski M, Segura E.** 2009. Membrane vesicles as conveyors of immune responses. Nature reviews. Immunology **9:**581-593.
263. **Kowal J, Arras G, Colombo M, Jouve M, Morath JP, Primdal-Bengtson B, Dingli F, Loew D, Tkach M, Thery C.** 2016. Proteomic comparison defines novel markers to characterize heterogeneous populations of extracellular vesicle subtypes. Proceedings of the National Academy of Sciences of the United States of America **113:**E968-977.
264. **Trams EG, Lauter CJ, Salem N, Jr., Heine U.** 1981. Exfoliation of membrane ecto-enzymes in the form of micro-vesicles. Biochimica et biophysica acta **645:**63-70.
265. **Harding C, Heuser J, Stahl P.** 1983. Receptor-mediated endocytosis of transferrin and recycling of the transferrin receptor in rat reticulocytes. The Journal of cell biology **97:**329-339.
266. **Pan BT, Teng K, Wu C, Adam M, Johnstone RM.** 1985. Electron microscopic evidence for externalization of the transferrin receptor in vesicular form in sheep reticulocytes. The Journal of cell biology **101:**942-948.
267. **Campbell TD, Khan M, Huang MB, Bond VC, Powell MD.** 2008. HIV-1 Nef protein is secreted into vesicles that can fuse with target cells and virions. Ethnicity & disease **18:**S2-14-19.
268. **daSilva LL, Sougrat R, Burgos PV, Janvier K, Mattera R, Bonifacino JS.** 2009. Human immunodeficiency virus type 1 Nef protein targets CD4 to the multivesicular body pathway. Journal of virology **83:**6578-6590.

269. **Fang Y, Wu N, Gan X, Yan W, Morrell JC, Gould SJ.** 2007. Higher-order oligomerization targets plasma membrane proteins and HIV gag to exosomes. PLoS biology **5:**e158.
270. **Narayanan A, Iordanskiy S, Das R, Van Duyne R, Santos S, Jaworski E, Guendel I, Sampey G, Dalby E, Iglesias-Ussel M, Popratiloff A, Hakami R, Kehn-Hall K, Young M, Subra C, Gilbert C, Bailey C, Romerio F, Kashanchi F.** 2013. Exosomes derived from HIV-1-infected cells contain trans-activation response element RNA. The Journal of biological chemistry **288:**20014-20033.
271. **Arakelyan A, Fitzgerald W, Zicari S, Vanpouille C, Margolis L.** 2017. Extracellular Vesicles Carry HIV Env and Facilitate Hiv Infection of Human Lymphoid Tissue. Scientific reports **7:**1695.
272. **Booth AM, Fang Y, Fallon JK, Yang JM, Hildreth JE, Gould SJ.** 2006. Exosomes and HIV Gag bud from endosome-like domains of the T cell plasma membrane. The Journal of cell biology **172:**923-935.
273. **Hanson PI, Cashikar A.** 2012. Multivesicular body morphogenesis. Annual review of cell and developmental biology **28:**337-362.
274. **Davies BA, Lee JR, Oestreich AJ, Katzmann DJ.** 2009. Membrane protein targeting to the MVB/lysosome. Chemical reviews **109:**1575-1586.
275. **Metcalf D, Isaacs AM.** 2010. The role of ESCRT proteins in fusion events involving lysosomes, endosomes and autophagosomes. Biochemical Society transactions **38:**1469-1473.
276. **Babst M, Katzmann DJ, Estepa-Sabal EJ, Meerloo T, Emr SD.** 2002. Escrt-III: an endosome-associated heterooligomeric protein complex required for mvb sorting. Developmental cell **3:**271-282.
277. **Babst M, Katzmann DJ, Snyder WB, Wendland B, Emr SD.** 2002. Endosome-associated complex, ESCRT-II, recruits transport machinery for protein sorting at the multivesicular body. Developmental cell **3:**283-289.
278. **Bilodeau PS, Winistorfer SC, Kearney WR, Robertson AD, Piper RC.** 2003. Vps27-Hse1 and ESCRT-I complexes cooperate to increase efficiency of sorting ubiquitinated proteins at the endosome. The Journal of cell biology **163:**237-243.
279. **Katzmann DJ, Babst M, Emr SD.** 2001. Ubiquitin-dependent sorting into the multivesicular body pathway requires the function of a conserved endosomal protein sorting complex, ESCRT-I. Cell **106:**145-155.
280. **Katzmann DJ, Stefan CJ, Babst M, Emr SD.** 2003. Vps27 recruits ESCRT machinery to endosomes during MVB sorting. The Journal of cell biology **162:**413-423.
281. **Stuffers S, Sem Wegner C, Stenmark H, Brech A.** 2009. Multivesicular endosome biogenesis in the absence of ESCRTs. Traffic **10:**925-937.
282. **Trajkovic K, Hsu C, Chiantia S, Rajendran L, Wenzel D, Wieland F, Schwille P, Brugger B, Simons M.** 2008. Ceramide triggers budding of exosome vesicles into multivesicular endosomes. Science **319:**1244-1247.

283. **Theos AC, Truschel ST, Tenza D, Hurbain I, Harper DC, Berson JF, Thomas PC, Raposo G, Marks MS.** A Lumenal Domain-Dependent Pathway for Sorting to Intralumenal Vesicles of Multivesicular Endosomes Involved in Organelle Morphogenesis. Developmental cell **10:**343-354.
284. **Buschow SI, Nolte-'t Hoen EN, van Niel G, Pols MS, ten Broeke T, Lauwen M, Ossendorp F, Melief CJ, Raposo G, Wubbolts R, Wauben MH, Stoorvogel W.** 2009. MHC II in dendritic cells is targeted to lysosomes or T cell-induced exosomes via distinct multivesicular body pathways. Traffic **10:**1528-1542.
285. **van Niel G, Charrin S, Simoes S, Romao M, Rochin L, Saftig P, Marks MS, Rubinstein E, Raposo G.** 2011. The tetraspanin CD63 regulates ESCRT-independent and -dependent endosomal sorting during melanogenesis. Developmental cell **21:**708-721.
286. **Dreux M, Garaigorta U, Boyd B, Decembre E, Chung J, Whitten-Bauer C, Wieland S, Chisari FV.** 2012. Short-range exosomal transfer of viral RNA from infected cells to plasmacytoid dendritic cells triggers innate immunity. Cell host & microbe **12:**558-570.
287. **Hoshino D, Kirkbride KC, Costello K, Clark ES, Sinha S, Grega-Larson N, Tyska MJ, Weaver AM.** 2013. Exosome secretion is enhanced by invadopodia and drives invasive behavior. Cell reports **5:**1159-1168.
288. **Kosaka N, Iguchi H, Yoshioka Y, Takeshita F, Matsuki Y, Ochiya T.** 2010. Secretory mechanisms and intercellular transfer of microRNAs in living cells. The Journal of biological chemistry **285:**17442-17452.
289. **Chairoungdua A, Smith DL, Pochard P, Hull M, Caplan MJ.** 2010. Exosome release of β-catenin: a novel mechanism that antagonizes Wnt signaling. The Journal of cell biology **190:**1079-1091.
290. **Geminard C, De Gassart A, Blanc L, Vidal M.** 2004. Degradation of AP2 during reticulocyte maturation enhances binding of hsc70 and Alix to a common site on TFR for sorting into exosomes. Traffic **5:**181-193.
291. **Sahu R, Kaushik S, Clement CC, Cannizzo ES, Scharf B, Follenzi A, Potolicchio I, Nieves E, Cuervo AM, Santambrogio L.** 2011. Microautophagy of cytosolic proteins by late endosomes. Developmental cell **20:**131-139.
292. **Alonso R, Mazzeo C, Rodriguez MC, Marsh M, Fraile-Ramos A, Calvo V, Avila-Flores A, Merida I, Izquierdo M.** 2011. Diacylglycerol kinase alpha regulates the formation and polarisation of mature multivesicular bodies involved in the secretion of Fas ligand-containing exosomes in T lymphocytes. Cell death and differentiation **18:**1161-1173.
293. **Hsu C, Morohashi Y, Yoshimura S, Manrique-Hoyos N, Jung S, Lauterbach MA, Bakhti M, Gronborg M, Mobius W, Rhee J, Barr FA, Simons M.** 2010. Regulation of exosome secretion by Rab35 and its GTPase-activating proteins TBC1D10A-C. The Journal of cell biology **189:**223-232.

294. **Laulagnier K, Grand D, Dujardin A, Hamdi S, Vincent-Schneider H, Lankar D, Salles JP, Bonnerot C, Perret B, Record M.** 2004. PLD2 is enriched on exosomes and its activity is correlated to the release of exosomes. FEBS letters **572:**11-14.
295. **Laulagnier K, Vincent-Schneider H, Hamdi S, Subra C, Lankar D, Record M.** 2005. Characterization of exosome subpopulations from RBL-2H3 cells using fluorescent lipids. Blood cells, molecules & diseases **35:**116-121.
296. **Loomis RJ, Holmes DA, Elms A, Solski PA, Der CJ, Su L.** 2006. Citron kinase, a RhoA effector, enhances HIV-1 virion production by modulating exocytosis. Traffic **7:**1643-1653.
297. **Ostrowski M, Carmo NB, Krumeich S, Fanget I, Raposo G, Savina A, Moita CF, Schauer K, Hume AN, Freitas RP, Goud B, Benaroch P, Hacohen N, Fukuda M, Desnos C, Seabra MC, Darchen F, Amigorena S, Moita LF, Thery C.** 2010. Rab27a and Rab27b control different steps of the exosome secretion pathway. Nature cell biology **12:**19-30; sup pp 11-13.
298. **Savina A, Fader CM, Damiani MT, Colombo MI.** 2005. Rab11 promotes docking and fusion of multivesicular bodies in a calcium-dependent manner. Traffic **6:**131-143.
299. **Hyenne V, Apaydin A, Rodriguez D, Spiegelhalter C, Hoff-Yoessle S, Diem M, Tak S, Lefebvre O, Schwab Y, Goetz JG, Labouesse M.** 2015. RAL-1 controls multivesicular body biogenesis and exosome secretion. The Journal of cell biology **211:**27-37.
300. **Fader CM, Sanchez DG, Mestre MB, Colombo MI.** 2009. TI-VAMP/VAMP7 and VAMP3/cellubrevin: two v-SNARE proteins involved in specific steps of the autophagy/multivesicular body pathways. Biochimica et biophysica acta **1793:**1901-1916.
301. **Proux-Gillardeaux V, Raposo G, Irinopoulou T, Galli T.** 2007. Expression of the Longin domain of TI-VAMP impairs lysosomal secretion and epithelial cell migration. Biology of the cell **99:**261-271.
302. **Rao SK, Huynh C, Proux-Gillardeaux V, Galli T, Andrews NW.** 2004. Identification of SNAREs involved in synaptotagmin VII-regulated lysosomal exocytosis. The Journal of biological chemistry **279:**20471-20479.
303. **Giri PK, Schorey JS.** 2008. Exosomes Derived from M. Bovis BCG Infected Macrophages Activate Antigen-Specific CD4(+) and CD8(+) T Cells In Vitro and In Vivo. PLoS ONE **3:**e2461.
304. **Smith VL, Cheng Y, Bryant BR, Schorey JS.** 2017. Exosomes function in antigen presentation during an in vivo Mycobacterium tuberculosis infection. Scientific reports **7:**43578.
305. **Segura E, Amigorena S, Thery C.** 2005. Mature dendritic cells secrete exosomes with strong ability to induce antigen-specific effector immune responses. Blood cells, molecules & diseases **35:**89-93.

306. **Mathivanan S, Fahner CJ, Reid GE, Simpson RJ.** 2012. ExoCarta 2012: database of exosomal proteins, RNA and lipids. Nucleic acids research **40:**D1241-1244.
307. **Laulagnier K, Motta C, Hamdi S, Roy S, Fauvelle F, Pageaux JF, Kobayashi T, Salles JP, Perret B, Bonnerot C, Record M.** 2004. Mast cell- and dendritic cell-derived exosomes display a specific lipid composition and an unusual membrane organization. The Biochemical journal **380:**161-171.
308. **Llorente A, Skotland T, Sylvanne T, Kauhanen D, Rog T, Orlowski A, Vattulainen I, Ekroos K, Sandvig K.** 2013. Molecular lipidomics of exosomes released by PC-3 prostate cancer cells. Biochimica et biophysica acta **1831:**1302-1309.
309. **Longatti A, Boyd B, Chisari FV.** 2015. Virion-independent transfer of replication-competent hepatitis C virus RNA between permissive cells. Journal of virology **89:**2956-2961.
310. **Lydic TA, Townsend S, Adda CG, Collins C, Mathivanan S, Reid GE.** 2015. Rapid and comprehensive 'shotgun' lipidome profiling of colorectal cancer cell derived exosomes. Methods **87:**83-95.
311. **Mittelbrunn M, Gutierrez-Vazquez C, Villarroya-Beltri C, Gonzalez S, Sanchez-Cabo F, Gonzalez MA, Bernad A, Sanchez-Madrid F.** 2011. Unidirectional transfer of microRNA-loaded exosomes from T cells to antigen-presenting cells. Nature communications **2:**282.
312. **Montecalvo A, Larregina AT, Shufesky WJ, Stolz DB, Sullivan ML, Karlsson JM, Baty CJ, Gibson GA, Erdos G, Wang Z, Milosevic J, Tkacheva OA, Divito SJ, Jordan R, Lyons-Weiler J, Watkins SC, Morelli AE.** 2012. Mechanism of transfer of functional microRNAs between mouse dendritic cells via exosomes. Blood **119:**756-766.
313. **Okoye IS, Coomes SM, Pelly VS, Czieso S, Papayannopoulos V, Tolmachova T, Seabra MC, Wilson MS.** 2014. MicroRNA-containing T-regulatory-cell-derived exosomes suppress pathogenic T helper 1 cells. Immunity **41:**89-103.
314. **Lian L, Qu L, Chen Y, Lamont SJ, Yang N.** 2012. A systematic analysis of miRNA transcriptome in Marek's disease virus-induced lymphoma reveals novel and differentially expressed miRNAs. PLoS One **7:**e51003.
315. **Nolte-'t Hoen EN, Buermans HP, Waasdorp M, Stoorvogel W, Wauben MH, t Hoen PA.** 2012. Deep sequencing of RNA from immune cell-derived vesicles uncovers the selective incorporation of small non-coding RNA biotypes with potential regulatory functions. Nucleic acids research **40:**9272-9285.
316. **Thery C, Regnault A, Garin J, Wolfers J, Zitvogel L, Ricciardi-Castagnoli P, Raposo G, Amigorena S.** 1999. Molecular characterization of dendritic cell-derived exosomes. Selective accumulation of the heat shock protein hsc73. The Journal of cell biology **147:**599-610.

317. **Muntasell A, Berger AC, Roche PA.** 2007. T cell-induced secretion of MHC class II–peptide complexes on B cell exosomes. The EMBO Journal **26:**4263-4272.
318. **Raposo G, Nijman HW, Stoorvogel W, Liejendekker R, Harding CV, Melief CJ, Geuze HJ.** 1996. B lymphocytes secrete antigen-presenting vesicles. The Journal of experimental medicine **183:**1161-1172.
319. **Segura E, Nicco C, Lombard B, Veron P, Raposo G, Batteux F, Amigorena S, Thery C.** 2005. ICAM-1 on exosomes from mature dendritic cells is critical for efficient naive T-cell priming. Blood **106:**216-223.
320. **Thery C, Duban L, Segura E, Veron P, Lantz O, Amigorena S.** 2002. Indirect activation of naive CD4+ T cells by dendritic cell-derived exosomes. Nature immunology **3:**1156-1162.
321. **Skokos D, Le Panse S, Villa I, Rousselle JC, Peronet R, David B, Namane A, Mecheri S.** 2001. Mast cell-dependent B and T lymphocyte activation is mediated by the secretion of immunologically active exosomes. Journal of immunology **166:**868-876.
322. **Skokos D, Botros HG, Demeure C, Morin J, Peronet R, Birkenmeier G, Boudaly S, Mécheri S.** 2003. Mast Cell-Derived Exosomes Induce Phenotypic and Functional Maturation of Dendritic Cells and Elicit Specific Immune Responses In Vivo. The Journal of Immunology **170:**3037-3045.
323. **Hwang I, Shen X, Sprent J.** 2003. Direct stimulation of naive T cells by membrane vesicles from antigen-presenting cells: distinct roles for CD54 and B7 molecules. Proceedings of the National Academy of Sciences of the United States of America **100:**6670-6675.
324. **Admyre C, Johansson SM, Paulie S, Gabrielsson S.** 2006. Direct exosome stimulation of peripheral humanT cells detected by ELISPOT. European journal of immunology **36:**1772-1781.
325. **Utsugi-Kobukai S, Fujimaki H, Hotta C, Nakazawa M, Minami M.** 2003. MHC class I-mediated exogenous antigen presentation by exosomes secreted from immature and mature bone marrow derived dendritic cells. Immunology letters **89:**125-131.
326. **Zhang P, Li Y, Xia J, He J, Pu J, Xie J, Wu S, Feng L, Huang X, Zhang P.** 2014. IPS-1 plays an essential role in dsRNA-induced stress granule formation by interacting with PKR and promoting its activation. Journal of cell science **127:**2471-2482.
327. **Bukong TN, Momen-Heravi F, Kodys K, Bala S, Szabo G.** 2014. Exosomes from hepatitis C infected patients transmit HCV infection and contain replication competent viral RNA in complex with Ago2-miR122-HSP90. PLoS Pathog **10:**e1004424.
328. **Cosset FL, Dreux M.** 2014. HCV transmission by hepatic exosomes establishes a productive infection. Journal of hepatology **60:**674-675.
329. **Masciopinto F, Giovani C, Campagnoli S, Galli-Stampino L, Colombatto P, Brunetto M, Yen TS, Houghton M, Pileri P, Abrignani S.** 2004.

Association of hepatitis C virus envelope proteins with exosomes. European journal of immunology **34:**2834-2842.

330. **Patman G.** 2014. Hepatitis: Exosomal route of HCV transmission exists in patients. Nature reviews. Gastroenterology & hepatology **11:**704.
331. **Ramakrishnaiah V, Thumann C, Fofana I, Habersetzer F, Pan Q, de Ruiter PE, Willemsen R, Demmers JA, Stalin Raj V, Jenster G, Kwekkeboom J, Tilanus HW, Haagmans BL, Baumert TF, van der Laan LJ.** 2013. Exosome-mediated transmission of hepatitis C virus between human hepatoma Huh7.5 cells. Proceedings of the National Academy of Sciences of the United States of America **110:**13109-13113.
332. **Ariza ME, Rivailler P, Glaser R, Chen M, Williams MV.** 2013. Epstein-Barr virus encoded dUTPase containing exosomes modulate innate and adaptive immune responses in human dendritic cells and peripheral blood mononuclear cells. PLoS One **8:**e69827.
333. **Dukers DF, Meij P, Vervoort MB, Vos W, Scheper RJ, Meijer CJ, Bloemena E, Middeldorp JM.** 2000. Direct immunosuppressive effects of EBV-encoded latent membrane protein 1. Journal of immunology **165:**663-670.
334. **Jaworski E, Narayanan A, Van Duyne R, Shabbeer-Meyering S, Iordanskiy S, Saifuddin M, Das R, Afonso PV, Sampey GC, Chung M, Popratiloff A, Shrestha B, Sehgal M, Jain P, Vertes A, Mahieux R, Kashanchi F.** 2014. Human T-lymphotropic virus type 1-infected cells secrete exosomes that contain Tax protein. The Journal of biological chemistry **289:**22284-22305.
335. **Verweij FJ, van Eijndhoven MA, Hopmans ES, Vendrig T, Wurdinger T, Cahir-McFarland E, Kieff E, Geerts D, van der Kant R, Neefjes J, Middeldorp JM, Pegtel DM.** 2011. LMP1 association with CD63 in endosomes and secretion via exosomes limits constitutive NF-kappaB activation. EMBO J **30:**2115-2129.
336. **Pegtel DM, Cosmopoulos K, Thorley-Lawson DA, van Eijndhoven MA, Hopmans ES, Lindenberg JL, de Gruijl TD, Wurdinger T, Middeldorp JM.** 2010. Functional delivery of viral miRNAs via exosomes. Proceedings of the National Academy of Sciences of the United States of America **107:**6328-6333.
337. **Haneklaus M, Gerlic M, Kurowska-Stolarska M, Rainey A-A, Pich D, McInnes IB, Hammerschmidt W, O'Neill LAJ, Masters SL.** 2012. Cutting Edge: miR-223 and EBV miR-BART15 Regulate the NLRP3 Inflammasome and IL-1β Production. The Journal of Immunology **189:**3795-3799.
338. **Lin Z, Swan K, Zhang X, Cao S, Brett Z, Drury S, Strong MJ, Fewell C, Puetter A, Wang X, Ferris M, Sullivan DE, Li L, Flemington EK.** 2016. Secreted Oral Epithelial Cell Membrane Vesicles Induce Epstein-Barr Virus Reactivation in Latently Infected B Cells. Journal of virology **90:**3469-3479.

339. **Hansen HP, Trad A, Dams M, Zigrino P, Moss M, Tator M, Schon G, Grenzi PC, Bachurski D, Aquino B, Durkop H, Reiners KS, von Bergwelt-Baildon M, Hallek M, Grotzinger J, Engert A, Paes Leme AF, Pogge von Strandmann E.** 2016. CD30 on extracellular vesicles from malignant Hodgkin cells supports damaging of CD30 ligand-expressing bystander cells with Brentuximab-Vedotin, in vitro. Oncotarget **7:**30523-30535.
340. **Meckes DG, Jr., Gunawardena HP, Dekroon RM, Heaton PR, Edwards RH, Ozgur S, Griffith JD, Damania B, Raab-Traub N.** 2013. Modulation of B-cell exosome proteins by gamma herpesvirus infection. Proceedings of the National Academy of Sciences of the United States of America **110:**E2925-2933.
341. **Kalamvoki M, Du T, Roizman B.** 2014. Cells infected with herpes simplex virus 1 export to uninfected cells exosomes containing STING, viral mRNAs, and microRNAs. Proceedings of the National Academy of Sciences of the United States of America **111:**E4991-4996.
342. **Skog J, Wurdinger T, van Rijn S, Meijer DH, Gainche L, Curry WT, Carter BS, Krichevsky AM, Breakefield XO.** 2008. Glioblastoma microvesicles transport RNA and proteins that promote tumour growth and provide diagnostic biomarkers. Nature cell biology **10:**1470-1476.
343. **Clayton A, Mitchell JP, Court J, Linnane S, Mason MD, Tabi Z.** 2008. Human tumor-derived exosomes down-modulate NKG2D expression. Journal of immunology **180:**7249-7258.
344. **Graves LE, Ariztia EV, Navari JR, Matzel HJ, Stack MS, Fishman DA.** 2004. Proinvasive properties of ovarian cancer ascites-derived membrane vesicles. Cancer research **64:**7045-7049.
345. **Hood JL, San RS, Wickline SA.** 2011. Exosomes released by melanoma cells prepare sentinel lymph nodes for tumor metastasis. Cancer research **71:**3792-3801.
346. **Liu C, Yu S, Zinn K, Wang J, Zhang L, Jia Y, Kappes JC, Barnes S, Kimberly RP, Grizzle WE, Zhang HG.** 2006. Murine mammary carcinoma exosomes promote tumor growth by suppression of NK cell function. Journal of immunology **176:**1375-1385.
347. **Szczepanski MJ, Szajnik M, Welsh A, Whiteside TL, Boyiadzis M.** 2011. Blast-derived microvesicles in sera from patients with acute myeloid leukemia suppress natural killer cell function via membrane-associated transforming growth factor-β1. Haematologica **96:**1302-1309.
348. **Whiteside Theresa L.** 2013. Immune modulation of T-cell and NK (natural killer) cell activities by TEXs (tumour-derived exosomes). Biochemical Society transactions **41:**245-251.
349. **Szajnik M, Czystowska M, Szczepanski MJ, Mandapathil M, Whiteside TL.** 2010. Tumor-derived microvesicles induce, expand and up-regulate biological activities of human regulatory T cells (Treg). PLoS One **5:**e11469.

350. **Kim JW, Wieckowski E, Taylor DD, Reichert TE, Watkins S, Whiteside TL.** 2005. Fas ligand-positive membranous vesicles isolated from sera of patients with oral cancer induce apoptosis of activated T lymphocytes. Clinical cancer research : an official journal of the American Association for Cancer Research **11:**1010-1020.
351. **Andreola G, Rivoltini L, Castelli C, Huber V, Perego P, Deho P, Squarcina P, Accornero P, Lozupone F, Lugini L, Stringaro A, Molinari A, Arancia G, Gentile M, Parmiani G, Fais S.** 2002. Induction of Lymphocyte Apoptosis by Tumor Cell Secretion of FasL-bearing Microvesicles. The Journal of experimental medicine **195:**1303-1316.
352. **Schuler PJ, Saze Z, Hong CS, Muller L, Gillespie DG, Cheng D, Harasymczuk M, Mandapathil M, Lang S, Jackson EK, Whiteside TL.** 2014. Human CD4+ CD39+ regulatory T cells produce adenosine upon co-expression of surface CD73 or contact with CD73+ exosomes or CD73+ cells. Clinical and experimental immunology **177:**531-543.
353. **Muller-Haegele S, Muller L, Whiteside TL.** 2014. Immunoregulatory activity of adenosine and its role in human cancer progression. Expert review of clinical immunology **10:**897-914.
354. **Clayton A, Mitchell JP, Court J, Mason MD, Tabi Z.** 2007. Human Tumor-Derived Exosomes Selectively Impair Lymphocyte Responses to Interleukin-2. Cancer research **67:**7458-7466.
355. **Bretz NP, Ridinger J, Rupp AK, Rimbach K, Keller S, Rupp C, Marme F, Umansky L, Umansky V, Eigenbrod T, Sammar M, Altevogt P.** 2013. Body fluid exosomes promote secretion of inflammatory cytokines in monocytic cells via Toll-like receptor signaling. The Journal of biological chemistry **288:**36691-36702.
356. **Wieckowski EU, Visus C, Szajnik M, Szczepanski MJ, Storkus WJ, Whiteside TL.** 2009. Tumor-derived microvesicles promote regulatory T cell expansion and induce apoptosis in tumor-reactive activated CD8+ T lymphocytes. Journal of immunology **183:**3720-3730.
357. **Liu C, Yu S, Zinn K, Wang J, Zhang L, Jia Y, Kappes JC, Barnes S, Kimberly RP, Grizzle WE, Zhang H-G.** 2006. Murine Mammary Carcinoma Exosomes Promote Tumor Growth by Suppression of NK Cell Function. The Journal of Immunology **176:**1375-1385.
358. **Hong CS, Muller L, Whiteside TL, Boyiadzis M.** 2014. Plasma exosomes as markers of therapeutic response in patients with acute myeloid leukemia. Frontiers in immunology **5:**160.
359. **Pucci F, Pittet MJ.** 2013. Molecular pathways: tumor-derived microvesicles and their interactions with immune cells in vivo. Clinical cancer research : an official journal of the American Association for Cancer Research **19:**2598-2604.
360. **Valenti R, Huber V, Filipazzi P, Pilla L, Sovena G, Villa A, Corbelli A, Fais S, Parmiani G, Rivoltini L.** 2006. Human Tumor-Released

Microvesicles Promote the Differentiation of Myeloid Cells with Transforming Growth Factor-β–Mediated Suppressive Activity on T Lymphocytes. Cancer research **66:**9290-9298.

361. **Caivano A, Laurenzana I, De Luca L, La Rocca F, Simeon V, Trino S, D'Auria F, Traficante A, Maietti M, Izzo T, D'Arena G, Mansueto G, Pietrantuono G, Laurenti L, Musto P, Del Vecchio L.** 2015. High serum levels of extracellular vesicles expressing malignancy-related markers are released in patients with various types of hematological neoplastic disorders. Tumour Biol **36:**9739-9752.
362. **Friedlander MR, Mackowiak SD, Li N, Chen W, Rajewsky N.** 2012. miRDeep2 accurately identifies known and hundreds of novel microRNA genes in seven animal clades. Nucleic acids research **40:**37-52.
363. **Wong N, Wang X.** 2015. miRDB: an online resource for microRNA target prediction and functional annotations. Nucleic acids research **43:**D146-152.
364. **Sharbati-Tehrani S, Kutz-Lohroff B, Bergbauer R, Scholven J, Einspanier R.** 2008. miR-Q: a novel quantitative RT-PCR approach for the expression profiling of small RNA molecules such as miRNAs in a complex sample. BMC Molecular Biology **9:**34.
365. **Schmittgen TD, Livak KJ.** 2008. Analyzing real-time PCR data by the comparative CT method. Nat. Protocols **3:**1101-1108.
366. **McCarthy FM, Burgess SC, van den Berg BHJ, Koter MD, Pharr GT.** 2005. Differential Detergent Fractionation for Non-electrophoretic Eukaryote Cell Proteomics. Journal of Proteome Research **4:**316-324.
367. **Schmidt MA, Pendarvis K.** 2017. Proteome rebalancing in transgenic Camelina occurs within the enlarged proteome induced by β-carotene accumulation and storage protein suppression. Transgenic Research **26:**171-186.
368. **Pathan M, Keerthikumar S, Ang C-S, Gangoda L, Quek CYJ, Williamson NA, Mouradov D, Sieber OM, Simpson RJ, Salim A, Bacic A, Hill AF, Stroud DA, Ryan MT, Agbinya JI, Mariadason JM, Burgess AW, Mathivanan S.** 2015. FunRich: An open access standalone functional enrichment and interaction network analysis tool. PROTEOMICS **15:**2597-2601.
369. **Money NP.** 1989. Osmotic Pressure of Aqueous Polyethylene Glycols : Relationship between Molecular Weight and Vapor Pressure Deficit. Plant physiology **91:**766-769.
370. **Cao Q, Mani R-S, Ateeq B, Dhanasekaran Saravana M, Asangani Irfan A, Prensner John R, Kim Jung H, Brenner JC, Jing X, Cao X, Wang R, Li Y, Dahiya A, Wang L, Pandhi M, Lonigro Robert J, Wu Y-M, Tomlins Scott A, Palanisamy N, Qin Z, Yu J, Maher Christopher A, Varambally S, Chinnaiyan Arul M.** 2011. Coordinated Regulation of Polycomb Group Complexes through microRNAs in Cancer. Cancer cell **20:**187-199.

371. **Lu TX, Munitz A, Rothenberg ME.** 2009. MicroRNA-21 is up-regulated in allergic airway inflammation and regulates IL-12p35 expression. Journal of immunology (Baltimore, Md. : 1950) **182:**4994-5002.
372. **Lu TX, Hartner J, Lim EJ, Fabry V, Mingler MK, Cole ET, Orkin SH, Aronow BJ, Rothenberg ME.** 2011. MicroRNA-21 limits in vivo immune response-mediated activation of the IL-12/IFN-gamma pathway, Th1 polarization, and the severity of delayed-type hypersensitivity. Journal of immunology **187:**3362-3373.
373. **Vennegaard MT, Bonefeld CM, Hagedorn PH, Bangsgaard N, Lovendorf MB, Odum N, Woetmann A, Geisler C, Skov L.** 2012. Allergic contact dermatitis induces upregulation of identical microRNAs in humans and mice. Contact dermatitis **67:**298-305.
374. **Alexander M, Hu R, Runtsch MC, Kagele DA, Mosbruger TL, Tolmachova T, Seabra MC, Round JL, Ward DM, O'Connell RM.** 2015. Exosome-delivered microRNAs modulate the inflammatory response to endotoxin. Nature communications **6:**7321.
375. **Oppmann B, Lesley R, Blom B, Timans JC, Xu Y, Hunte B, Vega F, Yu N, Wang J, Singh K, Zonin F, Vaisberg E, Churakova T, Liu M, Gorman D, Wagner J, Zurawski S, Liu Y, Abrams JS, Moore KW, Rennick D, de Waal-Malefyt R, Hannum C, Bazan JF, Kastelein RA.** 2000. Novel p19 protein engages IL-12p40 to form a cytokine, IL-23, with biological activities similar as well as distinct from IL-12. Immunity **13:**715-725.
376. **Pathan M, Keerthikumar S, Ang CS, Gangoda L, Quek CY, Williamson NA, Mouradov D, Sieber OM, Simpson RJ, Salim A, Bacic A, Hill AF, Stroud DA, Ryan MT, Agbinya JI, Mariadason JM, Burgess AW, Mathivanan S.** 2015. FunRich: An open access standalone functional enrichment and interaction network analysis tool. Proteomics **15:**2597-2601.
377. **Huang DW, Sherman BT, Tan Q, Collins JR, Alvord WG, Roayaei J, Stephens R, Baseler MW, Lane HC, Lempicki RA.** 2007. The DAVID Gene Functional Classification Tool: a novel biological module-centric algorithm to functionally analyze large gene lists. Genome biology **8:**R183.
378. **Kalra H, Simpson RJ, Ji H, Aikawa E, Altevogt P, Askenase P, Bond VC, Borras FE, Breakefield X, Budnik V, Buzas E, Camussi G, Clayton A, Cocucci E, Falcon-Perez JM, Gabrielsson S, Gho YS, Gupta D, Harsha HC, Hendrix A, Hill AF, Inal JM, Jenster G, Kramer-Albers EM, Lim SK, Llorente A, Lotvall J, Marcilla A, Mincheva-Nilsson L, Nazarenko I, Nieuwland R, Nolte-'t Hoen EN, Pandey A, Patel T, Piper MG, Pluchino S, Prasad TS, Rajendran L, Raposo G, Record M, Reid GE, Sanchez-Madrid F, Schiffelers RM, Siljander P, Stensballe A, Stoorvogel W, Taylor D, Thery C, Valadi H, van Balkom BW, Vazquez J, Vidal M, Wauben MH, Yanez-Mo M, Zoeller M, Mathivanan S.** 2012. Vesiclepedia: a compendium for extracellular vesicles with continuous community annotation. PLoS biology **10:**e1001450.

379. **Nahid MA, Pauley KM, Satoh M, Chan EK.** 2009. miR-146a is critical for endotoxin-induced tolerance: IMPLICATION IN INNATE IMMUNITY. The Journal of biological chemistry **284:**34590-34599.
380. **Taganov KD, Boldin MP, Chang KJ, Baltimore D.** 2006. NF-kappaB-dependent induction of microRNA miR-146, an inhibitor targeted to signaling proteins of innate immune responses. Proceedings of the National Academy of Sciences of the United States of America **103:**12481-12486.
381. **Li B, Wang X, Choi IY, Wang Y-C, Liu S, Pham AT, Moon H, Smith DJ, Rao DS, Boldin MP, Yang L.** 2017. miR-146a modulates autoreactive Th17 cell differentiation and regulates organ-specific autoimmunity. The Journal of clinical investigation **127:**3702-3716.
382. **Lu L-F, Boldin MP, Chaudhry A, Lin L-L, Taganov KD, Hanada T, Yoshimura A, Baltimore D, Rudensky AY.** 2010. Function of miR-146a in controlling Treg cell-mediated regulation of Th1 responses. Cell **142:**914-929.
383. **Xiang M, Birkbak NJ, Vafaizadeh V, Walker SR, Yeh JE, Liu S, Kroll Y, Boldin M, Taganov K, Groner B, Richardson AL, Frank DA.** 2014. STAT3 induction of miR-146b forms a feedback loop to inhibit the NF-kappaB to IL-6 signaling axis and STAT3-driven cancer phenotypes. Science signaling **7:**ra11.
384. **Lu L-F, Cho S, Wu C-J, Yasuda T, Cruz LO, Khan AA, Lin L-L, Nguyen DT, Miller M, Lee H-M, Kuo M-L, Broide DH, Rajewsky K, Rudensky AY.** 2016. MiR-23~27~24 clusters control effector T cell differentiation and function. The Journal of Immunology **196:**127.124-127.124.
385. **Hu R, O'Connell RM.** 2012. MiR-23b is a safeguard against autoimmunity. Nature medicine **18:**1009.
386. **Zhou R, Gong A-Y, Eischeid AN, Chen X-M.** 2012. miR-27b Targets KSRP to Coordinate TLR4-Mediated Epithelial Defense against Cryptosporidium parvum Infection. PLoS Pathogens **8:**e1002702.
387. **Zhu S, Pan W, Song X, Liu Y, Shao X, Tang Y, Liang D, He D, Wang H, Liu W, Shi Y, Harley JB, Shen N, Qian Y.** 2012. The microRNA miR-23b suppresses IL-17-associated autoimmune inflammation by targeting TAB2, TAB3 and IKK-α. Nature medicine **18:**1077.
388. **Cho S, Wu C-J, Yasuda T, Cruz LO, Khan AA, Lin L-L, Nguyen DT, Miller M, Lee H-M, Kuo M-L, Broide DH, Rajewsky K, Rudensky AY, Lu L-F.** 2016. miR-23~27~24 clusters control effector T cell differentiation and function. The Journal of experimental medicine.
389. **Takahashi R-u, Miyazaki H, Takeshita F, Yamamoto Y, Minoura K, Ono M, Kodaira M, Tamura K, Mori M, Ochiya T.** 2015. Loss of microRNA-27b contributes to breast cancer stem cell generation by activating ENPP1. Nature communications **6:**7318.
390. **Wan L, Zhang L, Fan K, Wang J.** 2014. miR-27b targets LIMK1 to inhibit growth and invasion of NSCLC cells. Molecular and Cellular Biochemistry **390:**85-91.

391. **Liu W, Lv C, Zhang B, Zhou Q, Cao Z.** 2017. MicroRNA-27b functions as a new inhibitor of ovarian cancer-mediated vasculogenic mimicry through suppression of VE-cadherin expression. RNA **23:**1019-1027.
392. **Li J, Hui L, Kang Q, Li R.** 2018. Down-regulation of microRNA-27b promotes retinal pigment epithelial cell proliferation and migration by targeting Nox2. Pathology - Research and Practice **214:**925-933.
393. **Kang H, Rho JG, Kim C, Tak H, Lee H, Ji E, Ahn S, Shin AR, Cho H-I, Huh YH, Song WK, Kim W, Lee EK.** 2017. The miR-24-3p/p130Cas: a novel axis regulating the migration and invasion of cancer cells. Scientific reports **7:**44847.
394. **Lin KY, Ye H, Han BW, Wang WT, Wei PP, He B, Li XJ, Chen YQ.** 2015. Genome-wide screen identified let-7c/miR-99a/miR-125b regulating tumor progression and stem-like properties in cholangiocarcinoma. Oncogene **35:**3376.
395. **Feliciano A, Garcia-Mayea Y, Jubierre L, Mir C, Hummel M, Castellvi J, Hernández-Losa J, Paciucci R, Sansano I, Sun Y, Ramón y Cajal S, Kondon H, Soriano A, Segura M, Lyakhovich A, Lleonart ME.** 2017. miR-99a reveals two novel oncogenic proteins E2F2 and EMR2 and represses stemness in lung cancer. Cell Death &Amp; Disease **8:**e3141.
396. **Chen D, Chen Z, Jin Y, Dragas D, Zhang L, Adjei BS, Wang A, Dai Y, Zhou X.** 2013. MicroRNA-99 family members suppress Homeobox A1 expression in epithelial cells. PLoS One **8:**e80625.
397. **Kim SW, Ramasamy K, Bouamar H, Lin AP, Jiang D, Aguiar RC.** 2012. MicroRNAs miR-125a and miR-125b constitutively activate the NF-kappaB pathway by targeting the tumor necrosis factor alpha-induced protein 3 (TNFAIP3, A20). Proceedings of the National Academy of Sciences of the United States of America **109:**7865-7870.
398. **Li Y, Zhang Z, Zhang X, Lin Y, Luo T, Xiao Z, Zhou Q.** 2016. A dual PI3K/AKT/mTOR signaling inhibitor miR-99a suppresses endometrial carcinoma. American journal of translational research **8:**719-731.
399. **Alajez NM, Shi W, Hui AB, Bruce J, Lenarduzzi M, Ito E, Yue S, O'Sullivan B, Liu FF.** 2010. Enhancer of Zeste homolog 2 (EZH2) is overexpressed in recurrent nasopharyngeal carcinoma and is regulated by miR-26a, miR-101, and miR-98. Cell death & disease **1:**e85.
400. **Yang X, Liang L, Zhang XF, Jia HL, Qin Y, Zhu XC, Gao XM, Qiao P, Zheng Y, Sheng YY, Wei JW, Zhou HJ, Ren N, Ye QH, Dong QZ, Qin LX.** 2013. MicroRNA-26a suppresses tumor growth and metastasis of human hepatocellular carcinoma by targeting interleukin-6-Stat3 pathway. Hepatology **58:**158-170.
401. **Yang X, Zhang XF, Lu X, Jia HL, Liang L, Dong QZ, Ye QH, Qin LX.** 2014. MicroRNA-26a suppresses angiogenesis in human hepatocellular carcinoma by targeting hepatocyte growth factor-cMet pathway. Hepatology **59:**1874-1885.

402. **Zhuang C, Wang P, Huang D, Xu L, Wang X, Wang L, Hu L.** 2016. A double-negative feedback loop between EZH2 and miR-26a regulates tumor cell growth in hepatocellular carcinoma. International journal of oncology **48:**1195-1204.
403. **Zhou J, Ju WQ, Yuan XP, Zhu XF, Wang DP, He XS.** 2016. miR-26a regulates mouse hepatocyte proliferation via directly targeting the 3' untranslated region of CCND2 and CCNE2. Hepatobiliary & pancreatic diseases international : HBPD INT **15:**65-72.
404. **Li X, Lian L, Zhang D, Qu L, Yang N.** 2014. gga-miR-26a targets NEK6 and suppresses Marek's disease lymphoma cell proliferation. Poult Sci **93:**1097-1105.
405. **Wang Y, Li Z, Zhao X, Zuo X, Peng Z.** 2016. miR-10b promotes invasion by targeting HOXD10 in colorectal cancer. Oncology letters **12:**488-494.
406. **Tsuchida A, Ohno S, Wu W, Borjigin N, Fujita K, Aoki T, Ueda S, Takanashi M, Kuroda M.** 2011. miR-92 is a key oncogenic component of the miR-17–92 cluster in colon cancer. Cancer Science **102:**2264-2271.
407. **Landais S, Landry S, Legault P, Rassart E.** 2007. Oncogenic Potential of the miR-106-363 Cluster and Its Implication in Human T-Cell Leukemia. Cancer research **67:**5699-5707.
408. **Baumjohann D.** 2018. Diverse functions of miR-17–92 cluster microRNAs in T helper cells. Cancer Letters **423:**147-152.
409. **Mogilyansky E, Rigoutsos I.** 2013. The miR-17/92 cluster: a comprehensive update on its genomics, genetics, functions and increasingly important and numerous roles in health and disease. Cell death and differentiation **20:**1603-1614.
410. **Mu P, Han Y-C, Betel D, Yao E, Squatrito M, Ogrodowski P, de Stanchina E, D'Andrea A, Sander C, Ventura A.** 2009. Genetic dissection of the miR-17~92 cluster of microRNAs in Myc-induced B-cell lymphomas. Genes & development **23:**2806-2811.
411. **Kumar P, Luo Y, Tudela C, Alexander JM, Mendelson CR.** 2013. The c-Myc-Regulated MicroRNA-17~92 (miR-17~92) and miR-106a~363 Clusters Target hCYP19A1 and hGCM1 To Inhibit Human Trophoblast Differentiation. Molecular and cellular biology **33:**1782-1796.
412. **Li L, Shi B, Chen J, Li C, Wang S, Wang Z, Zhu G.** 2017. An E2F1/MiR-17-92 Negative Feedback Loop mediates proliferation of Mouse Palatal Mesenchymal Cells. Scientific reports **7:**5148.
413. **Petrocca F, Vecchione A, Croce CM.** 2008. Emerging Role of miR-106b-25/miR-17-92 Clusters in the Control of Transforming Growth Factor β Signaling. Cancer research **68:**8191-8194.
414. **Ivanovska I, Ball AS, Diaz RL, Magnus JF, Kibukawa M, Schelter JM, Kobayashi SV, Lim L, Burchard J, Jackson AL, Linsley PS, Cleary MA.** 2008. MicroRNAs in the miR-106b Family Regulate p21/CDKN1A and

Promote Cell Cycle Progression. Molecular and cellular biology **28:**2167-2174.

415. **Choi HS, Jain V, Krueger B, Marshall V, Kim CH, Shisler JL, Whitby D, Renne R.** 2015. Kaposi's Sarcoma-Associated Herpesvirus (KSHV) Induces the Oncogenic miR-17-92 Cluster and Down-Regulates TGF-β Signaling. PLOS Pathogens **11:**e1005255.
416. **Skalsky RL, Corcoran DL, Gottwein E, Frank CL, Kang D, Hafner M, Nusbaum JD, Feederle R, Delecluse H-J, Luftig MA, Tuschl T, Ohler U, Cullen BR.** 2012. The Viral and Cellular MicroRNA Targetome in Lymphoblastoid Cell Lines. PLoS Pathogens **8:**e1002484.
417. **Honegger A, Schilling D, Bastian S, Sponagel J, Kuryshev V, Sültmann H, Scheffner M, Hoppe-Seyler K, Hoppe-Seyler F.** 2015. Dependence of Intracellular and Exosomal microRNAs on Viral E6/E7 Oncogene Expression in HPV-positive Tumor Cells. PLOS Pathogens **11:**e1004712.
418. **Smallwood DT, Apollonio B, Willimott S, Lezina L, Alharthi A, Ambrose AR, De Rossi G, Ramsay AG, Wagner SD.** 2016. Extracellular vesicles released by CD40/IL-4–stimulated CLL cells confer altered functional properties to CD4⁺ T cells. Blood **128:**542-552.
419. **Chen X-M, Splinter PL, O'Hara SP, LaRusso NF.** 2007. A Cellular Micro-RNA, let-7i, Regulates Toll-like Receptor 4 Expression and Contributes to Cholangiocyte Immune Responses against Cryptosporidium parvum Infection. The Journal of biological chemistry **282:**28929-28938.
420. **Sampson VB, Rong NH, Han J, Yang Q, Aris V, Soteropoulos P, Petrelli NJ, Dunn SP, Krueger LJ.** 2007. MicroRNA Let-7a Down-regulates MYC and Reverts MYC-Induced Growth in Burkitt Lymphoma Cells. Cancer research **67:**9762-9770.
421. **Ma X, Kumar M, Choudhury SN, Becker Buscaglia LE, Barker JR, Kanakamedala K, Liu M-F, Li Y.** 2011. Loss of the miR-21 allele elevates the expression of its target genes and reduces tumorigenesis. Proceedings of the National Academy of Sciences of the United States of America **108:**10144-10149.
422. **Stik G, Dambrine G, Pfeffer S, Rasschaert D.** 2013. The Oncogenic MicroRNA OncomiR-21 Overexpressed during Marek's Disease Lymphomagenesis Is Transactivated by the Viral Oncoprotein Meq. Journal of virology **87:**80-93.
423. **Melnik BC.** 2015. MiR-21: an environmental driver of malignant melanoma? Journal of Translational Medicine **13:**202.
424. **Lou Y, Liu S.** 2011. The TIPE (TNFAIP8) family in inflammation, immunity, and cancer. Molecular immunology **49:**4-7.
425. **McCormick C, Khaperskyy DA.** 2017. Translation inhibition and stress granules in the antiviral immune response. Nature Reviews Immunology **17:**647.

426. **Jarosinski K, Kattenhorn L, Kaufer B, Ploegh H, Osterrieder N.** 2007. A herpesvirus ubiquitin-specific protease is critical for efficient T cell lymphoma formation. Proceedings of the National Academy of Sciences of the United States of America **104:**20025-20030.
427. **Veiga IB, Jarosinski KW, Kaufer BB, Osterrieder N.** 2013. Marek's disease virus (MDV) ubiquitin-specific protease (USP) performs critical functions beyond its enzymatic activity during virus replication. Virology **437:**110-117.
428. **Mi W, Guan H, Lyu J, Zhao D, Xi Y, Jiang S, Andrews FH, Wang X, Gagea M, Wen H, Tora L, Dent SYR, Kutateladze TG, Li W, Li H, Shi X.** 2017. YEATS2 links histone acetylation to tumorigenesis of non-small cell lung cancer. Nature communications **8:**1088.
429. **Zhao D, Guan H, Zhao S, Mi W, Wen H, Li Y, Zhao Y, Allis CD, Shi X, Li H.** 2016. YEATS2 is a selective histone crotonylation reader. Cell research **26:**629-632.
430. **Duprè S, Chiaraluce R, Nardini M, Cannella C, Ricci G, Cavallini D.** 1984. Continuous spectrophotometric assay of pantetheinase activity. Analytical Biochemistry **142:**175-181.
431. **Mahadevan NR, Rodvold J, Sepulveda H, Rossi S, Drew AF, Zanetti M.** 2011. Transmission of endoplasmic reticulum stress and pro-inflammation from tumor cells to myeloid cells. Proceedings of the National Academy of Sciences of the United States of America **108:**6561-6566.
432. **Zhang H, Yue Y, Sun T, Wu X, Xiong S.** 2017. Transmissible endoplasmic reticulum stress from myocardiocytes to macrophages is pivotal for the pathogenesis of CVB3-induced viral myocarditis. Scientific reports **7:**42162.

Appendix A

PRIMER SEQUENCES USED IN THE STUDY

Gene	Tm	Forward	Reverse	Reference
GAPDH	55	GGAGTCCACTGGTGTCTTCA	AGCACCACCCTTCAGATGAG	This study
AvBD1	58	AAACCATGCGGATCGTGTACCTGC	CAATGCTAAACTGCACACCTTTA	This study
AvBD2	58	TGTCCCAGCCATCTAATC	GGCTTTGCTGTAGCATTTA	This study
AvBD3	58	GGAGGATTCTGTCGTGTT	CAGGGCATCAACCTCATA	This study
AvBD4	58	CATCGTGCTCCTCTTTGT	TTCCCATGAGGGCATTTC	This study
AvBD5	58	GATCCTGACTCTCCTCTTTG	GGGTAATCCTCGAGCAAG	This study
AvBD10	58	CTGTTCTCCTCTTCCTCTTC	CCAGAGATGGTGAAGGTG	This study
Cathelicidin	58	GTGGACTCCTACAACCAA	GATGGTGAAGTTGAGGTTG	This study
LEAP2	58	TTCTGGAGAGGAGTCTCA	CTTCCTGCATAGCATTGTG	This study
CATHB1	58	GGAGGTGAGCTTCCTTGT	CTGCTCTATGGACACGGT	This study
CATH1	58	CGTGCTCGATGTCACCTG	GTAGAGGTTGTATCCTGCAATCA	This study
CATH2	58	ATCAATCTACGCTGCAGAGAC	GGATGGTGATGGTGACCTTAG	This study
CATH3	58	GTGGACTCCATGGCTGAC	TTCTCCTGATGGCTTTGTAGAG	This study
IL-1B	58	GCATCAAGGGCTACAAGCTCTACA	TGTCCAGGCGGTAGAAGATGAA	This study
IL-18	58	AGGTGAAATCTGGCAGTGGAAT	ACCTGGACGCTGAATGCAA	This study
NOS2A	58	GGGAGAATCCAGTGGTCCAATCTA	GTGGCATACTGAATATGGCGACAG	This study
IL-8	58	CCCTCGCCACAGAACCAA	CAGCCTTGCCCATCATCTTT	This study
IFN-α	58	CGCAACCTTCACCTCACCATCAAA	TGTGAGGTTGTGGATGTGCAGGAA	This study
MX1	58	ATGGGCAAATGGACTTCTGCAACG	TGCCAGATGTGGGATAGTAGCCTT	This study
OASL	58	TACTATTCCCTGGAGGATGAGTGGGT	ACCAAGTCCCAGTTCTTGCCTT	This study
IFNG	58	GTGAAGAAGGTGAAAGATATCATGGA	GCTTTGCGCTGGATTCTCA	This study
MHC I	58	CATCGTGGTTGGTGTTG	CGATGTTGTAGCCCTTC	This study
MHC II	58	ACGGACGTGATGCAGAA	CGGCACACGTAGCTGTC	This study
SOCS1	58	AGGCTGTAGGATGGTAGCGC	GTCAAGTAGACATCGCGGGTC	This study
SOCS2	58	CTGCTGACCATCTCGGTCAA	AGCCTGAACTTGCCGTCCT	This study
SOCS3	58	AGCTGCCAGCCCCTATCAA	TTCCCTCTGCCAGCCTCTTA	This study
T-bet/TBX21	58	AGGAGGTTTCCTTTGGGAAGCTGA	TGGTTGGTACTTGTGCAGCGACT	This study
IL-12p40	58	TTGCCGAAGAGCACCAGCCG	CGGTGTGCTCCAGGTCTTGGG	This study
IL-12p19	58	TGCAGGGACCTCTCTCAG	CTCCATGTCCTCCTCTCCA	This study
GATA3	58	TGGGCTCTACTACAAGCTGCACAA	AGACTTTCCCAAGAGCAGCTCCTT	This study
IL-4	58	GCTCTCAGTGCCGCTGATG	GAAACCTCTCCCTGGATGTCAT	Rath et al 2013
IL-10	58	GAGCTGAGGGTGAAGTTTGAGGAA	CTTTGACACAGACTGGCAGCCAAA	This study
IL-13	58	ATCCAGAAGCTCAACAGA	CTTCCGATCCTTGAAAGC	This study
CD3	58	CGTAAACTCCACTCTCCA	CGACCACAATCCCTGATA	This study
CD8α	58	CAACCAGATGCTGTACTTC	GCAGATGTCCTTGTTGAC	This study
CD4	58	TTGCAGGAAAGGAGGTGATCCTGA	TCCAGGCTCAAGTCTGACACCTT	This study
CD107	58	GAGCTAACTTTCCACTACAATC	CCAATACGTGCCTGAATAAC	This study
Bu.1	58	CAGTGTTTGCTGGTGATAA	GGAAACTTTGCTGAGCTG	This study
CD11c	58	CCATCGGATGAAGACATTC	GTCGAAGTCGGAGAAGT	This study
CD18	58	CAGAGTGTCCCAAGATCAA	CACCAGCTTTGGTGAAAC	This study
SIRT1	58	TCTTTCCGAACCACCAA	GTATTCCACAAGACACAGAC	This study
SIRT2	58	GGAATCGCCCGGTTCAT	CCCAGGTTGGCGTACAG	This study
SIRT3	58	GAGTGTCGTCGAGTAGTG	GGGTAAGGGATGTTGTACT	This study
SIRT4	58	CTTCACACCAAAGCTGGGAG	CCAGGGTTCAGAGCTTCAAA	This study
SIRT5	58	TGGTCATCACCCAGAAC	GCAGATCGGACTCTTGTA	This study
SIRT6	58	CTTCCAATGTGGTGTTCC	CTCAAAGGTGGTGTCAAAT	This study
SIRT7	58	CCTCGTCGTCCAAAGCTCTA	CCAGCTCCTCCATCAGCAG	This study
MDV2 (HPRS24)	58	CCTCGGCATAGTCCAATA	CACGTTTGTAGACCTGAAC	This study
MDV3 (HVT/FC126)	58	CCAGATCAGCATTTCCATAC	GGTTGGAGTTGTTCCATAAA	This study

Appendix B

MIRDB PREDICTED CELLULAR TARGETS MDV-1 MIRNA

MDV1-miR-M1	MDV1-miR-M2	MDV1-miR-M4	MDV1-miR-M5	MDV1-miR-M11	MDV1-miR-M6	MDV1-miR-M7
TAF4	SPPL2B	ZNF652	GABRA1	KCNK10	MBNL2	PAPPA
MAGT1	TNFAIP8	S1PR1	USP47	NUFIP2	MCFD2	
SIK1	TAB3	CNTN4	GALNT7	HELZ	FMR1	
HIPK1	RPS6KA1	WEE1	NCOA2	PAPD5	MEMO1	
KBTBD2	KIAA0240	XRN1	FAM76B	PLXNA2	YY1	
MEGF11	ZNRF2	ITK	ZSWIM6	FAM154B	G3BP2	
MAL	LRCH3	HIVEP2	ADAM28	NRXN1	ARIH1	
RBFOX1	ARFGEF2	RREB1		SEMA6A	DET1	
DCUN1D4	RASGEF1C	LZTFL1		TRIP11	RAB10	
SLC1A2	UBE2W	FBXO33		PHF12	ZMYM4	
LOC101749175	ZNF410	SPI1		RELL1	SLC8A3	
MPHOSPH6	RDH12	BACH1		TAB2	ALS2CL	
MDGA2	PSD3	ATXN1L		SLC1A1	RAB1A	
SCN8A	ZHX3	KIAA1468		BCL11A	CTNNA3	
TRIB2	MFSD10	1-Mar		IQGAP1	PTPRG	
ACPP	IDH1	RPS6KA5		FAN1	MSI2	
TMEM47	C11ORF41	RAB5C		FIGN	MEF2C	
AUTS2	ALS2CR8	KBTBD2		NEK6	KBTBD8	
GAPVD1	BTRC	JARID2		LOC421259	HIPK3	
RNF165	GFOD2	TSPAN14		VAPB	LRIT1	
PDE7B	C14H7ORF62	ARID2		PBX3	TMEM194B	
IPO7		GABRA1		SET	TPK1	
LOC100858906		RPS6KA3		CLASP2	RASA1	
B3GALT2		TAB2		SUB1	ARL14EPL	
		SNX3		NAA30	KIF26B	
		USP44		GPR161	LOC426820	
		ATRNL1		TP53INP1	TMEM47	
		RGL1		KLF9	GPR17	
		TSHZ3		ITGB8	TRMT10A	
		TRIM66		TMEM50A	MAF	
		KRAS		GNAS		
		ANO5		RUNX3		
		VKORC1L1		CACNA1C		
		OPRL1		RFXDC2		
		ELL2		DCX		
		PAPLN		FLRT2		
		RORA		MLL		
		DYNC1I1		SLC30A1		
		NEDD4L		XRN1		
		VAV3		SESN3		
		SULT1C3		YTHDF2		
		SLC2A12		ARGLU1		
		KDM2A		MAGI1		
		GPD1L		KLHL24		
		HAUS6		SMURF2		
		TRPS1		TPPP		
		PSMC3		STK17B		
		COMMD8		PHF21A		
		LRRC59		FAM164A		
		COL21A1		MLEC		
		STRN3		RBMX		
		CHAF1A		TMED5		
		RC3H2		THBS1		
		TADA2B		SETBP1		
		TAPT1		SYN3		
		DENND6A		RBM12B		
		SEL1L3		MAFB		
		SLC1A3		PPP2R5E		
		SLC15A1		TGFB2		
		TOE1		NUP153		
		C13H5ORF41		HLF		
				HIVEP3		
				PRKRIP1		
				HSPA2		
				GRIN2A		
				ARIH1		
				ANO5		
				CELF1		
				B3GNT5		
				LMX1A		
				SDK2		
				TNPO1		
				CCDC126		
				SYT11		
				GALNT1		
				AMMECR1		
				AXIN2		
				FBXO42		
				CDK19		
				ADAMTS17		

Appendix C

IACUC PERMISSIONS

University of Delaware
Institutional Animal Care and Use Committee
Application to Use Animals in Application to use animals in Research
(New and 3-Yr submission)

RECEIVED
JUL 22 2016
IACUC

Title of Protocol: Characterization of Marek's Disease Viruses (for Pathogenicity, Therapeutic and Vaccine Efficacy Studies)	
AUP Number: 64R-2016-0	**← (4 digits only — if new, leave blank)**
Principal Investigator: Mark S. Parcells, Ph.D.	
Common Name (Strain/Breed if Appropriate): Chickens (SPF and/or Commercial Broilers or Layers) **Genus Species:** Gallus gallus	
Date of Submission: 7/19/16	

Official Use Only

IACUC Approval Signature: Glenn Tallman, DVM

Date of Approval: 8/10/2016

Principal Investigator Assurance

1. I agree to abide by all applicable federal, state, and local laws and regulations, and UD policies and procedures.
2. I understand that deviations from an approved protocol or violations of applicable policies, guidelines, or laws could result in immediate suspension of the protocol and may be reportable to the Office of Laboratory Animal Welfare (OLAW).
3. I understand that the Attending Veterinarian or his/her designee must be consulted in the planning of any research or procedural changes that may cause more than momentary or slight pain or distress to the animals.
4. I declare that all experiments involving live animals will be performed under my supervision or that of another qualified scientist. All listed personnel will be trained and certified in the proper humane methods of animal care and use prior to conducting experimentation.
5. I understand that emergency veterinary care will be administered to animals showing evidence of discomfort, ailment, or illness.
6. I declare that the information provided in this application is accurate to the best of my knowledge. If this project is funded by an extramural source, I certify that this application accurately reflects all currently planned procedures involving animals described in the proposal to the funding agency.
7. I assure that any modifications to the protocol will be submitted to by the UD-IACUC and I understand that they must be approved by the IACUC prior to initiation of such changes.
8. I understand that the approval of this project is for a maximum of one year from the date of UD-IACUC approval and that I must re-apply to continue the project beyond that period.
9. I understand that any unanticipated adverse events, morbidity, or mortality must be reported to the UD-IACUC immediately.
10. I assure that the experimental design has been developed with consideration of the three Rs: reduction, refinement, and replacement, to reduce animal pain and/or distress and the number of animals used in the laboratory.
11. I assure that the proposed research does not unnecessarily duplicate previous experiments. ***(Teaching Protocols, including cooperative extension demonstrations, Exempt)***
12. I understand that by signing, I agree to these assurances. Mark S. Parcells Signature of Principal Investigator **7/19/16** Date

Rev202/2016

#64R-2016-0

NAMES OF ALL PERSONS WORKING ON THIS PROTOCOL

I certify that I have read this protocol, accept my responsibility and will perform only those procedures that have been approved by the IACUC.

Name	Signature
1. Mark S. Parcells, Principal Investigator	
2. Phaedra Tavlarides-Hontz, Technician	
3. Sabari Nath Neerukonda, PhD student	
4.	
5. Click here to enter text.	
6. Click here to enter text.	
7. Click here to enter text.	
8. Click here to enter text.	
9. Click here to enter text.	
10. Click here to enter text.	

If after hours participation is required by students on project involving **agricultural animals**, please describe how this is handled and the times and days that students may be on site

Any and all undergraduate students or additional graduate students will participate in active training for any and all animal handling procedures. All non-survival sampling (tissue removal) or euthanasia will be carried out by the PI or trained PhD student. Undergraduates and MS students will be employed to monitor animals, feed, water and transport birds or tissues only.

The Animal Use Protocol form has been developed to facilitate review of requests for specific research, teaching, or biological testing projects. The review process has been designed to communicate methods and materials for using animals through administrative officials and attending veterinarians to the Institutional Animal Care and Use Committee (IACUC). This process will help assure that provisions are made for compliance with the Animal Welfare Act, the Public Health Service Policy on Humane Care and Use of Laboratory Animals and the Guide for the Care and Use of Laboratory Animals.

Please read this form carefully and fill out all sections. Failure to do so may delay the review of this application. Sections that do not apply to your research must be marked "NA" for "Not Applicable."

This application form must be used for all NEW or THREE-YEAR RENEWAL protocols.

All answers are to be completed using Arial 12 size font.

All questions must be answered in their respective boxes and NOT as attachments at the end of this form.

Please complete any relevant addenda:

- Hybridoma/Monoclonal Antibodies ("B")
- Polyclonal Antibodies ("C")
- Survival Surgery ("D")
- Non-Survival Surgery ("E")
- Wildlife Research ("F")

If help is needed with these forms, contact the IACUC Coordinator at extension 2616, the Facility Manager at extension 2400 or the Attending Veterinarian at extension 2980.